NATURA

TUR2021

3rd International Conference on Tourmaline
Elba Island, Italy
September 9-11, 2021

Ferdinando Bosi
Federico Pezzotta
Giovanni B. Andreozzi
Editors

VOLUME 111 (1) 2021

SISN
SOCIETÀ ITALIANA
DI SCIENZE NATURALI

msnm
Museo di Storia Naturale di Milano

Direttore responsabile
Anna Alessandrello
Museo di Storia Naturale di Milano

Grafica editoriale
Michela Mura
Museo di Storia Naturale di Milano

Editors and co-chairmen
Ferdinando Bosi
Sapienza University of Rome

Federico Pezzotta
Museo di Storia Naturale di Milano

Giovanni B. Andreozzi
Sapienza University of Rome

In copertina Tourmaline crystals with quartz and "lepidolite", Grotta d'Oggi, Elba Island. (Photo A. Miglioli).

Editore
Società Italiana di Scienze Naturali
Corso Venezia, 55 - 20121 Milano
www.scienzenaturali.org
E-mail: info@scienzenaturali.org

Autorizzazione 1112
Tribunale di Milano del 3 febbraio 1949

Poste Italiane S.p.a. - Spedizione in Abbonamento Postale - D.L. 353/2003 (conv. in L. 27/02/2004 n° 46) art. 1 comma 2, LO/MI

ISSN 0369-6243 (print)

Stampa
Litografia Solari
Via Lambro 7/15 - 20068 Peschiera Borromeo (MI)

Finito di stampare
Agosto 2021

This volume contains 52 abstracts and keynote abstracts presented at the 3rd International Conference on Tourmaline (*TUR2021*), held on Elba Island, Italy, from 9 to 11 September 2021 (https://www.tur2021.com).

The Conference has been organized along with the sponsorship of SIMP (Italian Society of Mineralogy and Petrology), and support of the Sapienza University of Rome and Natural History Museum of Milan.

The abstract volume is the joint effort of all conference participants and covers many aspects of tourmaline regarding the latest discoveries across the range of crystallography, mineralogy, petrology, geochemistry, isotopic analyses, ore-deposits research, gem science, and much more.

All the abstracts published in this volume were critically read and approved by the scientific committee for presentation at *TUR2021*.

We wish to express our deepest gratitude to the members of the scientific committee of *TUR2021*: J. Cempírek, (Masaryk University), A. Dini (National Research Council of Italy), B.L. Dutrow (Louisiana State University), A. Ertl (University of Vienna), D.J. Henry (Louisiana State University), H.R. Marschall (Goethe University Frankfurt), M. Novák (Masaryk University), R.B. Trumbull (Helmholtz Centre Potsdam-GFZ), V.J. van Hinsberg (McGill University, Montreal).

Particular thanks are due to Alessandra Altieri and Beatrice Celata for all their effort and cooperation in the organizational and editing aspects of the abstracts.

The publication of this abstract volume was made possible through the support of the NATURA journal staff, namely Michela Mura and the managing director Anna Alessandrello, to whom we express our gratitude.

Ferdinando Bosi
Federico Pezzotta
Giovanni B. Andreozzi
(Co-chairmen of *TUR2021*)

PATRONAGE AND SPONSORSHIP

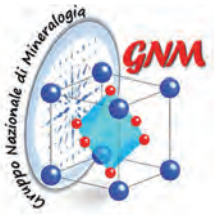

Color anomalies at the termination of pegmatitic gem-tourmaline crystals from Elba Island (Tyrrhenian Sea, Italy): a genetic model

Alessandra Altieri[1]*, Federico Pezzotta[2], Giovanni B. Andreozzi[1], Ferdinando Bosi[1]

Elba tourmalines are renowned for their beauty, elegance and the wide spectrum of colors, even within an individual crystal.

The most famous Elba tourmaline variety is represented by the "black cap" crystals (Fig. 1), which are characterized by a transparent prismatic sector (yellow-green, olive-green, colorless, or pink) with a sharp transition to black color at the analogous termination. However, in some pegmatitic veins the dark terminations of the tourmaline crystals are not black, but they are made up by multiple thin sectors of bluish, greenish, brownish or even purplish-to-reddish colors (Pezzotta, 2021 in press).

It is well known that tourmaline crystals are able to register the chemical-physical variations of the crystallizing environment during their growth (Hawthorne & Dirlam, 2011). Thus, the color anomalies at the analogous termination observed in tourmaline crystals from Elba likely reflect processes occurred in tourmaline-rich pegmatites during the latest stages of crystallization. The goal of this study is to describe such color anomalies and to propose a model for their genesis.

To achieve this goal, ten selected tourmaline samples from pegmatitic veins, located in the eastern border of the Monte Capanne monzogranite pluton, were analyzed using a multi-analytical approach, including electron microprobe (WDS mode) and Mössbauer spectroscopy. Compositional data were collected along a straight traverse parallel to the *c*-axis from the base to the termination of each crystal.

All studied samples show a (more or less) dark colored termination at the analogous pole, ranging from purple-red to brown, green, blue and black. Analytical results suggest that the color variation stems from uptake of increasing content of Mn and/or Fe (Fig. 2A).

The increase in Mn and Fe is quite significant in several samples (MnO > 5 wt% and FeO > 2 wt%) and determines the evolution from the initial elbaite/fluor-elbaite composition to celleriite, foitite or schorl at the crystal termination (Fig. 2B). The compositional anomalies observed at the analogous termination of Elba tourmalines suggest that chemical-physical variation occurred during the latest stages of crystallization.

Fig. 1 - Tourmaline crystals of elbaite-tsilaisite composition with a typical dark-colored termination at the analogous pole. Specimen 5 cm across, from Grotta d'Oggi (San Piero in Campo, Elba Island). (Private collection. Photo: A. Miglioli).

In the studied samples, the increase in Mn and Fe during the latest stages of crystals growth is consistent with the substitution of Li and Al at the *Y* site. However, this substitution can occur in different ways according to whether Mn and Fe totally or partially replace Li and Al (Fig. 2B).

In the crystals from Elba, a partial substitution occurred at *Y*, according to the simplified mechanism $(1.5Li^{+} + 0.5Al^{3+}) \leftrightarrow 2(Mn^{2+},Fe^{2+})$. As this substitution determines a total charge variation, it is balanced by the incorporation of cation vacancy (□) replacing Na at the *X* site:

$Na^{+} + (1.5Li + 0.5Al)^{\Sigma 3+} \leftrightarrow \square + 2(Mn,Fe)^{\Sigma 4+}$

It is interesting to point out that this partial substitution, in presence of an excess of Mn over Fe, led to the formation of celleriite at the termination of some crystals,

[1] Sapienza University of Rome, Piazzale Aldo Moro 5, 00185 Rome, Italy.
[2] Museo di Storia Naturale di Milano, Corso Venezia 55, 20121 Milano, Italia.

* Corresponding author: alessandra.altieri@uniroma1.it

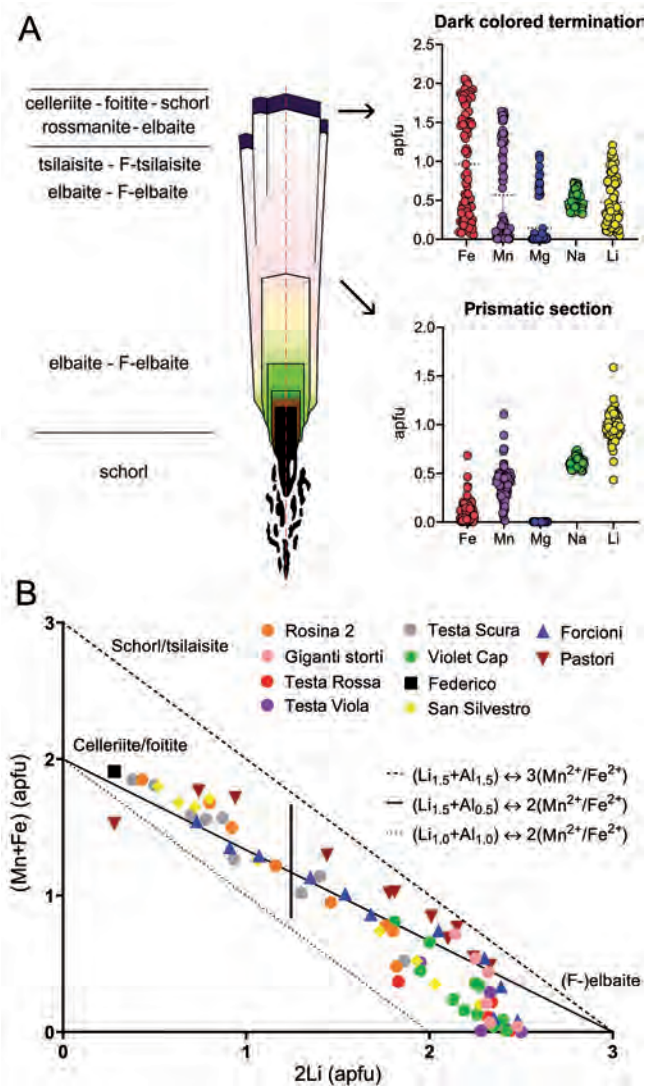

Fig. 2 - A) Compositional variations in typical tourmaline crystals from Elba pegmatites. The representative abundances of Li, Na, Mg, Mn, Fe (apfu) are reported for the prismatic sections and the dark colored terminations. Each point represents the result of a spot analysis. B) Plot of the content of 2Li vs (Mn + Fe) at the *Y* site for each analyzed zone of the tourmaline samples studied. The three lines (dashed, dotted and full) represent different degree of substitution. The bold vertical full line distinguishes the compositions occurring at the crystal dark terminations (left) from those occurring in the prismatic sectors (right).

representing the first world occurrence of this new tourmaline species approved in 2019 by IMA-CNMNC (Bosi *et al*., 2021 in press).

In the studied samples, an addition peculiar feature is the rhythmic behavior of Mn and Fe observed at the terminations, where Fe and Mn oscillatory pattern led to an alternation of either celleriite and rossmanite or celleriite and foitite (Fig. 3).

Further inspection to paragenetic relations in the cavities in which tourmaline samples were collected reveal abundant petalite, pollucite and lepidolite. The occurrence of such mineral phases provides evidence that the initial steps of crystal growth occurred in pegmatite portions characterized by an advanced degree of geochemical evolution. At this stage, the pegmatitic melt appears to be depleted in Mn and Fe, as such elements were stored in early crystallized minerals, such as biotite and spessartine. Therefore, tourmalines occurring in the cavities initially crystallized as elbaite/fluor-elbaite. However, a sharp increase in Mn and Fe must have occurred in the latest stages of crystallization. Actually, microstructural observations indicate that the latest growth sectors of tourmalines occur right after an event of pocket rupture. Here, we hypothesize that Mn and Fe entered the fluids due to the alteration of the early-crystallized minerals rich in these elements (such as biotite and spessartine) occurring in the pegmatitic rock surrounding the cavities. Consequently, the latest stage fluids enriched in Mn and Fe were responsible for tourmaline chemical evolution (or in some cases, crystallization re-start), which caused the observed color anomalies at the termination of the crystals.

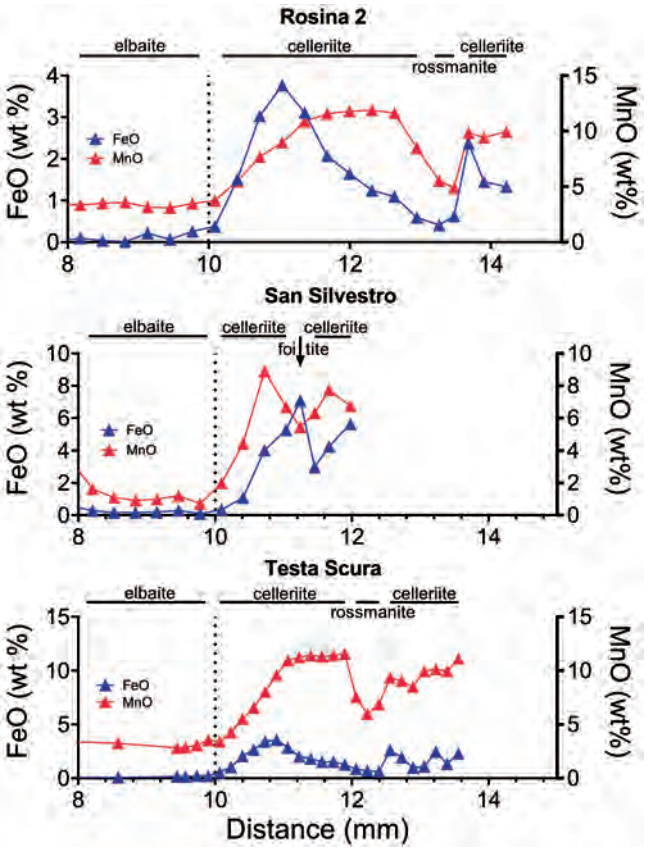

Fig. 3 - Variation in MnO and FeO (wt%) along a straight traverse parallel to the *c*-axis of three selected crystals, from the upper section to the dark termination. The dashed line marks the transition between the upper section and the dark colored termination of the crystals.

REFERENCES

Bosi F., Pezzotta F., Altieri A., Andreozzi G. B., Ballirano P., Tempesta G., Cempírek J., Škoda R., Filip J., Čopjacová R., Novák M., Kampf A. R., Scribner E. D., Groat L. A. & Evans R. J., 2021 in press – Celleriite, $\square(Mn^{2+}_2Al)Al_6(Si_6O_{18})(BO_3)_3(OH)_3(OH)$, a new mineral species of the tourmaline supergroup. *American Mineralogist*. <doi:10.2138/am-2021-7818>

Hawthorne F. C. & Dirlam D. M., 2011 – Tourmaline the indicator mineral: from atomic arrangement to Viking Navigation. *Elements*, 7: 307-312.

Pezzotta F., 2021 in press – Tourmalines from Elba Island (Tuscany, Italy): from discovery to present days. *The Mineralogical Record*.

Tetrahedral substitutions in tourmaline-supergroup minerals from the bond-topological and bond-valence perspective

Peter Bačík

The *T* site in tourmaline is tetrahedrally coordinated and TO_4 tetrahedra form the six-membered ring interconnected by the pairs of O^{2-} anions (Ertl *et al*., 2018). Each TO_4 tetrahedron shares O anions with the *T* (2×), *Y*, *Z* (2×) and *X* (2×) sites. It has the lowest bond-length distortion from all tourmaline cation sites resulting from its smaller size and higher rigidity than other polyhedra (Ertl *et al*., 2002).

The *T* site is dominantly occupied by Si^{4+}. Determination of possible substituents can be based on the bond valence calculation defining the "Goldilocks zone" of structural site. It is defined by the zone of structurally stable bond lengths with a minimal induced distortion (Bačík & Fridrichová, 2021). It is quite narrow for *T* site; it allows unlimited substitution of Be^{2+} for Si^{4+} and limited substitution of Al^{3+} and B^{3+}. The calculated Si–O distance of 1.624 Å and the empirical bond length of 1.619–1.621 Å (Bačík & Fridrichová, 2021 and references therein) are very similar to Be^{2+}–O 1.635 Å bond length calculated for ideal bond valence. Two other typical substituents for Si^{4+} – Al^{3+} and B^{3+} – have either longer (Al^{3+}–O 1.746 Å calculated bond length) or shorter bonds (B^{3+}–O 1.475 Å calculated, 1.482 Å empirical bond length) than Si^{4+}. Consequently, B^{3+} causes compression and Al^{3+} expansion of tetrahedra. Other possible substituting cations form very long bonds (Ti^{4+} 1.819 Å, Fe^{3+} 1.870 Å), therefore, their presence at *T* site may be significantly limited (Bačík & Fridrichová, 2021).

Substitution mechanisms for incorporation of trivalent and divalent cations at the tetrahedral sites require charge-balancing in two possible ways. The first tetrahedral substitution (TS1) of lower-charged *T* cation involves the exchange of higher-charged cation at the neighboring Y site, i.e. $^{T}Al(^{T}B) + {}^{Y}Al \rightarrow {}^{T}Si + {}^{Y}Mg$, and $^{T}Be + 2\,{}^{Y}Al \rightarrow {}^{T}Si + 2\,{}^{Y}Mg$. The second type of substitution (TS2) requires the exchange of higher-charged cation at the *X* site, i.e. $^{T}Al(^{T}B) + {}^{X}Ca \rightarrow {}^{T}Si + {}^{X}Na$, and $^{T}Be + {}^{X}Y \rightarrow {}^{T}Si + {}^{X}Na$. In reality, both mechanisms or their combination can be active, however, here, only ideal substitutions will be examined in terms of bond-valence and bond-length variations.

For these purposes, selected structural topological graphs were constructed. These involve tetrahedral ring, neighboring ZO_6 octahedra and either triplet of YO_6 octahedra for TS1 and *X* site for TS2. The bond valences were given considering distribution in the real structure. Therefore, the starting values for the dravite composition in the TO_4 tetrahedron were higher for non-bridging *T*–O6 and *T*–O7 bonds and lower for bridging *T*–O6 and *T*–O7 bonds.

The topological graphs for the TS1 showed that decrease in bond-valence in the Al^{3+}- and B^{3+}-bearing tetrahedron can be well compensated by an increase in bond valences at neighboring ring tetrahedra followed by increase in bond valence at *Y* site connected to involved tetrahedra. This can be satisfied by the $AlMg_{-1}$ substitution at the *Y* site. Consequently, the $(Al^{3+}, B^{3+})Si^{4+}_{-1}$ substitution influences bond valences in the half of tetrahedral ring. The decrease in bond valence at the *T* site may also interfere with the bond valences at *Z* site, but the excess of ca. 10 *vu* (valence units) can be distributed relatively evenly among *Z*–O bonds with up to 0.03 *vu* for each bond.

However, there is a difference between B^{3+} and Al^{3+}, if bond lengths calculated from bond valences are considered. Boron shrinks the TO_4 tetrahedron, aluminum expands it. Since the neighboring polyhedra are similarly compressed the for both substitutions, the B substitution causes significant contraction of the local structure and is limited by the ability of structure to accommodate it. Therefore, tetrahedral B is structurally limited to tourmaline composition with the most compressed structural arrangement, i.e., Al-enriched tourmalines. In contrast, tetrahedral Al is less restricted, because the expansion of the Al-bearing tetrahedron can be settled by the compression of the neighboring polyhedra.

The situation is more complicated for the $Be^{2+}Si^{4+}_{-1}$ substitution due to the large difference in charge. Consequently, this substitution requires exchange of either four-valent for divalent cation or two trivalent for two divalent cations at the *Y* site. The second option was studied as trivalent Al is far more common than tetravalent Ti, Sn or

Comenius University, Ilkovičova 6, Mlynská dolina, 842 15, Bratislava, Slovakia.
Earth Science Institute of the Slovak Academy of Sciences, Dúbravská cesta 9, P.O. BOX 106, 84005 Bratislava, Slovakia.
E.mail: peter.bacik@uniba.sk

any other cation in tourmaline. If the same mechanism of bond-valence distribution as in $(Al^{3+}, B^{3+})Si^{4+}_{-1}$ substitution is assumed, the disparity among bond valences will be very large, almost 1 *vu*. This would result in extreme bond-length distortion of the tetrahedron with the difference of ca. 0.4 Å between the longest and the shortest bond. However, if the change in bond valence is distributed to other tetrahedra around the ring, the difference between extreme bond valences is reduced to 0.7 *vu* and to 0.28 Å in bond lengths. Consequently, the second mechanism would result in less distorted and more stable structural arrangement.

Tetrahedral substitution 2 occurs in adachiite, which is the end member with (Si_5Al) *T*-site occupancy. The decrease in charge is balanced by the substitution of Ca^{2+} for Na^+ at the *X* site. In this case, however, the distribution of bond valences differs from TS1. The *X*–O4 and *X*–O5 bonds have significantly smaller bond valence, ca. 0.07-0.09 *vu* for Na^+ and 0.13-0.15 *vu* for Ca^{2+} based on the empirical bond lengths. Consequently, the variation in bond valence is more limited than for the *Y* site and it is necessary to include not only 3 (for B and Al) or 4-5 (Be) T-to-neighboring-site connections, but more. In TS2, the bond valences were altered in all around the whole ring. This mechanism allowed distribution of *X*–O bond valences increasing from 0.7 vu for $^{X}Na^+$ to 0.12-0.18 *vu* for Ca^{2+} substituted with Al^{3+} and B^{3+} and to 0.20-0.28 *vu* for Y^{3+} substituted with Be^{2+}.

The tetrahedral substitution of B^{3+} and Al^{3+} resulted in a slight change in bond valences below 0.2 *vu* in the bridging bonds of neighboring tetrahedra, variations in the other tetrahedra are even smaller. However, TS2 of Be^{2+} produces variations above 0.4 *vu*, which could cause significant distortion and destabilize the tetrahedral ring.

If the bond lengths are considered, Al^{3+} substitution causes an expansion of TO_4 tetrahedron up to 0.2 Å, which could be well relaxed by the contraction at the *X* site and slight distortion of *T*-ring. However, the compression of B^{3+}-bearing tetrahedron would not be so easily relaxed at the *X* site. More importantly, this mechanism could apply only in liddicoatitic tourmalines which have sufficiently compressed structure to handle this substitution. Interestingly, TS2 with $^{T}Be^{2+}$ would not produce significant bond-length variations, all are below 0.2 Å and majority below 0.1 Å.

The testing of this mechanisms on real samples (from the AMCSD database) is limited by their scarcity and in case of Be^{2+} by its usually low content in tourmalines usually up to few tens of ppm. However, these models can be used for prediction of bond lengths in TO^{4+} tetrahedron. The average T–O bond lengths in natural tourmalines with tetrahedral B and Al falls very well around the junction of Si_6 and (Si_5B) tourmaline if compared with ^{T}B. In comparison with ^{T}Al, the correlation is worse due to usually mutual ^{T}B and ^{T}Al substitution causing greater scattering of these samples.

Similarly, the substitution models show similar predictions for individual *T*–O bonds. The substitution of ^{T}B results in *T*–O4, *T*–O5 and *T*–O7 shortening in both substitution models and real samples. However, for T–O6 bond, the TS1 model predicts slight prolongation of the bond, the TS2 model suggests its significant shortening. Real samples are slightly increasing with low B content, with higher content, it stabilizes at ca. 1.605 Å. This indicates that TS1 is preferential substitution model for B incorporation in the natural samples.

In contrast, ^{T}Al substitution should produce prolongation of tetrahedral bonds. For bridging *T*–O4 and *T*–O5 bonds, TS1 predicts smaller, TS2 larger prolongation. For *T*–O7, both models predict the same prolongation and for *T*–O6 bonds, TS1 estimates larger and TS2 smaller prolongation. Tourmalines with high ^{T}Al content follow these trends, those with lower ^{T}Al proportion are more scattered due to simultaneous presence of ^{T}B. Interestingly, the *T*–O6 bond length in adachiite is approaching TS2 prediction, while all other samples follow the TS1 trend quite well.

In conclusion, tetrahedral substitution is allowed by either increase in charge in the octahedral sites or at the *X* site. Consequently, a significant substitution for Si^{4+} usually occurs in Al-rich tourmalines (B and Be) or produce the adachiite composition. The proposed bond-valence based models offered predictions of tetrahedral substitutions which are in good agreement with empirical data.

This research was funded by the projects APVV–18–0065 and VEGA-1/0137/20.

REFERENCES

Bačík P. & Fridrichová J., 2021 – Cation partitioning among crystallographic sites based on bond-length constraints in tourmaline-supergroup minerals. *American Mineralogist*, 106: 851-861.

Ertl A., Hughes J. M., Pertlik F., Foit F. F., Wright S. E., Brandstätter F. & Marler B., 2002 – Polyhedron distortions in tourmaline. *Canadian Mineralogist*, 40: 153-162.

Ertl A., Henry D. J. & Tillmanns E., 2018 – Tetrahedral substitutions in tourmaline: a review. *European Journal of Mineralogy*, 30: 465-470.

Creating a comprehensive, standardized dataset of tourmaline geochemical analyses integrating localities and petrogenesis

Marko Bermanec[1]*, Jason R. Williams[2], Robert M. Hazen[3], Shaunna M. Morrison[3]

The occurrence and distribution of tourmaline group minerals can provide insights into a wide range of environments on Earth. The combination of their physical and chemical resistance to geological and geochemical processes, as well as their ubiquitous occurrence under a wide range of pressure and temperature conditions, make tourmaline minerals important petrogenetic indicators of fluid and host rock compositions (Henry & Dutrow, 2018).

This project aims to create a comprehensive repository of geochemical, temporal, and spatial data of tourmaline mineral supergroup occurrences in order to advance data-driven discovery in mineralogy and petrology. Similar approaches have been taken to create a comprehensive database of garnet supergroup minerals (Chiama *et al*., 2020) and a similar approach is used here to generate a robust database of chemical and physical attributes of tourmaline supergroup minerals that are useful for characterizing a range of metamorphic, hydrothermal, igneous, and sedimentary environments. Gathering data from existing literature into a single open-access, machine-readable database will provide an outstanding platform for researchers to explore tourmaline spatial and temporal history as well as related geologic processes by means of statistical and machine learning techniques (Hazen *et al*., 2019).

Note that other work has mentioned existing compilations of tourmaline data, but to our knowledge those data have not yet been made available in an open access source.

The project intends to compile data from a variety of sources such as already existing databases (e.g. EarthChem, RRUFF and the Handbook of Mineralogy) as well as individual peer-reviewed publications.

A special emphasis is put on accumulation of "dark data" which is not present in existing geochemical databases or in supplementary data of peer-reviewed publications (Hazen, 2014; Wilkinson *et al*., 2016; Hazen *et al*., 2019). "Dark data" mostly appears in publications prior to 1990 which have been recorded in PDF files. It is difficult to extract these analytical data using an automated approach, thus making "dark data" time-consuming to compile in a database. However, these data are valuable and should not be neglected, especially when constructing a comprehensive database.

Fig. 1 - A map of countries that have schorl, elbaite or dravite occurrences reported in the Mindat database shaded in purple.

Formational environments are directly reflected in chemical compositions of tourmalines, which can be complemented with locality information, paragenetic modes, age, *P—T* conditions, and other geochemical data to form a platform for big data abductive discoveries in mineralogy and petrology. This would not be possible without the accumulation of deductive and inductive information in the form of traditional measurements, calculations, and observations (Hazen, 2014).

Each chemical element, isotope ratio, or other attribute represents a single column of the database while the rows represent individual tourmaline analyses and also marked with the "Project ID" representing the line number for easier identification of the total number of samples in the database.

[1] Faculty of Science, University of Zagreb, HR - 10000 Zagreb, Republic of Croatia.
[2] Southern Illinois University Carbondale, School of Earth Systems and Sustainability, Carbondale, IL 62901, USA.
[3] Earth and Planets Laboratory, Carnegie Institution for Science, Washington, DC 20015, USA.
E-mail: jasbfree@siu.edu
rhazen@carnegiescience.edu
smorrison@carnegiescience.edu

* Corresponding author: marko.bermanec@gmail.com

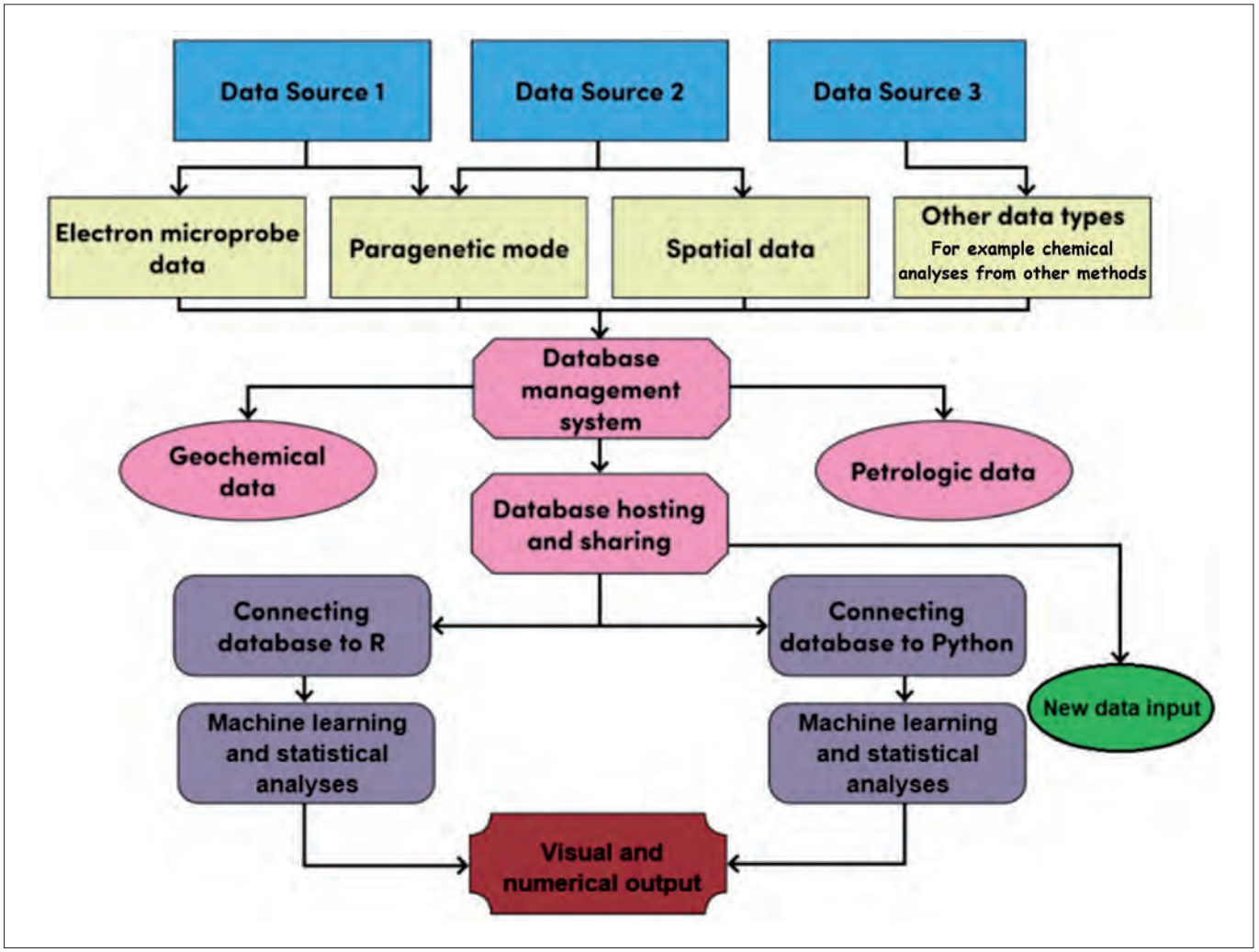

Fig. 2 - A visual representation of the intended database workflow and its features.

Apart from the geological data, a reference section is also added to the database to enable future researchers to easily access the original source. Data are recorded for the title, journal, authors, and year of publication of the source material.

Ultimately, our objective is for this open-access database to provide a compilation of extensive scientific data related to the occurrence and composition of tourmaline group minerals. Scientists will have the ability to contribute their data in the future to expand the database even further.

REFERENCES

Chiama K., Rutledge R., Gabor M., Lupini I., Hazen R. M., Zhang S. & Boujibar A., 2020 − Garnet: a comprehensive, standardized, geochemical database incorporating locations and paragenesis. *Geological Society of America, Abstracts with Programs*.

Hazen R. M., 2014 – Data-driven abductive discovery in mineralogy. *American Mineralogist,* 99 (11-12): 2165-2170. <doi: 10.2138/am-2014-4895>

Hazen R. M., Downs R. T., Eleish A., Fox P., Gagné O. C., Golden J. J., Grew E. S., Hummer D. R., Hystad G., Krivovichev S. V., Li C., Liu C., Ma X., Morrison S. M., Pan F., Pires A. J., Prabhu A., Ralph J., Runyon S. E. & Yhong H., 2019 – Data-driven discovery in mineralogy: Recent advances in data resources, analysis, and visualization. *Engineering*, 5: 397-405. <doi: 10.1016/j.eng.2019.03.006>

Henry D. J. & Dutrow B. L., 2018 − Tourmaline studies through time: contributions to scientific advancements. *Journal of Geosciences*, 63 (2): 77-98. <doi: 10.3190/jgeosci.255>

Wilkinson M. D., Dumontier M., Aalbersberg I. J., Appleton G., Axton, M., Baak, A., Blomberg N., Boiten J.-W., Bonino da Silva Santos L., Bourne P. E., Bouwman J., Brookes A. J., Clark T., Crosas M., Dillo I., Dumon O., Edmunds S., Evelo C. T., Finkers R., Gonzalez-Beltran A., Gray A. J.G., Groth P., Goble C., Grethe J. S., Heringa J., 't Hoen P. A. C., Hooft R., Kuhn T., Kok R., Kok J., Lusher S. J., Martone M. E., Mons A., Packer A. L., Persson B., Rocca-Serra P., Roos M., van Schaik R., Sansone S.A., Schultes E., Sengstag T., Slater T., Strawn G., Swertz M. A., Thompson M., van der Lei J., van Mulligen E., Velterop J., Waagmeester A., Wittenburg P., Wolstencroft K., Zhao J. & Mons B., 2016 – The FAIR Guiding Principles for scientific data management and stewardship. *Scientific Data*, 3: 160018. <doi: 10.1038/sdata.2016.18>

Pegmatite occurrences in Moslavačka gora, Northern Croatia

Vladimir Bermanec[1]*, Marko Bermanec[2], Snježana Mikulčić Pavlaković[3], Lyudmila Kuznetsova[4], Viktor Zagorsky†

The magmatic and metamorphic complex of Moslavačka gora lies between the rivers of Sava and Drava and is located around 50 km east from Zagreb. The orientation of Moslavačka gora today is NNW - SSE and it is in accordance with its genesis as an inselberg of the Sava zone between the Tisza and the Dacia Mega - Unit on the Northeast and the internal Dinarides on the Southwest (Schmid *et al.*, 2008).

The age of granitic intrusions of Moslavačka gora has been estimated (Palinkaš *et al.*, 2000). The muscovite dating from the Srednja Rijeka pegmatite gave a plateau age of 73.2±0.8 Ma using the Ar/Ar method. The intrusion of the granitic rock into an earlier metamorphic complex leads to partial melting and the formation of migmatites surrounding the intrusion body. These granitic rocks, migmatites and amphibolites show graduations from one rock type to another and are therefore regarded as a single petrological unit (Pamić, 1990). These rocks are sometimes covered by a weathering crust over 10 m (Balen, 1999). This alteration crust is also present and most evident in the kaolinization of the granitic rocks.

Pegmatitic veins scaling from 1 cm thickness to several decimeters are present in the granitic rocks of Moslavačka gora. These pegmatites are found in quarries at Vrtlinska, Pleterac, Garjevica and Srednja Rijeka. The contact between these pegmatitic veins and the host rock varies from very sharp to diffuse. Tourmaline samples from the Srednja Rijeka quarry have been studied.

Pegmatites found in the Srednja Rijeka quarry contain microcline, albite, quartz, muscovite, biotite and tourmaline. Some observed accessory minerals include andalusite, spessartine and dumortierite.

Tourmalines from Moslavačka gora have attracted a lot of attention and have already been analyzed by several authors (e.g. Balen & Broska, 2011). However, little attention has been given to the mineralogical characteristics of this mineral occurrence. Tourmaline occurs in single crystals as well as in aggregates. The latter often form thin crusts consisting of tiny needles up to 4 mm in length. Apart from these crusts they often form tourmaline nodules with quartz (Balen & Broska, 2011). The biggest tourmaline crystals are found in pegmatitic veins, where they form crystals up to 1 cm in diameter and several centimeters in length (Fig. 1). Such crystals from pegmatitic veins have also been studied.

All these described tourmalines are macroscopically black and not transparent. In thin sections, however, they show a significant zonation, probably due to different Fe^{2+}/Fe^{3+} ratios. Such zonations can be observed in sections perpendicular to the *c* axis and very often they show different shades of brown and green color (Fig. 2), but some crystals show blue zones as well.

[1] Faculty of Science, University of Zagreb, HR - 10000, Aleja Narodnih heroja 3, Sisak, Republic of Croatia.
[2] Faculty of Science, University of Zagreb, HR - 10000 Zagreb, Republic of Croatia.
E-mail: marko.bermanec@gmail.com
[3] Croatian Natural History Museum, Demetrova street 1, HR - 10000 Zagreb, Croatia.
E-mail: snjezana.mikulcic@hpm.hr
[4] Vinogradov Institute of Geochemistry, Siberian Division, Russian Academy of Sciences, Favorskogo street 1a, Irkutsk, 664033 Russia.
E-mail: lkuzn@igc.irk.ru

* Corresponding author: vberman@public.carnet.hr

Fig. 1 - A large sample of a pegmatitic vein with several large tourmaline crystals from Srednja Rijeka quarry.

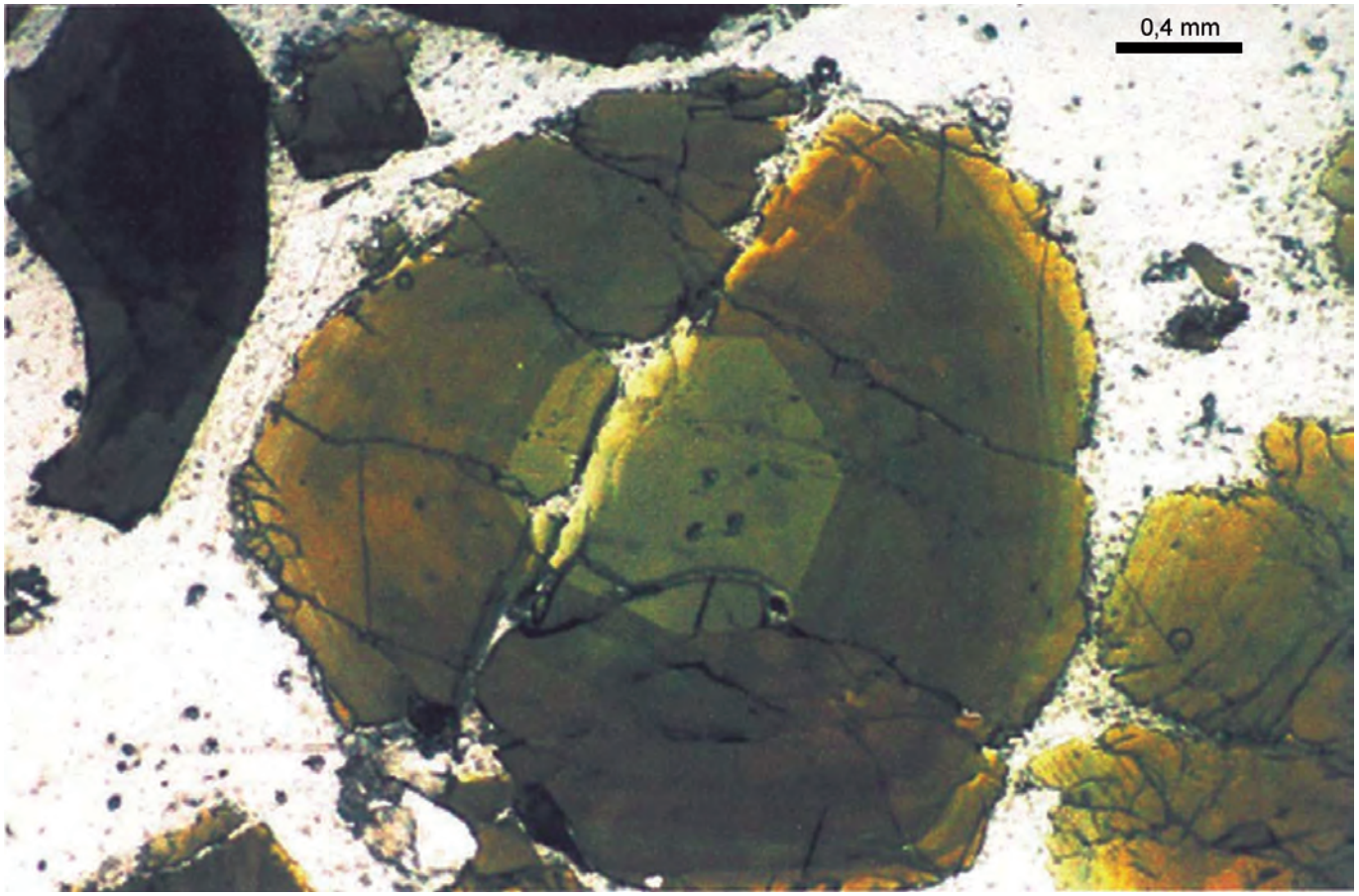

Fig. 2 - Zonation of the tourmaline from Srednja Rijeka in thin section perpendicular to the *c* axis.

Apart from the colour zonation, these tourmalines vary in chemical composition as well, most obviously in the Fe^{2+}/Fe^{3+} ratio. However, some chemical analyses of tourmaline samples from Srednja Rijeka gave strange results. When normalizing the crystallochemical formula to 31 anions, by using wet chemical analyses, these formulae showed excess Si and Al. Since no obvious inclusions have been detected in tourmaline thin sections, further structural analysis and refinements are suggested, as well as microprobe analyses of different tourmaline zones, which could be helpful for further interpretation of the formation conditions.

REFERENCES

Balen D., 1999 – Metamorfne reakcije u amfibolskim stijenama Moslavačke gore. *Dissertation, Faculty of Science, University of Zagreb*.

Balen D. & Broska I., 2011 − Tourmaline nodules: products of devolatilization within the final evolutionary stage of granitic melt?. *Geological Society*, London, Special Publications 350 (1): 53-68.

Palinkaš L., Balogh K., Strmić S., Pamić J. & Bermanec V., 2000 − Ar/Ar dating and fluid inclusion study of muscovite from the pegmatite of Srednja Rijeka, within granitoids of Moslavačka gora Mt., North Croatia. *Vijesti Hrvatskog Geološkog Društva*, 37 (3): 95-96.

Pamić J., 1990 – Alpinski granitoidi, migmatiti i metamorfiti Moslavačke gore i okolne podloge Panonskog bazena (Sjeverna Hrvatska, Jugoslavija). *Rad JAZU*, Zagreb, 10: 7-87.

Schmid S. M., Bernoulli D., Fügenschuh B., Matenco L., Schefer S., Schuster R., Tischler M. & Ustaszewski K., 2008 – The Alpine-Carpathian-Dinaridic orogenic system: correlation and evolution of tectonic units. *Swiss Journal of Geosciences*, 101: 139-183.

Anortho-schorl from Langesundsfjord (Norway)

Fernando Cámara[1]*, Ferdinando Bosi[2], Henrik Skogby[3], Ulf Hålenius[3], Beatrice Celata[2], Marco E. Ciriotti[4]

Some previous studies report of optically anomalous tourmaline with biaxial character, which is incompatible with its putative *R*3*m* symmetry. A crystal fragment of sample GEO-NRM19252409 (Swedish Museum of Natural History) coming from Langesundsfjord (Norway) showing zonation with biaxial optic behavior in the rims was studied by means of electron microprobe, single-crystal X-ray diffraction, Mössbauer, infrared and optical absorption spectroscopy and optical measurements. The latter were performed with a spindle stage in a Leitz Dialux microscope equipped with a CCD camera using Excelibr spreadsheet (Steven & Gunter, 2018), using a 30 μm thin section of the crystal cut perpendicular to *c* axis. Conoscopic image showed a biaxial interference figure, with negative optic sign. Measure $2V_x$ was 15.6° (white light). The biaxial character of the sample is not due to internal stress since it cannot be removed by heating and cooling. Orientation of the optical indicatrix was obtained using the same crystal mounting at a Rigaku XtaLAB Synergy-S diffractometer (Mo*K*α) and showed *c*^*X* = 2°, *b*^*Z* = 164.3° and *a*^*Z* = 75.8°. Complete data collection was obtained on a full sphere up to 0.50 Å. Diffraction data were refined with a standard *R*3*m* space group model [*a* 16.0013(2) Å, *c* 7.2263(1) Å] and with a non-conventional triclinic *R*1 space group model from Hughes *et al*. (2011), keeping the same hexagonal triple cell for comparison purposes but with unconstrained unit-cell parameters: *a* 16.0093(5) Å, *b* 16.0042(5) Å, *c* 7.2328(2) Å, α 90.008(3)°, β 89.856(3)°, γ 119.90(9)°. Trigonal R_{int} = 6.6%, R_{all} = 1.75% (3136 unique reflections) vs. triclinic R_{int} = 4.1%, R_{all} = 2.53% (17342 unique reflections). In both structure models, protons bonded to O3 sites were located and their coordinates refined. No proton was observed close to O1, in agreement with chemistry. Crystal-chemical analysis resulted in the chemical formula $(Na_{0.98}K_{0.01}\square_{0.01})_{\Sigma1.00}{}^{Y}(Fe^{2+}{}_{1.73}Mg_{0.12}Al_{0.90}Ti_{0.21}Mn_{0.02}V_{0.0}{}_{1}Zn_{0.01})_{\Sigma3.00}{}^{Z}(Al_{4.88}Fe^{3+}{}_{0.30}Fe^{2+}{}_{0.19}Mg_{0.63})_{\Sigma6.00}(Si_6O_{18})(BO_3)(OH)_3[(OH)_{0.29}F_{0.22}O_{0.49}]_{\Sigma1.00}$, which agrees well in terms of calculated site scattering (*X* 10.9 epfu, *Y* 63.7 epfu, *Z* 83.7 epfu) and refined site scattering (*X* 11.4 epfu, *Y* 63.4 epfu, *Z* 83.6 epfu). The ordering of about 0.19 apfu of Fe^{2+} at the *Z* sites comes from the structure refinement of the *R*1 model that showed that one out of 6 independent *Z* sites (*Zd* site) shows higher refined site scattering (15.5 eps vs. mean 13.3 eps for the other 5 sites) as well as larger mean bond length (1.968 Å vs. 1.925, s.d. 0.006, Å for the other 5 sites) and larger octahedral angle variance (53° vs. 42°, s.d. 3). All these features support the local ordering of Fe^{2+} at the *Zd* site.

A less pronounced ordering of Al is also observed at the *Yc* site (lower refined scattering and smaller mean bond length than the other two *Y* sites), which shares one edge

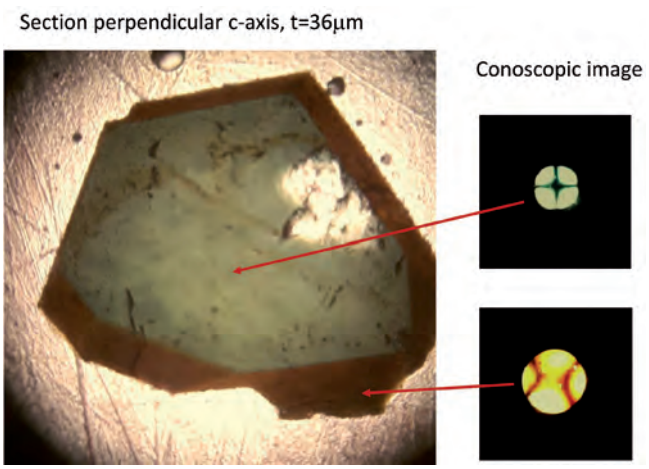

Fig. 1 - The studied sample showing the zonation and the location of the studied crystal fragment as well as the correspondent conoscopic images.

[1] University of Milan, Via Mangiagalli 34, 20133 Milano, Italia.
[2] Sapienza University of Rome, Piazzale Aldo Moro 5, I-00185 Roma, Italia.
E-mail: ferdinando.bosi@uniroma1.it, beatrice.celata@uniroma1.it
[3] Department of Geosciences, Swedish Museum of Natural History, Box 50 007, SE-104 05 Stockholm, Svezia.
E-mail: henrik.skogby@nrm.se, ulf.halenius@nrm.se
[4] Associazione Micromineralogica Italiana, Via San Pietro 55, I-10073 Devesi-Cirié, Torino, Italia.
E-mail: marco.ciriotti45@gmail.com

* Corresponding author: fernando.camara@unimi.it

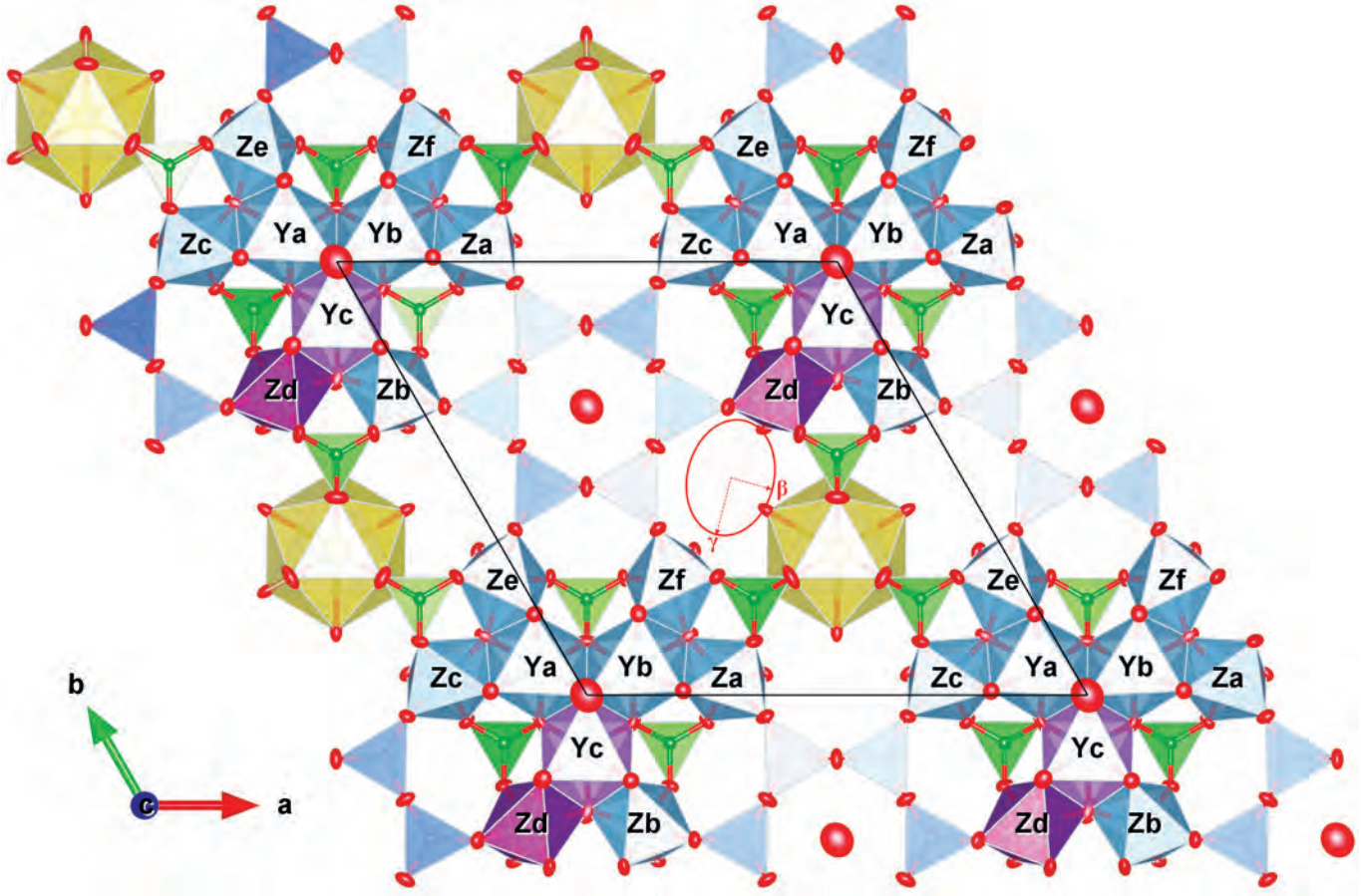

Fig. 2 - The [001] projection of the *R*1 structure model sowing the location of *Y*c and *Z*d sites (b). The direction of experimentally determined γ (and β) directions is reported as the approximate acute bisectrix section of the optical indicatrix (in red).

with the *Zd* site. Optical absorption spectra also show evidence of Fe^{2+} at the *Z* sites. Interestingly, the elongation of the *Zd*-octahedron is along a direction which forms an angle of ca. 73° with *a* unit-cell parameter and is coincident with the direction for γ-refraction index. All these evidences support the triclinic character of the tourmaline structure from Langesundsfjord, and put on evidence that even in the presence of excellent statistical residual factors from excellent X-ray diffraction data, the lowering of symmetry due to cation ordering may have been overseen in many other tourmaline samples in absence of an opportune check of the optical behavior.

Although the symmetry of the present sample is not trigonal, the basic structure type of tourmaline is retained. Thus, it can be classified as the triclinic dimorph of schorl.

REFERENCES

Hughes J. M., Rakovan J., Ertl A., Rossman G. R., Baksheev I. & Bernhardt H.-J., 2011 − Dissymmetrization in tourmaline: the atomic arrangement of sectorally zoned triclinic Ni-bearing dravite. *Canadian Mineralogist*, 49 (1): 29-40. <doi: 10.3749/canmin.49.1.29>

Steven C. J. & Gunter M. E., 2018 − EXCELIBR: An Excel spreadsheet for solving the optical orientation of uniaxial and biaxial crystals. *The Microscope*, 65 (4): 147-152.

Tourmaline breakdown: preliminary results from experimental studies

Beatrice Celata[1]*, Paolo Ballirano[1], Ferdinando Bosi[1], Vincenzo Stagno[1], Henrik Skogby[2], Giovanni B. Andreozzi[1]

Subducting oceanic crust and sediments experience a continuous dehydration process, which involves hydrous minerals such as clays and borosilicates. Once the breakdown conditions of borosilicates are reached, B-rich aqueous fluids are then released in the subducting system leading to B-metasomatism of the hosting and neighboring rocks, which may play a key role on the overall system rheology (Ota *et al*., 2008). Some of the released B can still be stored in deeply subducted sediments through mineral phases which are stable at higher pressure and temperature conditions (e.g. phengite), until further breakdown would make their structure collapse and lead again to dehydration and boron leaking. Mapping out every step of this breakdown sequence would help to trace the water and boron path deep down the Earth.

In this study, tourmaline high temperature (HT) and high temperature-high pressure (HT-HP) breakdown conditions and mechanisms were investigated.

In-situ HT behavior of a Fe-rich fluor-elbaite from Minas Gerais (Brazil) and a Mn-bearing elbaite from Anjanabonoina (Madagascar), both crystal-chemically fully characterized (Bosi *et al*., 2019, 2021, respectively), was investigated at room pressure through X-Rays Powder Diffraction (XRPD). Temperature was progressively raised at fixed T steps, monitoring the occurrence of the first peaks of any newly formed phases (Fig. 1). For Fe-rich fluor-elbaite and Mn-bearing elbaite the breakdown temperature was thus constrained at 803 and 825 °C, respectively.

[1] Department of Earth Science, Sapienza University of Rome, Piazzale Aldo Moro 5, I-00185 Rome, Italy.
E-mail: paolo.ballirano@uniroma1.it
ferdinando.bosi@uniroma1.it
vincenzo.stagno@uniroma1.it
gianni.andreozzi@uniroma1.it
[2] Department of Geosciences, Swedish Museum of Natural History, SE-10405 Stockholm, Sweden.
E-mail: henrik.skogby@nrm.se

* Corresponding author: beatrice.celata@uniroma1.it

In both cases the structural breakdown was preceded by a thermally-induced oxidation process (of Fe^{2+} to Fe^{3+} and of Mn^{2+} to Mn^{3+}, respectively) starting at ~ 500 °C, which was counterbalanced by H^+ loss (namely deprotonation). In addition, between the octahedrally-coordinated *Y* and *Z* sites a partial intra-crystalline cation exchange (Fe-Al and possibly Li-Al for the two samples, respectively) was observed. The breakdown products were then collected and analyzed *ex-situ* with XRPD for phases identification, and they resulted to be mostly represented by a B-bearing mullite (approximately 75% of the total) for both tourmaline samples.

Further HT-HP experiments were carried out on a schorl from the Seagull batholith (Yukon Territory, Canada), previously crystal-chemically characterized (Andreozzi *et al*., 2020), at various temperatures ranging from 500 to 950 °C and constant pressure of 3.5 GPa applied through a Walker-type multi anvil press. Experimental products were characterized *ex-situ* through a multi-analytical approach: textural aspects were investigated through Scanning Electron Microscope (SEM), the chemical composition was obtained through Electron Micro-Probe (EMP), and Fe oxidation state (in the assemblage

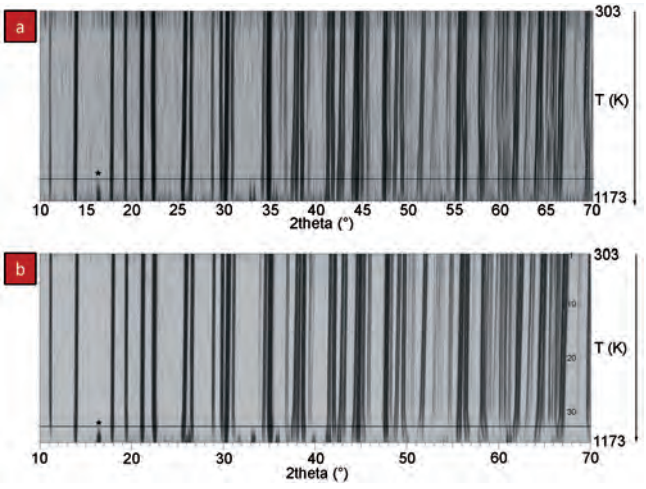

Fig. 1 - Pseudo-Guinier plot of XRPD data of Fe-rich fluor-elbaite a) and Mn-bearing elbaite b). The horizontal lines at 1076 and 1098 K (803 and 825 °C), respectively, represent the first occurrence of the B-mullite peaks, the most intense of which is marked by the "*" symbol.

tourmaline + its breakdown products) was constrained through Mössbauer spectroscopy. Integrating the obtained results, the breakdown temperature of the Canadian schorl at 3.5 GPa was constrained at approximately 700 °C. Breakdown products were mostly represented by garnet (Fig. 2 and Tab. 1), with minor Al-bearing phases still under study. Further arguments on the schorl HT-HP breakdown mechanism, possibly preceded by the oxidation process from Fe^{2+} to Fe^{3+} counterbalanced by the H^{+} loss already observed at HT, are still in the making.

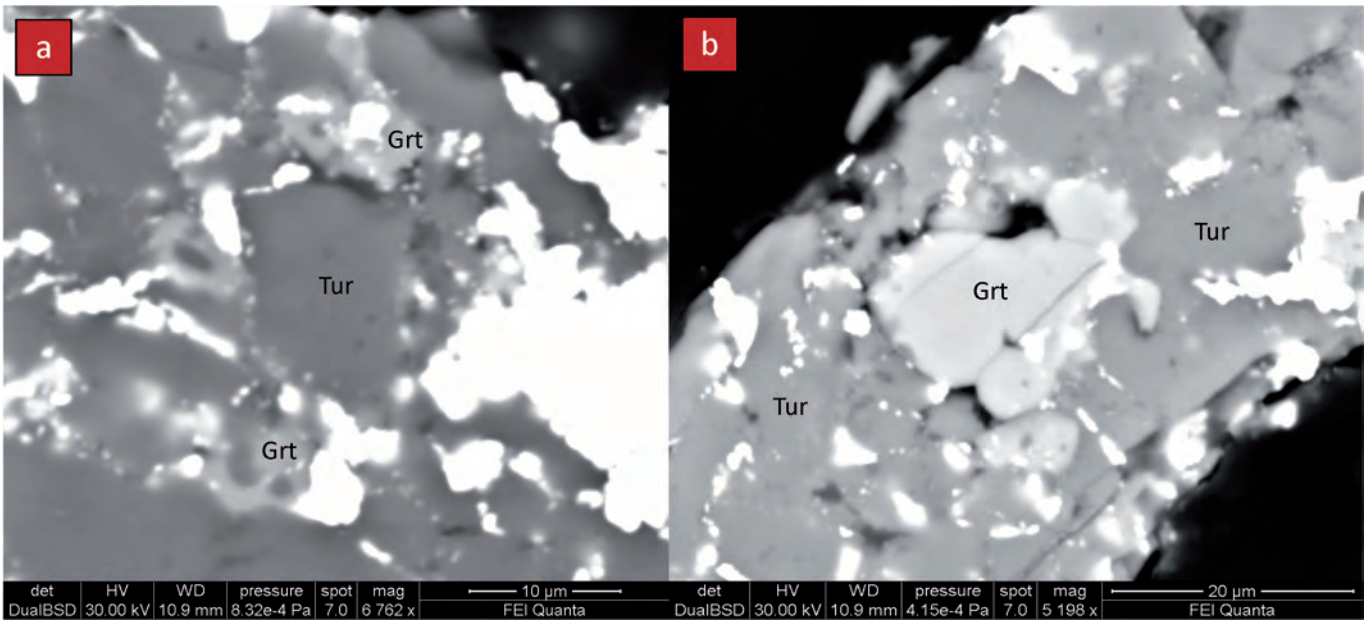

Fig. 2 - SEM image of experimental tourmaline-garnet assemblages at 3.5 GPa and temperatures of a) 700 °C, b) 750 °C.

Table 1 - EMP data collected on experimental tourmaline-garnet assemblage at 3.5 GPa and 700 °C.

Phase	SiO_2	TiO_2	Al_2O_3	FeO	MgO	CaO	Na_2O	K_2O	F	Tot
Tur	34.44	0.43	31.16	17.50	0.42	0.05	2.58	0.02	0.98	87.58
Grt	36.06	0.14	21.10	39.44	0.15	0.57	0.11	0.00	0.43	98.01

REFERENCES

Andreozzi G. B., Bosi F., Celata B., Capizzi L. S., Stagno V. & Beckett-Brown C. E., 2020 – Crystal-chemical behavior of Fe^{2+} in tourmaline dictated by structural stability: insights from a schorl with formula $Na^{Y}(Fe^{2+}{}_2Al)^{Z}(Al_5Fe^{2+})(Si_6O_{18})(BO_3)_3(OH)_3(OH,F)$ from Seagull batholith (Yukon Territory, Canada). *Physics and Chemistry of Minerals*, 47: 25.

Bosi F., Skogby H. & Hålenius U., 2019 − Thermally induced cation redistribution in fluor-elbaite and Fe-bearing tourmalines. *Physics and Chemistry of Minerals*, 46: 371-383.

Bosi F., Celata B., Skogby H., Hålenius U., Tempesta G., Ciriotti M. E., Bittarello E. & Marengo A., 2021 − Mn-bearing purplish-red tourmaline from the Anjanabonoina pegmatite, Madagascar. *Mineralogical Magazine*, 85: 242-253.

Ota T., Kobayashi K., Katsura T. & Nakamura E., 2008 − Tourmaline breakdown in a pelitic system: implications for boron cycling through subduction zones. *Contribution to Mineralogy and Petrology*, 155: 19-32.

Tourmaline in the elbaite-subtype pegmatites from the Czech Republic: towards the general evolution trends

Jan Cempírek*, Tomáš Flégr

Elbaite-subtype of rare-element group of granitic pegmatites defined by Novák & Povondra (1995) from the Moldanubian Zone of the Bohemian Massif represents mineralogically variable rock suite. Composition of elbaite-subtype pegmatites is characterized by relatively low and variable amounts of albite, low activity of P and F and high activity of B, and especially by the presence of tourmaline as the major carrier of Li, typically associated by (typically late-stage) borate minerals and B-bearing silicates (including e.g. hambergite, datolite, danburite, boromuscovite, tusionite, B-bearing polylithionite), scarcity of white mica (Ply>>Tri; Ms is absent or extremely rare), and high contents of Mn in garnet and columbite; the black tourmaline (dravite-schorl-elbaite) is characterized by strong enrichment in Mn (and in some cases F), low vacancy and dominant Na whereas composition of pink tourmaline in pockets ranges from elbaite to less common liddicoatite (Novák & Povondra, 1995).

Several recent detailed studies (e..g. Zahradníček, 2012; Flégr, 2016; Buřival & Novák, 2018; Novotný & Cempírek, 2021; Bosi *et al*., 2021 in press) on the most significant pegmatites (Řečice, Dolní Rožínka, Pikárec, Rudolfov, Ctidružice, Biskupice) significantly improved the amount of compositional and paragenetic information on the tourmaline which allows some general genetic interpretations of its evolution.

Tourmaline evolution typically starts with Mg-rich schorl pegmatite border zone (exceptionally Fe-dravite), followed by Al-rich schorl to Li-bearing schorl in the wall and intermediate zone; initial F contents are generally low (≤0.3 apfu). The graphic Tur + Qtz intergrowths that evolve to dark prismatic crystals in pockets typically occur at the transition between the coarse-grained intermediate zone and the albite zone (commonly with cleavelandite); they usually feature various degree of Mn-enrichment represented by Li,Mn-rich schorl (Řečice, Dolní Rožínka) or tsilaisite-celleriite-princivalleite (Pikárec, Rudolfov) with relatively low Li and F contents. The dark prismatic crystals at the base of the pegmatite pocket are usually followed by a metasomatic pink prismatic Li,F-rich tourmaline (fluor-elbaite, elbaite) in pockets. The transition is usually abrupt or can be visible as diffuse zoning which usually represents a recrystallization zone.

Hydrothermal tourmaline assemblages are characterized by fibrous/acicular or long-prismatic crystal habitus, or intergrowths with quartz (elbaite, rarely darrellhenryite or fluor-liddicoatite); they can show very complex sector zoning (Ca,F-poor and Ca,F-rich zones) or homogeneous (Fe-enriched elbaite). B-rich fluids typically cause partial metasomatic replacement of earlier generations, resulting in quartz-tourmaline (fluor-elbaite to fluor-liddicoatite) aggregates along tourmaline grain boundaries in older units. Typical textures of metasomatic (hydrothermal) replacement, including recrystallization (compositional mixing) are shown on Figure 1.

Increase of Ca is typical for late stages of tourmaline formation (e. g. Řečice, Rudolfov, Dolní Rožínka), locally reaching composition of fluor-liddicoatite. Late hydrothermal tourmalines may also form in border pegmatite zones, xenoliths and on exocontacts – primary biotite is typically replaced by Al-deficient schorl-dravite or Fe^{3+},Ti-rich bosiite.

The evolution of the primary tourmaline can be characterized as fractionation from Mg-, Fe-, to Fe-Al- and Mn,Al-dominant compositions with low to moderate F and Li. It is followed by of Li,Al,F-rich tourmalines in pockets and hydrothermal (metasomatic) veinlets that may be widespread in all pegmatite zones. The elbaite-subtype pegmatites are characterized by very high B activity during most stages of their evolution, with high F+Li contents restricted to late magmatic (albite zone) and hydrothermal stages.

Department of Geological Sciences, Faculty of Science, Masaryk University, Kotlářská 2, 611 37 Brno, Czech Republic.

* Corresponding author: jan.cempirek@gmail.com

This work was supported by the research projects GAČR 19-05198S and MUNI/A/1594/2020.

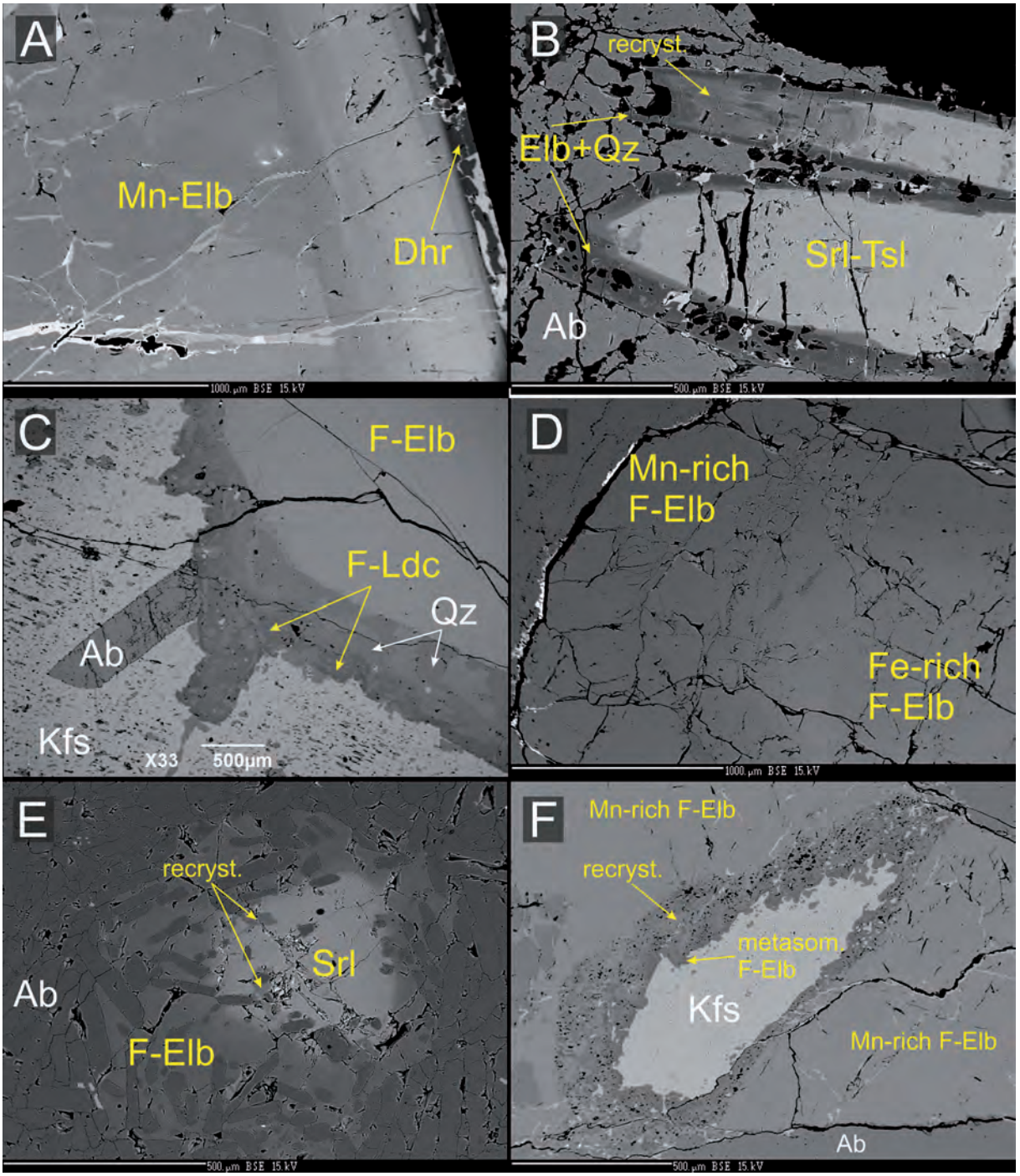

Fig. 1 - Metasomatic and recrystallization in tourmaline from Rudolfov (A,F), Biskupice (B), Řečice (C), and Ctidružice (D,E) pegmatites.

REFERENCES

Bosi F., Pezzotta F., Altieri A., Andreozzi G., Ballirano P., Tempesta G., Cempírek J., Škoda R., Filip J., Čopjaková R., Novák M., Kampf A., Scribner E., Groat L. A. & Evans R. J., 2021 in press − Celleriite, $\square(Mn^{2+}{}_2Al)Al_6(Si_6O_{18})(BO_3)_3(OH)_3(OH)$ a new mineral species of the tourmaline supergroup. *American Mineralogist*. <doi:10.2138/am-2021-7818>

Buřival Z. & Novák M., 2018 − Secondary blue tourmaline after garnet from elbaite-subtype pegmatites. *Journal of Geosciences*, 63: 111-122.

Flégr T., 2016 − Compositional evolution of tourmaline from elbaite-subtype pegmatite Řečice. *MSc thesis, Faculty of Science, Masaryk University*, Brno.

Novák M. & Povondra P., 1995 − Elbaite pegmatites in the Moldanubicum: a new subtype of the rare-element class. *Mineralogy and Petrology*, 55: 159-176.

Novotný F. & Cempírek J., 2021− Mineralogy of the elbaite-subtype pegmatite from Dolní Rožínka. *Acta Musei Moraviae, Scientiae geologicae*, 106: 3-33.

Zahradníček L., 2012 − Vývoj textur a chemického složení zonálních turmalínů z elbaitového pegmatitu v Pikárci u Křižanova. *MSc thesis, Faculty of Science, Masaryk University*, Brno.

Calculation of the pyroelectric coefficient of tourmalines from single crystal X-ray data

Irina Chernyshova[1]*, Oleg Vereshchagin[1], Olga Frank-Kamenetskaya[1], Olga Malyshkina[2]

Tourmalines with general crystal-chemical formulae $^{[9]}X\,^{[6]}Y_3\,^{[6]}Z_6\,(^{[4]}TO_4)_6\,(^{[3]}BO_3)_3V_3W$ (Henry *et al.*, 2011) belong to polar symmetry class with a singular polar axis (space group *R*3*m*). It is worth to note, that pyroelectric effect (γ) was firstly discovered in tourmaline. Stability in a wide range of temperatures and pressures makes tourmaline a promising material with pyroelectric and piezoelectric properties (Chernyshova *et al*., 2021 in press).

The emergence of a polarized state in linear pyroelectrics occurs due to the sharing of electrons of neighboring atoms, i.e. due to short-range forces, which are large only at distances of the order of interatomic ones (Kittel, 2004). The action of directed short-range forces leads to a rigid fixation of dipole moments in the entire region of existence of a solid state. In this case, external electric fields are unable to reorient the spontaneous polarization.

According to previous studies performed by various experimental methods, the pyroelectric coefficient of tourmalines varies widely: from 1 to 20 $\mu Cm^{-2}K^{-1}$ at room temperature (Chernyshova *et al*., 2021 in press). Revealing the relationships between the chemical composition, crystal structure and pyroelectric properties of tourmaline will allow deeper penetration into the structural nature of its unique properties and carry out crystal-chemical design of new nature-like materials with improved properties.

Zhou *et al.* (2018) made meaningful steps in this direction, proposing a γ - calculation method, based on structural analysis data at different temperatures. Intrinsic electric dipole moment (*P*) is calculated using atoms coordinates and chemical composition of tourmaline. Pyroelectric effect is calculated as the difference between *P* in a temperature range. Based on the Rietveld refinement Zhou *et al*. (2018) calculated pyroelectric effect of Mg-tourmaline and concluded, that the deformations of $[TO_4]$ – and $[BO_3]$ – polyhedra along *c*-axis are the main contributors in γ values.

This result raises many questions. First of all, Rietveld refinement results are not precise enough for such a calculation in general and especially in this particular case, which is clear from irregular changes of average bond lengths in $[XO_9]$ –, $[YO_6]$ –, $[ZO_6]$ – and $[TO_4]$ – polyhedra (Fig. 1). Furthermore, $[TO_4]$ – and $[BO_3]$ – polyhedra are most stable and invariant regarding their chemical composition in tourmaline structure. Whereas ionic substitutions and cations disordering occur in $[XO_9]$ –, $[YO_6]$ –, and $[ZO_6]$ – polyhedra. Therefore, deformation of $[XO_9]$ –, $[YO_6]$ – and $[ZO_6]$ – polyhedra should be main factors affecting pyroelectric properties.

Correlations between the chemical composition of octahedral sites (primarily the oxidation state of cations) and the pyroelectric coefficient confirm last assumption (Chernyshova *et al*., 2021 in press). Finally, the γ values obtained by Zhou *et al*. (2018) strongly increase with temperature from 5 $\mu Cm^{-2}K^{-1}$ (25 °C) to 35 $\mu Cm^{-2}K^{-1}$ (300 °C) and greatly exceed all known γ for tourmalines.

In course of current work, we have used method proposed Zhou *et al*. (2018) for tourmaline with known γ value in order to evaluate its applicability. To solve this goal, we chose synthetic Ni-tourmaline (Lebedev *et al.*, 1988; Vereshchagin *et al.*, 2015) of simple chemical composition (No 1, Table 1). Single-crystal X-ray diffraction was collected by means of diffractometer Agilent Technologies (Oxford Diffraction) «Supernova»: MoKα (λ= 0.71073) in a temperature range -170 – +75 °C and refined by SHELX (Sheldrick, 2015). Besides that, single crystal X-ray data for Fe and Mg-bearing tourmalines in temperature range 20 – 850 °C (No 2-4, Table 1) were used for comparison.

According to the refinement results of Ni-tourmaline, average bond lengths of its polyhedra increase regularly in temperature range -170 – +75 °C: $X > Z >> Y > T$ (Fig. 1). The refinement results of Fe- and Mg-tourmalines crystal structure (No 2-4, Table 1) showed, that significant changes in bond lengths occur in the range of 400 – 800 °C (Fig. 1). These changes are associated with disordering of cations over *Y*- and *Z*-sites (Menken, 2014). Since no changes higher than determination error occur up to 400 °C, it is impossible to use these data to calculate γ.

[1] Institute of Earth Sciences, St Petersburg State University, Universitetskaya nab. 7/9, 199034 St Petersburg, Russia.
E-mail: o.vereshchagin@spbu.ru
ofrank-kam@mail.ru
[2] Tver State University, Zhelyabova st. 33, 170100 Tver, Russia.
E-mail: olga.malyshkina@mail.ru

* Corresponding author i.a.chernyshova@yandex.ru

Table 1 - Characterization of chemical composition and X-ray experiment of studied tourmalines.

No	$X_{0\text{-}1}\,Y_3Z_6$	T, °C	R_1, I > 2σ(I)	References
1	$Na_{1.00}(Ni_{1.80}Al_{1.20})\,(Al_{4.86}Ni_{1.14})$	-170–75	0.02-0.02	Our data
2	$(Na_{0.66}Ca_{0.18}\square_{0.16})\,(Mg_{2.46}Al_{0.54}Fe^{2+}_{0.01}Ti_{0.01})\,(Al_{5.64}Mg_{0.36})$	20–800	0.01-0.02	
3	$(Na_{0.76}Ca_{0.05}K_{0.01}\square_{0.18})\times$ $(Fe^{2+}_{1.71}Al_{0.62}Mg_{0.19}Ti_{0.12}Mn_{0.10}Fe^{3+}_{0.09}Li_{0.07}Zn_{0.01})\,(Al_{5.76}Mg_{0.24})$	20–850	0.01-0.01	Menken, 2012
4	$(Na_{0.84}Ca_{0.06}K_{0.01}\square_{0.09})\,(Fe^{3+}_{2.62}Al_{0.26}Mg_{0.04}Ti^{4+}_{0.07}Mn^{2+}_{0.02})\,Al_6$		0.03-0.04	
5	$(Na_{0.73}Ca_{0.16}K_{0.01}\square_{0.10})\,(Mg_{2.22}Al_{0.51}Fe^{3+}_{0.30}Fe^{2+}_{0.10}Ti_{0.05})\,Al_6$	25–300	-	Zhou *et al.*, 2018

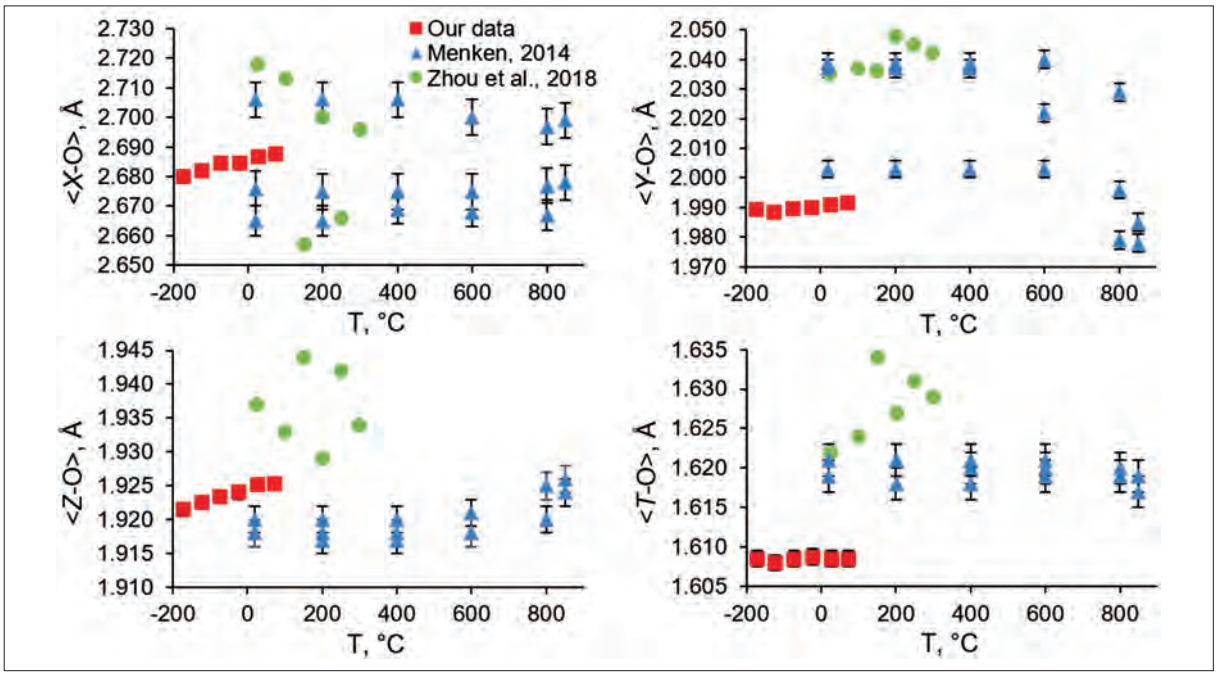

Fig. 1 - Average bond lengths of *X* (a), *Y* (b), *Z* (c) and *T* (d) polyhedra *vs.* temperature.

The results of calculating the γ values of synthetic Ni-tourmaline showed that γ is 2.4 $\mu Cm^{-2}K^{-1}$ in the temperature range -170 – -20 °C, which is consistent with the γ value of this tourmaline obtained by the dynamic method (2.7 $\mu Cm^{-2}K^{-1}$, Chernyshova *et al.*, 2021 in press). The γ value sharply increases to 35 $\mu Cm^{-2}K^{-1}$ upon passing through 0 °C in the range -30 – ±20 °C and is 3.7 $\mu Cm^{-2}K^{-1}$ in temperature range 30 – 75 °C. This pattern requires additional explanation.

The work was carried out using the analytical capabilities of Resource Centre for X-ray Diffraction Studies in St. Petersburg State University. This work was supported by grant of the President of the Russian Federation MK-1832.2021.1.5.

REFERENCES

Chernyshova I. A., Vereshchagin O. S., Malyshkina O. V., Goncharov A. G. & Frank-Kamenetskaya O. V., 2021 in press – The influence of chemical composition and cation oxidation state on pyroelectric properties of tourmalines. *Java Simple Serial Connector*.

Henry D. J., Novák M., Hawthorne F. C., Ertl A., Dutrow B. L., Uher P. & Pezzotta F., 2011 – Nomenclature of the tourmaline-supergroup minerals. *American Mineralogist*, 96 (5-6): 895-913. <doi:10.2138/am.2011.3636>

Kittel C., 2004 – Introduction to solid state Physics. *Wiley*, New York.

Lebedev A. S., Kargalcev S. V. & Pavlychenko V., 1988 – Synthesis and properties of tourmaline series Al-Mg-(Na) and Al-Fe-(Na). In: Proceedings of Genetic and Experimental Mineralogy: Growth and Properties of Crystals. *Nauka*, Novosibirsk, Russia: 58-75. (In Russian).

Menken J. S., 2014 – Effect of thermal treatment on the cation exchange and disordering in tourmaline. *Graduate College Dissertations and Theses*. Paper 254.

Sheldrick G. M., 2015 – Crystal structure refinement with SHELXL. *Acta Crystallographica,* C71: 3-8. <doi: 10.1107/S2053229614024218>

Vereshchagin O. S., Frank-Kamenetskaya O. V. & Rozhdestvenskaya I. V., 2015 – Crystal structure and stability of Ni-rich synthetic tourmaline. Distribution of divalent transition-metal cations over octahedral positions. *Mineralogical Magazine*, 79 (4): 997-1006. <doi:10.1180/minmag.2015.079.4.09>

Zhou G., Liu H., Chen K., Gai X., Zhao C., Liao L., Shen K., Fan Z. & Shan Y., 2018 – The origin of pyroelectricity in tourmaline at varying temperature. *Journal of Alloys and Compounds*, 744: 328-336. <doi:10.1016/j.jallcom.2018.02.064>

Insights into the magmatic-hydrothermal evolution at the Panasqueira W-Cu-Sn deposit, Portugal from chemical and B-isotopic studies of tourmaline and white mica: a review

Marta S. Codeço

Tourmaline and white mica are common gangue minerals in hydrothermal ore deposits. These minerals are the most abundant alteration phases throughout the Panasqueira W-Sn-Cu deposit and, therefore, the prime indicators for the composition and source of the mineralizing fluids. The deposit consists of sub-horizontal ore-bearing quartz veins hosted by metasedimentary rocks above a late-Variscan granite and its greisen cupola (e.g., Kelly & Rye, 1979).

This contribution summarizes the results of three studies that combine in-situ analyses of major elements by EPMA, trace elements by laser ablation ICP-MS, and boron isotopes by SIMS in tourmaline and white mica at the Panasqueira deposit (Codeço *et al*., 2017, 2019, 2021). The SIMS results were also used to test the application of B-isotope exchange between muscovite and tourmaline as a geothermometer (Codeço *et al*., 2019). In addition, the bulk chemical changes caused by the hydrothermal alteration are addressed, based on analyses of altered and unaltered host rocks, granite, and greisen from drill core samples presented by Codeço *et al*. (2021).

Whole-rock data from altered host rocks show enrichments in W, Sn, Cu, Zn, As, F, Li, Rb, and Cs relative to the unaltered metasediments. Most of these elements are also enriched in the greisen relative to the unaltered granite. The observed variations in whole-rock composition with distance to ore veins reflect the alteration intensity and different modal abundances of tourmaline and mica (Codeço *et al*., 2021).

Tourmaline has intermediate schorl-dravite compositions and is chemically zoned, with increases in Fe/Mg and F from core to rim, while Ca and Al contents decrease (Codeço *et al*., 2017). White mica comprises muscovite, phengite, and celadonite components and has systematic variations in Fe/Mg according to the setting within the deposit (greisen, vein selvage, alteration zone, late mineralized fault), indicating an evolution with time (Codeço *et al*., 2019). In contrast, tourmaline compositions are similar throughout the deposit (but greisen is tourmaline-free). This is ascribed to a stronger dependence of tourmaline on host-rock compositions, while white mica is the better recorder of the changing fluid composition (Codeço *et al*., 2021). The in-situ trace-element data show that Rb, Cs, Ba, Li, Nb, Ta, W, and Sn are preferentially partitioned into white mica over tourmaline while Zn, V, and Sr show the opposite trend (Fig. 1) (Codeço *et al*., 2021).

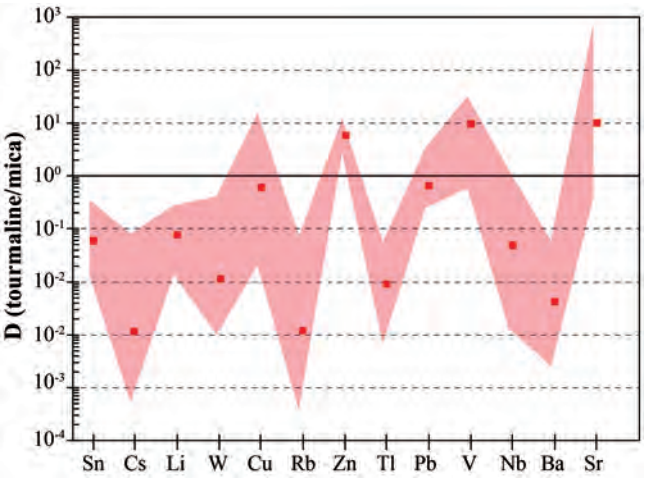

Fig.1 - Trace-element partitioning between tourmaline and white mica expressed as apparent D values. The squares show the median values for each element, and the shadowed field corresponds to the full range of values. Adapted from Codeço *et al*. (2021).

The B-isotope composition ($\delta^{11}B$) of coexisting tourmaline and white mica pairs are shown in Figure 2, along with the derived isotope exchange temperatures. Boron isotopic compositions of tourmaline in direct contact with mica have median values of -9‰ (Fig. 2). There is no isotopic zoning but a slight variation with distance from the ore veins. White mica has a more variable composition. The median $\delta^{11}B$ values of mica from greisen and vein selvages overlap (-17 to -18‰), whereas late-stage muscovite has lower values (down to -23‰). The B-isotope

GFZ German Research Centre for Geosciences, Telegrafenberg, 14473 Potsdam, Germany.
Institute of Earth and Environmental Science, University of Potsdam, 14476 Potsdam, Germany.
E.mail: marta.codeco@gfz-potsdam.de

composition of tourmaline-mica pairs from vein selvages provides an estimate for the temperature of vein formation (450 ±50°C). The temperature estimate for a late-mineralized fault zone is about 260°C (Fig. 2). The higher temperatures agree well with Ti-in-quartz thermometry from wall-rock alteration zones (503 ± 24°C) and arsenopyrite geothermometry (438 ±44°C) from vein selvages (Fig. 2). The lower temperature of late mineralization overlaps with the range of fluid inclusion homogenization temperatures in vein quartz (360 to 230 °C).

In summary, the B-isotope data from both minerals are consistent with a magmatic source of fluids during the stages of mineralization represented by mica and tourmaline samples, which supports the concept of multiple injections of magmatic-hydrothermal fluids (Codeço *et al*., 2017, 2019).

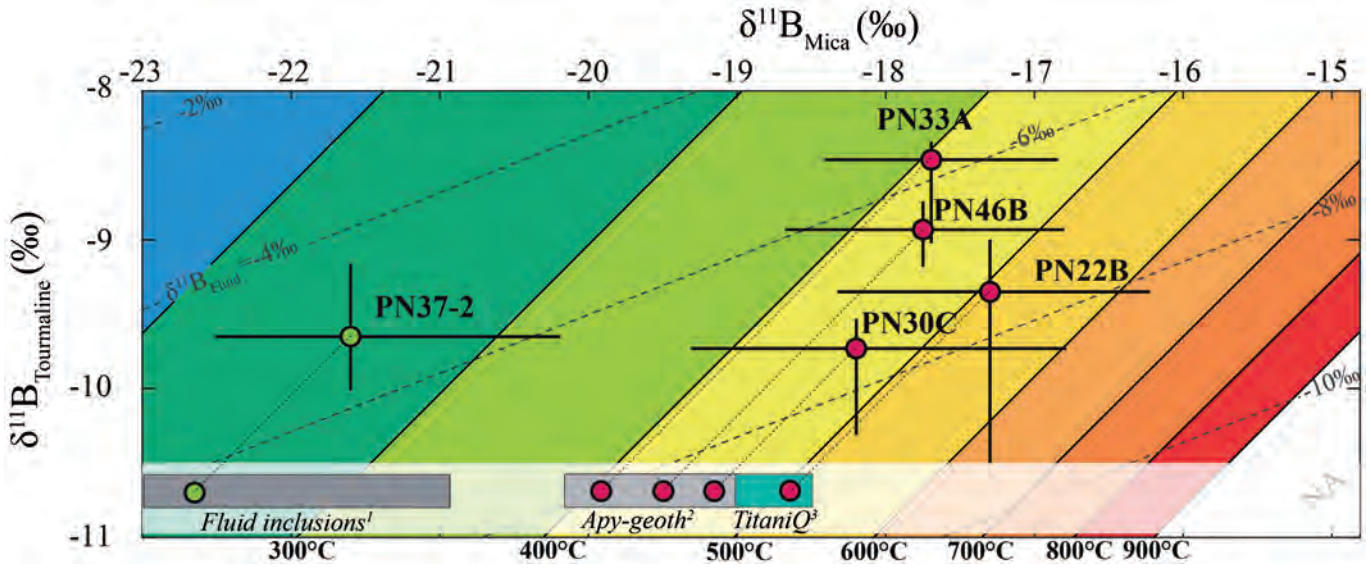

Fig. 2 - Temperature and $\delta^{11}B_{fluid}$ estimates calculated from Panasqueira mica-tourmaline pairs using the fractionation factors of Wunder *et al*., 2005 (mica-fluid) and Meyer *et al*., 2008 (tourmaline-fluid). Solid lines are isotherms, and dashed lines are isopleths of $\delta^{11}B_{fluid}$ composition. The median $\delta^{11}B$ values of tourmaline-mica pairs are indicated by circles, with the red and green symbols representing vein selvages and late fault zone, respectively. The black lines correspond to the 25th to 75th percentile range. Independent temperature estimates are shown in gray bars at the bottom of the plot: [1]Fluid inclusions from Kelly & Rye (1979), Bussink (1984), Jaques & Pascal (2017), and Lecumberri-Sanchez *et al*. (2017); [2]Arsenopyrite geothermometry (Apy-geoth) from Jaques & Pascal (2017); [3]Ti-in-quartz (TitaniQ) geothermometry from Codeço *et al*. (2017). Adapted from Codeço *et al*. (2019).

REFERENCES

Bussink R. W., 1984 – Geochemistry of the Panasqueira tungsten-tin deposit, Portugal. *Geologica Ultraiectina*, 33: 1-170.

Codeço M. S., Weis P., Trumbull R. B., Pinto F., Lecumberri-Sanchez P. & Wilke F. D. H. H., 2017 – Chemical and boron isotopic composition of hydrothermal tourmaline from the Panasqueira W-Sn-Cu deposit, Portugal. *Chemical Geology*, 468: 1-16.

Codeço M. S., Weis P., Trumbull R. B., Glodny J., Wiedenbeck M. & Romer R. L., 2019 – Boron isotope muscovite-tourmaline geothermometry indicates fluid cooling during magmatic-hydrothermal W-Sn ore formation. *Economic Geology,* 114: 153-163.

Codeço M. S., Weis P., Trumbull R. B., Van Hinsberg V., Pinto F., Lecumberri-Sanchez P. & Schleicher A. M., 2021 – The imprint of hydrothermal fluids on trace-element contents in white mica and tourmaline from the Panasqueira W–Sn–Cu deposit, Portugal. *Mineralium Deposita,* 56: 481-508.

Kelly W. C. & Rye R. O., 1979 – Geologic, fluid inclusion, and stable isotope studies of the tin-tungsten deposits of Panasqueira, Portugal. *Economic Geology,* 74 (8): 1721-1822.

Jaques L. & Pascal C., 2017 – Full paleostress tensor reconstruction using quartz veins of Panasqueira Mine, central Portugal; part I: Paleopressure determination. *Journal of Structural Geology,* 102: 58-74

Lecumberri-Sanchez P., Vieira R., Heinrich C. A. A., Pinto F. & Walle M., 2017 – Fluid-rock interaction is decisive for the formation of tungsten deposits. *Geology,* 45: 579-582.

Meyer C., Wunder B., Meixner A., Romer R. L. & Heinrich W., 2008 – Boron-isotope fractionation between tourmaline and fluid: An experimental reinvestigation. *Contribution to Mineralogy and Petrology,* 156 (2): 259-267.

Wunder B., Meixner A., Romer R. L., Wirth R. & Heinrich, W., 2005 – The geochemical cycle of boron: Constraints from boron isotope partitioning experiments between mica and fluid. *Lithos*, 84 (3-4): 206-216.

Does silicate-borosilicate melt immiscibility occur in natural settings? An assessment based on experimentally synthesized tourmaline nodules

Miguel Francisco Cruz[1]*, Vincent J. van Hinsberg[2]

Silicate-borosilicate liquid immiscibility would help explain phenomena observed in highly evolved melts, perhaps most notably local concentrations of tourmaline in granites and pegmatites. Two lines of evidence suggest that such liquid immiscibility is possible.

First: Orbicular or nodular tourmaline, observed in natural evolved melts (e.g. in the Třebíč Granite, Fig. 1), is hypothesized to form when, as the magma cools, a highly evolved melt unmixes into two melts, one being a boron-rich melt – volumetrically minor compared to the host B-poorer melt and therefore tending to form spherical nodules within the host – that crystallizes to predominantly tourmaline (see for example Drivenes *et al*., 2015). However, these tourmaline nodules are not strictly, or even typically spherical, but can take a variety of forms less consistent with liquid-liquid unmixing, and have alternatively been interpreted as magmatic fluid related (Sinclair & Richardson, 1992), hydrothermal replacement (Rozendaal & Bruwer, 1995), or as primary magmatic crystallisation of tourmaline with their shape controlled by nutrient supply (Perugini & Poli, 2007).

The second line of evidence is experimental: Immiscibility has been observed in B-rich silicate melts in the lab (e.g. Veksler *et al*., 2002). However, the synthetic melts studied by these authors were also doped with other incompatible elements to unnaturally high levels, and the effects of B alone – as well as the relevance to natural B-rich melts – are thus unclear. Indeed, Pichavant (1981) and van Hinsberg (2011) do not observe liquid immiscibility in B-rich melts up to 18 wt% B_2O_3, which exceeds the B-content of common natural granitic melts.

To resolve the ambiguity in whether silicate-borosilicate liquid immiscibility is possible for natural geological environments, we evaluated immiscibility in the granite-B_2O_3 chemical system experimentally. We investigated apparent equilibrium at different temperatures for melts that closely approximate natural compositions, using either a tourmaline-free granite to which we progressively added up to 50 wt% B_2O_3, or using a granite that hosts orbicular tourmaline (the Třebíč Granite of Fig. 1), in which case we homogenized a mixtures of the tourmaline nodule and the host granite up to 5 wt% B_2O_3.

Experiments were run H_2O-free at 1 atm in sealed quartz tubes in a box furnace, or were run H_2O-saturated at 1 kbar in sealed gold capsules in a rapid-quench cold-seal pressure vessel. All experimental charges were first homogenized to a single melt at 1200°C (dry, 1 atm) or 900°C (wet, 1 kbar). They were then cooled slowly over several days to a dwell temperature between 400 and 700°C where they were held for > 3 days, and then finally quenched rapidly.

The dry, 1-atm experiments showed no textural nor compositional evidence for liquid immiscibility, even at unnaturally high 50 wt% B_2O_3 contents, which rules out that B alone can induce liquid immiscibility, in agreement with experiments by Pichavant (1981). Liquid immiscibility was similarly absent in the H_2O-saturated 1-kbar experiments, but the run products of some of these displayed (among other interesting textures) nodular/orbicular tourmalines

Fig. 1 - Tourmaline nodules in the Třebíč Granite, Czech Republic as observed during the Tourmaline2017 post-conference fieldtrip.

[1] Department of Earth Sciences, Indiana University Purdue University Indianapolis, 723 W Michigan St., Indianapolis, IN 46202, USA.
[2] GEOTOP Research Centre, Department of Earth and Planetary Sciences, McGill University, Montreal, Canada.
Email: V.J.vanHinsberg@gmx.net

* Corresponding author: miguelx9@gmail.com

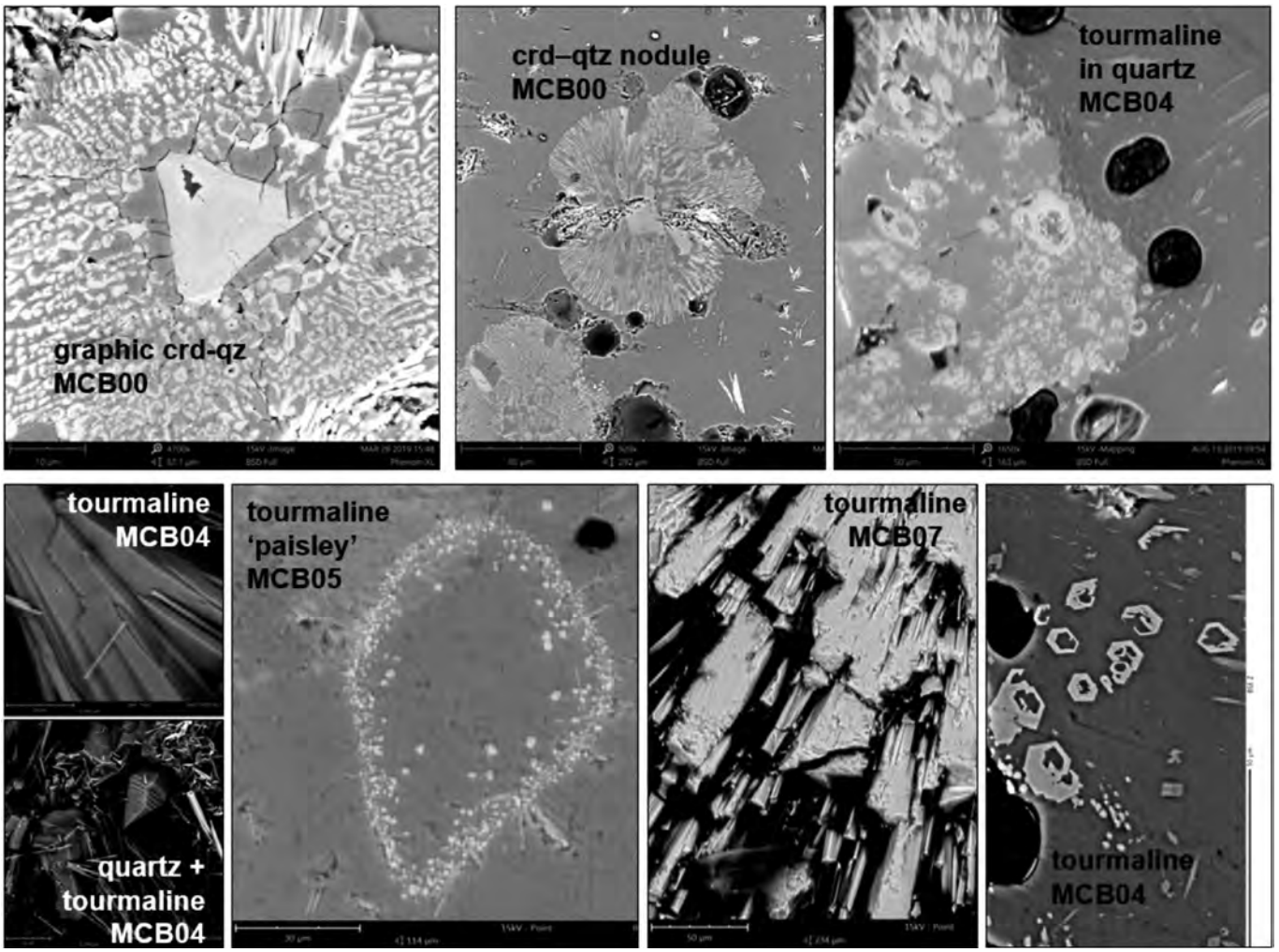

Fig. 2 - Back-scattered electron images of mineral textures in the experimental run products.

(Fig. 2). These micronodules have symplectitic quartz and tourmaline (or cordierite for lower B_2O_3 runs), intergrown at the scale of ~2 μm, and coexist with fluid, glass, and biotite. These do not represent crystallisation of a borosilicate immiscible melt given that such a melt was not observed in higher temperature experiments and cordierite replaces tourmaline in the nodules at lower melt B content.

We hypothesize that the nodules formed as tourmaline (or cordierite) crystallized, which saturated quartz in the immediate surrounding melt, and as quartz crystallizes, this in turn saturated in tourmaline. Length scales of the intergrowth could be related to differential transport rates of mineral nutrients, similar to how the nodules on Elba were interpreted by Perugini & Poli (2007).

In conclusion, B does not induce liquid immiscibility in granitic systems, and tourmaline nodules are best explained as the result of a magmatic crystallisation process with local B-enrichment, or to represent the transition from magmatic to hydrothermal conditions and formation from a fluid in the cooling magmatic body.

REFERENCES

Drivenes K., Larsen R. B., Müller A., Sørensen B. E., Wiedenbeck M. & Raanes M. P., 2015 – Late-magmatic immiscibility during batholith formation: assessment of B isotopes and trace elements in tourmaline from the Land's End granite, SW England. *Contributions to Mineralogy and Petrology*, 169: 1-27.

Perugini D. & Poli, G, 2007 – Tourmaline nodules from Capo Bianco aplite (Elba Island, Italy): an example of diffusion limited aggregation growth in a magmatic system. *Contributions to Mineralogy and Petrology*, 53: 493-508.

Pichavant M., 1981 – An experimental study of the effect of boron on a water-saturated haplogranite at 1 kbar pressure: geological applications. *Contributions to Mineralogy and Petrology*, 76: 430-439.

Rozendaal A. & Bruwer L., 1995 – Tourmaline nodules: indicator of hydrothermal alteration and Sn–Zn–(W) mineralization in the Cape Granite Suite, South Africa. *Journal of African Earth Sciences*, 21: 141-155.

Sinclair D. W. & Richardson J. M., 1992 – Quartz–tourmaline orbicles in the Seagull Batholith, Yukon Territory. *The Canadian Mineralogist*, 30: 923-935.

van Hinsberg V. J., 2011 – Preliminary experimental data on trace-element partitioning between tourmaline and silicate melt. *The Canadian Mineralogist*, 49, 153-163.

Veksler I. V., Thomas R. & Schmidt C., 2002 – Experimental evidence of three coexisting immiscible fluids in synthetic granitic pegmatite. *American Mineralogist*, 87: 775-779.

Boron, oxygen and hydrogen isotope composition of zoned tourmalines from the Monte Capanne miarolitic LCT pegmatite field

Andrea Dini

Granitic pegmatites are widespread in the Late Miocene Monte Capanne monzogranite pluton (Elba Island), but it is only along its eastern border that they display a marked Li-Cs-Ta (LCT) signature (Fig. 1). Such LCT pegmatites are of particular interest since, at a small scale, they contain much of the features typical of many other important pegmatite districts around the world. Indeed, Elba pegmatites show a variety of inner structures, different host-rocks, complex and rich mineralogy (e.g.: elbaite, petalite, pollucite, microlite, etc.), and a wide range of the degree of geochemical evolution (Pezzotta, 2000).

The Monte Capanne pluton is a slightly peraluminous monzogranite intrusion (Dini *et al.*, 2002) formed by the downward stacking of multiple magma pulses. Earlier emplacement of K-feldspar megacryst-rich magma sheets was followed by the emplacement of a larger magma batch that produced the megacryst-poor San Piero facies. Several evidences indicate that the NW part of the pluton acted as the feeding zone, while the eastern part developed as a "tongue" in the footwall of a low angle detachment (Fig. 1). Cordierite and tourmaline bearing leucogranites (Dini *et al.*, 2002), were emplaced as swarms of sub-parallel, sub-vertical dykes trending WSW-ENE (10-40 cm thick) throughout the entire pluton and crosscutting also the contact aureole. Leucogranite, sub-vertical dyke swarms continue along the eastern border of the pluton where their strike change to NNE-SSW. Here they acted as feeders of large leucogranite sills (same direction of dykes but gently dipping to the east) emplaced along the contact with, and within the metamorphic aureole.

The eastern side of the Monte Capanne pluton is crosscut by at least three NNE-SSW swarms of leucogranite dykes, but miarolitic LCT pegmatites are associated only with the easternmost one. The LCT pegmatite dykes display an overall NNE-SSW strike, like the leucogranite dykes, but their attitude can be much more variable (variably dipping to the west) as well as their thickness (from few cm up to 1-2 m). Miarolitic LCT pegmatites occur near the pluton contact, hosted by the monzogranite rocks (both in megacryst-rich and -poor facies), the meta-ophiolites of the contact aureole and the leucogranite sills. The age is constrained by isotopic dating (U-Pb and ^{40}Ar-^{39}Ar) of the Monte Capanne monzogranite (6.9 Ma) and late mafic porphyry dykes (6.85 Ma).

Internal structures and parageneses of the miarolitic LCT pegmatites have been described by Pezzotta (2000). Many dykes display aplitic fine-grained borders, with a basal line-rock highlighted by tiny tourmaline crystals, and a coarse grained pegmatitic core characterized by early quartz-tourmaline graphic aggregates that evolve to prismatic, zoned schorl-elbaite crystals inside the miarolitic cavities. Crystallization occurred in closed system conditions as indicated by continuous evolution from iron-rich to iron-poor and lithium-rich composition. Late brecciation of the pegmatite bodies is responsible for reversal zoning (dark overgrowths at elbaite crystal tips) as well as some tourmaline veining in the granite and meta-ophiolitic hosts. Recent studies identified a large number of tourmaline supergroup end-members (see Pezzotta, this volume and references therein).

This contribution provides new isotopic data (B, O, H) on zoned tourmalines and quartz from: 1) granite and leucogranite hosts; 2) LCT pegmatites and 3) late hydrothermal veins. Analyses have been performed on micro-

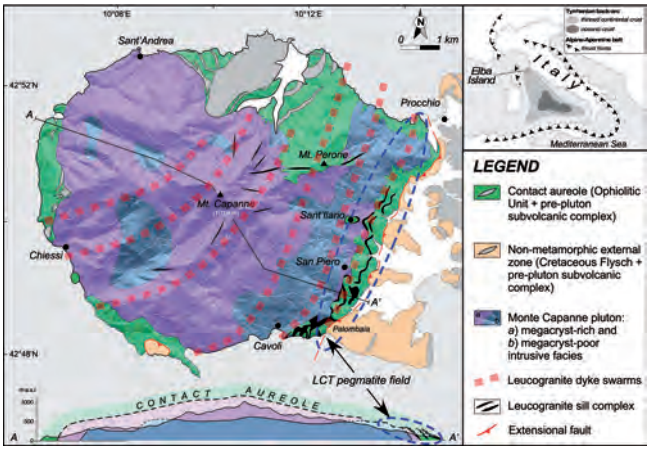

Fig. 1 - Geological sketch of Monte Capanne pluton (Elba Island).

Istituto di Geoscienze e Georisorse - CNR, Via Moruzzi 1, 56124 Pisa (PI), Italia.
E-mail: a.dini@igg.cnr.it

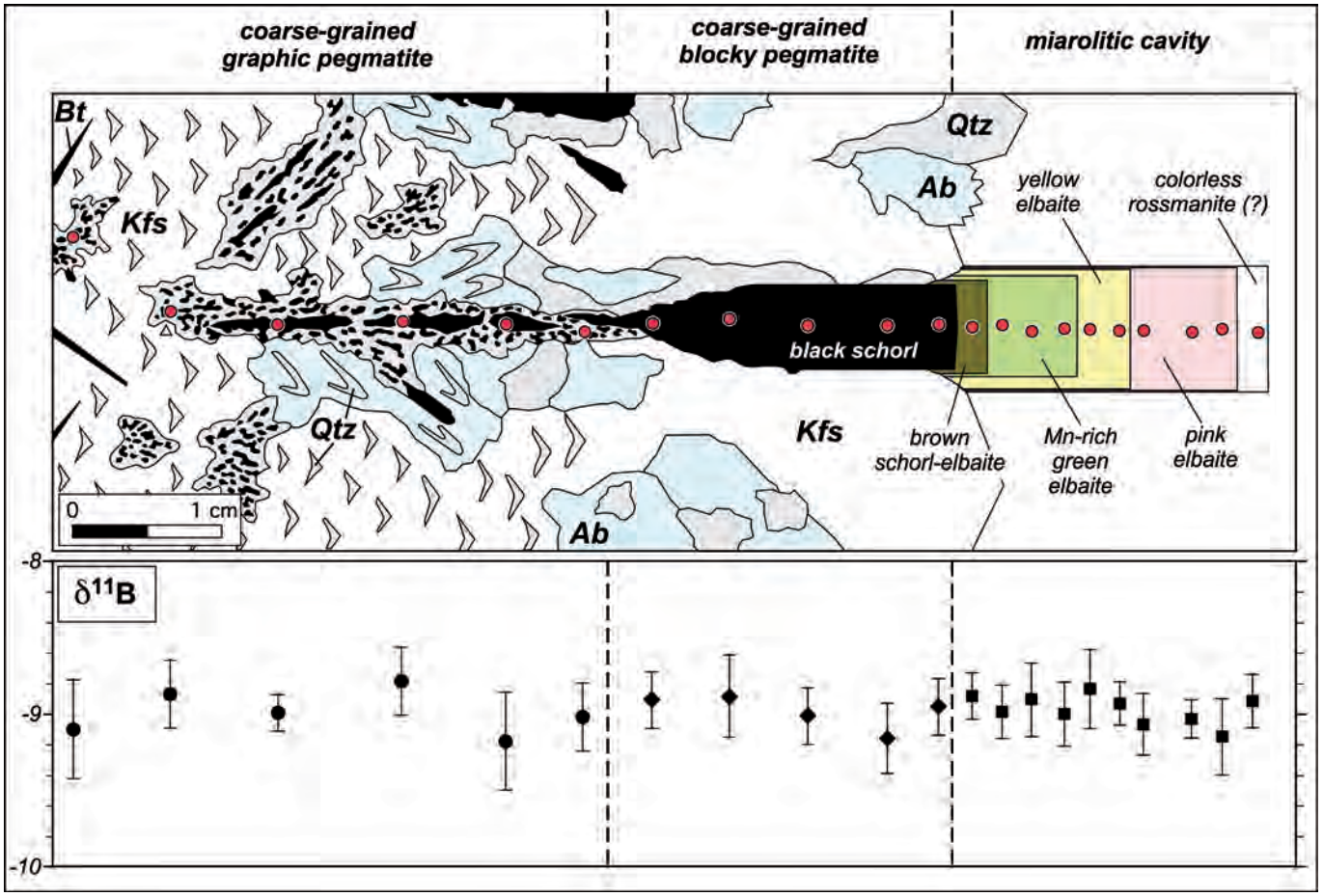

Fig. 2 - Boron isotopic composition of a transect from graphic schorl, to prismatic schorl, to strongly zoned elbaite-rossmanite (?). Sample coming from Forcioni pegmatite dyke (found in 1994), near the northern end of the Monte Capanne LCT pegmatite field.

drilled samples at IGG-CNR (Pisa) using a Neptune Plus MC-ICPMS (B), laser fluorination coupled with Delta XP spectrometer (O) and thermal reduction apparatus coupled with a Delta Plus XP IRMS spectrometer (H).

The boron isotopic composition of tourmaline from Monte Capanne LCT pegmatites has been already studied by Tonarini *et al*. (1998). They found an almost constant boron isotopic composition (average $\delta^{11}B = 9.05 \pm 0.37$ 1sd ‰) throughout the entire sequence from early graphic schorl, to prismatic schorl and late elbaite. The new boron isotope dataset confirms previous results and indicate that such a behavior characterizes the evolution of the entire LCT pegmatite system from Palombaia to Procchio. Pegmatitic $\delta^{11}B$ are consistent with ratios measured in granite-leucogranite, in the late dark overgrowths as well as the few analyzed tourmalines from hydrothermal veins. $\delta^{11}B$, $\delta^{18}O$ and δD are consistent with the crustal signature of these magmatic rocks and provide temperature of crystallization ($\Delta^{18}O_{tur\text{-}qtz}$; 700-350°C) that are coherent with fluid inclusion studies and petrological constraints. The lack of isotopic fractionation during the progressive extraction of boron from the growing medium (for decreasing temperature and variable chemical conditions) indicates that available theoretical and experimental fractionation factors must be cautiously applied to the study of pegmatitic systems.

REFERENCES

Dini A., Innocenti F., Rocchi S., Tonarini S. & Westerman D. S., 2002 – The magmatic evolution of the late Miocene laccolith-pluton-dyke granitic complex of Elba Island, Italy. *Geological Magazine*, 139: 257-279.

Pezzotta F., 2000 – Internal structures, parageneses and classification of the miarolitic Li-bearing complex pegmatites of Elba Island (Italy). *Memorie della Società Italiana di Scienze Naturali e del Museo di Storia Naturale di Milano*, 30: 29-43.

Tonarini S., Dini A., Pezzotta F. & Leeman W. P, 1998 – Boron isotopic composition of zoned (schorl-elbaite) tourmalines, Mt. Capanne Li-Cs pegmatites, Elba Island (Italy). *European Journal of Mineralogy*, 10: 941-951.

Sn-rich tourmaline from the Land's End granite, SW England

Kristian Drivenes

Tourmaline and Sn-W mineralizations are closely associated. However, the commodity of a deposit is not necessarily reflected by the chemical composition of tourmaline. Sn-rich tourmalines have been observed in Sn-mineralizations throughout the world (Mlynarczyk & Williams-Jones, 2006), whereas W-content in tourmaline is typically very low, even in mineralized areas. Tourmaline from a Sn-bearing hydrothermal quartz-tourmaline rock at Nanjizal, Land's End, was investigated in order to understand how Sn is distributed in tourmaline. It is located 10s-100 meters from two small, formerly worked lodes, and comprises almost exclusively quartz and tourmaline, with minor K-feldspar, apatite and cassiterite. Tourmaline occurs as replacements of former granite minerals and as overgrowths on former tourmaline generations. The relationship with cassiterite is not straightforward, but typically, cassiterite nucleates on clusters of late-stage tourmaline, and tourmaline, cassiterite and quartz crystallized simultaneously. The tourmaline generation coexisting with cassiterite is acicular with strong green/blue-colorless pleochroism. This association is recognized throughout the Land's End granite, but the Sn-content of rocks including this tourmaline generation may vary from a few 100 ppm to several wt%, the quartz-tourmaline rock at Nanjizal being an example of the latter.

Tourmaline is strongly zoned, both optically and chemically. Homogenous zones in the tourmaline generation associated with cassiterite rarely exceed 10 μm, and high-resolution BSE imaging revealed distinct growth zones less than 50 nm wide. Numerous low-resolution combined EDS/WDS maps of zoned areas were collected, and areas where Sn was detected were selected for high-resolution mapping. Quantitative maps (Fig. 1) were produced by correlating quantitative WDS analyses with mapped x-ray intensities.

Sn-rich zones are patchy or concentric. The highest recorded value was 2.48 wt% SnO_2 in a patchily zoned rim, and several zones with >1 wt% SnO_2 were observed. Submicron inclusions of cassiterite, Fe- and Ti-oxides are easily distinguished on BSE and x-ray maps (Fig. 1). Thus, the high Sn-values are not due to cassiterite inclusions, but structurally bound in tourmaline. High Sn-values (>0.4 wt% SnO_2) are coupled with a substantial substitution of Fe for Al (Fig. 1) in the Z-site, and in analyses with more than ca. 20 wt% FeO, structural formula calculation indicate that some Fe is present as Fe^{3+}. Trends between Sn and other elements are erratic, except for a weak positive correlation with Sr.

The fluid was saturated with respect to Sn, but Sn-rich zones in tourmaline are rare compared to cassiterite. This may indicate that co-precipitation of tourmaline and cassiterite was limited, or that Sn-content of the fluid is not the only parameter controlling the incorporation of Sn in tourmaline. Cassiterite precipitation from granite-derived fluids typically requires oxidation, and combined with the inferred Fe^{3+} in the Sn-rich zones this may indicate that oxidation of the ore fluid caused cassiterite precipitation and the Sn-rich tourmaline zones. Alternatively, the Sn-rich zones may be the result of local redistribution of Sn from granite minerals by dissolution-reprecipitation processes.

Independent researcher, Eyvind Lokkens veg 9, 7092 Tiller, Norway.
E.mail: kristian.drivenes@gmail.com

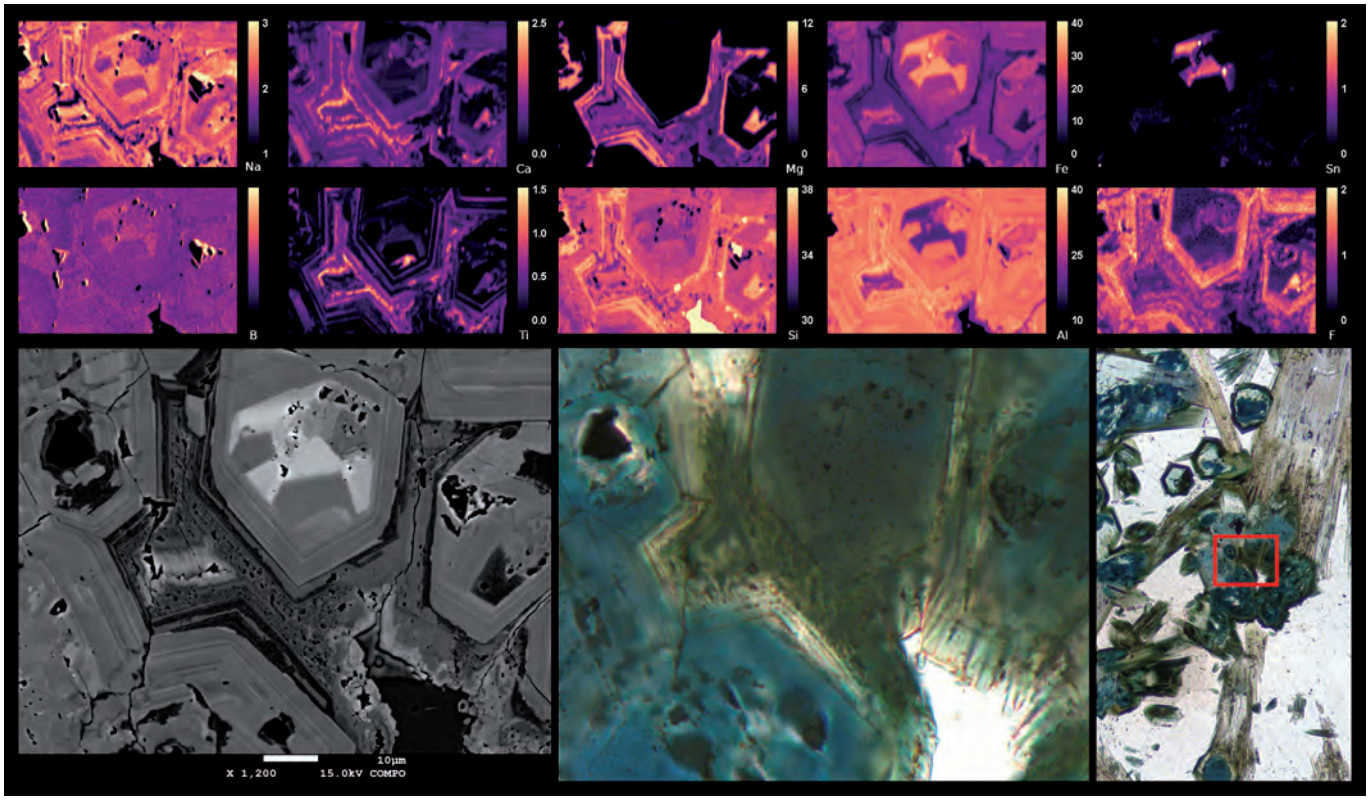

Fig. 1 - Optical, backscatter electron, and x-ray maps of tourmaline. B, F, Ti, Sn and Ca by WDS. Na, Al, Si Fe, and Mg by EDS. Scale is in wt% oxide. The maps were collected using a JEOL 8530FPlus at 12 kV, 120 nA. 300 nm defocus and step size, and 500 ms dwell time. Small, bright spots in the BSE image are cassiterite and Fe-oxide inclusions.

REFERENCES

Mlynarczyk M. S. J. & Williams-Jones A. E., 2006 – Zoned tourmaline associated with cassiterite: implications for fluid evolution and tin mineralization in the San Rafael Sn–Cu deposit, southeastern Peru. *The Canadian Mineralogist*, 44 (2): 347-365.

Petrogenetic utility of magnesian tourmaline: extraordinary origin of everyday tourmaline

Barbara L. Dutrow*, Darrell J. Henry

As more studies emerge, the petrogenetic utility of tourmaline continues to expand since its original description as one of the Big Three sedimentary provenance indicators (e.g., Krynine, 1946). The discovery that tourmaline rims are in chemical equilibrium with coexisting minerals in metamorphic rocks opened new avenues for deciphering the history of metamorphic terranes and the clastic sources for their detritus (Henry & Guidotti, 1985). This relationship between tourmaline chemistry and its original host-rock composition continues to open new avenues to its petrogenetic utility. Since that publication, more than 500 studies utilized tourmaline chemistry in conjunction with the AFM environmental diagram for provenance determinations (Fig. 1).

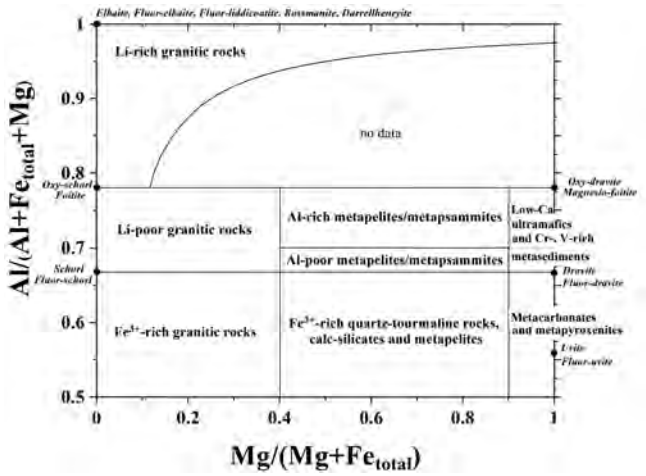

Fig. 1 - AFM diagram relating tourmaline compositions to host rock environment (modified after Henry & Guidotti, 1985). Note overlapping Mg-rich fields.

Department of Geology and Geophysics, Louisiana State University, Baton Rouge, Louisiana, USA.
E-mail: glhenr@lsu.edu

* Corresponding author: dutrow@lsu.edu

Most of the tourmaline compositions used to define the AFM host-rock fields relate to commonly encountered chemistries. Due to the paucity of data for the Mg-rich portion of the diagram, numerous host-rocks fields overlap, rendering the Mg-rich tourmalines less petrogenetically useful. These tourmalines are typically dravite (fluor), uvite (fluor), oxy-dravite, and magnesio-foitite.

To expand the utility of tourmaline compositions, numerous samples (ca. 100) of tourmaline from more unusual chemical environments have been analysed for major element chemistry by electron probe microanalysis (EPMA). Such data have the potential to modify, differentiate, and improve compositional boundaries for the Mg-rich compositions and provide data for development of new discrimination diagrams. Here, the highlights focus on the Mg-rich tourmalines in calcareous, calc-silicate, and evaporitic host-rocks.

Magnesian and calcic tourmaline species commonly occur in (meta)carbonate host-rocks. Two notable localities are the Brumado magnesite deposit of Brazil and the Tanzanian (TZ) carbonate and rhyolite localities. The Brumado tourmalines, typically distinctive, flattened euhedral brown and green crystals set in a magnesite matrix, are magnesian (X_{Mg}>0.86). A single crystal may range in composition to encompass species of fluor-uvite, uvite, dravite and magnesio-foitite with the green crystals containing >1.5 wt% V_2O_3. Tanzania tourmalines are typically found as lustrous vivid green V-Cr-bearing tourmalines, some of which occur in a pure white calcite matrix (marble). Other TZ tourmalines from the Arusha district have calcite-rich matrices that apparently replace volcanic breccias, preserving the morphology of the Fe-stained clasts. In one such sample, a large (3 mm) transparent, pale yellow single crystal of tourmaline is a nearly homogeneous, highly magnesian, dravite (n =12) with X_{Mg} = 0.99, Al_{tot} = 6.51 apfu, X_{Na} = 0.70, X_{Ca} = 0.22 and F= 0.02-0.14 apfu. In another TZ sample, dravite and uvite occur in dolomitic marbles partially replaced by calcite. Here, dravite is characterized by X_{Mg} = 0.95, Al_{tot} = 6.00 apfu, X_{Na} = 0.45, X_{Ca}=0.36 and F= 0.2-0.3 apfu whereas uvite has X_{Na} = 0.38 and X_{Ca}=0.46. This sample coexists with minor rutile, phlogopite, apatite and orthoclase. Tourmaline occurs in rocks across the spectrum of Mg-Ca carbonates.

Tourmaline from calc-silicate, typically metamorphosed, rocks are associated with magnesian and calcic minerals. Coexisting phases can include pargasite, chlorite, scapolite, talc, phlogopite, and minor carbonate (dolomite and/or calcite), apatite and titanite. In one such sample from New York, US, compositional zoning is prevalent, with tourmalines ranging from dravite to uvite to fluor-uvite. The Mg-rich nature of the host rocks is reflected in the tourmaline, X_{Mg} = 0.95, while X_{Na} = 0.28 – 0.50 with F = 0.07 – 0.34 apfu. Such zoning may reflect the influence of the devolatization reactions during metamorphism.

Tourmaline from evaporites and their metamorphosed equivalents are rare in the rock record. Forming at temperatures as low as 150°C, tourmalines of the oxy-dravite to povondraite trend are found in caprocks of active salt domes in the Gulf of Mexico (Henry *et al*., 1999). Recently, samples collected from the Arignac, Gypsum Mine in Ariege, Pyrenees, France contain tourmaline associated with gypsum, anhydrite, high-Mg calcite, and minor phlogopite, celestine, rutile, F-bearing apatite, and zircon (Fig. 2). Tourmaline has anhydrite inclusions and is weakly zoned: X_{Mg} = 0.92 – 0.98, X_{Na} = 0.54 – 0.77, Al_{tot} = 5.7 – 5.9 apfu, and F = 0.01 – 0.12 apfu. Traces of Ti and Fe contribute to the dark tourmaline color (Fig. 2).

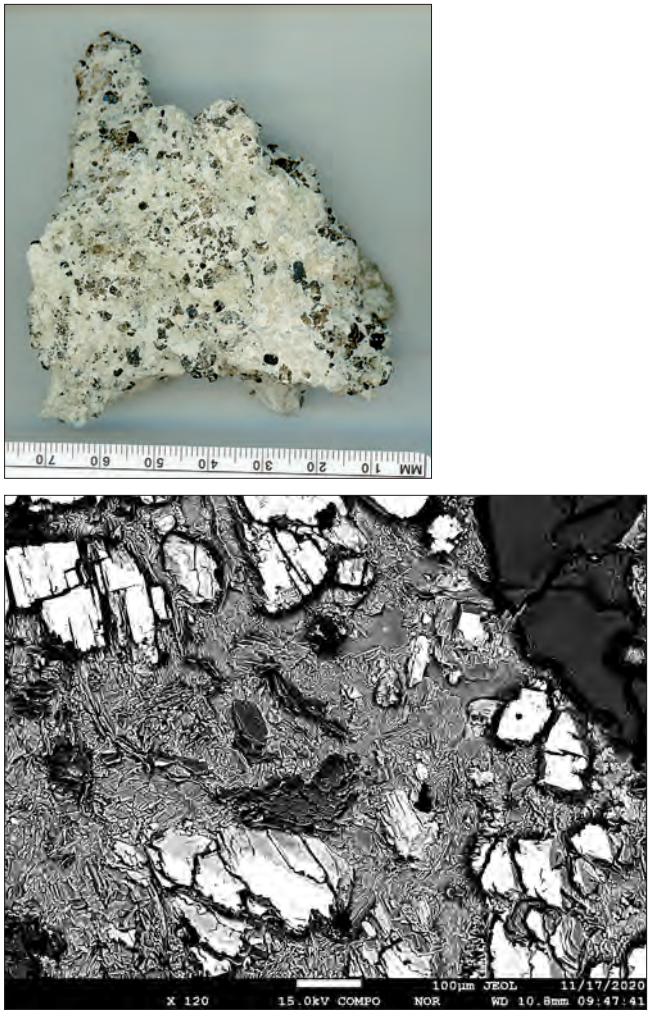

Fig. 2 - (top) Sample of tur-bearing evaporate from France. (bottom) BSE image showing a matrix of gypsum (grey), anhydrite (white), tourmaline (dark grains, upper right). Scale bar is 100 µm.

Another unusual host for meta-evaporitic tourmaline is danburite ($Ca_2B_2Si_2O_8$). In the Alto Chapare magnesio-riebeckite asbestos mining district, in the Chapare province, Cochabamba Department, Bolivia, tourmaline microinclusions occur in danburite (A. Petrov, person. comm.) Tourmalines are strongly zoned, but zones are too small for multiple EPM analyses to distinguish their chemistries (Fig. 3). A 5 µm EPMA analytical spot produced an average dravite composition with X_{Mg} = 0.69, X_{Na} = 0.96, Al_{tot} = 4.9 apfu, and F = 0.05 apfu. The Na-rich composition may result from partitioning of Ca into the danburite likely sequestering Ca from the coexisting tourmaline.

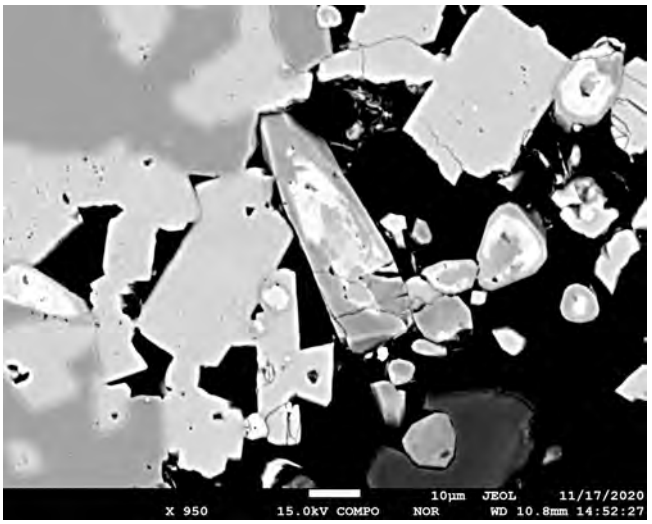

Fig. 3 - BSE image of zoned tourmaline (center) in danburite. Sample disaggregated during preparation. Scale bar is 10 µm.

In most Mg-rich samples, minor and trace elements are low; Fe, Mn, Ti are < 1.0 apfu and typically much lower, ca. ~0.1 apfu. Vanadium, Cr, and Zn were analysed in all samples, but only the TZ samples contained amounts above EPMA detection limits.

These data allow for new variations of environmental diagrams for magnesian tourmaline associated with host rocks in unusual and uncommon compositional environments. The addition of diagrams that takes into account Cr, Al, Ti, V and minor elements may be applicable for the magnesian tourmaline. As tourmaline in these environments continue to be revealed, new petrogenetic utility will be derived from the unusual to the usual compositions; tourmaline as an indicator mineral expands to wide-ranging and rare geochemical environments, both in the solid and fluid realm.

Funding for this research, by NSF-IF EAR 1151434, is gratefully acknowledged.

REFERENCES

Henry D. J. & Guidotti C. V., 1985 − Tourmaline as a petrogenetic indicator mineral - an example from the staurolite-grade metapelites of NW Maine. *American Mineralogist*, 70, 1-15.

Henry D. J., Kirkland B. L. & Kirkland D. W., 1999 − Sector-zoned tourmaline from the cap rock of a salt dome. *European Journal of Mineralogy*, 11, 263-280.

Krynine P. D., 1946 − The tourmaline group in sediments. *Journal of Geology*, 54, 65-87.

Why was it not possible to synthesize Li-rich tourmaline?

Andreas Ertl

Several attempts by different groups in the past were not successful to synthesize the Li-, Al- and OH-rich member of the tourmaline supergroup, named elbaite.

More than 100 years ago, Vernadsky proposed the name "Elbait" for Li-, Na-, and Al-rich tourmaline from Elba Island, Italy, with the simplified formula $(Li,Na)HAl_6B_2Si_4O_{21}$ (Vernadsky, 1914; Ertl, 2008). Most likely the type material for pink elbaite with the newly calculated formula $\sim(Na_{0.7}\square_{0.3})(Al_{1.9}Li_{1.1})Al_6(B_{0.9}O_3)_3[Si_{5.9}Al_{0.1}O_{18}](OH)_3[(OH)_{0.6}O_{0.4}]$ (F = 0.1 wt%) was found at Fonte del Prete, San Piero in Campo, Campo nell'Elba, Elba Island, Livorno Province, Tuscany, Italy (Ertl, 2008). For the 1914 work the chemical analysis from another author was used (Schaller, 1913). Around 20 years later the formula for elbaite was updated to $H_8Na_2Li_3Al_3B_6Al_{12}Si_{12}O_{62}$ (Winchell, 1933), which is commonly used to date written as $Na(Li_{1.5}Al_{1.5})Al_6(BO_3)_3[Si_6O_{18}](OH)_3(OH)$.

Later the F-analogue of elbaite with the formula $Na(Li_{1.5}Al_{1.5})Al_6(Si_6O_{18})(BO_3)_3(OH)_3F$ was found and eventually described with the name fluor-elbaite as new member of the tourmaline supergroup (Bosi *et al.*, 2013).

The group around David London synthesized Li-bearing tourmalines as the basis for elucidating the stability field of elbaite. Based on their experiments it was noted that the calculated Li content increases with increasing pressure (*P*) and temperature (*T*) (London, 2011; London & Morgan, 2011). A further study including single-crystal X-ray diffraction data and quantitative light elements (Li, B, H) data has shown that a pronounced negative correlation between temperature during crystal growth (at a constant pressure of 260 MPa) and $^{[4]}$B (from refinement) in three synthetic Li-bearing olenites was found (Ertl *et al.*, 2012). While the measured Li content (~0.5 Li apfu) did not change significantly, tourmalines synthesized below 500°C belonged to oxy-tourmalines with an O dominant W site David London synthesized these tourmaline samples at temperatures of 400-600 °C. All investigated samples contained $^{[4]}$B and $^{[4]}$Al beside the Si content (Ertl *et al.*, 2012). While the amount of $^{[4]}$B was ~0.5 apfu in the tourmaline sample synthesized at 600 °C, the amount of $^{[4]}$B increased significantly to ~1.2 apfu, while the amount of $^{[4]}$Al decreased slightly to ~0.2 apfu, in the sample synthesized at 400 °C.

Natural tourmalines, which can be assigned to elbaite, were not found very often. Tourmalines from a Li-pegmatite from the famous Himalaya mine were investigated chemically (including light elements) and structurally (Ertl *et al.*, 2010). Only one sample was assigned to an (Al-rich) elbaite. It contained ~1.1 apfu Li and the W site was occupied by $[(OH)_{0.54}F_{0.46}]$. This sample had ~0.4 vacancies at the *X* site and contained ~0.2 apfu $^{[4]}$B. All other investigated Li-rich tourmaline samples belong to fluor-elbaite with F contents in the range ~0.6-0.8 apfu F (Ertl *et al.*, 2010). Tourmalines from the Cruzeiro pegmatite, Minas Gerais, Brazil, showed comparable chemical data (Bosi *et al.*, 2005). Elbaite samples with ~1.4 apfu Li exhibited ~0.4 vacancies at the *X* site and contained ~0.3-0.4 apfu F. All other Li-rich tourmaline samples from the Cruzeiro pegmatite belong to fluor-elbaite with F contents in the range >0.5-0.8 apfu F (Bosi *et al.*, 2005). All these investigated elbaite samples contain significant amounts of F, from ~0.3 apfu up to <0.5 apfu F. And all these samples contain relatively high *X*-site vacancies (~0.4 pfu).

Three small Li-rich tourmaline crystals from a miarolitic pegmatite from Wolkenburg, Saxony, Germany, showed interesting relationships (Ertl *et al.*, 2009). These crystals are crystallized at similar *PT* conditions, but in different tiny pockets. The most Li-rich tourmalines is a fluor-elbaite. It contains ~1.1 apfu Li, ~0.3 vacancies at the *X* site and ~0.7 apfu F. The tourmaline with the second highest Li content is an elbaite. It contains ~1.0 apfu Li, ~0.45 vacancies at the *X* site and ~0.4 apfu F. The tourmaline sample with the lowest Li content is a rossmanite. It contains ~0.7 apfu Li, ~0.5 vacancies at the *X* site and ~0.3 apfu F. It seems that the Li and the F content are somehow positively correlated. Less F means less Li^{1+} and therefore more Al^{3+}. To produce a charge balanced formula the vacancies at the *X* site increase. There seems to be only a small gap, where "real" elbaite, which is (OH)-dominant at the W site, exists. Such elbaite samples have already

Institut für Mineralogie und Kristallographie, University of Vienna, Althanstrasse 14, 1090 Wien, Austria.
E.mail: andreas.ertl@a1.net

relatively high vacancies at the *X* site. If the F content in such a pocket is still lower, the Li content in tourmaline will be smaller, the Al content higher and the vacancies will start to dominate the *X* site. Such a tourmaline can be assigned to rossmanite.

This is also an explanation why most Li-rich tourmalines belong to the fluor-elbaite species. All these Li-rich tourmalines contain only small amounts of $(B,Al)^{3+}$-substitutions at the Si site. Usually such substitutions are ≤0.2 apfu.

Synthetic Al-rich and Li-bearing tourmalines always contain no F, but relatively high amounts of $^{[4]}B$. It is known that such a substitution is favored by lower temperatures (Ertl *et al.*, 2018). The temperature over a range of ~400–700 °C (Fig. 3 in Ertl *et al.*, 2008) is the most important factor.

Once the F content is too small, like in the pink mushroom tourmaline from Momeik, Myanmar, the amount of $^{[4]}B$ increases significantly (to ~0.7 apfu), because of the lower amount of Li (0.75 apfu) and the high amount of Al (Ertl *et al.*, 2007). Boron at the tetrahedral site always needs Al in both octahedral coordinated sites, because of the short-range order.

Fluorine is positively correlated to the average *X*-site charge (Ertl *et al.*, 2009; 2010), depending also on the temperature conditions. Means a smaller amount of F produces higher *X*-site vacancies in such tourmaline samples and higher *X*-site vacancies produce tourmalines with lower amounts of Li. The endmember of such a tourmaline is called rossmanite.

How to produce synthetic Li-rich tourmaline? The best way to produce Li-rich tourmaline is to synthesize fluor-elbaite at moderate pressures and temperatures >550 °C. You need relatively high amounts of Li and F in the starting material. If F is decreased in the starting material then elbaite starts to crystallize. However, there might not crystallize any elbaite, if no F at all is in the starting material.

This work was supported by the Austrian Science Fund (FWF) project no. P 31049-N29.

REFERENCES

Bosi F., Andreozzi G. B., Federico M., Graziani G., & Lucchesi S., 2005 – Crystal chemistry of the elbaite-schorl series. *American Mineralogist*, 90: 1784-1792.

Bosi, F., Andreozzi, G.B., Skogby, H., Lussier, A.J., Abdu, Y.A. & Hawthorne, F.C., 2013 – Fluor-elbaite, $Na(Li_{1.5}Al_{1.5})Al_6(Si_6O_{18})(BO_3)_3(OH)_3F$, a new mineral species of the tourmaline supergroup. *American Mineralogist*, 98: 297-303.

Ertl, A., 2008 – About the nomenclature and the type locality of elbaite: A historical review. *Mitteilungen der Österreichischen Mineralogischen Gesellschaft*, 154: 35-44.

Ertl A., Hughes J. M., Prowatke S., Ludwig T., Brandstätter F., Körner W. & Dyar M. D., 2007 – Tetrahedrally-coordinated boron in Li-bearing olenite from "mushroom" tourmaline from Momeik, Myanmar. *The Canadian Mineralogist*, 45: 891-899.

Ertl A., Tillmanns E., Ntaflos T., Francis C., Giester G., Körner W., Hughes J. M., Lengauer C. & Prem M., 2008 – Tetrahedrally coordinated boron in Al-rich tourmaline and its relationship to the pressure-temperature conditions of formation. *European Journal of Mineralogy*, 20: 881-888.

Ertl A., Kolitsch U., Meyer H.-P., Ludwig T., Lengauer C. L., Nasdala L. & Tillmanns E., 2009 – Substitution mechanism in tourmalines of the "fluor-elbaite"-rossmanite series from Wolkenburg, Saxony, Germany. *Neues Jahrbuch für Mineralogie Abhandlungen*, 186: 51-61.

Ertl A., Rossman G. R., Hughes J. M., London D., Wang Y., O'Leary J. A., Dyar M. D., Prowatke S., Ludwig T. & Tillmanns E., 2010 – Tourmaline of the elbaite-schorl series from the Himalaya Mine, Mesa Grande, California, U.S.A.: A detailed investigation. *American Mineralogist*, 95: 24-40.

Ertl A., Giester G., Ludwig T., Meyer H.-P. & Rossman G. R., 2012 – Synthetic B-rich olenite: Correlations of single-crystal structural data. *American Mineralogist*, 97: 1591-1597.

Ertl A., Henry D. J. & Tillmanns E., 2018 – Tetrahedral substitutions in tourmaline: A review. *European Journal of Mineralogy*, 30: 465-470.

London D., 2011 – Experimental synthesis and stability of tourmaline: a historical overview. *The Canadian Mineralogist*, 49 (1): 117-136.

London D. & Morgan VI G. B., 2011 – Synthesis and stability of elbaite. *GAC-MAC-SEG-SGA Joint Annual Meeting*, Ottawa, May 25-27, Abstracts, 34: 123.

Schaller W. T., 1913 – Beitrag zur Kenntnis der Turmalingruppe. *Zeitschrift für Kristallographie*, 51: 321-343.

Vernadsky W., 1914 – Über die chemische Formel der Turmaline. *Zeitschrift für Kristallographie*, 53: 273-288.

Winchell A. N., 1933 – Elements of Optical Mineralogy. Pt. II. *John Wiley & Sons*, Fourth Edition.

Fluor-Elbaite tourmaline from the Emmons pegmatite, Greenwood, Oxford Co., Maine

Alexander U. Falster*, William B. Simmons, Karen L. Webber

The Emmons is a highly evolved pegmatite in the Oxford pegmatite field in SW Maine. The pegmatite is the most mineral-rich in the field, with 170 identified species and is inferred to have formed by direct anatexis of the hosting migmatite complex. Webber *et al*. (2019) proposed an anatectic origin for the Oxford district pegmatites via a process related to decompressional melting associated with post-Appalachian compression (relaxation) and increased thermal input accompanying the early stages of rifting of Pangea. The pegmatite is well-zoned with a wall zone of distinctive comb-structure tapered schorl crystals associated with quartz, microcline, albite, muscovite, and almandine. The intermediate zone consists of albite, microcline, quartz, schorl-elbaite, and almandine-spessartine with a garnet line and two schorl layers in the lower portion. A core margin zone is comprised of ball muscovite with associated fluorapatite, Nb-Ta oxides, and cassiterite. The core zone consists of quartz, microcline, albite and muscovite, with masses of primary lithiophilite and montebrasite and masses of pollucite. Miarolitic cavities are common and may contain ball muscovite, albite, quartz, elbaite, beryl and numerous accessory minerals. The pegmatite is the type location for the recently approved species tantalowodginite. Albite replacement units include albite, quartz, schorl-elbaite, fluorapatite, columbite-tantalite, cassiterite, beryl, bertrandite, hydroxylherderite, and perhamite.

Although elbaitic tourmaline is not as abundant in the pegmatites of Greenwood township as it is in the Paris Hill, Mt. Apatite and Poland areas, rare gem-quality crystals occur in several miarolitic cavities, either as dark green or blue unzoned crystals or as polychrome crystals (Fig. 1).

Chemically, the tourmaline is mainly elbaite/fluor-elbaite (Fig. 2-4). Brownish fibrous crystals are “fluor-foitite.” Fluor-elbaite and elbaite occur in both green and red tourmaline, but all blue tourmaline is fluor-elbaite or fluor-schorl. The elbaite from the Emmons is distinctive, with the highest MnO content of up to 6.4 wt%, in the Oxford pegmatite field. The Ca (liddicoatite) component is small (Fig. 2) and is only present in the red and green

MP2 Research Group, Maine Mineral & Gem Museum, 99 Main Street, Bethel, Maine 04217, USA.

* Corresponding author: afalster@mainemineralmuseum.org

Fig. 1 - Color-zoned elbaite from the Emmons pegmatite (the tallest crystal is 6.5 cm long).

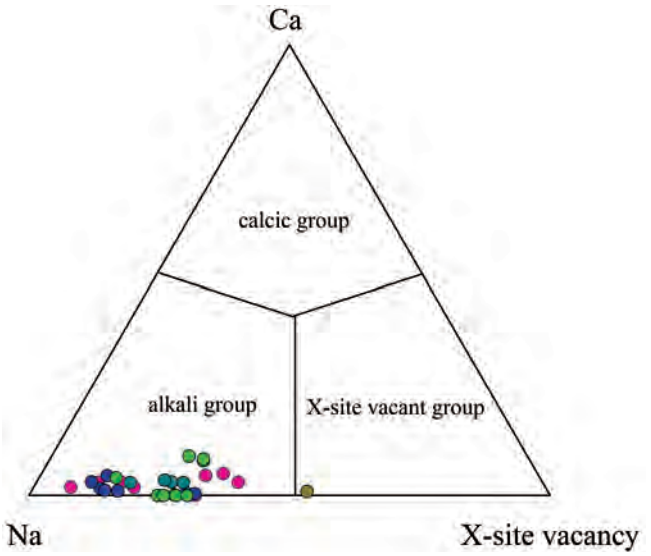

Fig. 2 - X-site occupancy ternary diagram.

tourmaline. Fig. 5 shows the Y-site occupancy of Fe, Mn and Mg and the color progression from high-Fe blue colors to intermediate-Fe green colors and a distinctive purple red in high-Mn tourmaline.

Magnesium is only present in trace amounts or not detectable. Chemical zoning is shown in Fig. 6. The green tourmaline crystal A reveals an early growth core. It is interesting to note that the orientation of the final crystal is not parallel to the substrate crystal. The X-ray map of the purple-red crystal in B shows the highest Mn in the core. However, some crystals show the highest Mn in the intermediate zone of the crystal as seen in C. In both crystals B and C, Mn drops dramatically but briefly resumes a higher concentration of Mn and a thin outermost rim of more Fe-rich elbaite forms before growth stops. The late-stage increase in Fe is likely related to the breakdown of Fe-bearing phases or Fe-bearing complexes. The late overgrowth of Fe is more prominent on the pedial than the prismatic faces.

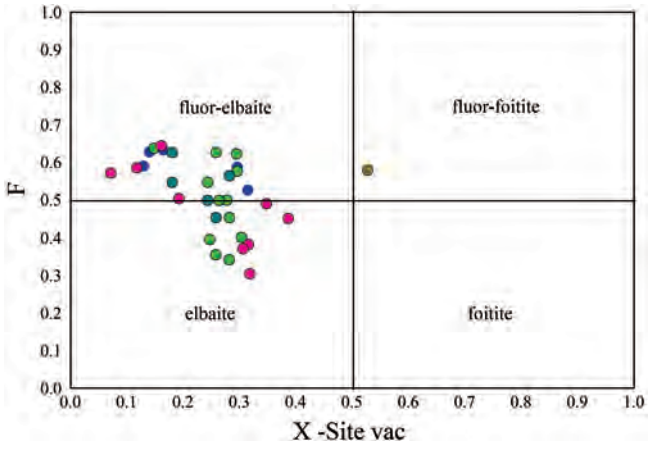

Fig. 3 - F versus X-site vacancy plot. Symbol color corresponds to the tourmaline color.

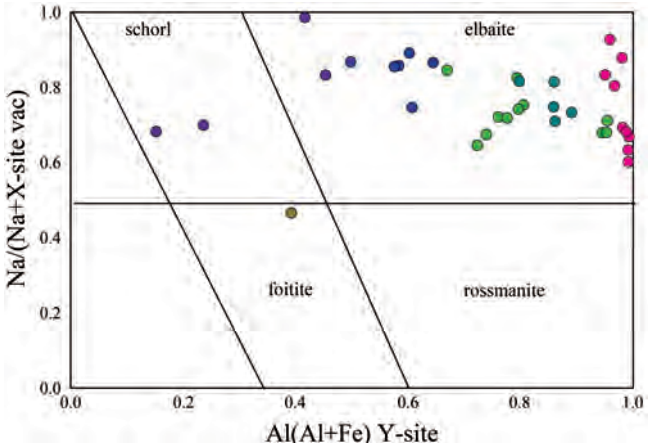

Fig. 4 - Species plot of tourmaline from the Emmons pegmatite. Symbol color corresponds to the tourmaline color.

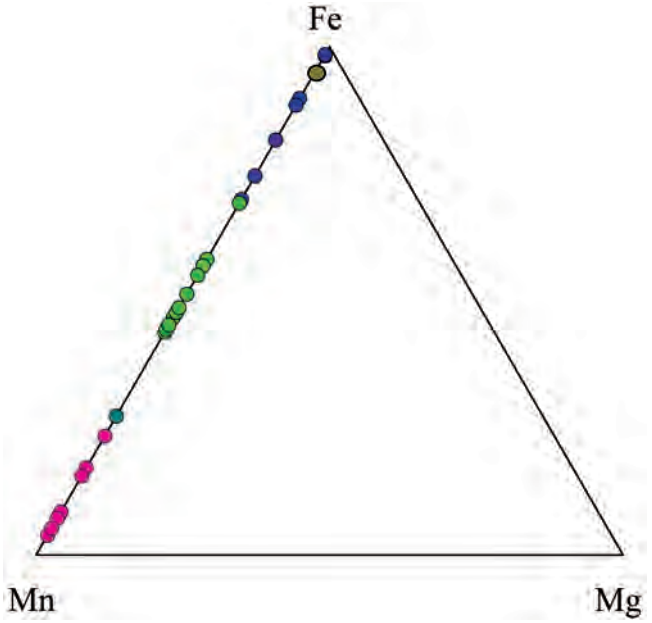

Fig. 5 - Y-site Mn-Fe-Mg ternary diagram.

REFERENCE

Webber K. L., Simmons W. B., Falster A. U. & Hanson S. L., 2019 – Anatectic pegmatites of the Oxford County pegmatite field, Maine, USA. *The Canadian Mineralogist*, 57 (5): 811-815. <doi:10.3749/canmin.AB00028>

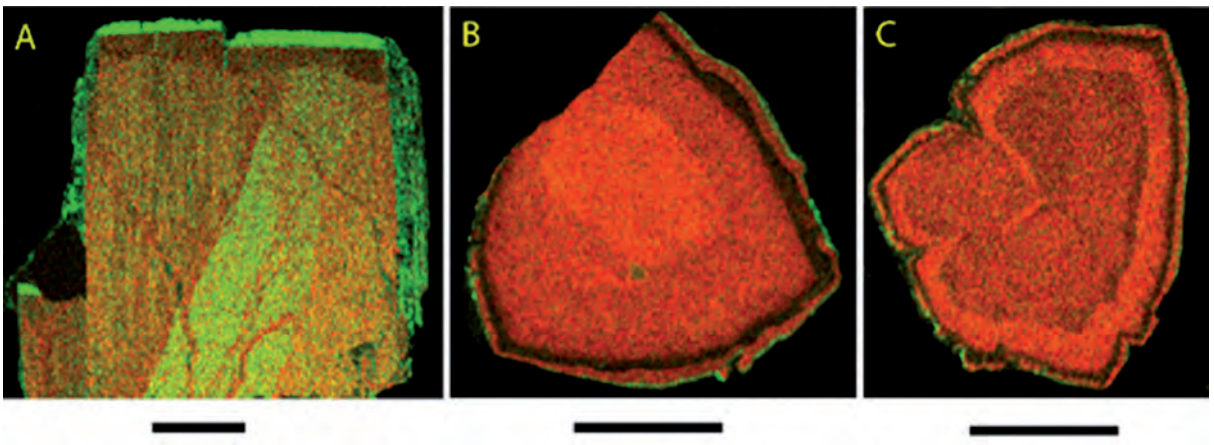

Fig. 6 - X-ray maps of a green (A) and two purple-red tourmalines (B and C). Green is Fe, red is Mn. Note: the X-ray maps of B and C are from crystals found in the same pocket, yet, B shows highest Mn in the core, whereas C has the highest Mn in the intermediate zone of the crystal. Scale bar is 1 mm.

An overview of environmental/industrial applications of tourmaline

Jan Filip

Complex borosilicate minerals from a tourmaline-group have attracted attention to scientist already several centuries ago (Henry & Dutrow, 2018). Besides mineralogy, crystallography, spectroscopy, (isotope) geochemistry, thermodynamics and petrology, there is a growing interest in such minerals also in different research fields than geosciences, such as in material science, environmental engineering, nanoscience and nanotechnology, and many other fields (see Fig. 1). The importance of tourmaline-group minerals (TGM) in "applied" sciences lies mainly in their specific crystal structure providing them unique physical and chemical properties – TGM possess spontaneous polarity (permanent electric dipole giving to tourmaline piezoelectric properties) and contain surface-active sites. With respect to above-mentioned unique electric and surface properties, tourmaline-group minerals have been investigated and tested for possible application in environmental technologies, including oxidation, adsorption and biological processes of contaminant removal from polluted waters.

One of the most recent published research is focused on the activation of persulfate on tourmaline surface-active sites leading to chemical degradation of organic pollutants (Zhang *et al*., 2021); the advantage of such process include possible repetitious use of tourmaline-based catalyst and non-radical degradation mechanism. Similarly, TGM (schorl) has been used as heterogeneous catalyst in Fenton-like reaction of wastewater discoloration (Xu *et al.*, 2009). In other studies, TGM are used as sorbents e.g., for extraction of Cu(II), Pb(II), Zn(II) and Cd(II) from aqueous solutions (Jiang *et al.*, 2006). Furthermore, TGM

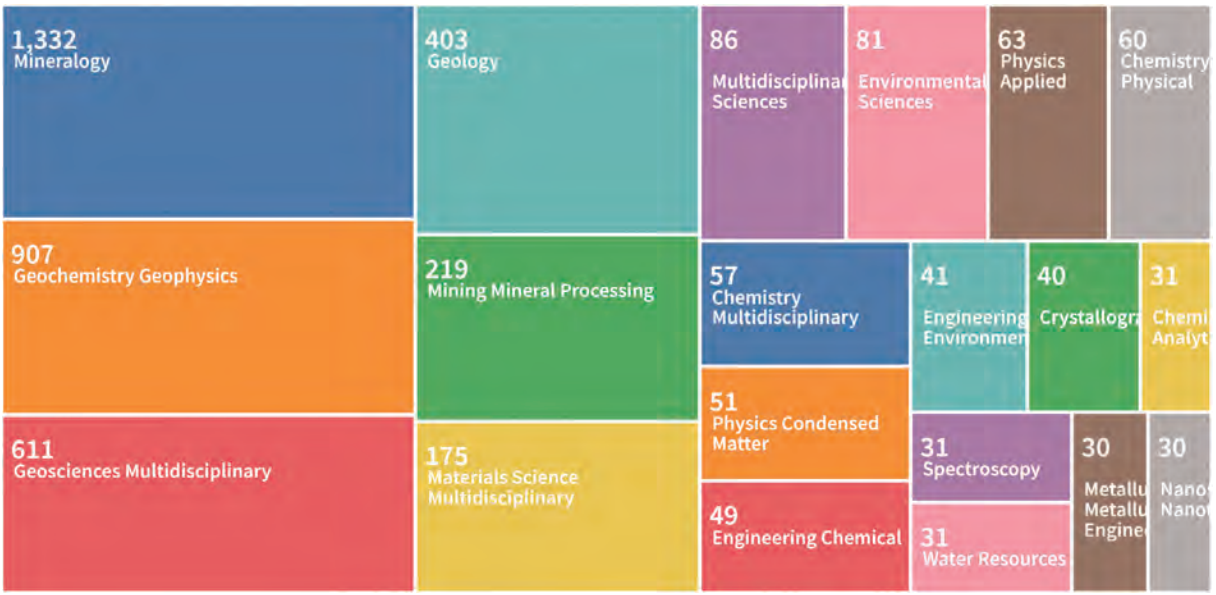

Fig. 1 - Coverage of tourmaline topics in various categories of research (data derived from Web of Science, July 8, 2021).

Regional Centre of Advanced Technologies and Materials, Czech Advanced Technology and Research Institute (CATRIN), Palacký University Olomouc, Šlechtitelů 27, Olomouc, Czech Republic.
E-mail: jan.filip@upol.cz

are used in various (nano)composites (Fig. 2) designed as heterogeneous catalysts for broad range of environmental technologies, namely for the efficient (photo)degradation of organic pollutants (Sun *et al.*, 2021a).

Besides above-mentioned research fields, tourmaline is used e.g. in ceramics for curling irons and other personal-care electronics/products where reduction of static electricity is needed, in conductometric sensors for gas detection (Sun *et al.*, 2021b), in infrared-radiation heating textiles (Tian *et al.*, 2021), and also in biocosmetics, alternative medicine and therapy etc. In this contribution, the most important applications of TGM will be reviewed and presented in relation to specific properties of tourmaline structure.

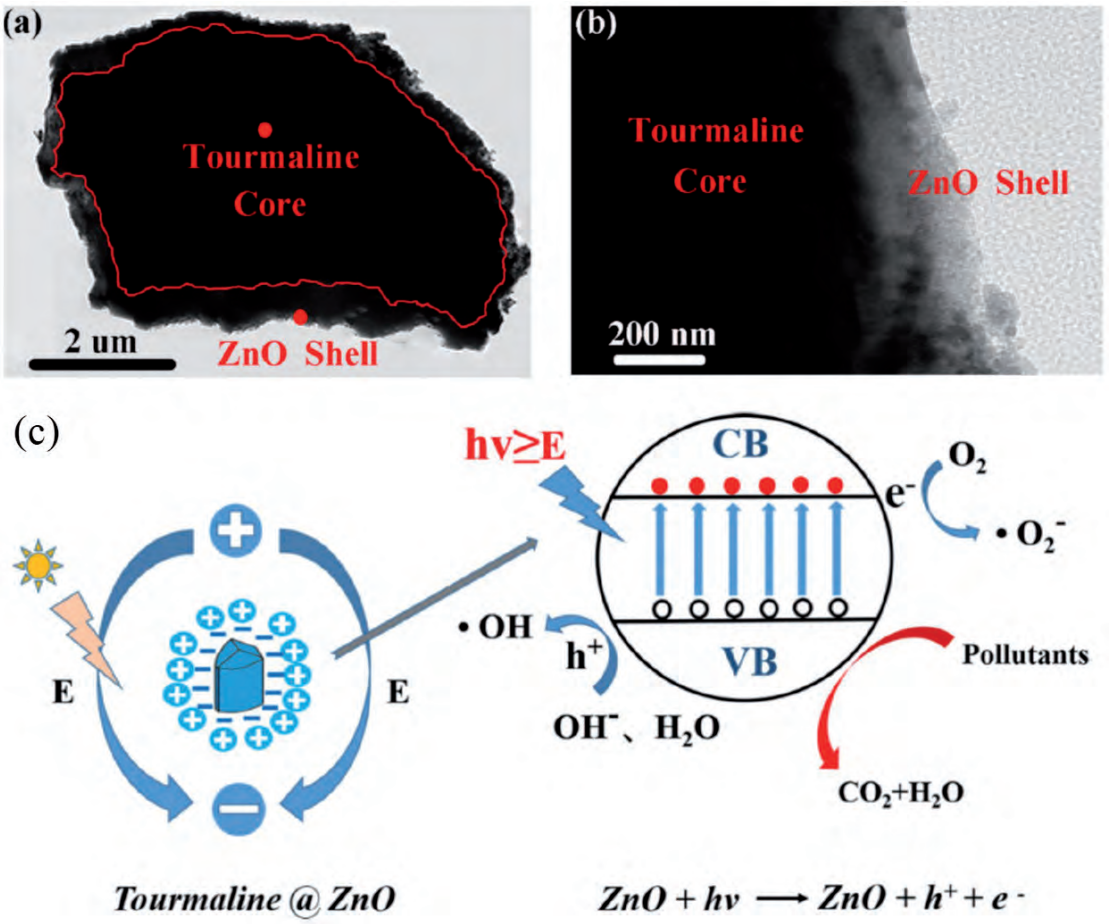

Fig. 2 - Illustration of tourmaline@ZnO nanocomposite (a, b) and mechanism of their photocatalytic reaction with pollutants (c). Adapted from Sun *et al.*, 2021a.

REFERENCES

Henry D. J. & Dutrow B. L., 2018 – Tourmaline studies through time: contributions to scientific advancements. *Journal of Geosciences*, 63: 77-98. <doi: 10.3190/jgeosci.255>

Jiang K., Sun T. H., Sun L. N. & Li H. B., 2006 – Adsorption characteristics of copper, lead, zinc and cadmium ions by tourmaline. *Journal of Environmental Sciences*, 18 (6): 1221-1225. <doi: 10.1016/S1001-0742(06)60066-1>

Sun L., Guo Y., Fu L., Hu Y., Pan S., Huang J. & Zhen Q., 2021a – Construction of the Core–Shell Tourmaline@ZnO Micro-nano Structure Towards the Highly Efficient Degradation of Organic Pollutants. *Journal of Electronic Materials*, 50: 3885-3896. <doi: 10.1007/s11664-021-08894-9>

Sun L., Guo Y., Hu Y., Pan S. & Jiao Z., 2021b – Conductometric n-butanol gas sensor based on Tourmaline@ZnO hierarchical micro-nanostructures. *Sensors & Actuators: B. Chemical*, 337: 129793. <doi: 10.1016/j.snb.2021.129793>

Tian T., Wei X., Elhassan A., Yu J., Li Z. & Ding B., 2021 – Highly flexible, efficient, and wearable infrared radiation heating carbon fabric. *Chemical Engineering Journal*, 417: 128114. <doi: 10.1016/j.cej.2020.128114>

Xu H. Y., Prasad M. & Liu Y., 2009 – Schorl: A novel catalyst in mineral-catalyzed Fenton-like system for dyeing wastewater discoloration. *Journal of Hazardous Materials*, 165 (1-3): 1186-1192. <doi: 10.1016/j.jhazmat.2008.10.108>

Zhang Y., Zhao H., Wen J., Ding S. & Wang W., 2021 – Insights into the nonradical degradation mechanism of antibiotics in persulfate activation by tourmaline. *Separation and Purification Technology*, 270: 118772. <doi: 10.1016/j.seppur.2021.118772>

Differentiating tourmaline species via reflectance spectroscopy: enhancing tourmaline as a mineral vector in ore deposits

Bill Fischer[1,2]*, Daniel Marshall[1], Dean Riley[3], Scott Hiebert[3]

The A.M. breccia is part of the Giant Copper deposit of southern British Columbia. It is the only well-defined zoned-tourmaline breccia pipe in the Canadian Cordillera. The A.M. breccia shares similarities with other tourmaline breccia pipes, most notably the tourmaline breccia pipes of Chile and Peru. Similarities can also be drawn to tourmaline breccia pipes of the Cascadia arc. Tourmaline is a hallmark alteration mineral within the A.M. breccia and is spatially associated with Cu. Observed changes in tourmaline chemistry range from alkali-rich (schorlitic-dravitic) to calcic-rich (feruvitic-uvitic). Tourmaline sub-species appear dependent on their spatial location to the A.M. breccia. Tourmalines outside of the pipe contain higher Mg^{2+} (dravitic-uvitic). Within the pipe tourmaline preferentially incorporates Fe^{2+} (schorlitic-feruvitic). However, these chemical variations are currently indistinguishable in hand specimens.

Spectral reflectance data were collected from 587 tourmaline grains to determine if discerning chemical changes in tourmaline can be determined in real-time and be made more cost-effective. Spectral reflectance clearly differentiates tourmaline associated with ore and ore-bearing breccia textures from tourmaline occurring distal to the pipe contact or within barren tourmaline breccia pipes. Fe-rich tourmaline within the A.M. breccia show spectral characteristics similar to end-member schorl (Fe-rich) spectrum first presented by Bierwirth (2006; Fig 1).

Fe-rich tourmaline demonstrates Mg-OH features above 2,361 and Fe-OH features greater than 2,253 nm, but never display Fe-OH and Mg-OH features below 2,253 and 2,361 nm, respectively. Tourmaline distal to the A.M. breccia and within Cu barren pipes demonstrate spectra similar to end-member dravite (Mg-rich). Mg-rich tourmaline have Fe-OH features less than or equal to 2,253 nm and Mg-OH features never exceed 2,361 nm (Fig. 2).

Tourmaline spectral data demonstrate that tourmaline sub-species can be identified via spectral reflectance; proving that spectral reflectance data can be a cost-effective and time-saving alternative to monitoring chemical changes in tourmaline within and around an ore deposit. Although chemical variation in tourmaline is not always present in an ore system, determining tourmaline variants spectrally can quickly and efficiently determine if tourmaline is a worthy mineral vector for an exploration project.

Airborne spectral data via remote drone was also successful at identifying a tourmaline anomaly confined to

[1] Simon Fraser University, Burnaby, British Columbia, Canada.
[2] Imperial Metals Corporation, Vancuver, British Columbia, Canada.
[3] EchoLabs, Vancuver, British Columbia, Canada.

* Corresponding author: wtfische@sfu.ca

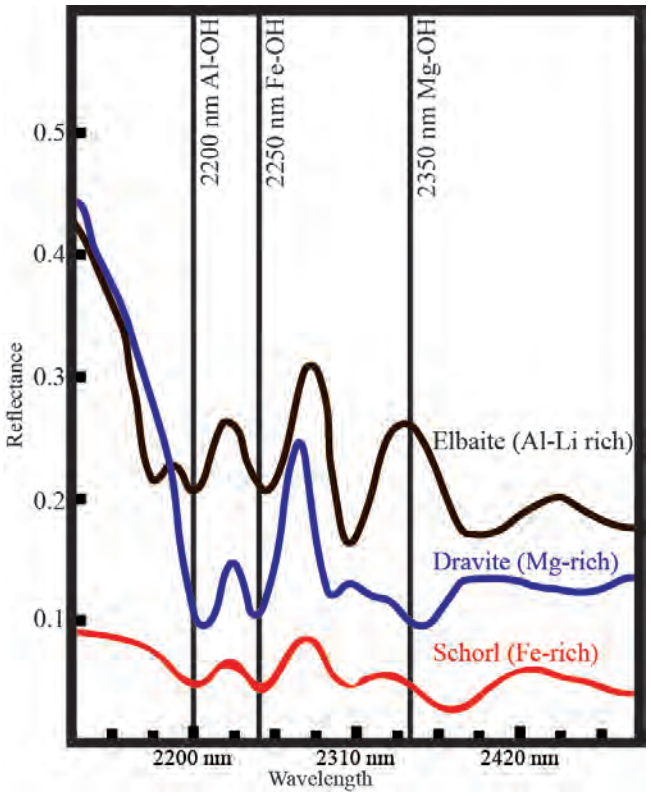

Fig. 1 - Short-wave infrared (SWIR) spectra of end-member alkali-rich tourmalines; schorl, dravite and elbaite. (Figure modified from Bierwirth, 2006).

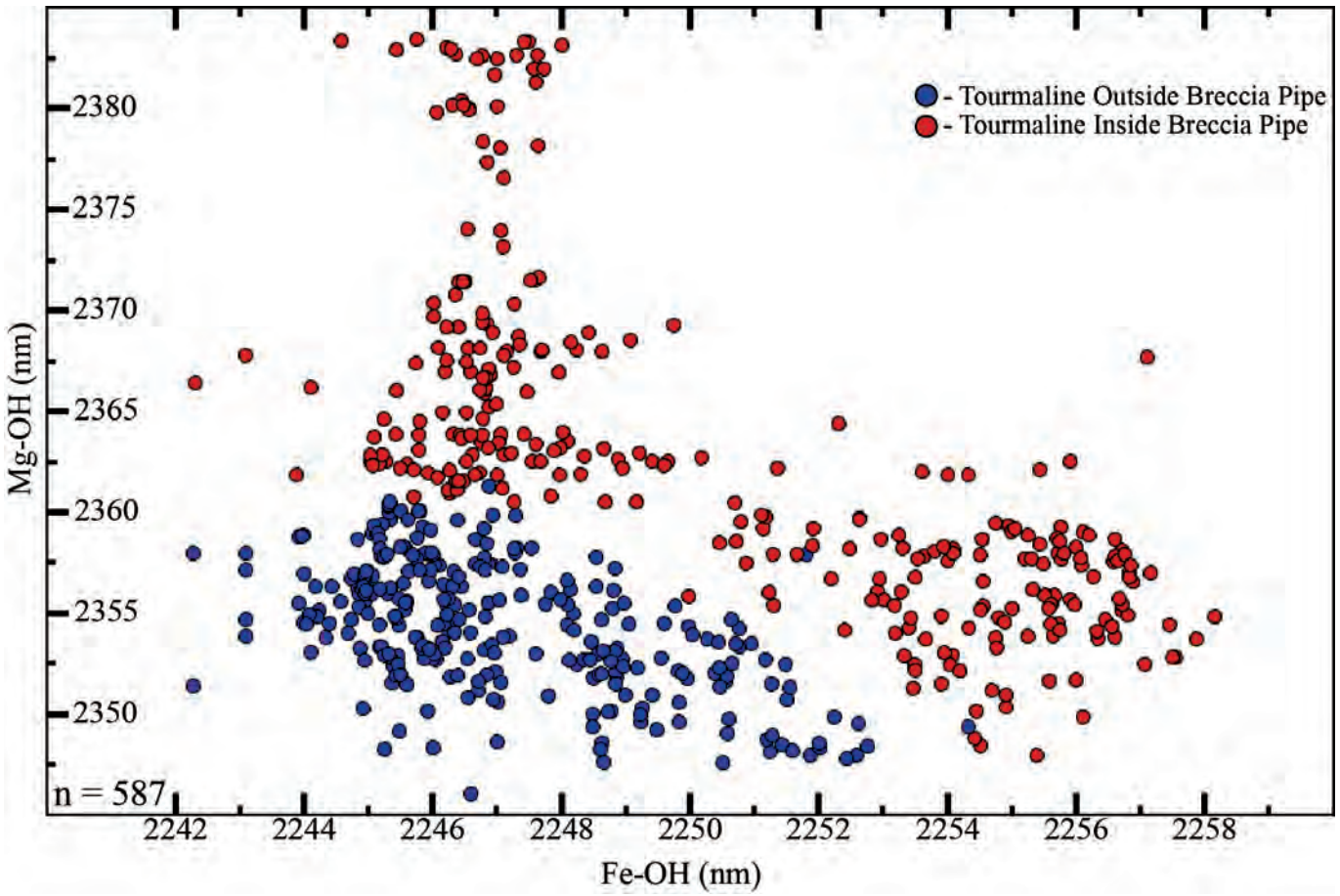

Fig. 2 - Fe-OH vs. Mg-OH plot for tourmaline within and distal to the A.M. breccia pipe.

Tab. 1 - Characteristic of Tourmaline Spectra.

Name	A1-OH Absorption Feature	Fe- OH Absorption Feature	Mg-OH Absorption Feature
Tourmaline Outside Breccia Pipe	2199.80 - 2209.62 nm	2242.27 - 2254.32 nm	2346.10 - 2361.34 nm
Tourmaline Inside Breccia Pipe	2201.26 - 2212.27 nm	2242.30 - 2258.16 nm	2247.99 - 2383.47 nm

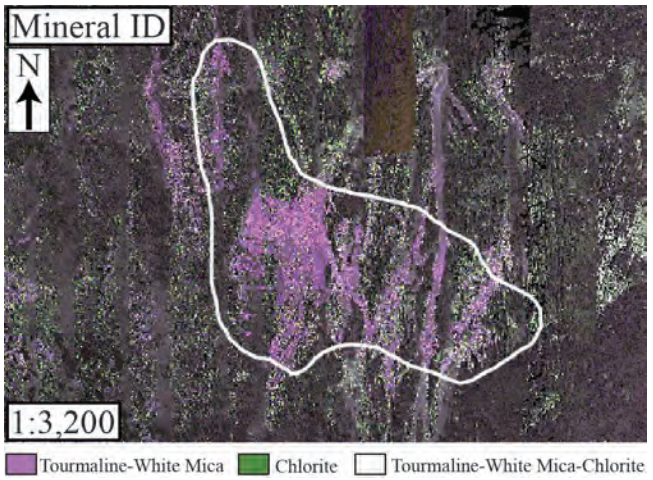

Fig. 3 - False color mineral map displaying dominant minerals at and around the A.M. breccia. White outline represents A.M. breccia contact.

the A.M. breccia (Fig. 3). The identification of tourmaline via an airborne spectral survey can quickly identify new tourmaline breccia pipes at Giant Copper and other tourmaline-associated ore deposits regionally.

REFERENCES

Bierwirth P. N., 2006 − Laboratory and Imaging Spectroscopy of Tourmaline - A Tool for Mineral Exploration. Internal Report. *Defence Imagery and Geospatial Organisation*: 1-12.

Spectroscopic and crystal-chemical study of brown, red and green magnesium-dominant tourmalines

Jana Fridrichová[1]*, Peter Bačík[1,2], Andreas Ertl[3], Radek Škoda[4]

Dravite is the most common Mg-bearing tourmaline-supergroup mineral, which belongs to the alkali tourmalines (Henry *et al*., 2011). It was firstly described by G. Tschermak (1884) in his publication *Lehrbuch der Mineralogie* as a tourmaline rich in Mg and Na, and named it after the Drava river, which flows near the type-locality near Dobrova (today Slovenia), which was part of the Austro-Hungarian Empire (Ertl, 2007). Tschermak (1884) described the chemical composition corresponding to the formula $NaMg_3(Al,Mg)_6B_3Si_6O_{27}(OH)$, which (exception made for the OH) is in very good agreement with the present formula of dravite.

Fluor-uvite, originally defined by Kunitz (1929), was considered to have the following ideal formula: $CaMg_3(Al_5Mg)(Si_6O_{18})(BO_3)_3(OH)_4$. This formula was based on the examination of tourmalines from Uva (Sri Lanka), De Kalb (New York) and Gouverneur (New York), with OH contents of approximately 4 *apfu*. However, all the other analyses performed on the samples from these localities showed a F range of 0.5 –1.0 *apfu*. Dunn *et al*. (1977) designated a sample of uvite from Uva (Sri Lanka) as a neotype, with an anion content of $OH_{2.90}F_{0.76}O_{0.34}$.

The W site would be dominated by F and uvite should have been described as an F-endmember, thus it was renamed as fluor-uvite (Henry *et al*., 2011).

Dravitic and uvitic tourmalines display a relatively large colour variability if their Fe content is limited. Brown dravite was found e.g. in the Gemerská Poloma (Slovakia), Yinnietharra Station (Australia), Jajarkot district (Nepal), Escadinha mine (Minas Gerais, Brazil), Sahatany Pegmatite Field (Madagascar). Red (along with green and brown) uvite occurs on its type locality at Brumado mine (Bahia, Brazil).

Specific colour varieties typical for Mg-rich tourmalines are shades of green. Green tourmalines can be divided in two groups according to their chemical composition: V- and Cr-enriched (with typical emerald green colour) and V- and Cr-poor (greyish green to green colour). Emerald-green tourmalines, often named as "chrome-dravite", occur e.g. in Landanai (Arusha Region, Tanzania) and Pyant Gyi mine (Mandalay Division, Myanmar). Green to brown-green tourmalines occur in Lengenbach quarry (Switzerland). Green to grayish-green tourmaline crystals occur in the Forshammar pegmatite (Sweden).

The tourmaline from Gemerská Poloma is almost homogeneous and has a dravitic composition with very high X_{Mg} (0.95 – 0.96), a very low *X*-site vacancy (up to 0.17) and Ca content (up 0.05 *apfu*). The Fe content is also very low (up to 0.14 *apfu*), and the content of Al varies between 5.97 and 6.27 *apfu*. The dravite from Yinnietharra Station is magnesium-dominant (2.74 Mg *apfu*, 0.06 Fe *apfu*) with a relatively high content of Ti (0.13 *apfu*). The dravite from Jajarkot district is also strongly magnesium-dominant (2.52 Mg *apfu*, 0.05 Fe *apfu*) and slightly enriched in Al (total Al equals to 6.34 *apfu*). Brown dravites found in Escadinha mine (2.47 Mg *apfu*, 0.04 Fe *apfu*, total Al 6.41 *apfu*) and in Sahatany Pegmatite Field (2.46 Mg *apfu*, 0.07 Fe *apfu*, total Al = 6.45 *apfu*) are chemically very similar to the abovementioned occurrences.

In comparison to the other studied Mg-dominant tourmalines, the red uvite from Brumado mine (Bahia, Brazil) has an increased content of Fe (0.50 *apfu*), Mg attains to 2.92 *apfu*. Interestingly, a part (at least 0.03 *apfu*) of iron might be trivalent according to the calculation of charge-balanced formula, which along with the slightly increased content of Ti (0.06 *apfu*) could have an impact on the colour of uvite.

Although the markedly green colour of tourmalines from Landanai and Pyant Gyi mine suggest the presence of Cr, it is only a minor element attaining max. 0.03 *apfu* in Pyant Gyi mine and 0.04 *apfu* in Landanai. The content of V is more significant: ~ 0.04 *apfu* in Pyant Gyi mine and 0.14 *apfu* in Landanai. Thus, this composition is very far from "chrome-dravite" or "vanadium-dravite". Moreover, none of the tourmalines from both localities is

[1] Comenius University, Faculty of Natural Sciences, Department of Mineralogy, Petrology and Economic Geology, Ilkovičova 6, 842 15 Bratislava, Slovakia.
[2] Earth Science Institute of the Slovak Academy of Sciences, Dúbravská cesta 9, P.O. BOX 106, 84005 Bratislava, Slovakia.
[3] Institut für Mineralogie und Kristallographie, Universität Wien, Althanstrasse 14, 1090 Wien, Austria.
[4] Masaryk University, Department of Geological Sciences, Kotlářská 2, 611 37 Brno, Czech Republic.

* Corresponding author: jana.fridrichova@uniba.sk

a dravite at all because their composition (studied only on one sample for each locality) corresponds to uvite (Ca = 0.76 *apfu* in Pyant Gyi mine and 0.57 *apfu* in Landanai). Both uvites are strongly Mg-dominant (3.58 Mg *apfu*, Fe below detection limit in Pyant Gyi mine and 3.31 Mg *apfu*, 0.002 Fe *apfu* in Landanai).

Green to brown-green tourmaline from Lengenbach contains 2.82 Mg *apfu*, 0.09 Fe *apfu*, 0.07 Ti *apfu*, and 0.02 V *apfu*.

The dravite from Forshammar displays chemical zoning with high Mg/(Mg+Fe) value which decreases from core (~0.85) to intermediate zone (0.76-0.79) but increases in the rim and vein tourmaline (0.93). The core has the highest proportion of *X*-site vacancies and Al content, while the intermediate zone is the most enriched in Fe and Na. The rim is slightly depleted in Al and has the highest content of Na compared to the inner zones. Tourmaline veins crosscut the pre-existing tourmaline and are relatively more enriched in Na and Ca.

Based on powder XRD and structure refinement, uvitic samples from Brumado mine and Landanai, along with dravitic samples from Yinnietharra Station, have *c* parameter higher than 7.20 Å, which indicates a significant abundance of Mg at Z site. However, all the samples have $c > 7.17$ Å; therefore, some proportion of ^{Z}Mg is very likely to occur in all samples.

The optical spectra of the studied samples clearly manifested their division into two groups. Brown and red tourmalines have a strong absorption (absorption edge?) in the blue and green regions, in the red uvite from Brumado it spreads to the yellow region. This results from Fe^{2+}–Ti^{4+} intervalence charge transfer transitions (IVCT transitions) at around 470 nm (21,200 cm^{-1}). In the Brumado sample, which contains around a ten times higher amount of Fe, the Fe^{2+}–Fe^{3+} IVCT band at around 525 nm (ca. 19,000 cm^{-1}) shifts the absorption edge to the yellow region. An additional band at around 730-750 nm (13,300-13,700 cm^{-1}) results from $^{5}T_{2g} \rightarrow {}^{5}E_{g}$ electronic transition on $^{Y}Fe^{2+}$ or $^{Y}Fe^{2+}$-$^{(Y,Z)}Fe^{3+}$exchange-coupled pair.

The optical spectra of green tourmalines have similar features with two distinct bands at 600-614 nm and 445-469 nm. These can be assigned to $^{4}A_{2g}(^{4}F) \rightarrow {}^{4}T_{1g}(^{4}F)$ a $^{4}A_{2g}(^{4}F) \rightarrow {}^{4}T_{2g}(^{4}F)$ electronic transitions in Cr^{3+} and $^{3}T_{1g}(^{4}F) \rightarrow {}^{3}T_{2g}(^{4}F)$ and $^{3}T_{1g}(^{4}F) \rightarrow {}^{3}T_{1g}(^{4}F)$ in V^{3+}.

The colour of dravite, just like the colour of other minerals, is the result of a combination of structural properties (e.g. short-range order) and chemical composition (the presence of typical chromophores). The low content of iron and titanium is typical for coloured dravites. High Fe^{3+} and Ti^{4+} contents cause dark (macroscopically black) colour of Fe-rich tourmalines (e.g., da Fonseca-Zang *et al*., 2008). Therefore, most of the tourmalines with an intermediate composition between schorl and dravite are macroscopically black. However, although the content of the abovementioned elements may be low, it could influence the dravite colour. It has been shown that blue colour in tourmaline is related to the spin-allowed crystal field transitions of Fe^{2+} in deformed octahedral sites while usual IVCT transitions (Fe^{2+}-Ti^{4+}, Fe^{2+}-Fe^{3+}) are responsible for brown and red-brown colour (e.g., da Fonseca-Zang *et al*., 2008). Brown tourmalines from Gemerská Poloma, Jajarkot, Escadinha mine, Yinnietharra, Sahatany and Brumado are relatively richer in Ti (0.05-0.13 *apfu*), thus their colour may be the result of Fe^{2+}-Ti^{4+} (and in Brumado also Fe^{2+}-Fe^{3+}) IVCT transitions. The reason for the greyish-green colour of the dravite from Forshammar is still unknown and cannot be estimated from the available data. The intensely-green colour of dravite, as the samples from Pyant Gyi Mine and Landanai show, can be caused by the presence of vanadium and/or chromium, as it is observed in other silicates such as beryl (variety emerald), uvarovite and goldmanite from the garnet group (Nassau, 1978). The colour of dravite from Lengenbach is probably the result of slightly increased Ti (Fe^{2+}-Ti^{4+} IVCT transitions responsible for brown shades) as well as V content (green shades).

This research was funded by the projects APVV–18–0065 and VEGA-1/0137/20.

REFERENCES

da Fonseca-Zang W. A., Zang J. W. & Hofmeister W., 2008 – The Ti-influence on the tourmaline colour. *Journal of Brazilian Chemical Society*, 19: 1186-1192.

Dunn P. J., Appleman D., Nelen J. A. & Norberg J., 1977 – Uvite, a new (old) commom member of the tourmaline group and its implications for collectors. *Mineralogical Record*, 8 (2): 100-108.

Ertl A., 2007 – Über die Typlokalität und die Nomenklatur des Minerals Dravit. *Mitteilungen der Österreichischen Mineralogischen Gesellschaft*, 153: 265-271.

Henry D., Novák M., Hawthorne F. C., Ertl A., Dutrow B., Uher P. & Pezzotta F., 2011 – Nomenclature of the tourmaline supergroup-minerals. *American Mineralogist*, 96: 895-913.

Kunitz W., 1929 – Beiträge zur Kenntnis der magmatischen Assoziationen. I. Die Mischungsriehen in der Turmalingruppe und die genetischen Beziehungen zwischen Turmalinen und Glimmern [hypothetical end member]. *Chemie der Erde*, 4: 208-251.

Nassau K., 1978 – The origins of color in minerals. *American Mineralogist*, 63: 219-229.

Tschermak G., 1884 – Lehrbuch der Mineralogie, IX. *Alfred Hölder*, Wien.

Tourmalines from exocontact and endocontact zones from the Manjaka pegmatite, Sahatany Valley, Madagascar

Petr Gadas[1]*, Milan Novák[1], Jan Filip[2], Václav Mandovec[1]

Tourmalines are indicators of a variety of geological processes due to their ability to incorporate large number of elements and refractory behaviour. They are highly compatible with Mg; hence, they are used as monitors of external contamination in granitic pegmatites from host rocks (e.g., Novák, 2013; Novák *et al*., 2017).

The Manjaka pegmatite is an excellent example of pegmatite where tourmalines are locally developed in the exocontact and endocontact of the pegmatite enclosed in calc-silicate rock. The pegmatite forms an EW-trending elongated body, 0.5 to 2 m thick, of a complicated shape (Fig. 1a). Typical major to minor minerals include albite > K-feldspar, quartz, tourmaline (black, brown, yellow, red, pink), and spodumene (colorless to pinkish; localy replaced by boralsilite and/or vránaite, Cempírek *et al*., 2016) and numerous accessory minerals e.g., fluorapatite, Cs-rich beryl, columbite-tantalite, pollucite, rhodizite-londonite; however, micas are almost absent (Simmons *et al*., 2001). Pegmatite crosscut or was emplaced along the foliation (Fig. 1a) of a strongly deformed, Mg-rich, calc-silicate rock consisting of diopside ($Di_{94-100}Hd_{0-4}Jhs_{0-4}$), plagioclase ($An_{26-32}$), K-feldspar ($Kfs_{73-96}Ab_{1-10}Cls_{0-26}$), phlogopite, tremolite, dolomite, quartz, and tourmaline. Contacts are often sharp; locally a narrow zone with common dark zoned brown to yellow tourmaline (Ca-rich dravite to Na-rich uvite), is developed in exocontact (Figs. 1b, 2a-b) as subhedral grains, 0.1-0.2 mm in size, in the matrix consisting of diopside, plagioclase, K-feldspar, phlogopite, tremolite, and rare dolomite. Prismatic yellow to red zoned crystals (elbaite to fluor-elbaite), up to ~1 cm long, crystallized from contact inwards.

We examined tourmalines on two profiles from endocontact to exocontact. Chemical composition of tourmaline in Fig. 3 shows that tourmaline from endocontact evolves from Fe,Mn-rich elbaite core with low Mg (< 0.19 apfu) to Mg-free elbaite to fluor-elbaite in rim. Both tourmalines have low to moderate Ca (< 0.17 apfu). Heterogeneous grains of uvite-dravite from exocontact contain variable Ca (0.09-0.65 apfu) and Na (0.26-0.805 apfu) but almost constant and high Mg (2.28-3.28 apfu). The substitutions $2R^{2+}$ = LiAl and NaAl = CaMg dominate in endocontact- and exocontact-tourmalines, respectively.

Common tourmaline in exocontact and accessory minerals (e.g., Cs-beryl, microlite, Ta-rich titanite) show

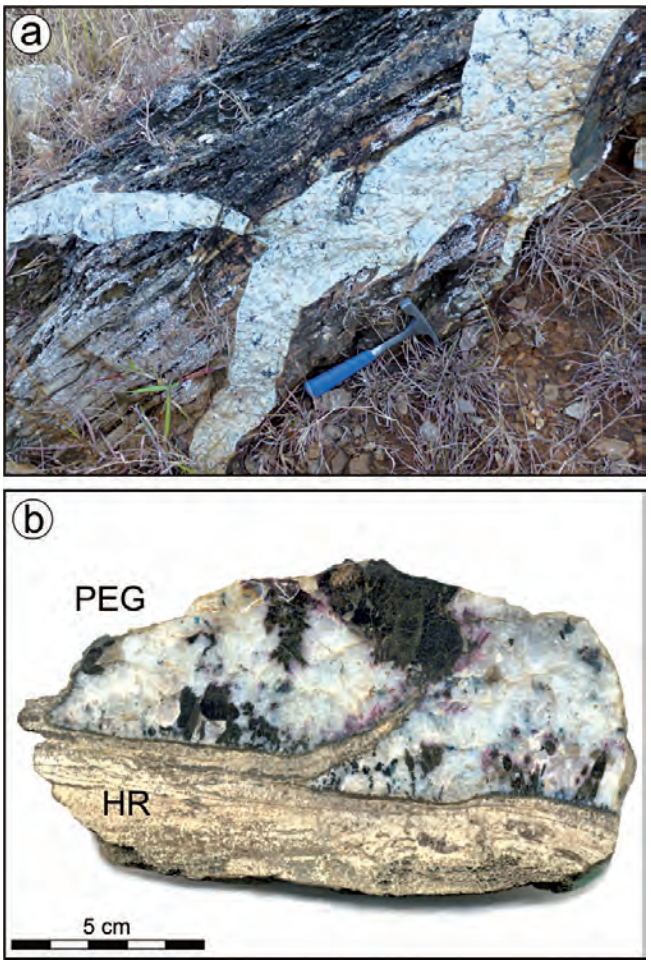

Fig. 1 - a) Apophyses of pegmatite; b) hand-size polished sample of contact of pegmatite and host rock.

[1] Department of Geological Sciences, Masaryk University, Brno, Czech Republic.
[2] Regional Centre of Advanced Technologies and Materials, Palacký University, Olomouc, Czech Republic.

* Corresponding author: gadas@sci.muni.cz

that fluids rich in B, Ta, Be, Cs escaped from pegmatite melt and facilitated origin of the exocontact assemblage with dominant newly formed tourmaline. Low concentrations of Mg in cores of zoned elbaite crystals show low Mg in the pegmatite melt which likely was not contaminated from host rock in situ during pegmatite melt emplacement. Magnesium in tourmaline cores from endocontact was likely sourced during early contamination - pre-emplacement stage as well as Ca in core and rim (see Novák, 2013).

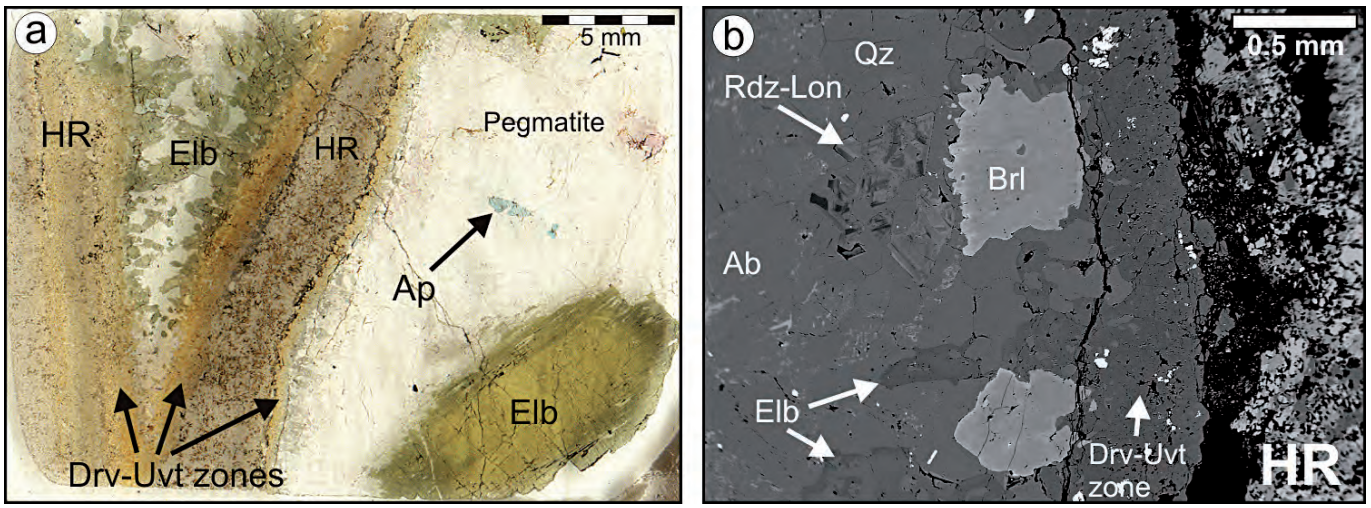

Fig. 2 - a) Thin-section through the contact of pegmatite and host rock; b) BSE image of the contact of pegmatite and host rock (HR).

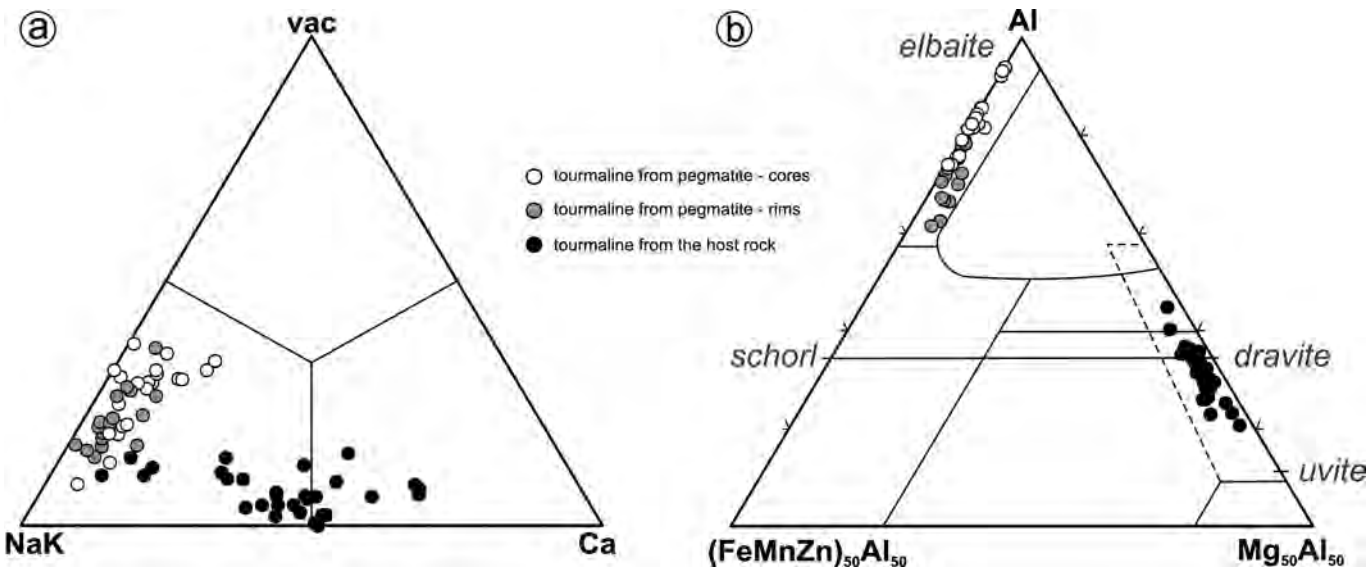

Fig. 3 - a) Chemical composition of tourmalines from pegmatite and from host rock in the X-site diagram (upper) and b) Y+Z-sites using the Al - Fe(+Mn, Zn) - Mg diagram of Henry & Guidotti (1985).

REFERENCES

Cempírek J., Grew E. S., Kampf A. R., Chi Ma, Novák M., Gadas P., Škoda R., Vašinová-Galiová M., Pezzotta F., Groat L. A. & Krivovichev S. V., 2016 – Vránaite, ideally $Al_{16}B_4Si_4O_{38}$, a new mineral related to boralsilite, $Al_{16}B_6Si_2O_{37}$, from the Manjaka pegmatite, Sahatany Valley, Madagascar. *American Mineralogist*, 101: 2108-2117.

Henry D. J. & Guidotti C. V., 1985 – Tourmaline as a petrogenetic indicator mineral - an example from the staurolite-grade metapelites of NW Maine: *American Mineralogist*, 70: 1-15.

Novák M., 2013 – Contamination processes in complex granitic pegmatites. *PEG 2013. Contribution to the 6th International Symposium on Granitic Pegmatites*: 100-103.

Novák M., Prokop J., Losos Z. & Macek I., 2017 – Tourmaline, an indicator of external Mg-contamination of granitic pegmatites from host serpentinite; examples from the Moldanubian Zone, Czech Republic. *Mineralogy and Petrology*, 111, 625-641.

Simmons W. B., Pezzotta F., Falster A. U. & Weber K. L., 2001 – Londonite, a new mineral species: the Cs-dominant analogue of rhodizite from Antadrokomby granitic pegmatite, Madagascar. *The Canadian Mineralogist,* 39, 747-755.

Gem deposit research and implications for exploration

Lee A. Groat

Gems have been prized for millenia for their color, luster, transparency, durability, and high value to volume ratio. However, gems are also of scientific interest because their deposits are evidence of unusual geological conditions; e.g., emeralds are rare because they require Be and Cr (and/or V), which concentrate in very different environments.

Gem deposits can also provide important tectonic information. Stern *et al.* (2013) noted that jadeitite deposits form in subduction zones, and ruby and sapphire form where continental plates collide; all are "Plate Tectonic Gemstones", and ruby in particular is "a robust indicator of continental collision" (Stern *et al.*, 2013).

Gem deposits may be classified according to the geological environment in which they formed: magmatic (e.g., diamond from kimberlite), hydrothermal (e.g., tourmaline in pegmatite), metamorphic (e.g., ruby in marble), sedimentary (e.g., opal), and alluvial (e.g., diamond in placers). Some gem deposits, notably sapphire and emerald, can form via either magmatic or metamorphic processes. For example, although most emerald deposits are associated with granitic intrusions ("tectonic-magmatic related" in the classification scheme of Guiliani *et al.*, 2019), in Colombia, which produces the world's finest emeralds, there is no evidence for magmatism. Instead, the gems formed as a result of hydrothermal growth associated with tectonic activity ("tectonic-metamorphic related in a sedimentary environment" in Giuliani *et al.*, 2019).

Although gems are valuable, little has been done to establish exploration protocols for gem materials other than diamond. Studies of known occurrences are an important foundation for the development of exploration guidelines. Such studies can also define the compositional range of the gems for use in origin determination, a service that is seeing increased demand in the gem trade.

For several decades the author has studied colored gem deposits in Canada in order to ascertain how they formed, determine what they can tell us about the local and regional geology, and develop exploration guidelines for use in Canada and elsewhere.

Ercit *et al.* (2003) suggested that gem elbaite crystals (Fig. 1) occurring in miarolitic cavities in pegmatites of the O'Grady batholith, Northwest Territories, formed through differentiation of parental melts that sequentially produced hornblende granite, pegmatititc granite, and pegmatite. The pegmatites were classified as mixed NYF + LCT by Černý & Ercit (2005). Future exploration should concentrate on unexplored parts of the batholith, on satellite dikes, and on other members of the Selwyn plutonic suite.

Fig. 1 - Elbaite (10 cm in longest dimension) from the O'Grady pegmatites, Northwest Territories, Canada. (Photo: B.S. Wilson).

Department of Earth, Ocean and Atmospheric Sciences, University of British Columbia, 2020-2207 Main Mall, Vancouver, BC V6T 1Z4, Canada.
E-mail: lee.groat@ubc.ca

Fig. 2 - Left: pink sapphire (2.1 cm long) in marble from the Goat claims, British Columbia, Canada. Right: 0.20 ct pink sapphire faceted from Goat claim material. Stone courtesy of B.S. Wilson. (Photos: M. J. Bainbridge).

Dzikowski *et al.* (2014) showed that ruby and pink sapphire (Fig. 2) at the Goat claims in British Columbia formed via the reaction muscovite → corundum + K-feldspar + H_2O at peak metamorphism. Approximately 120 km SE, our research into sapphire on the Blue Jay claims suggests that partial melting played a significant role in their formation. Our studies of these gem corundum occurrences suggest that future exploration should focus on the margins of the gneissic domes within metamorphic core complexes in the Omineca terrane.

For several sapphire occurrences on Baffin Island in Nunavut (Fig. 3), Belley *et al.* (2017) inferred that the protolith was dolomitic argillaceous marl and that the corundum formed via three equally important sequential metamorphic reactions: Corundum formation was made possible by three equally important sequential metamorphic reactions: (1) formation of nepheline, diopside, and K-feldspar (inferred) at granulite facies peak metamorphic conditions; (2) partial retrograde replacement of the peak assemblage by phlogopite, oligoclase, calcite, and scapolite (Me_{50}–Me_{67}) as a result of CO_2-, H_2O-, Cl-, F-bearing fluid influx at 1782.5 ± 3.7 Ma (P-T < 720 ºC, 6.2 kbar); and (3) retrograde breakdown of scapolite + nepheline (with CO_2- and H_2O-bearing fluid) to form albite, muscovite, corundum, and calcite. Belley *et al.* (2017) also showed that the most prospective areas for sapphire on Baffin Island are contiguous to the thrust fault separating the Lake Harbour Group and Narsajuaq terranes, where the retrograde amphibolite facies overprint of the granulite peak assemblages is most pervasive.

Belley & Groat (2019) described vivid blue, cobalt-enriched (0.03–0.07 wt.% CoO) spinel in metasedimentary rocks from two locations on Baffin Island (Fig. 4). Similar to the sapphire they are inferred to have formed under peak granulite facies metamorphic conditions. Belley & Groat (2019) suggested that marbles containing abundant metamorphosed dolomitic marl (magnesian calc-silicate) layers offer the best potential for gemstone discoveries on southern Baffin Island, and that meta-marl-rich units may be traceable stratigraphically.

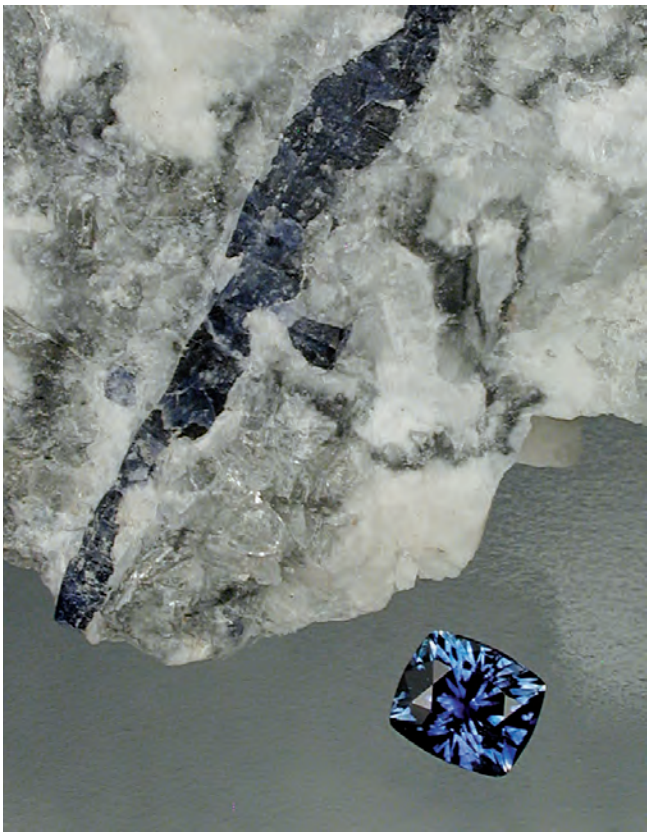

Fig. 3 - Sapphire crystal embedded in matrix (36 × 4 mm) and gem (1.17 ct) from Baffin Island, Nunavut, Canada. (Photo: B. S. Wilson

The author and his students have shown that the emerald occurrences Taylor 2 (Ontario), Lened (Northwest Territories), Tsa da Glisza (Yukon), and Anuri (Nunavut) are all associated with granitic intrusions ("tectonic-magmatic related" in Guiliani *et al.*, 2019). True North Gems Ltd. developed approximately 100 exploration targets from research on these occurrences and geochemical data; only 20 of the targets have been evaluated to date.

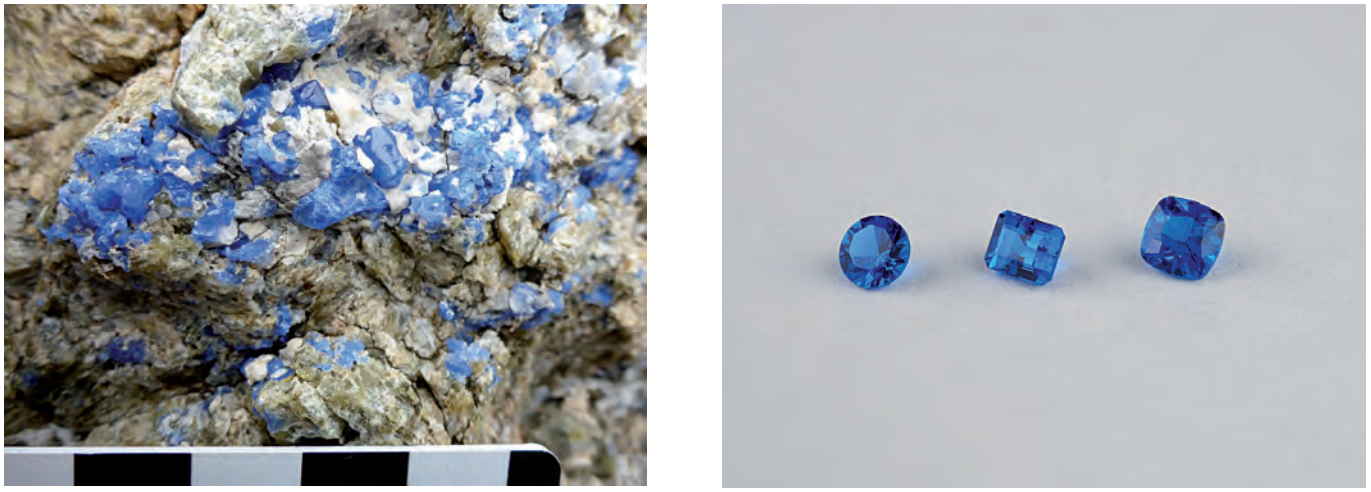

Fig. 4 - Left: cobalt-bearing spinel with white carbonate in metasedimentary rock, Baffin Island, Nunavut, Canada. Scale in cm. (Photo: author). Right: Cobalt-bearing spinel gemstones; the largest weighs 0.16 ct. Stones courtesy of B. S. Wilson. (Photo: T. Fa/Panotora).

Hewton *et al.* (2013) showed that the Mountain River occurrence in the Northwest Territories (Fig. 5) resulted from inorganic thermochemical sulfate reduction via the circulation of basinal brines through sedimentary rocks. Thus it is most likely "tectonic-metamorphic-related" (Giuliani *et al.*, 2019). Mountain River is the first confirmed occurrence of this type outside of Colombia and suggests that there is potential for Colombian-type emerald mineralization in NW Canada. The Mountain River discovery inspired Lake (2017) to learn the methods used to explore for emerald in Colombia and to apply them to the Yukon and Northwest Territories. He outlined a prospective area of >15,000 km^2.

Exploration will also continue to benefit from advances in technology. A number of studies have shown that ground penetrating radar can be used to explore for miarolitic cavities in pegmatites (Aranha *et al.*, 2018 and references therein). Companies exploring for sapphire on Baffin Island have used ultraviolet light to find coexisting scapolite, and imaging spectroscopy in the shortwave infrared region could also be used, as suggested by Turner *et al.* (2017). In order to efficiently explore for emerald in NW Canada, the author and his students are working on a method to determine the mineralogy and composition of individual particles in silt samples. Future exploration in many areas could benefit from the use of drones and geospatial analysis, as have been used to successfully explore for peridot in British Columbia (Belley *et al.*, 2020).

It is evident that there is much scope for future research on gem deposits, and it is expected that this will lead to a better knowledge of local and regional geology and more success in exploration.

Fig. 5 - Emerald in extensional quartz-carbonate veins, Mountain River occurrence, Northwest Territories, Canada. (Photos: D. J. Lake).

REFERENCES

Aranha P. R. A., Horn A. H. & Joncew H. C., 2018 – Use of GPR in pegmatite mining: example of a sheetlike body from northern Minas Gerais, Brazil. *Romanian Journal of Mineral Deposits*, 91 (1-2): 7-12.

Belley P. M. & Groat L. A., 2019 – Metacarbonate-hosted spinel on Baffin island, Nunavut, Canada: insights into the origin of gem spinel and cobalt-blue spinel. *The Canadian Mineralogist*, 57: 147-200.

Belley P. M., Dzikowski T. J., Fagan A., Cempírek J., Groat L. A., Mortensen J. K., Fayek M., Giuliani G. & Gertzbein P., 2017 – Origin of scapolite-hosted sapphire (corundum) near Kimmirut, Baffin Island, Nunavut, Canada. *The Canadian Mineralogist*, 55: 669-699.

Belley P. M., Shang P. & Lake D. J., 2020 – Gem exploration using a camera drone and geospatial analysis: a case study of peridot exploration in British Columbia, Canada. *Journal of Gemmology*, 37 (1): 80-90.

Černý P. & Ercit T. S., 2005 – The classification of granitic pegmatites revisited. *The Canadian Mineralogist*, 43 (6): 2005-2026.

Dzikowski T. J., Cempírek J., Groat L. A., Dipple G. M. & Giuliani G., 2014 – Origin of gem corundum in calcite marble: The Revelstoke occurrence in the Canadian Cordillera of British Columbia. *Lithos*, 198-199: 281-297.

Ercit T. S., Groat L. A. & Gault R. A., 2003 – Granitic pegmatites of the O'Grady batholith, N.W.T., Canada: A case study of the evolution of the elbaite subtype of rare-element granitic pegmatite. *The Canadian Mineralogist*, 41: 117-137.

Giuliani G., Groat L.A., Marshall D., Fallick A.E. & Branquet Y., 2019 – Emerald deposits: a review and enhanced classification. *Minerals*, 9 (2), 105.

Hewton M. L., Marshall D., Ootes L., Loughrey L. E., Creaser R. A. & Hanley J., 2013 – Colombian-style emerald mineralization in the northern Canadian Cordillera: Integration into a regional Paleozoic fluid flow regime. *Canadian Journal of Earth Sciences*, 50 (8): 857-871.

Lake D. J., 2017 – Are There Colombian-Type Emeralds in Canada's Northern Cordillera? Insights from Regional Silt Geochemistry, and the Genesis of Emerald at Lened, NWT. *M.Sc. thesis, University of British Columbia*, Vancouver, Canada.

Stern R. J., Tsujimori T., Harlow G. & Groat L. A., 2013 – Plate tectonic gemstones. *Geology*, 41: 723-726.

Turner D., Groat L. A., Rivard B. & Belley P. M., 2017 – Reflectance spectroscopy and hyperspectral imaging of sapphire-bearing marble from the Beluga occurrence, Baffin Island, Nunavut. *The Canadian Mineralogist*, 55: 787-797.

Tourmaline crystallography, crystal chemistry and nomenclature: current status

Darrell J. Henry*, Barbara L. Dutrow

Four years after the Tourmaline 2017 Conference and twenty-four years after the original Tourmaline Conference in 1997 (both in the Czech Republic), tourmaline studies remain a vibrant and evolving area of scientific endeavor. One indication of this ongoing interest is the sustained large numbers of tourmaline papers published over the years (Fig. 1). Many more papers involving tourmaline have been published in the last 24 years than in the previous 400 years.

With more complete determinations of the crystallography and chemical variability of tourmaline, tourmaline investigations have expanded to numerous disciplines. Two key concepts modified the way in which tourmaline is considered and classified (e.g., Henry & Dutrow, 2018). The first concept is that two distinct types of OH-bearing sites occur, the *V* and *W* sites, in which F^{1-} occupies only the *W* site and O^{2-} prefers that site. Consequently, the general chemical formula of tourmaline was revised to $X\,Y_3\,Z_6\,T_6\,(BO_3)_3\,O_{18}\,(V)_3\,(W)$, where the most common substituents are X = Na, Ca, K or □ (X-site vacancy); Y = Al, Li, Fe^{2+}, Mg, Mn^{2+}, Fe^{3+}, V^{3+}, Cr^{3+}, Ti^{4+}; Z = Al, Mg, Cr^{3+}, V^{3+} and Fe^{3+}; T = Si, Al, B; V = OH^{1-}, O^{2-} and W = F^{1-}, O^{2}, OH^{1-} (Hawthorne & Henry, 1999). X, Y, Z, T and B represent groups of cations that occupy the *X, Y, Z, T* and *B* sites, respectively, in the R3m tourmaline structure – note that the designated sites are italicized. The V-group anions occupy the *O(3)* anionic crystallographic site and the W-group anions occupy the *O(1)* crystallographic site. The second concept is that there are order-disorder phenomena involving cations across multiple cationic sites in tourmaline. This feature is especially common in tourmalines with dominant O^{2-} in the *W* site. These features lead the IMA Subcommittee on Tourmaline Nomenclature, chaired by Milan Novák, to establish tourmaline as a supergroup mineral with three *X*-site-based primary groups: alkali-, calcic- and *X*-site vacancy-groups (Henry *et al*., 2011). A guideline used to define tourmaline species was the dominant-valency rule; stating that in a relevant site the dominant ion of the dominant valence state is used for nomenclature purposes (Hatert & Burke, 2008). This principle has recently been the approach used to establish species by the IMA-CNMNC (Bosi *et al*., 2019). In the case of tourmaline, the number of tourmaline species has expanded greatly in the last 24 years from 13 species in 1997 to 38 species in 2021 (Fig. 2). Fittingly, Elba is the type or co-type locality of 5 tourmaline species.

Additional tourmaline species are certainly forthcoming. Experimental studies of tourmaline have suggested that tourmalines with other more unusual cations are likely. Berryman *et al*. (2015) synthesized "potassium-dravite" at UHP conditions at 4 GPa. This implies that K-dominance in magnesian tourmaline, such as found in maruyamaite, is likely a signal of UHP conditions. Vereshchagin *et al*. (2018, 2020) were able to synthesize Ni- and Pb-dominant tourmaline and further suggest that there is no crystallographic reason to exclude the occur-

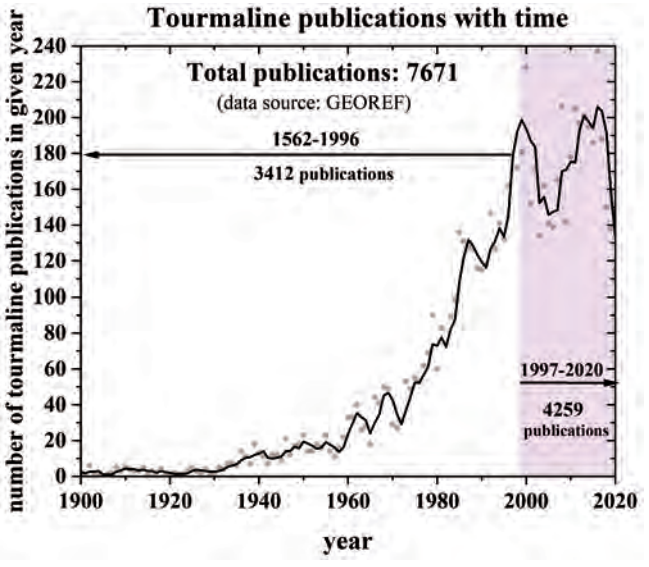

Fig. 1 - Numbers of papers published on various aspects of tourmaline (data from GEOREF). Data are from plotted for 1900 through 2020, but publications include those going back to 1562. The solid curve represents a 3-year running average of publications.

Department of Geology and Geophysics, Louisiana State University, Baton Rouge, Louisiana, USA.
E-mail: dutrow@lsu.edu

* Corresponding author: glhenr@lsu.edu

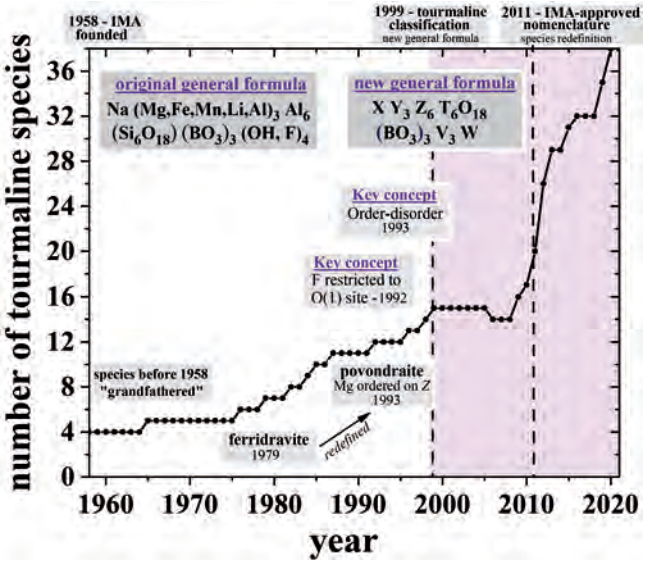

Fig. 2 - Number of tourmaline species from 1958 through 2020.

rence of Ni-, Co- and Cu-dominant tourmaline species. The primary impediment appears to be the unusual geochemical environments that must include boron and these cations. Studies of natural tourmaline establish that tourmalines enriched in Pb, Ni, Co and Cu do occur, but do not reach site dominance - yet (e.g., Henry & Dutrow, 2001; Baksheev & Kudryavtseva, 2004; Sokolov & Martin, 2009).

Tourmaline analytical challenges remain and specifically include easily accessible quantification of light elements (e.g., H, B, Li) and the oxidation states of Fe. In addition, evaluation of the order-disorder in tourmaline can be a significant issue (e.g., Bosi, 2018). Each of these factors potentially influences the proper classification of tourmaline. Fortunately, progress has been made either to estimate light elements through a variety of calculation schemes or to directly measure these cations through improving analytical approaches such as Mössbauer spectroscopy, SIMS, LA-ICPMS or LIBS. In addition, in some subsystems it may be possible to establish tourmaline species through simple graphical approaches (e.g., Fig. 3). Much progress has occurred and will continue into tourmaline's future.

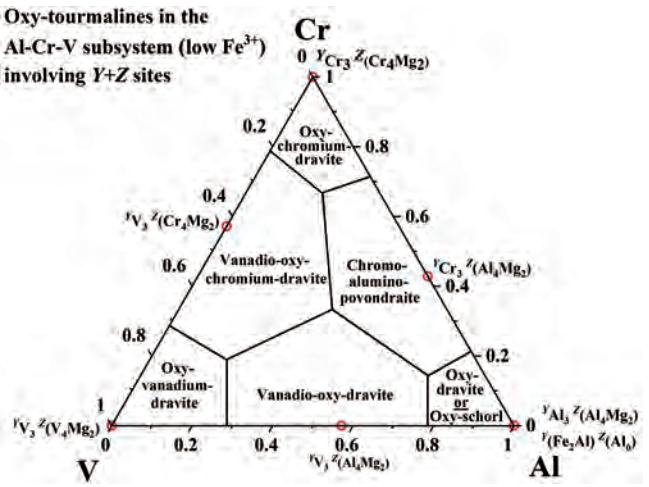

Fig. 3 - Graphical limits of oxy-tourmaline species in the Al-Cr-V subsystem considering Al-Cr-V over the sum of the *Y* and *Z* sites i.e., unnecessary to determine ordering to define species (Henry & Dutrow 2018; Bosi *et al*., 2020).

REFERENCES

Baksheev I. A. & Kudryavtseva O. E., 2004 − Nickeloan tourmaline from the Berezovskoe gold deposit, Middle Urals, Russia. *The Canadian Mineralogist*, 42: 1065-1078.

Berryman E., Wunder B., Wirth R., Rhede D., Schettler G., Franz G. & Heinrich W., 2015 − An experimental study on K and Na incorporation in dravitic tourmaline and insight into the origin of diamondiferous tourmaline from the Kokchetav Massif, Kazakhstan. *Contributions to Mineralogy and Petrology*, 169: 1-16.

Bosi F., 2018 − Tourmaline crystal chemistry. *American Mineralogist*, 103: 298-306.

Bosi F., Hatert F., Hålenius U., Pasero M., Miyawaki R. & Mills S. J., 2019 − On the application of the IMA−CNMNC dominant-valency rule to complex mineral compositions. *Mineralogical Magazine*, 83: 627-632.

Bosi F., Altieri A., Cámara F. & Ciriotti M. E., 2020 − Chromium-rich vanadio-oxy-dravite from the Tzarevskoye uranium–vanadium deposit, Karelia, Russia: a second world-occurrence of Al–Cr–V–oxy-tourmaline. *Mineralogical Magazine*, 84: 797-804.

Hatert F. & Burke E. A. J., 2008 − The IMA-CNMNC dominant-constituent rule revisited and extended. *The Canadian Mineralogist*, 46: 717-728.

Hawthorne F. C. & Henry D. J., 1999 − Classification of the minerals of the tourmaline group. *European Journal of Mineralogy*, 11: 201-216.

Henry D. J. & Dutrow B. L., 2001 − Compositional zoning and element partitioning in nickeloan tourmaline from a metamorphosed karstbauxite from Samos, Greece. *American Mineralogist*, 86: 1130-1142.

Henry D. J. & Dutrow B. L., 2018 − Tourmaline studies through time: contributions to scientific advancements. *Journal of Geosciences*, 63, 77-98.

Henry D. J., Novák M., Hawthorne F. C., Ertl A., Dutrow B. L., Uher P. & Pezzotta F., 2011 − Nomenclature of the tourmaline-supergroup minerals. *American Mineralogist*, 96: 895-913.

Sokolov M. & Martin R. F., 2009 − Evidence for the existence of a Pb-dominant member of the tourmaline group. *Eos, Transactions, American Geophysical Union*, 90 @Abstract MA31A-02.

Vereshchagin O. S., Frank-Kamenetskaya O. V., Rozhdestvenskaya I. V. & Zolotarev A. A., 2018 − Incorporation of 3d elements in tourmalines: structural adjustments and stability. *European Journal of Mineralogy*, 30 (5): 917-928.

Vereshchagin O. S., Wunder B., Britvin S. N., Frank-Kamenetskaya O. V., Wilke F. D. H., Vlasenko N. S. & Shilovskikh V. V., 2020 − Synthesis and crystal structure of Pb-dominant tourmaline. *American Mineralogist*, 105: 1589-1592.

Tourmaline-quartz development across the magmatic-to-hydrothermal transition in peraluminous granites from NW Argentina

Darrell J. Henry[1]*, Eduardo O. Zappettini[2], Barbara L. Dutrow[1]

Textural and chemical characteristics of tourmaline and quartz developed in tourmaline-rich orbicules, greisens, pegmatites and tourmalinite segregations associated with the peraluminous leucogranitic Tusaquillas Batholith Complex of NW Argentina exhibit both magmatic and subsolidus hydrothermal features. Tourmaline-bearing lithologies, irregularly distributed throughout the Tusaquillas Composite Batholith, are most commonly associated with late-stage magmatic-to-hydrothermal portions near the margins or apex of the plutonic complex (Fig. 1).

Imaging of quartz by optical-CL and SEM-CL show three developmental stages. Stage-1 quartz, considered likely magmatic, develops as large grains in pegmatites that have optical-CL homogeneity, as anhedral relict grains partially replaced by stage-2 quartz in tourmalinite segregations, orbicules and greisens, and as idiomorphic crystals with oscillatory zoning in SEM-CL in orbicules. Stage-2 quartz, interpreted as hydrothermal, partially replaces stage-1 quartz and generation-1 tourmaline. Stage-3 quartz, a late hydrothermal stage, occurs as weakly luminescing quartz in healed quartz fractures with abundant fluid inclusions, commonly associated with the crystallization of irregular late-stage tourmaline (Fig. 2).

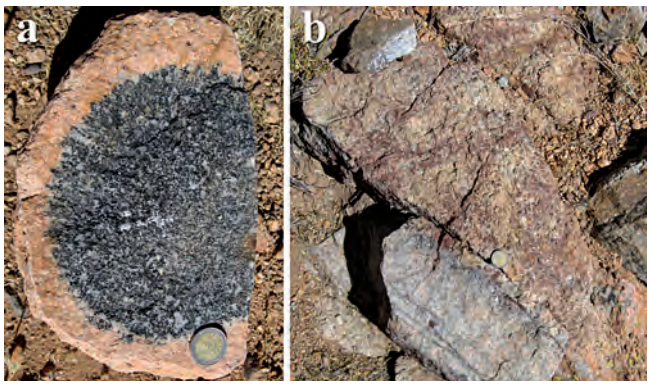

Fig. 1 - Outcrop images of two tourmaline-bearing lithologies. (a) Tourmaline-rich orbicule embedded in granite. Coin for scale. (b) Reddish greisen zone enriched in quartz, muscovite, tourmaline, topaz and hematite. Horizontal field of view is ~1.5 m.

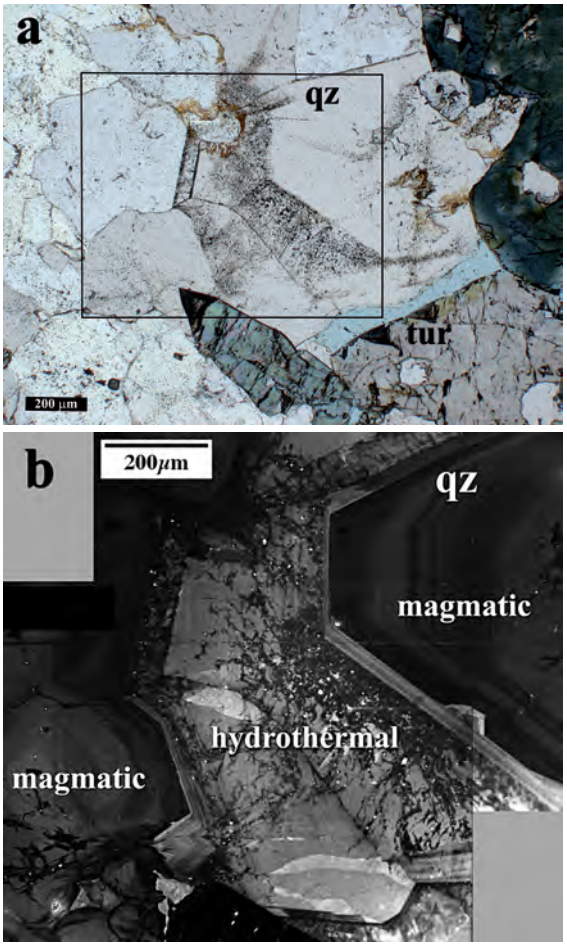

Fig. 2 - Quartz in tourmaline-rich orbicule. (a) PPL optical image. Cloudy zones contain abundant fluid inclusions. (b) SEM-CL image showing euhedral, oscillatory-zoned, magmatic stage-1 quartz and stage-2 hydrothermal quartz. Stage-3 quartz develops as irregular dark CL fluid-inclusion-bearing cross-cutting veins.

[1] Department of Geology and Geophysics, Louisiana State University, Baton Rouge, Louisiana, USA.
E-mail: dutrow@lsu.edu
[2] Instituto de Geología y Recursos Minerales, San Martín, Provincia de Buenos Aires, Argentina.
E-mail: eduardo.zappettini@segemar.gov.ar

* Corresponding author: glhenr@lsu.edu

Multiple generations of tourmaline span the magmatic to hydrothermal stages of development across most of the tourmaline-bearing lithologies. (1) Tourmaline in the tourmalinite segregation is dominated by clusters of weakly oscillatory zoned blue-green to yellow-brown generation-1 tourmaline with minor late or crosscutting generations-2 and -3 darker tourmaline (Fig. 3a). (2) In the pegmatite, tourmaline is optically zoned with the interior zone-1 core region being pale green-brown and the exterior rim zone-2 being green-to-orange with distinct oscillatory-zoning. These two zones are considered part of the initial growth of tourmaline in the overall pegmatite stage of development (i.e., generation 1). (3) Tourmaline-bearing orbicule samples generally have anhedral grains of generation-1 tourmaline with up to three color/compositional zones (Fig. 3b). There is also late, dark-blue generation-2 tourmaline that crosscuts generation-1 tourmaline. (4) Tourmaline from greisen samples contains a generation-1 tourmaline with broad oscillatory zoning exemplified by a series of blue and pale green-brown bands. Minor amounts of dark blue generation-2 tourmaline are observed near the margins of generation-1 tourmaline.

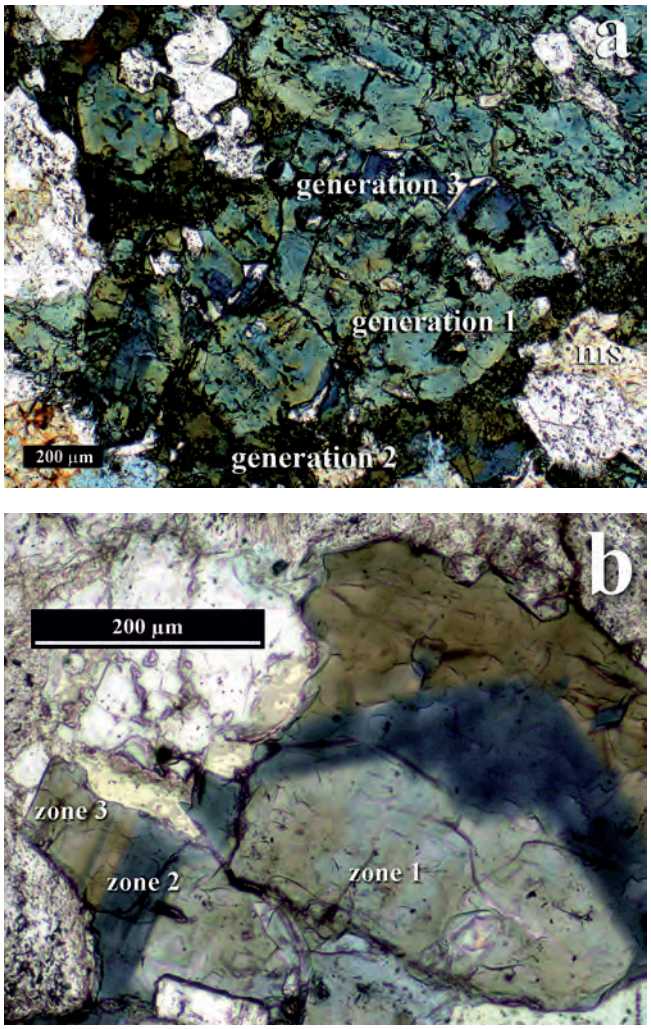

Fig. 3 - Optical images of tourmaline from two different lithologies. (a) Tourmaline segregation. Cluster of tourmaline crystals showing three generations of development. (b) Tourmaline-rich orbicule. This generation-1 tourmaline has three distinct optical and compositional zones.

Generation-1 tourmaline in all lithologies is compositionally similar being highly aluminous (range of average values of Al_{total}= 6.31-6.95 apfu), markedly Fe- and $^{X}\square$-rich [X_{Mg} = 0.01-0.17, $^{X}\square$ = 0.21-0.51] with variable F and ^{W}O [F = 0.00-0.57 apfu, ^{W}O = 0.00-0.40] (Fig. 4). Generation-1 magmatic tourmaline has compositions reflecting the chemical environment of the host lithologies and with compositional zoning patterns characteristic of both closed- and open-system behavior. Like generation-1 tourmaline, later-stage generations-2 and -3 tourmaline compositions are highly aluminous [range of average values of Al_{total}= 6.38-6.79 apfu], markedly Fe- and $^{X}\square$-rich [X_{Mg} = 0.00-0.20, $^{X}\square$ = 0.28-0.40], variably F- and ^{W}O-enriched [F = 0.07-0.57 apfu, ^{W}O = 0.00-0.31], but notably lower in Ca and Ti [<0.01 apfu]. The later-stage tourmaline is considered to have developed during the transition to hydrothermal conditions. External chemical contributions to tourmaline compositions from the country rocks appears to be minor-to-nonexistent.

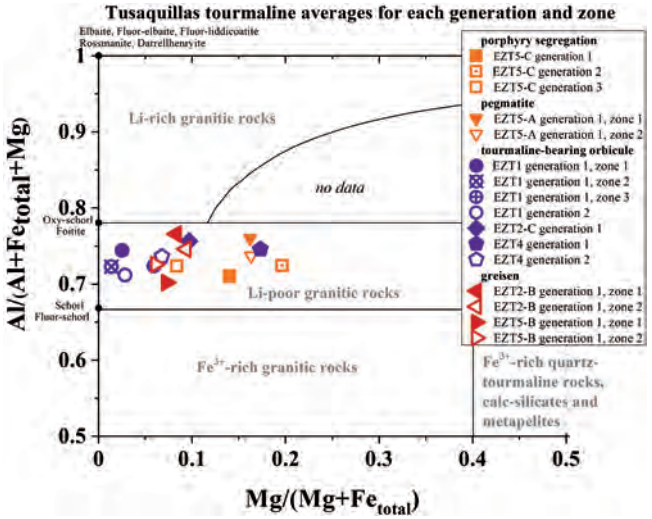

Fig. 4 - Average compositions for each tourmaline generation and each zone within generation-1 tourmaline in lithologies of the peraluminous Tusaquillas Complex (modified after Henry & Dutrow, 2018 with areas defined by Henry & Guidotti, 1985).

Tourmaline-bearing lithologies of the Tusaquillas Composite Batholith system exhibit many textural and chemical similarities attributed to the magmatic-to-hydrothermal transitions found in other comparable low-pressure peraluminous leucogranite systems and their common accompanying late Sn-W mineralization.

REFERENCES

Henry D. J. & Dutrow B. L., 2018 − Tourmaline studies through time: contributions to scientific advancements. *Journal of Geosciences*, 63: 77-98.

Henry D. J. & Guidotti C. V., 1985 − Tourmaline as a petrogenetic indicator mineral - an example from the staurolite-grade metapelites of NW Maine. *American Mineralogist*, 70: 1-15.

Tourmaline breccias in the Río Blanco-Los Bronces porphyry Cu-Mo district, central Chile: a geochemical and stable isotope study

Michael Hohf[1], Robert B. Trumbull[2]*, Patricio Cuadra[3], Marco Solé[3]

The supergiant Río Blanco-Los Bronces (RB-LB) porphyry Cu-Mo district in Chile has an estimated total resource of more than 200 Mt of copper, a large part of which is in mineralized tourmaline-cemented breccia bodies (e.g., Frikken *et al*., 2005; Toro *et al*., 2012). Despite the close association with mineralization, only a handful of geochemical studies of the tourmaline exist. This study is based on samples of mineralized tourmaline breccia from La Americana and Sur-Sur sectors (herein: mine area) and barren tourmaline breccia from the Diamante prospect NW of the mine area. The geochemical data comprise major-element analyses by EPMA and boron isotope analyses by SIMS. Our aim is to test for a relationship between the chemical and/or boron isotopic composition tourmaline and copper mineralization as an aid in exploration. Also, the boron isotope composition of tourmaline is combined with sulfur isotope data to help constrain the source of the mineralizing fluid.

The RB-LB district is hosted in a late Eocene to mid Miocene volcaniclastic-sedimentary sequence that was intruded by the granodioritic San Francisco Batholith dated between ca. 16 to 8 Ma (Toro *et al*., 2012). Most mineralization in the district (stockwork veins and breccia bodies) is associated with a string of quartz diorite and dacite porphyry intrusions of ca. 7 to 5 Ma age distributed over 10 km along a NW-SE fault zone. Tourmaline-cemented breccias in the RB-LB district are typically monomictic "crackle breccia" with angular clasts lithologically identical to the respective host rock (Fig. 1). Clasts show strong K-feldspar and sericite alteration and are cemented with tourmaline, quartz, locally biotite, albite, magnetite and/or specularite, sulphide minerals, anhydrite and rock flour.

[1] Geological Institute, Technischen Universität Bergakademie Freiberg, 09599 Freiberg, Germany.
E-mail: michaelhohf@gmail.com
[2] GFZ - German Research Centre for Geosciences, 14473 Potsdam, Germany.
[3] CODELCO-Chile, División Andina, Los Andes, Chile.
E-mail: pcuadra.geo@gmail.com
MSole@codelco.cl

* Corresponding author: bobby@gfz-potsdam.de

Fig.1 - Tourmaline breccia showing K-alteration rims on larger clasts; small clasts are entirely altered.

Tourmaline typically forms masses of tiny acicular grains in the breccia matrix, but larger prismatic crystals occur locally in vugs. Tourmaline is black in hand specimen and brown-green to bluish in thin section. Optical zoning is common and diverse, with irregular patchy zoning as well as concentric zoning (locally oscillatory). However, consistent chemical zoning trends were not observed and the majority of grains are too fine-grained to assess chemical zoning at all.

Based on X-site occupancy, nearly all tourmaline data plot in the alkali subgroup with exceptional analyses extending to the calcic subgroup. There is no distinction of mineralized vs. barren samples in the X-site. The strongest variations in tourmaline composition are in the Mg/(Mg+Fe) ratio, which ranges from 0.11 to 0.89 overall, and in total Al contents (3.9 to 7.4 apfu). Importantly, these variations appear to differ systematically between the mineralized and the barren breccia samples, and this may have exploration significance. Tourmaline from the barren Diamante breccia shows a strong negative correlation of Fe and Mg and no correlation of Fe and Al, while the mineralized samples from the mine area show the opposite trends (Fig. 2). This difference is attributed to a larger proportion of trivalent Fe in the mineralized breccias, permitting Fe^{3+}-Al^{3+} substitution in tourmaline.

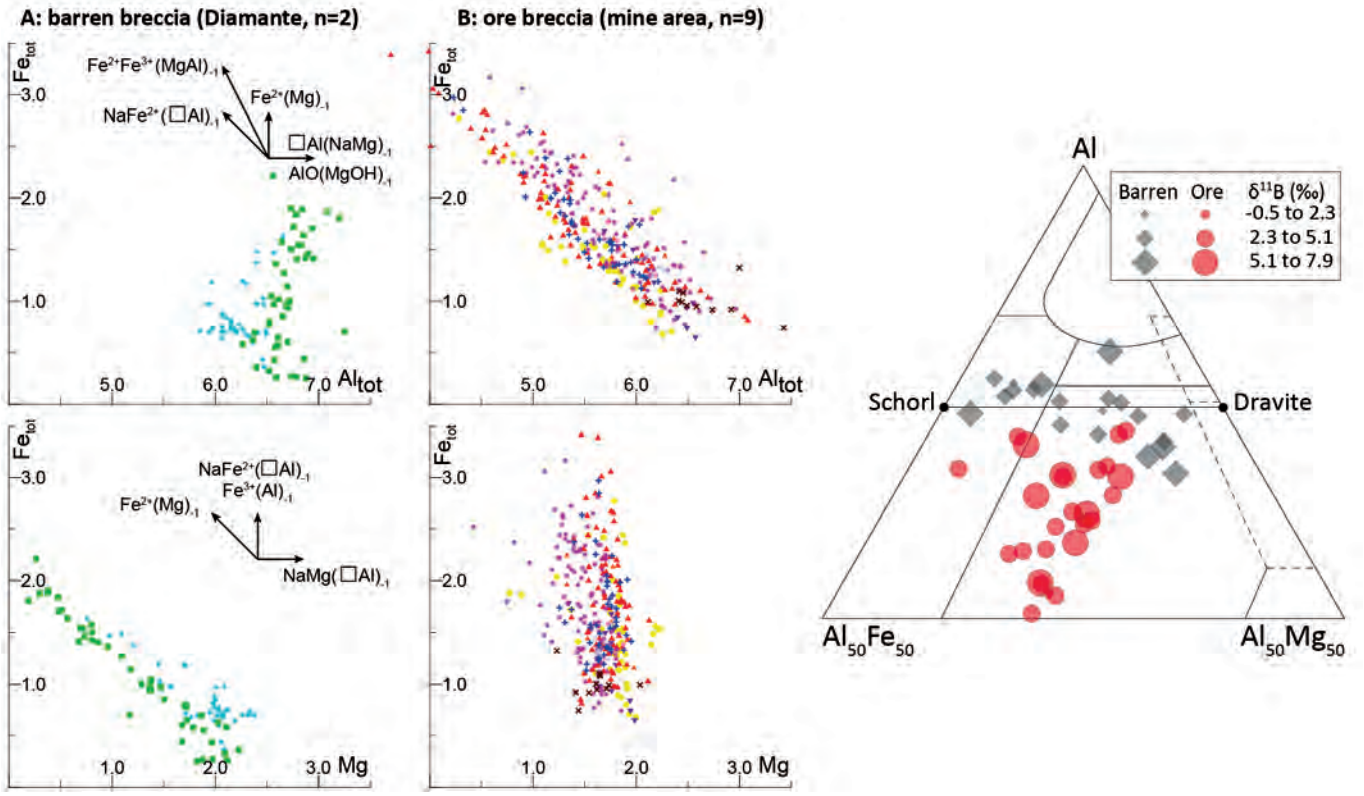

Fig. 2 - Tourmaline compositions from the RB-LB district. Left: Fe, Mg and Al variations in barren and ore breccias; note contrasting trends in Al-Fe and Mg-Fe between the two groups. Right: combined plot of Al-Mg-Fe variations and B-isotope ratio ($\delta^{11}B$ keyed to symbol size).

The implication is that mineralized breccias formed from more oxidized fluids, which is consistent with specularite and anhydrite in the breccia cement. Oxidation could result from boiling of magmatic-hydrothermal fluid, which was suggested from a fluid inclusion study of Sur-Sur breccia (Frikken *et al*., 2005).

The total range in boron isotope compositions, expressed in $\delta^{11}B$ values, is from -0.5 to 7.9‰ (1‰ uncertainty). Most grains were too small for multiple analyses but the larger grains were found to be homogeneous within the uncertainty level. Importantly, there is no correlation between chemical and isotopic composition and no difference between mineralized and non-mineralized breccias (Fig. 2). For a mineralization temperature estimated at 400-500°C (Frikken *et al*., 2005) the estimated fluid $\delta^{11}B$ range is 4.7 to 8.2 ‰.

Positive $\delta^{11}B$ values suggest an ultimately marine-related source of boron. For the RB-LB geologic setting this could be either from seafloor-altered crust in the arc magma source or from assimilation of evaporite-bearing strata beneath the Abanico basin. Both explanations could explain the boron isotope values but $\delta^{34}S$ values (Frikken *et al*., 2005; Hohf, 2021) clearly favor the magmatic option. This is supported by B-isotope compositions of quartz-hosted melt inclusions in post-mineral dikes at the El Salvador porphyry Cu deposit ($\delta^{11}B$ = -5 to 12‰: Wittenbrink *et al*., 2009).

REFERENCES

Frikken P., Cooke D. R., Walshe J. L., Archibald D. A., Skarmeta J., Serrano L. & Vargas R. A., 2005 − Mineralogical and isotopic zonation in the Sur-Sur tourmaline breccia, Río Blanco-Los Bronces Cu-Mo deposit, Chile: Implications for ore genesis. *Economic Geology,* 100: 935-961.

Hohf M., 2021 − Magmatic-hydrothermal events, mineralogy and geochemistry of tourmaline breccia in the giant Río Blanco-Los Bronces porphyry copper deposit, Central Chile. *Dissertation, Technischen Universität Bergakademie Freiberg*. <https://nbn-resolving.org/urn:nbn:de:bsz:105-qucosa2-744100>

Toro J .C., Ortúzar J., Zamorano J., Cuadra P., Hermosilla J. M. & Spröhnle C., 2012 − Protracted magmatic-hydrothermal history of the Río Blanco-Los Bronces District, Central Chile: Development of the world's greatest known concentration of copper. *Society of Econonic Geologists, Special Publications*, 16: 105-126.

Wittenbrink J., Lehmann B., Wiedenbeck M., Wallianos A., Dietrich A. & Palacios C., 2009 − Boron isotope composition of melt inclusions from porphyry systems of the Central Andes: a reconnaissance study. *Terra Nova*, 21 (2): 111-118.

Thermal expansion of tourmaline: a systematic investigation

Guy Hovis[1], Ferdinando Bosi[2], Mario Tribaudino[3]*

In recent papers we have explored the thermal expansion of minerals in the pyroxene (Hovis *et al*., 2021) and amphibole (Tribaudino *et al*., 2021 in press) mineral systems. The present contribution extends this work to minerals of the tourmaline system with the presentation of volume - temperature (V-T) data for fifteen mineral specimens in this system. As with the previously studied systems, the aims of this work were to (1) learn the effects of chemical composition on thermal expansion in this system, (2) apply appropriate thermal expansion models to the data collected, and (3) discover how mineral structure adjusts to increasing temperature. The chosen samples are all natural, and represent a sampling of the chemical variability in natural tourmalines. Available analyses were recalculated, correcting previous erroneous name assignments.

X-ray powder diffraction measurements were conducted from room T to ~928 °C at mostly 50 °C intervals on a PANalytical Empyrean X-ray powder diffraction system equipped with an Anton-Parr HTK 1200N heating stage.

Deterioration in X-ray peak quality at some point during sample heating was generally found, although the temperature at which such deterioration began varied from sample to sample. Also, off-trend unit-cell dimensions with increasing T was found at some temperature. This however never occurred below 400 °C, allowing a comparison between the axial and volume thermal expansion between room and 400 °C. Within this range thermal expansion data were fitted by empirical linear and polynomial Berman models.

[1] Department of Geology and Environmental Geosciences, Lafayette College, Easton, PA 18042, USA.
E-mail: hovisguy@lafayette.edu
[2] Department of Earth Science, Sapienza University of Rome, Piazzale Aldo Moro 5, I-00185 Rome, Italy.
E.mail: ferdinando.bosi@uniroma1.it
[3] Department of Chemical, Life and Environmental Sciences, University of Parma, Viale G.P. Usberti 157/A, I-43100 Parma, Italy.

* Corresponding author: mario.tribaudino@unipr.it

Volume thermal expansion in a linear model varies between 2.06(4)x10^{-5} and 2.30(4)x10^{-5} in foitite and fluor-liddicoatite respectively, a rather small variability when compared to other mineral families.

Axial expansion along the *a* axis averages at 0.53(4) with maximum and minimum values between 0.60 and 0.47, whereas along the *c* axis it averages 0.97(5), with minimum and maximum between 0.90 and 1.06 x10^{-5}/K. Despite the limited variation the lower expansion of the Fe^{2+} bearing tourmalines is apparent (Fig. 1), whereas Li and Fe^{2+} tourmalines expand less along the *c* axis. Higher expansion along the *c* axis is in line with previous investigations, and confirms the limiting effect of the silicate rings to thermal expansion.

At temperatures higher than 400 °C the behaviour of the tourmalines varies. We have defined four groups: 1) shown by dravite, fluor-liddicoatite and fluor-uvite, with a trend dictated just by thermal expansion, but for a higher value in the *c* axis at the highest temperature for fluor-liddicoatite. Within this group the thermal expansion of

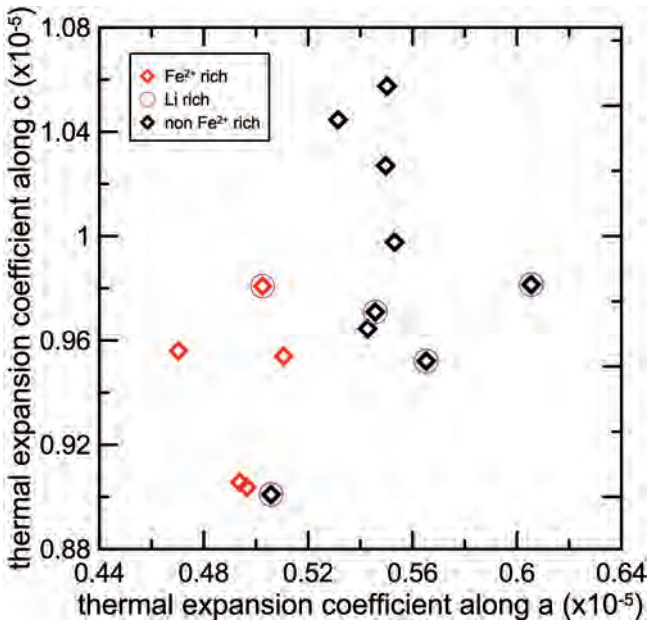

Fig. 1 - Thermal expansion along the *a* and *c* axes in the tourmalines studied. The Fe^{2+}-poor tourmalines with the lower *c* expansion is the olenitic sample (namely, Vac-Al-B-rich elbaite).

dravite was taken as reference; 2) rossmanite, fluor-buergerite and elbaite overshoot the *c* parameter and undershoot the *a* parameter at a temperature higher than 800 °C; 3) Fe-rich elbaite and fluor-uvite, as well as olenitic sample show a much more marked deviation at 600 °C. In the olenitic sample the *a* parameter decreases at higher temperature, in a trend resembling previous observation by Celata *et al*., 2021; 4) schorl and foitite, which show a marked irreversible degradation at T > 600 °C, can be gathered in a single trend for Fe^{2+}-rich tourmalines (Fig. 2).

The different behaviour was interpreted as arising from coupled interaction of the oxidation-deprotonation, which involved mostly the Fe^{2+}-bearing tourmalines, and cation ordering which involved mostly the Fe^{2+}- and Li-bearing samples. Seemingly, the Mg-bearing dravite samples are not affected by cation ordering at higher temperature.

Different Fe^{2+} content also explains the different high temperature behaviour shown by the three fluor-uvite samples.

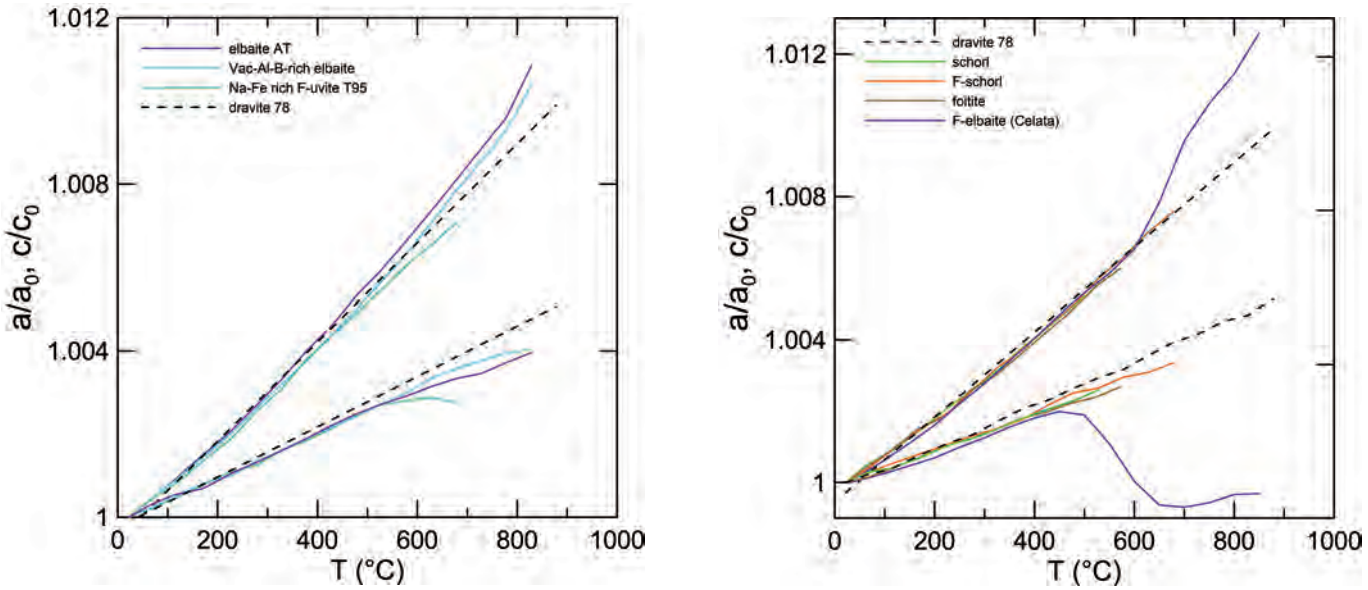

Fig. 2 - Thermal expansion along the *a* and *c* axes in group 3 (left) and group 4 (right) tourmalines.

REFERENCES

Celata B., Ballirano P., Andreozzi G. B. & Bosi F., 2021 − In-situ high-temperature behaviour and breakdown conditions of fluor-elbaite. *Physics and Chemistry of Minerals*, 48: 24-31.

Hovis G. L., Tribaudino M., Leaman A., Almer C., Altomare C., Morris M., Maksymiw N., Morris D., Jackson K., Scott B., Tomaino G. & Mantovani L., 2021 − Thermal expansion of minerals in the pyroxene system and examination of various thermal expansion models. *American Mineralogist*, 106: 883-899.

Tribaudino M., Hovis G. L., Almer C. & Leaman A., 2021 in press − Thermal expansion of minerals in the amphibole supergroup. *American Mineralogist*.

Crystal-chemical effects of heat treatment on Mg-dominant tourmalines

Petra Kardošová[1]*, Peter Bačík[1,2], Jana Fridrichová[1], Marcel Miglierini[3,4], Tomáš Mikuš[5], Daniel Furka[6], Samuel Furka[6], Radek Škoda[7]

Crystal-chemical effects of heat treatment on tourmalines have been studied in several investigations. Castañeda *et al*. (2006) produced colour changes in Li-bearing tourmaline from Brazil where the original green elbaitic tourmaline turned brown or bluish-grey. The original green colour was caused by the presence of Fe^{2+} in the Y site, and colour change was related to a local disorder of crystal structure. Pink tourmaline did not change the colour due to Mn^{+2}, indicating that the divalent Mn did not oxidize to trivalent manganese. Blue tourmaline turned red by heating to 700 °C for 48 h. This colour change can be described by the oxidation of Fe^{2+} and the release of H^+ from the OH groups (Castañeda *et al*., 2006). The compression of <H-O> bond lengths is similar to the bond length values of naturally oxidized tourmalines caused by the replacement of Fe^{2+} by Fe^{3+} in Y octahedra (Pieczka & Kraczka, 2004).

Temperature of 700 °C is in the middle of the interval between the initiating temperature of Fe^{2+} and $Mn^{2?}$ oxidation and the temperature of tourmaline structural disintegration, which is estimated at 880–920°C (Pieczka & Kraczka, 2004). The composition of schorlitic tourmalines heated to 700 °C changed to oxidized member with the ideal formula $NaFe_3^{3+}Al_6Si_6O_{18}(BO_3)_3(O_2OH)O$, which is similar to the formula of the hypothetical end member 'buergerite' $NaFe_3^{3+}Al_6Si_6O_{18}(BO_3)_3O_3(OH)$ (Henry *et al*., 2011).

As a result of the high-temperature treatment, the tourmaline fragments (originally black) turned dark brownish-red (oxidized) or greyish-black (reduced) when viewed through very thin edges (Filip *et al*., 2012). Heat treatment was also performed on Fe-dominant tourmalines from Dolní Bory, Czech Republic and Vlachovo, Slovakia at 450°C, 700°C and 900°C in which the Fe oxidation was observed at 700°C and structural breakdown at 900°C (Bačík *et al*., 2011). This breakdown may be driven by diffusion between octahedral sites after the Fe oxidation (Ertl *et al*., 2012).

We present a detailed study of thermally driven oxidation of Fe in the structure of Mg-dominant tourmaline. High-temperature changes were evidenced using ^{57}Fe Mössbauer, infrared, and optical absorption spectroscopy, and electron microprobe. Tourmaline samples were thermally treated in air at temperature of 700, 800 and 900°C.

Heat experiments were performed on the following samples: (1) dravite from Yunnan, China (CHD) forms euhedral brown thick prismatic crystals, with pyramidal faces, 2-3 cm in size; (2) schorlitic-dravite from Rubeho Mts., Tanzania (TSCH) forms black thin prismatic crystals, with pyramidal faces, up to 2 cm long; (3) Cr-bearing fluor-uvite from Merelani Hills, Tanzania (TUV) forms anhedral black thick prismatic crystals, with pyramidal faces up to 1,5 cm in size. After the heat treatment, no apparent visual changes were observed.

According to their chemical composition analysed by electron microprobe, all samples are Mg dominant, but with variable X_{Mg} (Mg/(Mg+Fe)). The TSCH sample schorlitic dravite from Tanzania with X_{Mg} of 0.5-0.8. CHD sample is Mg-dominant dravite with $X_{Mg} > 0.9$. The TUV sample Cr-bearing fluor-uvite (up to Cr 0.095 apfu) with $X_{Mg} > 0.99$).

Mössbauer spectroscopy was planned to use for determination of Fe charge and its changes after the heat treatment but only the TSCH sample had sufficient Fe content for analysis. Tourmaline heated at 700°C did not

[1] Comenius University, Faculty of Natural Sciences, Department of Mineralogy, Petrology and Economic Geology, Ilkovičova 6, Mlynská dolina, 842 15 Bratislava, Slovakia.
[2] Earth Science Institute of the Slovak Academy of Sciences, Dúbravská cesta 9, P.O. BOX 106, 84005 Bratislava, Slovakia.
[3] Slovak University of Technology, Faculty of Electrical Engineering and Information Technology, Institute of Nuclear and Physical Engineering, Ilkovičova 3, 812 19 Bratislava, Slovakia.
[4] Department of Nuclear Reactors, Faculty of Nuclear Sciences and Physical Engineering, Czech Technical University in Prague, V Holešovičkách 2, 180 00 Prague, Czech Republic.
[5] Earth Science Institute of the Slovak Academy of Sciences, Dúbravská cesta 9, P.O. BOX 106, 84005 Bratislava, Slovakia.
[6] Comenius University, Faculty of Natural Sciences, Department of Physical and Theoretical Chemistry, Ilkovičova 6, 842 15 Bratislava, Slovakia.
[7] Masaryk University, Department of Geological Sciences, Kotlářská 2, 611 37 Brno, Czech Republic.

* Corresponding author: kardosova6@uniba.sk

show any change in Fe oxidation state, but Fe oxidized to trivalent at 800°C and 900°C.

The influence of the possible cation oxidation on the OH groups bonded at the edges of YO_6 octahedra was determined by IR spectroscopy. TSCH and CHD samples show decrease in absorbance of OH bands which indicates deprotonization and Fe oxidation present. TUV sample does not show any significant decrease in absorbance. This suggests that no oxidation could take a place due to a very low Fe, Mn and V content and Cr cannot oxidize at normal atmosphere.

Optical absorption spectroscopy was used to illustrate possible oxidation of the transition metals. In the samples with at least some Fe content – CHD and TSCH – Fe oxidation was indicated by change of absorption bands. However, all changes in the optical spectra happened in the NIR region, therefore, original brown and black colour did not change. Almost Fe-free TUV sample with Cr as dominant chromophore displayed no significant changes in optical spectra.

This research was funded by the projects APVV–18–0065 and VEGA-1/0137/20.

REFERENCES

Bačik P., Ozdín D., Miglierini M., Kardošová P., Pentrák M. & Haloda J., 2011 – Crystallochemical effects of heat treatment on Fe-dominant tourmalines from Dolní Bory (Czech Republic) and Vlachovo (Slovakia). *Physics and Chemistry of Minerals*, 38: 599-611.

Castañeda C., Eeckhout S. G., da Costa G. M., Botelho N. F. & De Grave E., 2006 – Effect of heat on tourmaline from Brazil. *Physics and Chemistry of Minerals*, 33: 207-216.

Ertl A., Kolitsch U., Dyar M. D., Hughes J. M., Rossman G. R., Pieczka A., Henry D. J., Pezzotta F., Prowatke S., Lengauer C. L., Körner W., Brandstätter F., Francis C. A., Prem M. & Tillmanns E., 2012 – Limitations of Fe^{2+} and Mn^{2+} site occupancy in tourmaline: Evidence from Fe^{2+}- and Mn^{2+}-rich tourmaline. *American Mineralogist*, 97: 1402-1416.

Filip J., Bosi F., Novák M., Skogby H., Tuček J., Čuda J. & Wildner M., 2012 – Iron redox reactions in the tourmaline structure: High-temperature treatment of Fe^{3+}-rich schorl. *Geochimica et Cosmochimica Acta*, 86: 239-256.

Henry D., Novák M., Hawthorne F. C., Ertl A., Dutrow B. L., Uher P. & Pezzotta F., 2011 – Nomenclature of the tourmaline-supergroup minerals. *American Mineralogist*, 96: 895-913.

Pieczka A. & Kraczka J., 2004 – Oxidized tourmalines. A combined chemical, XRD and Mossbauer study. *European Journal Mineralogy*, 16: 309-321.

B-isotopic study of maruyamaite from the new locality within the Kokchetav massif

Andrey Korsakov[1]*, Denis Mikhailenko[1,2,3], Kira Musiyachenko[1,4], Le Zhang[2,3], Yi-Gang Xu[2,3]

Maruyamaite is a K-bearing dravite with a maximum recorded K content of 2.7 wt % and 3.44 wt % in natural and synthesized samples, respectively (Shimizu & Ogasawara, 2005; Berryman *et al.*, 2014). So far the findings of this unusual tourmaline were restricted only to one locality – Kumdy-Kol microdiamond deposit (Kokchetav Massif), where it was first described in a tourmaline-quartz-K-feldspar rock (Shimizu & Ogasawara, 2005). Some authors claim maruyamaite to be an indicator of the ultra-high pressure (UHP) conditions because of the presence of diamond inclusions (Shimizu & Ogasawara, 2005). However, these diamond inclusions found in zircon and tourmaline are the only reliable marker of UHP in this rock. Another theory associates the formation of K-bearing tourmaline in these rocks with the infiltration of boron-bearing fluids at crustal conditions (Marschall *et al.*, 2009). The B-isotopic composition of the tourmaline K-rich cores (with and without diamond inclusions) is quite similar for the tourmalines from the Kumdy-Kol unit (δ11B +7‰; Ota *et al.*, 2008; Marschall *et al.*, 2009). However, this B-isotopic composition is not typical for tourmaline from other UHPM localities (Marschall *et al.*, 2009).

Recently reported findings of maruyamaite at the Barchi-Kol site (Musiyachenko *et al.*, 2021), located 17 km west of the Kumdy-Kol deposit. This is the second described locality for the maruyamaite in the world. Here, we present a B-isotopic study of the Barchi-Kol K-tourmaline. We also provide estimates of the fluid regime and the P–T conditions of the formation of mineral paragenesis associated with maruyamaite.

Tourmaline-bearing sample of the Barchi-Kol site consists of garnet, tourmaline, quartz, potassium feldspar, biotite, and muscovite. The volumetric content of tourmaline in the samples is ~15–20%. Findings of tourmaline inclusions in garnet, garnet inclusions in tourmaline and inclusions of both in extracted zircons allow suggesting that these phases formed together. Furthermore, inclusions of biotite and K-feldspar in tourmaline and garnet porphyroblasts, have identical composition to biotite and K-feldspar from the rock matrix. Despite an extensive study of solid inclusions no UHPM mineral-indicators (e.g. coesite or diamond) were detected in samples from this locality. Tourmaline crystals have a pronounced compositional zoning in K, Na, Ca, and Ti. Potassium zoning pattern is opposite to that in Na with high K concentrations in spindle-shaped zones concentrated in the inner part of the grain. Areas of maruyamaite composition (2.1 wt % K_2O) are surrounded by zones of low-K-dravite (0.2 wt % K_2O) (Fig. 1A). B-isotopic compositions of K-rich and K-poor zones within the maruyamaite from the Barchi-Kol are presented at Fig. 1B. δ11B vary from -6 to -8.6 ‰ in contrast to maruyamaite (δ11B +7‰) from the Kumdy-Kol deposit.

Results of the petrographic observations, thermodynamic modelling and mineral-thermometer calculations suggest that all rock forming minerals crystallized at the same time at 650-800°C and <1.4 GPa (Musiyachenko *et al.*, 2021). The significant amount of tourmaline in the sample implies high boron concentrations in the crystallization environment. According to (Marschall *et al.*, 2009), this environment can be achieved only by an external influx of boron-rich fluids. However, the significant differences in B-isotopic composition of maruyamaite-forming fluids from Kumdy-Kol deposit and Barchi-Kol locality could imply different fluid sources.

[1] Sobolev Institute of Geology and Mineralogy, Russian Academy of Sciences, Novosibirsk, Koptuga aven. 3, 630090, Russia.
[2] CAS Center for Excellence in Deep Earth Science, Guangzhou, 510640, China.
[3] State Key Laboratory of Isotope Geochemistry, Guangzhou Institute of Geochemistry, Chinese Academy of Science, Guangzhou, Kehua street, Tianhe district, 510640 China.
[4] Department of Earth, Ocean and Atmospheric Sciences, The University of British Columbia, 2020-2207 Main Mall, Vancouver, BC Canada V6T 1Z4.
E-mail: mikhailenkodenis@gmail.com
kmusiyachenko@gmail.com
zhangle@gig.ac.cn
yigangxu@gig.ac.cn

* Corresponding author: korsakov@igm.nsc.ru

This work was financially supported by the Russian Science Foundation 18-17-00186.

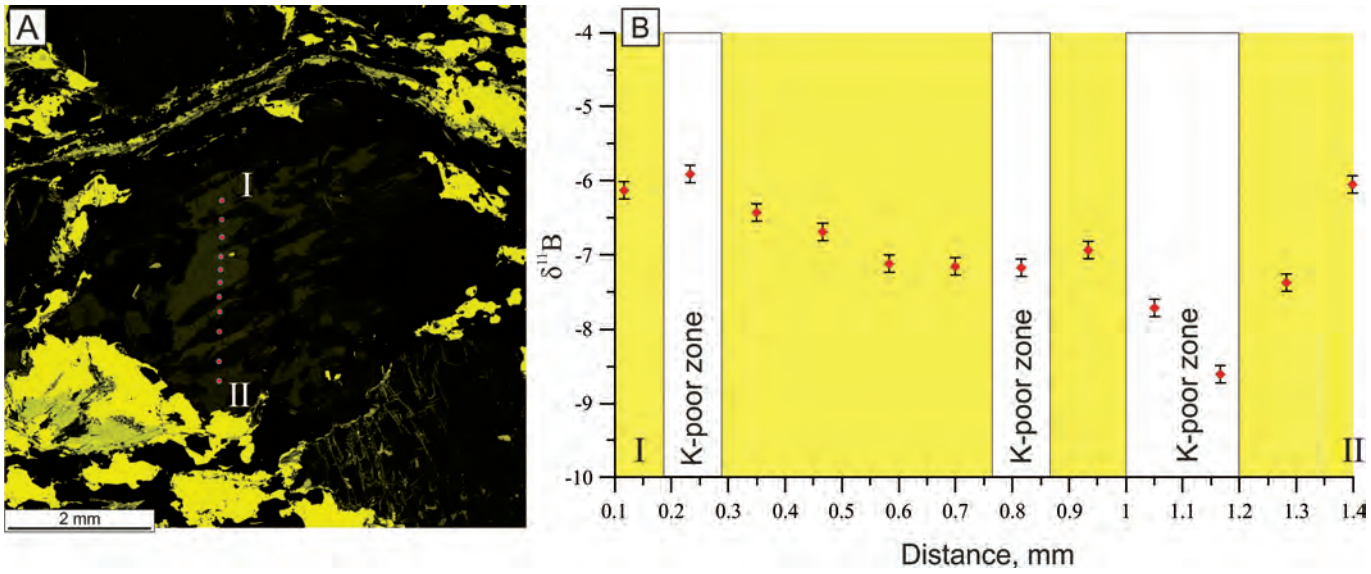

Fig. 1 - A) SEM image of K-distribution within the maruyamaite crystal from the Barchi-Kol locality. B) isotopic profile accross this crystal.

REFERENCES

Berryman E., Wunder B. & Rhede D., 2014 − Synthesis of K-dominant tourmaline. *American Mineralogist*, 99: 539-542.

Marschall H. R., Korsakov A. V., Luvizotto G. L., Nasdala L. & Ludwig T., 2009 − On the occurrence and boron isotopic composition of tourmaline in (ultra) high-pressure metamorphic rocks. *Journal of the Geological Society,* London, 166: 811-823.

Musiyachenko K. A., Korsakov A. V. & Letnikov F. A., 2021 − A New Occurrence of Maruyamaite. *Doklady Earth Sciences*, 498: 403-408.

Ota T., Kobayashi K., Kunihiro T. & Nakamura E., 2008 − Boron cycling by subducted lithosphere; insights from diamondiferous tourmaline from the Kokchetav ultrahigh-pressure metamorphic belt. *Geochimica et Cosmochimica Acta* 72, 3531–3541.

Shimizu R. & Ogasawara Y., 2005 − Discovery of K-tourmaline in diamond-bearing quartz-rich rock from the Kokchetav Massif, Kazakhstan. *Mitteilungen der Österreichischen Mineralogischen Gesellschaft*, 150: 141.

Crystal chemistry of natural Pb-rich tourmalines

Monika Kubernátová*, Jan Cempírek

Lead is one of the cations with a large ionic radius (1.35 Å) and should therefore enter the tourmaline structure as a divalent cation Pb^{2+} at the nine-coordinated X-site. The lead contents typically found in tourmaline are between tens and hundreds of ppm. Elevated lead contents in tourmaline are rare; they were described from a few localities only, such as Anjanabonoina, Madagascar, Momeik, Myanmar or from Kreuzeck Mountains, Austria (for references, see Kubernátová, 2021). The highest lead contents known up to date were described from amazonite pegmatites in Alto Ligonha, Mozambique (up to 15.4 wt.% PbO) and Minh Tien, Vietnam (17.5 wt.% PbO; Sokolov & Martin, 2009).

The Minh Tien locality was recently revisited along with another four potentially interesting localities of amazonitic pegmatites where Pb-rich tourmaline could appear, including Ifasina and Ambatofinandrahana (Madagascar), Rio Grande do Sul (Brazil), and Tennvatn (Norway). The studied samples from amazonitic pegmatites contain greenish K-feldspar (var. amazonite), white albite, black green, blue and sometimes also pink tourmaline, typically associated with lepidolite, topaz, beryl, and accessory zircon, cassiterite, tusionite, and other phases (Kubernátová, 2021). At Minh Tien, Pb-rich tourmaline occurs in four textural-paragenetic types (Fig. 1A); all primary (Tur 1) and hydrothermal (Tur 2, 3, 4) types are enriched in Ca and variable contents of Pb. Of the other hand, primary tourmaline Tur 1 from the localities in Madagascar and Brazil is relatively Pb-poor, in contrast to the hydrothermal Tur 2 which forms euhedral Pb-poor crystals overgrown by Pb-rich skeletal crystals intergrown with quartz (Fig. 1B). The studied Tennvatn samples contain Fe,F-rich heterogeneous hydrothermal tourmaline with elevated Li (up to 2500 ppm, confirmed using LA-ICP-MS); its PbO contents are only rarely above the EMPA detection limit.

Department of Geological Sciences, Faculty of Science, Masaryk University, Kotlářská 267/2, 611 37 Brno, Czech Republic.
E-mail: jan.cempirek@gmail.com

* Corresponding author: monca.kubernatova@centrum.cz

Composition of tourmaline and associated minerals was characterized using EMPA. Very high PbO contents were locally found in tourmaline from Ifasina, Madagascar (up to 15 wt.%), Minh Tien, Vietnam (up to 14.15 wt.%), Rio Grande do Sul (12.77 wt.%) and Ambatofinandrahana, Madagascar (11.72 wt.% PbO). The tourmaline from Tennvatn is Pb-poor and only locally contains elevated PbO contents (≤0.14 wt.%).

We observed two general compositional trends of Pb-rich tourmalines (Fig. 1C-D): 1) at Minh Tien, tourmaline evolves from sodic do Ca-rich with elevated Pb-contents and typically Ca>Pb, significant Pb-enrichment where Pb>Ca is related to the latest Tur 4 that forms domains only few tens of micrometers large; 2) at Madagascar and Brazil localities, tourmaline evolves from sodic to Pb-rich with Pb>Ca – the Ca contents are very low. Again, the highest Pb is related to the latest Tur 2b (Fig. 1B). The main substitutions that take place in the studied tourmalines are from fluor-schorl to fluor-elbaite and/or fluor-liddicoatite (or to the Pb-dominant analogue of fluor-liddicoatite).

The observed paragenetic relationships indicate that the Pb-enrichment in tourmaline is related to both albitization of amazonite (in Minh Tien) and its hydrothermal alteration (all studied localities). Formation of Pb-rich tourmaline is not restricted to Ca-rich systems (and Pb-Ca_{-1} exchange) and takes place also in Na,Li,F-rich tourmalines. Hydrothermal tourmalines may locally reach compositions dominated by the theoretical Pb-analogue of fluor-liddicoatite. The study is currently being followed by further characterization using LA-ICP-MS and structural methods.

This work was supported by the projects GAČR 19-05198S and MUNI/A/1594/2020.

REFERENCES

Kubernátová M., 2021 – Lead in tourmaline supergroup minerals. *MSc thesis, Masaryk University*, Brno.

Sokolov M. & Martin R., 2009 – A Pb-Dominant member of the Tourmaline Group, Minh Tien Granitic Pegmatite, Luc Yen district, Vietnam. *Estudos Geológicos*, 19: 352-353.

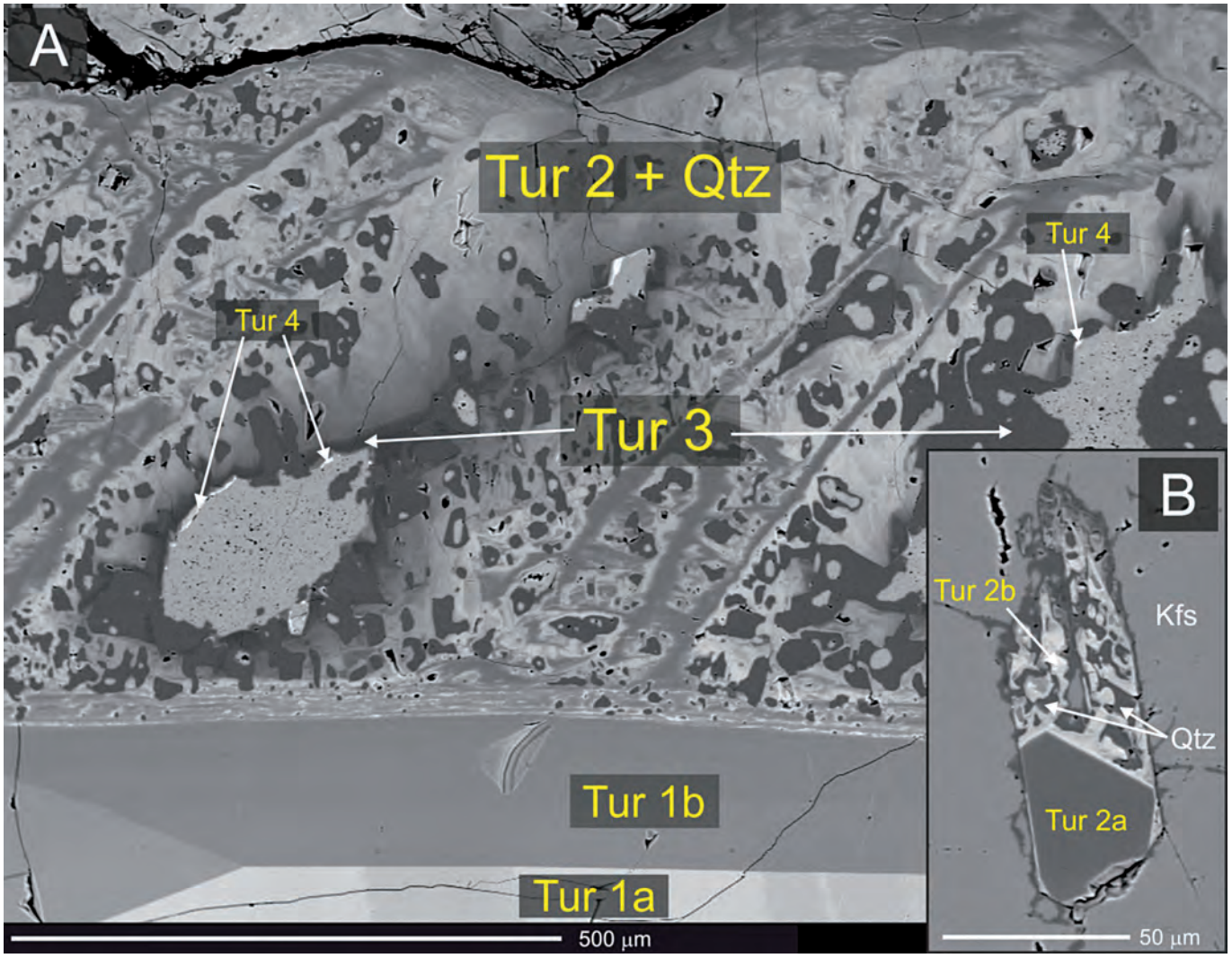

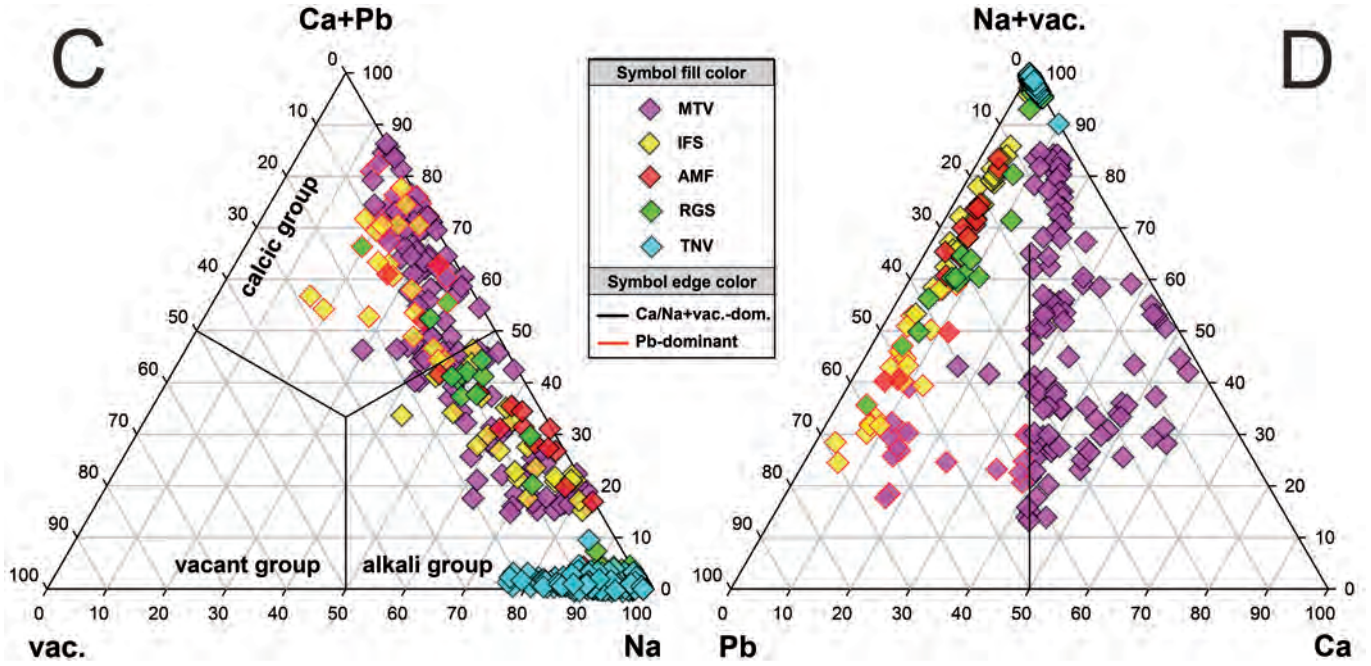

Fig. 1 - BSE images for Pb-tourmaline generations from Minh Tien (A) and Ifasina (B), and ternary diagrams representing occupancy of the X site based on the cation charge (C) and .based on the ratio of Ca, Pb and Na+vacancy (D).

Tourmaline as a gem: varieties, origin determination and future challenges for gem-testing laboratories

Brendan M. Laurs

Gem tourmaline mainly consists of elbaite-liddicoatite-rossmanite species or dravite-uvite species. The first group is hosted by granitic pegmatites, and typically forms the most commonly encountered tourmaline varieties in the gem trade (e.g. pink-to-red *rubellite* [Fig. 1], green *verdelite*, blue *indicolite*, yellow *Canary* from Zambia, colourless *achroite* and so-called *Paraíba-type* consisting of intense blue, violetish blue to greenish blue tourmaline that mainly owes its colour to copper). By contrast, dravite-uvite gem tourmalines are typically found in magnesian-to-calcic metamorphic rocks, and these gems mostly range from yellow to orange to brown (e.g. *Savannah* tourmaline) or deep green (so-called *chrome* tourmaline, although usually with V>Cr).

Recently, a single example of blue dravite was documented from Sri Lanka (Nasdala *et al.*, 2021). Black tourmaline (typically schorl-elbaite) may also be encountered as an unusual gem material.

Nearly all of the transparent tourmaline varieties (except for Canary) may occur in bicoloured or multicolored crystals; well-known examples include pink-green 'watermelon' tourmaline from various localities and distinctive oscillatory-zoned liddicoatite from Madagascar. In addition, textural sub-types of gem tourmaline include chatoyant *cat's-eye* material (most commonly seen in green and blue varieties of elbaite-liddicoatite-rossmanite) and *trapiche* tourmaline showing six-spoked growth features (i.e. green dravite-uvite).

In recent years, the most important localities for producing gem tourmaline consisted of various countries in Africa (Nigeria, Mozambique, Namibia, Tanzania and Kenya), as well as Madagascar, Brazil and Afghanistan. In addition, the Democratic Republic of Congo in Central Africa recently emerged as a significant source (Laurs *et al.*, 2017).

Of all types of gem tourmaline, the brightly coloured Cu-bearing material from Paraíba State in Brazil is the most highly prized (e.g. US$60,000/ct for top-quality gemstones weighing 4.00–4.99 ct), ranking as the second-most valuable coloured stone after untreated Burmese ruby. Cu-bearing tourmaline from other localities commands much lower prices ($14,000/ct for stones of equivalent size), while values for other gem tourmalines are significantly less (e.g. chrome = $1,000/ct, blue/green = $650/ct, bicoloured = $600/ct, green = $600/ct, red = $575/ct, cat's-eye = $500/ct and pink = $475/ct, according to 2021 GemGuide listings).

Fig. 1 - A matrix specimen of pink tourmaline, albite ("cleavelandite") and lepidolite from Paprok, Afghanistan (12 x 12 cm), is shown together with a carved free-form 16.55 ct rubellite from Mozambique. (Specimens courtesy of Pala International, Fallbrook, California, USA. Photo: Robert Weldon).

Gem-A: The Gemmological Association of Great Britain, 1106 2nd St., #317, Encinitas, CA 92024, USA.
E-mail: brendanlaurs@gmail.com

Given the exceedingly high value of Paraíba material, there is significant demand for origin determination of Cu-bearing tourmalines to be performed by gemmological laboratories. In addition to the most highly sought-after material from São José da Batalha in Paraíba State, this tourmaline variety also comes from other sources in northeast Brazil (two principal mines Rio Grande do Norte State), and also from Mozambique and Nigeria. To address the needs of the gem trade, origin determination is done mainly to differentiate material simply by country (Brazil vs. Mozambique vs. Nigeria), rather than according to the specific deposit. Actually two localities in Mozambique are known: Mavuco (the main source, which produces Cu-bearing elbaite of various colours) and Maraca (liddicoatite that is violet before heat treatment; Milisenda & Müller, 2017). As is the case for the other localities, Nigeria produces blue-to-green and also violet material (before heating), and in addition a new variety of Cu-bearing tourmaline from Nigeria was recently documented that contains a distinct amount of Fe, resulting in a blue colour that resembles some non-Cu-bearing stones from Namibia (Krzemnicki, 2021). Although the gemmological properties of Paraíba-type tourmaline from the various localities mostly overlap, the Cu-bearing elbaites can be effectively differentiated by their trace-element contents (e.g. Katsurada *et al.*, 2019 and references therein; Wang *et al.*, 2021; see Fig. 2).

In addition to origin determination, gemmological laboratories are also tasked with identifying treatments and synthetics. While gem tourmaline has not been produced synthetically (as the crystals produced so far range up to only about 1-2 mm; Setkova *et al.*, 2019), treatments are quite common. The most widespread treatment is heating at relatively low temperature to improve colouration (e.g. to remove a greyish component, to lighten dark tones or, most importantly, to produce an attractive blue colour in violet Cu-bearing tourmaline). In addition, the pink-to-red colouration is commonly improved by irradiating pale-colored tourmaline with gamma rays (or, less commonly, by an electron beam; e.g. Suwanmanee *et al.*, 2021). Nevertheless, because the colouration produced by heat and irradiation statements is stable–and generally undetectable by routine gem testing–gem labs are not called upon to identify them. Of greater concern is the identification of clarity enhancement by fracture filling (typically with epoxy resin or oil) to improve a stone's apparent clarity. The filled fissures can be identified by careful microscopic examination, Raman and infrared spectroscopy, and UV imaging (e.g. Dai *et al.*, 2017). Fissure-filling is particularly important to detect in Paraíba-type tourmaline (e.g. Fig. 3), due to its high value.

During the examination of tourmaline gemstones, sometimes interesting internal features are seen that provide insight into the stone's geographic origin or formation conditions. For example, inclusions of native copper are occasionally encountered in Cu-bearing tourmaline (Fig. 4a), and their presence is indicative of a Brazilian source. Other inclusions documented in tourmaline include cassiterite (Delaunay *et al.*, 2020) and pyrochlore crystals (Fig. 4b; both indicative of a granitic pegmatite origin), while pyrite inclusions have been identified in dravite from Mozambique (consistent with its non-pegmatitic origin). Elongate growth tubes are commonly oriented parallel to the *c*-axis of gem tourmaline (Fig. 4c), and may produce chatoyancy if present in great enough abundance. Microscopic colour zoning in gem tourmaline also provides useful insights. Fractures and channels may be surrounded by narrow zones of pink colouration due to post-crystallization exposure to radioactive solutions, and is known in Cu-bearing tourmaline from Mozambique (e.g. Leblan *et al.*, 2015 and references therein), as well as in rubellite (Jia & Sit, 2017). In addition, Hänni *et al.* (2019) documented dark pink halos surrounding columbite-tantalite inclusions in a polished slice of liddicoatite from Madagascar. Colour-zoning patterns seen in faceted or sliced specimens, particularly when viewed parallel to the *c*-axis, may reveal complicated growth relations that help reveal the history of gem tourmaline crystallisation.

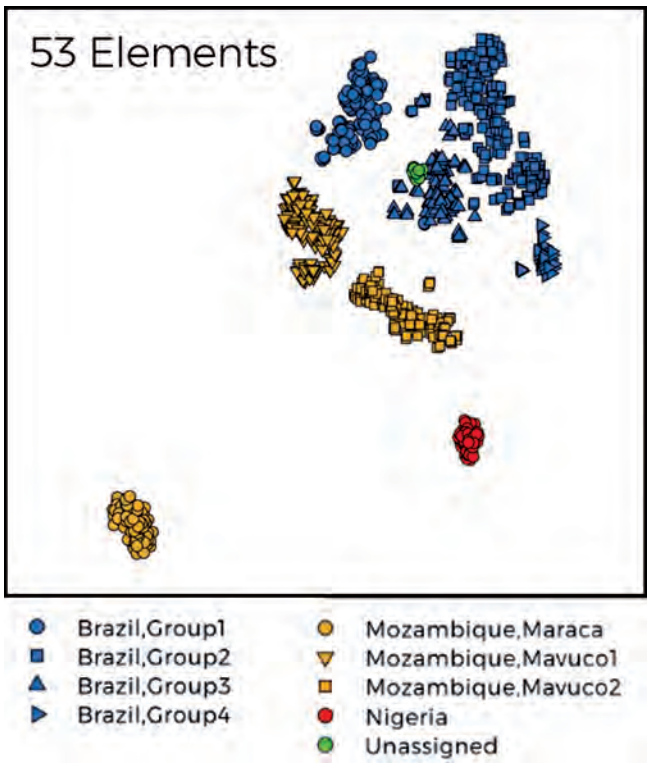

Fig. 2 - Paraíba-type tourmalines from various localities can be differentiated using statistical processing (i.e. t-distributed stochastic neighbour embedding, or t-SNE) of trace-element data, as obtained here by LA-ICP-TOF-MS analysis. (Image © SSEF).

Fig. 3 - This 2.6 ct Paraíba-type tourmaline from Mozambique is shown as received for gem testing with oil-filled fissures (left), and after the oil has been removed from the fractures by cleaning the stone in acetone (right). (Composite photo © SSEF).

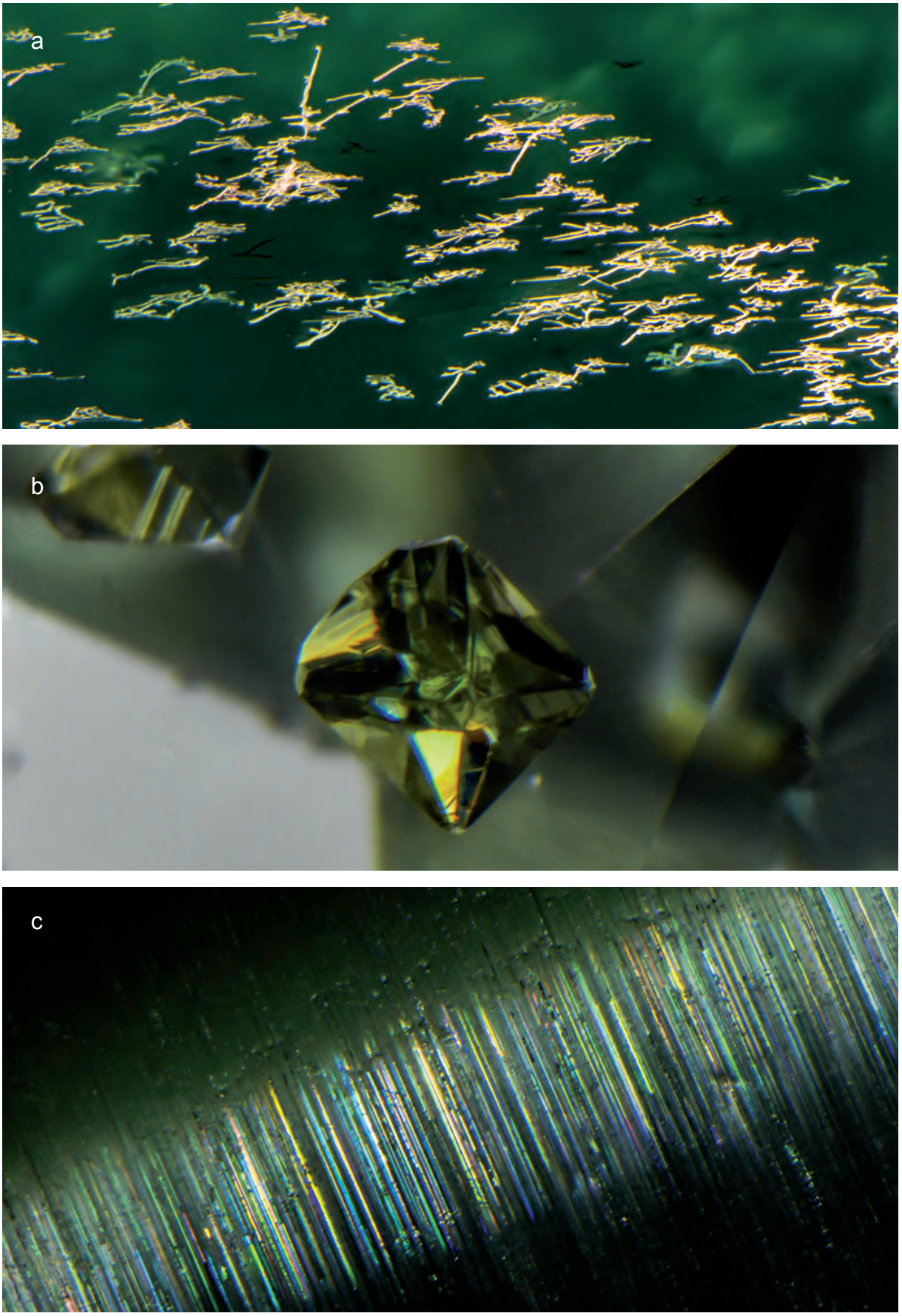

Fig. 4 - Inclusions seen in gem tourmaline include (from top to bottom): a) dendrites of native copper in a stone from São José da Batalha in Paraíba State, Brazil (image width 2.3 mm); b) pyrochlore in tourmaline from Myanmar (image width 1.9 mm); c) growth tubes oriented parallel to the *c*-axis, which are capable of causing chatoyancy, in a tourmaline from Minas Gerais, Brazil (image width 2.0 mm). (Courtesy of the John Koivula Inclusion Collection. Photomicrograph: Nathan D. Renfro, © GIA).

REFERENCES

Dai S., Qu W., Xia Y., Chen H., Chen D., Luo Q. & Xu S., 2017 − Research on the identification of filled tourmaline and its filling grade. *Journal of Mineralogy and Petrology*, 37 (3): 6-15.

Delaunay A., Fritsch E., Stephant N. & Hennebois U., 2020 − Gem Notes: Tourmaline with cassiterite inclusions. *Journal of Gemmology*, 37 (4): 349-350. <doi: 10.15506/JoG.2020.37.4.349>

Hänni H. A., Milisenda C. C. & Wang H. A. O., 2019 − Turmalin mit Coltan Einschlüssen – ein Beispiel von natürlicher Selbstbestrahlung [Tourmaline with coltan inclusions – An example of autoirradiation]. *Gemmologie: Zeitschrift der Deutschen Gemmologischen Gesellschaft*, 68 (3/4): 55-60.

Jia X. & Sit M. M., 2017 − Lab Notes: Rubellite with incredibly strong "pink sleeves". *Gems & Gemology*, 53 (1): 101.

Katsurada Y., Sun Z., Breeding C. M. & Dutrow B. L., 2019 − Geographic origin determination of Paraiba tourmaline. *Gems & Gemology*, 55 (4): 648-659. <doi: 10.5741/gems.55.4.648>

Krzemnicki M. S., 2021 − New copper-bearing tourmalines from Nigeria. *SSEF Facette*, 27: 21.

Laurs B. M., Falster A. U. & Simmons W. B., 2017 − Gem Notes: Tourmaline from Masisi, Democratic Republic of the Congo. *Journal of Gemmology*, 35 (8): 698-700. <doi: 10.15506/JoG.2017.35.8.691>

Leblan S., Fritsch E., Droux A. & Segura O., 2015 − Canalicules et fractures roses dans une tourmaline de type "Paraïba" [Tubules and pink fractures in a tourmaline from "Paraíba"]. *Revue de Gemmologie A.F.G.*, 192: 9-10.

Milisenda C. C. & Müller S., 2017 − REE photoluminescence in Paraíba type tourmaline from Mozambique. *35th International Gemmological Conference*, Windhoek, Namibia: 71-73.

Nasdala L., Wildner M., Giester G., Chanmuang N. C., Scicchitano M. R. & Hauzenberger C., 2021 − Blue dravite ('Indicolite') from the Elahera gem field, Sri Lanka. *Journal of Gemmology*, 37 (6): 618-630. <doi: 10.15506/JoG.2021.37.6.618>

Setkova T. V., Balitsky V. S. & Shapovalov Y .B., 2019 − Experimental study of the stability and synthesis of the tourmaline supergroup minerals. *Geochemistry International*, 57 (10): 1082-1094. <doi: 10.1134/s0016702919100094>

Suwanmanee W., Wanthanachaisaeng B., Utapong T. & Sutthirat C., 2021 − Colour enhancement of pink tourmaline from Nigeria by electron-beam and gamma irradiation. *Journal of Gemmology*, 37 (5): 514-526. <doi: 1010.15506/JoG.2020.37.5.514>

Wang H. A. O., Krzemnicki M. S., Büche S., Degen S., Franz L. & Schultz-Guttler R., 2021 − Multi-element correlation analysis of Cu-bearing tourmaline using LA-ICP-time-of-flight-MS. *EGU General Assembly*, 19-30 April.

Oscillatory zoned liddicoatite from Anjanabonoina, central Madagascar: trace element patterns determined by LA-ICP-MS

Aaron J. Lussier[1]*, Frank C. Hawthorne[2]

Large crystals of liddicoatite tourmaline from the Anjanabonoina pegmatite of central Madagascar are well-known for exhibiting distinct patterns of oscillatory zoning (OZ). This study follows two previous investigations, in which the crystal chemistry (Lussier *et al*., 2011) and variations of major chemical constituents (Lussier & Hawthorne, 2011) were thoroughly characterized. Here, the variations of elements present in trace concentrations are investigated. A thorough survey of potential elements (48 in total) by Laser Ablation - Inductively Coupled Plasma - Mass Spectrometry (LA-ICP-MS) confirmed the occurrence of 29 elements with mean abundances above limits of detection, typically ranging between <1 and ~200 ppm.

Here, trace element behaviour is systematically examined along a continuous analytical traverse (total length, ~90 mm; total data, ~8800 points) form the core to the edge of the crystal (Fig. 1). Four types of behaviours are observed: (1) OZ profiles in phase with those of major elements (*e.g*., Pb^{2+}, Ti^{4+}, Ta^{5+}, Nb^{5+}); (2) OZ profiles antiphase with those of major elements (*e.g*., $LREE^{3+}$); (3) no OZ (*e.g*, Be^{2+}, Ga^{3+}); and (4) anomalous compositional variation (Cu^{2+}).

For elements of type (1), each OZ corresponds to a predictable variation in abundance: a pronounced discontinuity, followed by a nonlinear change. For elements such as Ti^{4+}, Ta^{5+}, and Nb^{5+} (Fig. 2a), a discontinuous increase is followed by a smooth decrease, whereas for elements such as Bi^{3+} and Pb^{2+} (Fig. 2b), the opposite behaviours are observed. In each case, the absolute rate of abundance change with respect to distance (*da*/*dx*) is greatest towards the beginning of each zone, decreasing rapidly with growth. These trace element profile shapes very closely mirror those observed for major elements.

[1] Canadian Museum of Nature, P.O. Box 3443, Stn. D. Ottawa, Ontario, K1P 6P4 Canada.
[2] Department of Geological Sciences, University of Manitoba, Winnipeg, Manitoba, R3T 2N2 Canada.
E-mail: frank.hawthorne@umanitoba.ca

* Corresponding author: alussier@nature.ca

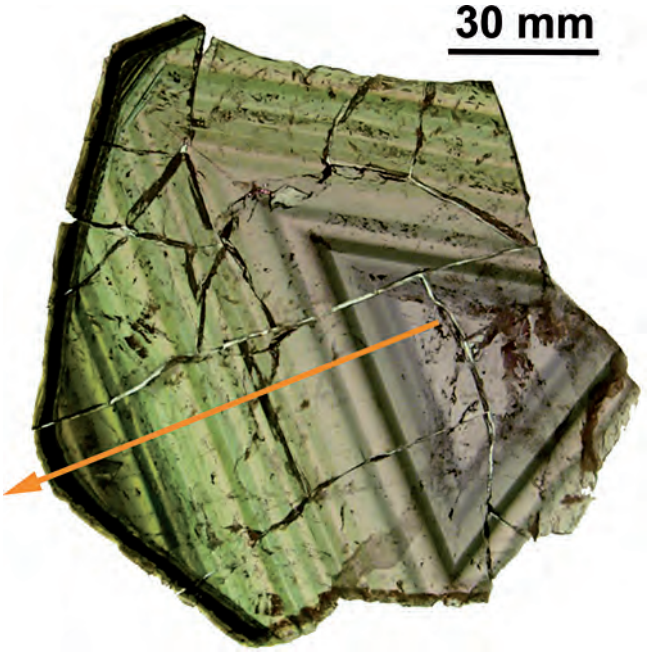

Fig. 1 - Studied liddicoatite slab, cut perpendicular to [001].

For elements of type (2), such as La^{3+} (Fig. 2c), each OZ again begins with a discontinuous decrease in abundance, followed by a nonlinear increase. However, *da*/*dx* is slight at the beginning of each zone, increasing with growth. Pronounced discontinuities in baseline abundances are also observed along the analytical traverse, *e.g*., a significant drop at ~20 mm. Hence, elements of type (2) show trends in both baseline abundance and individual OZ profiles that are unique, not observed for major elements.

By matching trace element ionic radii to known crystal chemical and crystal structural parameters, valence and site location are deduced; both are observed to exert significant influence on oscillatory behaviour. Generally, elements occurring at the *X*- (*e.g*., Bi^{3+}, REE^{3+}) and *Y*-site (*e.g*., Ti^{4+}, Nb^{5+}, Ta^{5+}) are likely to show pronounced OZ, whereas those occurring at the *T*-site (Be^{2+}, Ga^{3+}) are not.

The mean amplitude of individual zones (measured as the magnitude of the initial discontinuity) varies in nearly

linear proportion to the mean element abundance over the analytical traverse; however, along individual element profiles, OZ amplitudes are relatively consistent. Trace elements with the largest amplitudes include Ti^{4+} (amplitude, ~3100 ppm), Bi^{3+} (~175 ppm), and Sn^{5+} (~115 ppm), whereas elements with the smallest amplitudes include Sc^{3+} (~3 ppm), Th^{4+} (2.5 ppm), and Y^{3+} (1.3 ppm).

In major element profiles, significant differences in element behaviour were observed between OZs occurring parallel to the pyramidal {021} and prismatic {110} faces; these differences are echoed in profiles of trace elements, confirming the influence of growth face structure on oscillatory feedback processes.

In a growing crystal, much of the variation in major element composition is constrained by stoichiometry. By contrast, the incorporation of trace elements is affected by subtle differences in the ionic and crystallographic characteristics of the growth system. As undertaken here, the systematic, comparative study of multiple trace elements provides valuable insight into operating growth mechanisms that are imperceptible to investigations of major element chemistry.

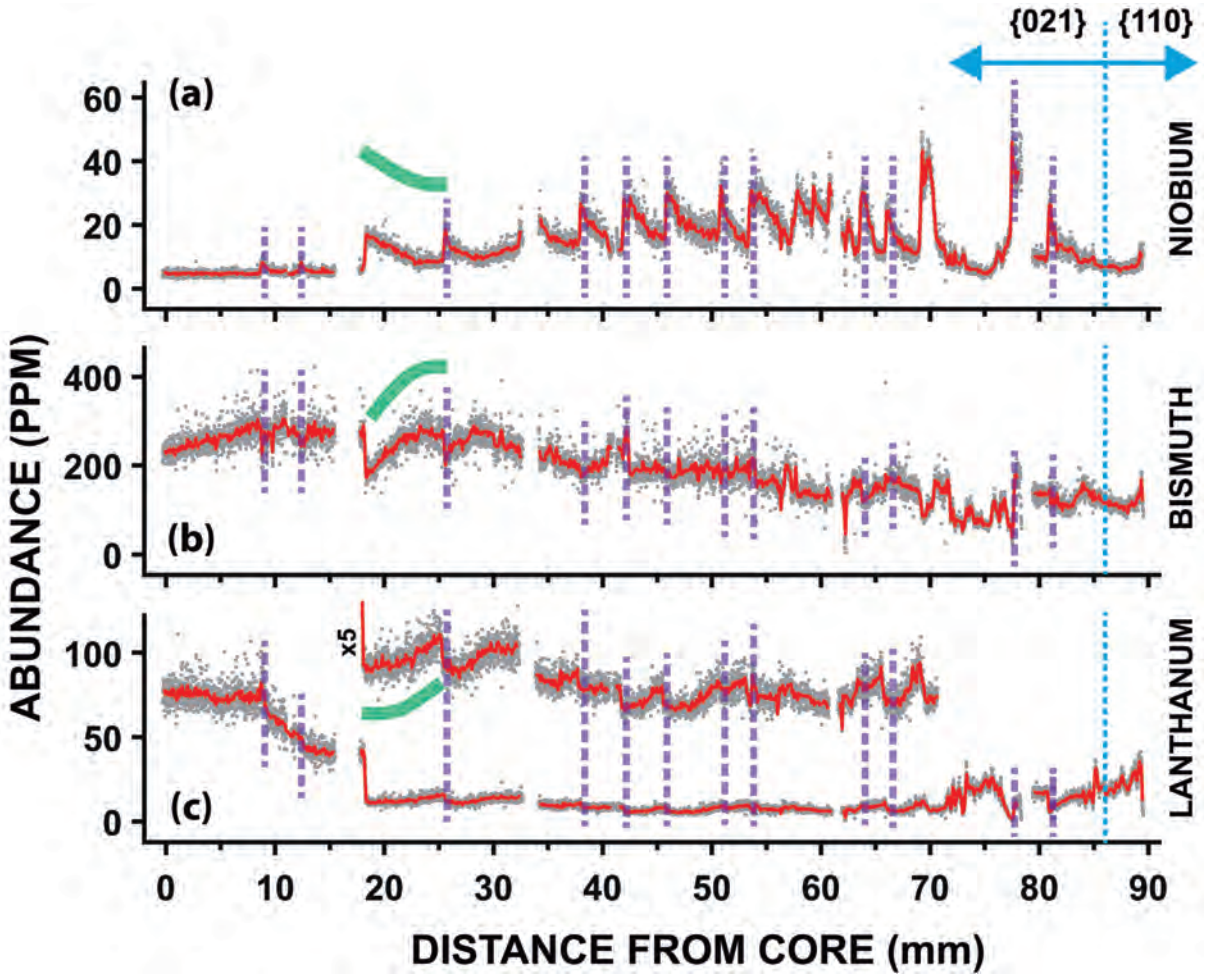

Fig. 2 - Example element profiles: niobium, bismuth, and lanthanum. Grey dots and red lines are all data points and averages of 10 consecutive points, respectively. The general shapes of individual OZ profile are outlined in green at 20 mm.

REFERENCES

Lussier A. J. & Hawthorne F. C., 2011 – Oscillatory zoned liddicoatite from central Madagascar. II. Compositional variation and substitution mechanisms. *The Canadian Mineralogist*, 49 (1): 89-104.

Lussier A J., Abdu Y., Michaelis V. K., Aguiar P. M., Kroeker S. & Hawthorne F. C., 2011 – Oscillatory zoned liddicoatite from Anjanabonoina, central Madagascar. I. Crystal chemistry and structure by SREF and ^{11}B and ^{27}Al MAS NMR spectroscopy. *The Canadian Mineralogist*, 49 (1): 63-88.

Tourmaline isotopes – ten years left behind

Horst R. Marschall

A decade has past since 'The Year of the Tourmaline', proclaimed by Henry *et al*. in 2011 for the publication of three major contributions to the field that saw their appearance in said year, i.e. the 406 pages special volume in the *Canadian Mineralogist*, the nomenclature of the tourmaline supergroup in the *American Mineralogist*, and the tourmaline issue of *Elements* in October of 2011. The Elements issue featured a range of overview articles on the petrology, gemology and geochemistry of the tourmaline supergroup. Shao-Yong Jiang and I had contributed a review on different isotope systems that had been analysed in tourmaline to reconstruct magmatic, metamorphic and metasomatic systems (Marschall & Jiang, 2011). Most studies to date still focus on boron isotopes, but some combine that with the detailed investigation of major- or trace-element zoning or with other stable or radiogenic isotope systems, such as $\delta^{18}O$, δD, $\delta^{7}Li$ or $^{87}Sr/^{86}Sr$ (e.g., Bast *et al*., 2014; Su *et al*., 2019; Xiang *et al*., 2020; Harlaux *et al*., 2021).

The past decade has seen various advancements in the analytical capabilities of isotope analyses of tourmaline. This includes the in-situ boron isotope analyses by laser-ablation coupled to a multi-collector ICP mass spectrometer (e.g., Hou *et al*., 2010; Míková *et al*., 2014; Albert *et al*., 2019). The advantage of this type of analysis compared to secondary-ion mass spectrometry (SIMS) lies in the shorter analysis time of approximately 2 min per spot, compared to typically 5 to 10 min for SIMS at comparable accuracies and precisions (0.4–1.0 ‰ 2SD). The spatial resolution, on the other hand, is better in SIMS, with a typical spot size of 5–10 µm diameter and <1 µm depth compared to 20–30 µm diameter and 10–20 µm depth for a laser spot; yet in many natural tourmaline samples that limitation is not crucial, because of their sufficient grain size and wide growth zones.

SIMS has also been operated in multi-collection mode, which resulted in lower uncertainty and shorter analyses times (Codeço *et al*., 2019; Xiang *et al*., 2020). The introduction of the more stable and reliable Hyperion radio-frequency oxygen plasma ion source on the Cameca instruments promises further improvements in the reproducibility of SIMS boron and oxygen isotope analyses of tourmaline (Marger *et al*., 2020).

As part of the analytical advancements, the well-known Harvard-Museum tourmaline triple along with the IAEA-B4 schorl was characterized for their oxygen and lithium isotopic compositions, and can thus be employed as reference materials for the in-situ analysis of tourmaline (Tab. 1). In addition, a larger compositional variety of tourmaline was characterized for their use as potential reference materials for the analysis of boron and oxygen isotope ratios (Tab. 1). The extended range in chemical composition of these potential reference materials enables us to quantify chemical matrix effects in the analysis of stable isotope ratios and thus improves analytical accuracy.

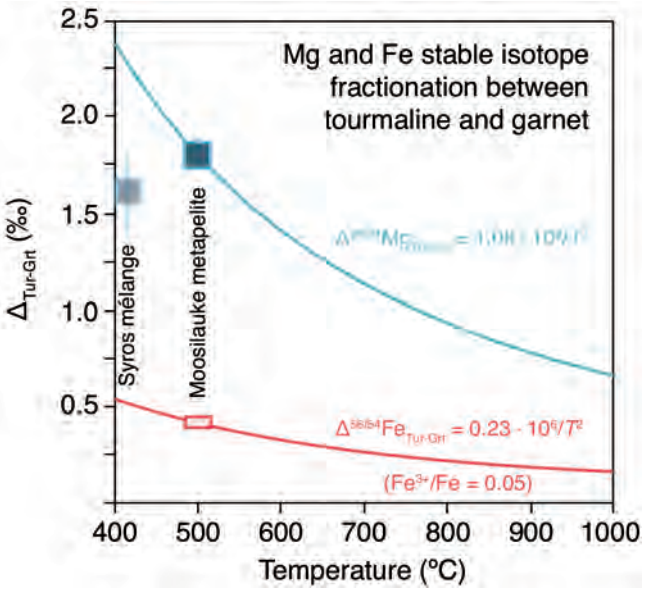

Fig. 1 - Mg (blue) and Fe (red) isotope fractionation between tourmaline and garnet as determined from ab-initio calculations and from experimentally determined force constants. Also shown are analyses from a natural metapelite sample from Mt. Moosilauke (New Hampshire). After Nie *et al*. (2021). Mg isotope fractionation for samples from Syros, Greece from a high-*P* mélange zone was calculated from tourmaline-glaucophane and glaucophane-garnet pairs (Pogge von Strandmann *et al*., 2015).

Institut für Geowissenschaften, Goethe-Universität, Altenhöferallee 1, 60438 Frankfurt am Main, Germany.
E-mail: marschall@fierce.uni-frankfurt.de

Table 1 - Tourmaline reference materials used for stable isotope analyses. Note that four out of eleven reference tourmalines originate from Elba island. References are: 1) Leeman & Tonarini, 2001; 2) Gonfiantini *et al*., 2003; 3) Hou *et al*., 2010; 4) Lin *et al*., 2019; 5) Marger *et al*., 2019; 6) Marger *et al*., 2020; 7) Wiedenbeck *et al*., 2021; 8) Wiedenbeck *et al*., unpublished data.

No.	name	supplier	composition	locality	$\delta^{11}B$	$\delta^{18}O$	$\delta^{17}O$	δD	$\delta^{7}Li$	references
1	HS.98144	Harvard Mineral Museum	elbaite	Minas Gerais, pegmatite	-10.4 -12.0	+13.76	+7.28	-99.4	+7.1 +7.9	1, 4, 6, 7
2	HS.108796		dravite	Madagascar, pegmatite	-6.6 -6.9	+10.07	+5.31	-47.3	+10.2	1, 6, 7
3	HS.112566		schorl	Alto Ligonha, pegmatite	-12.5 -13.9	+9.66	+5.08	-92.4	+5.5 +6.5	1, 4, 6, 7
4	IAEA-B4	IAEA	schorl	Elba island, pegmatite	-8.7	+11.09			+2.6 to +6.4	2–8
5	UNIL-T1	University of Lausanne	schorl	Elba island, pegmatite	-9.2	+10.82				5, 6
6	UNIL-T2		dravite	Nepal, metasediment	-10.0	+7.63				5, 6
7	UNIL-T3		schorl	Pakistan	-15.5	+10.37				5, 6
8	UNIL-T4		darrellhenryite	Elba island, pegmatite	-9.4	+11.32				5, 6
9	UNIL-T5		darrellhenryite	Elba island, pegmatite	-9.2	+11.29				5, 6
10	UNIL-T6		fluor-elbaite	Alaska, Tur-Qz	-10.8	+12.43				5, 6
11	IMR RB1	Chineses Academy Geol. Sci., Beijing	schorl	Shangdong, pegmatite	-13.0				+2.5	3, 4

The quantitative interpretation of stable isotope data in a geologic context requires accurate knowledge on stable isotope fractionation. Much progress has also been made on this front in recent years. The temperature-dependent equilibrium fractionation between tourmaline and coexisting minerals and fluids for various stable isotope systems was investigated. Three different avenues are taken to determine isotope fractionation factors: (1) analyses of mineral pairs from natural rocks that display tourmaline in an equilibrium assemblage; (2) laboratory experiments in which tourmaline is synthesised in equilibrium with other minerals, fluids or melts at specific *P–T* conditions, or (3) ab-initio calculations that enable the determination of stable isotope fractionation factors from bond strengths as a function of *P*, *T* and mineral composition (see Kowalski & Wunder, 2018). Calculations and natural mineral pairs have been presented for various stable isotope systems, such as the classical O and H, but also for the 'non-traditional' metal isotope systems Mg and Fe (Fig. 1). In-situ $\delta^{18}O$ analyses in tourmaline in metamorphic rocks are now being used, not only to distinguish between inherited and metamorphic grains, but indeed to determine the temperatures of formation of individual growth zones through tourmaline–quartz O isotope fractionation (Marger *et al*., 2019).

However, much of the focus has been on boron isotopes. The $\delta^{11}B$ fractionation between tourmaline and aqueous fluid is now known in great detail as a function of temperature, tourmaline major element composition, tetrahedral B content of tourmaline, and fluid pH (or B speciation in the fluid expressed as boric acid/borate ion ratio) (Kowalski & Wunder, 2018; Li *et al*., 2020). The isotope fractionation factors are well enough constrained, such that measured boron isotopes in coexisting tourmaline–mica pairs in natural rocks are now used to estimate the temperature of their formation (Codeço *et al*., 2019).

The application of boron isotopes in the geosciences has seen a real breakthrough over the past decade, driven by a number of detailed studies in the low- and high-temperature isotope geochemistry of boron including such diverse fields as weathering studies, environmental geology, paleoceanography, ore geology, mantle geochemistry and cosmochemistry (see Marschall & Foster, 2018). For example, a well-defined value for the B isotopic composition of mid-ocean ridge basalt and the mantle was established, which serves as a baseline for the interpretation of all other geological materials and reservoirs (Marschall *et al*., 2017). These advances were only possible, of course, with the improvement of the analytical protocols mentioned above.

The total variation of $\delta^{11}B$ tourmaline in nature reported to date spans a range of more than 66 ‰ from -29.9 ‰ in schorl from a Mesoarchaean granite dyke in Swaziland to +36.5 ‰ in dravite from an unconformity-related U deposits from the Athabasca Basin in Canada (Trumbull & Chaussidon, 1999; Mercadier *et al*., 2012). The natural range is thus approximately 100 times larger than the typical analytical uncertainties, which makes tourmaline boron isotopes such a sensitive geochemical tool.

Over the past decade tourmaline isotope geochemistry was employed in a large number of studies in the field of ore deposit research. In their review, Trumbull *et al*. (2020) list more than 2600 tourmaline boron isotope analyses from 119 different localities representing all types of hydrothermal ore deposits. An equally large number of studies have investigated S-type granites and pegmatites, many of them in the high Himalayas, where the boron isotopes are being employed to demonstrate the metasediment-derived melt character of the plutons, their magmatic differentiation and the interaction of the magma with the country rock during magmatic-hydrothermal evolution.

In both cases, a dominant distinction needs to be made in order to unravel the petrogenetic histories between, on the one hand, closed magmatic systems that evolve by cooling and internal differentiation and phase separation (e.g. Codeço *et al*., 2019; Li J. X. *et al*., 2020) and, on the other hand, open magmatic systems in which mineral precipitation and ore formation are governed by the influx and admixture of country rock or external fluids (e.g. Su *et al*., 2019; Harlaux *et al*., 2021; Carr *et al*., 2021). It is noteworthy that most cases are likely to transition from dominantly closed magmatic to open hydrothermal

systems in their cooling history (e.g. Xiang *et al*., 2020). The ubiquitous occurrence of tourmaline in and around peraluminous intrusions and most types of hydrothermal ore deposits along with its large chemical variability has drawn a lot of attention to this mineral group as a petrogenetic recorder. Some of the petrogenesis can be unravelled through the major and trace-element composition of tourmaline, yet this can be hindered or left ambiguous by potential changes in physical parameters (P, T, fO_2) that also influence mineral chemistry and thus complicate the decoding of the chemical evolution of the bulk system.

Studies employing stable and radiogenic isotopes are at an advantage here, as isotope signatures of minerals allow us to clearly distinguish between closed evolution of a system and the influx of externally-derived components. This becomes especially powerful where in-situ analytical methods are employed that enable us to determine the exact points in the petrogenetic history where material sources changed, mixed or unmixed. This can be taken even one step further with the combination of two or more isotope systems, as this helps to restrict the modelling parameters and can be used to quantify the processes involved. Recent studies have thus combined the petrographic and chemical investigation of tourmaline with a combination of $\delta^{11}B$ and other isotope systems, such as $\delta^{18}O$, $\delta^{7}Li$ or $^{87}Sr/^{86}Sr$ (e.g., Bast *et al*., 2014; Su *et al*., 2019; Xiang *et al*., 2020; Harlaux *et al*., 2021). Where one isotope system on its own may leave ambiguity, a combination of two systems will in many cases enable a clear distinction of different generations of minerals and their sources (Fig. 2).

There were also several attempts to employ tourmaline from Archaean near-surface, supra-crustal environments as monitors for the secular evolution of boron isotopes in seawater (see discussion in Marschall & Foster, 2018). However, the success of this approach is hampered by the fact that the tourmaline in those ancient metasediments and metabasalts evidently formed through multistage processes, which loads the reconstruction of seawater isotopic compositions with large propagated uncertainties. In addition, it is difficult to judge whether the supracrustal rocks formed in restricted basins or communicated with the global ocean. It should also be noted that no tourmaline has ever been found in modern seafloor sediments or basalts, making it impossible to test the isotopic reconstruction on modern samples.

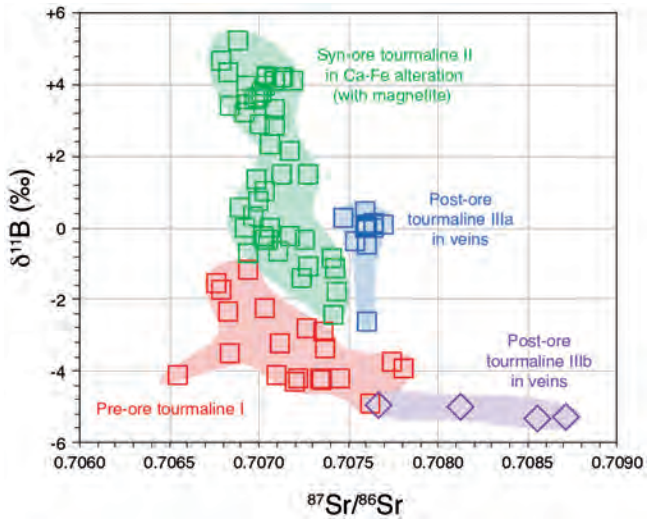

Fig. 2 - Boron isotopic composition vs. $^{87}Sr/^{86}Sr$ ratio of four generations of tourmaline from the Taocun giant iron oxide–apatite deposit. Pre-, syn- and post-ore tourmaline are distinct in B-Sr-isotope space showing that ore formation involved magmatic as well as externally-derived fluids (re-plotted from Su *et al*., 2019).

Similar obstacles burden the interpretation of tourmaline isotope data from continental supracrustal settings. For example, Cabral *et al*. (2021) report boron isotope data of dravite–magnesio-foitite from Palaeoproterozoic metalaterites from the Sao Francisco Craton. Laterites form by oxidative weathering under subaerial, tropical conditions, and the occurrence of such rocks at 2.2 Ga is evidence for an O_2-bearing atmosphere at this time in Earth history. Yet, laterites are leached in water-soluble elements, such as boron, requiring a subsequent event of boron metasomatism in the soils during diagenesis or metamorphism to supply the boron required for tourmaline formation. Hence, despite of its occurrence in supracrustal rocks, tourmaline unfortunately does not seem to directly record chemical or isotopic signatures of the ocean, the atmosphere or soils. However, future studies may be able to quantify the isotope fractionation pathways from the surface waters or soils to the physically and chemically robust recorder that is tourmaline. A combination of various stable and radiogenic isotope systems may help here too to constrain the parameters.

REFERENCES

Albert C., Lana C., Gerdes A., Schannor M. & Narduzzi F., 2019 – Archean magmatic-hydrothermal fluid evolution in the Quadrilátero Ferrífero (SE Brazil) documented by B isotopes (LA MC-ICPMS) in tourmaline. *Chemical Geology*, 481: 95-109.

Bast R., Scherer E. E., Mezger K., Austrheim H., Ludwig T., Marschall H. R., Putnis A. & Löwen K., 2014 – Boron isotopes in tourmaline as a tracer of metasomatic processes in the Bamble sector of Southern Norway. *Contributions to Mineralogy and Petrology*, 168: 1069.

Cabral A. R., DeFerreira T. H., Lana C., de Castro M. P. & Quieroga G., 2021 – Tourmaline composition and boron isotopes record lateritic weathering during the Great Oxidation Event. *Terra Nova*, 33: 46-55.

Carr P., Norman M. D., Bennett V. C. & Blevin P. L., 2021 – Tin enrichment in magmatic-hydrothermal environments associated with cassiterite mineralization at Ardlethan, Eastern Australia: insights from Rb-Sr and Sm-Nd isotope compositions in tourmaline. *Economic Geology*, 116: 147-167.

Codeço M. S., Weis P., Trumbull R. B., Glodny J., Wiedenbeck M. & Romer R. L., 2019 – Boron isotope muscovite-tourmaline geothermometry indicates fluid cooling during magmatic-hydrothermal W-Sn ore formation. *Economic Geology*, 114: 153-163.

Gonfiantini R., Tonarini S., Gröning M., Adorni-Braccesi A., Al-Ammar A. S., Astner M., Bächler S., Barnes R. M., Bassett R. L., Cocherie A., Deyhle A., Dini A., Ferrara G., Gaillardet J., Grimm J., Guerrot C., Krähenbühl U., Layne G., Lemarchand D., Meixner A., Northington D. J., Pennisi M., Reitznerová E., Ro-

dushkin I., Sugiura N., Surberg R., Tonn S., Wiedenbeck M., Wunderli S., Xiao Y. & Zack T., 2003 – Intercomparison of boron isotope and concentration measurements. Part II: evaluation of results. *Geostandards and Geoanalytical Research*, 27: 41-57.

Harlaux M., Kouzmanov K., Gialli S., Marger K., Bouvier A. S., Baumgartner L. P., Rielli A., Dini A., Chauvet A., Kalinaj M. & Fontboté L., 2021 – Fluid mixing as primary trigger for cassiterite deposition: Evidence from in situ $\delta^{18}O$–$\delta^{11}B$ analysis of tourmaline from the world-class San Rafael tin (-copper) deposit, Peru. *Earth and Planetary Science Letters*, 563: 116889.

Henry D., van Hinsberg V., Marschall H. & Dutrow B., 2011 - 2011: Year of the tourmaline. *Elements*, 7: 128.

Hou K. J., Li Y. H., Xiao Y. K., Liu F. & Tian Y. R., 2010 – In situ boron isotope measurements of natural geological materials by LA-MC-ICP-MS. *Chinese Science Bulletin*, 29: 3305-3311.

Kowalski P. M. & Wunder B., 2018 – Boron isotope fractionation among vapor–liquids–solids–melts: Experiments and atomistic modeling. In: Boron Isotopes. The Fifth Element. Marschall H. R. & Foster G. L. (eds.). *Advances in Isotope Geochemistry*, *Springer*, 33-69.

Leeman W. P. & Tonarini S., 2001 – Boron isotopic analysis of proposed borosilicate mineral reference samples. *Geostandards and Geoanalytical Research*, 25 (2-3): 399-403.

Li J. X., Fan W. M., Zhang L. Y., Ding L., Yue Y. H., Xie J., Cai F. L. & Sein K., 2020 – B-rich melt immiscibility in Late Cretaceous Nattaung granite, Myanmar: Implication by composition and B isotope in tourmaline. *Lithos*, 356-357: 105380.

Li Y. C., Chen H. W., Wei H. Z., Jiang S. Y., Palmer M. R., van de Ven T. G. M., Hohl S., Lu J. J. & Ma J., 2020 – Exploration of driving mechanisms of equilibrium boron isotope fractionation in tourmaline group minerals and fluid: A density functional theory study. *Chemical Geology*, 536: 119466.

Lin J., Liu Y. S., Hu Z. C., Chen W., Zhang C. X., Zhao K. D. & Jin X. Y., 2019 – Accurate analysis of Li isotopes in tourmalines by LA-MC-ICP-MS under "wet" conditions with non matrix-matched calibration. *Journal of Analytical and Atomic Spectrometry*, 34: 1145-1153.

Marger K., Luisier C., Baumgartner L. P., Putlitz B., Dutrow B. L., Bouvier A. S. & Dini A., 2019 – Origin of Monte Rosa whiteschist from in-situ tourmaline and quartz oxygen isotope analysis by SIMS using new tourmaline reference materials. *American Mineralogist*, 104: 1503-1520.

Marger K., Harlaux M., Rielli A., Baumgartner L. P., Dini A., Dutrow B. L. & Bouvier A. S., 2020 –Development and re-evaluation of tourmaline reference materials for in situ measurement of boron δ values by secondary ion mass spectrometry. *Geostandards and Geoanalytical Research*, 44 (3): 593-615.

Marschall H. R. & Foster G. L., 2018 – Boron Isotopes. The Fifth Element. *Advances in Isotope Geochemistry, Springer*.

Marschall H. R. & Jiang S.-Y., 2011 – Tourmaline isotopes: no element left behind. *Elements*, 7: 313-319.

Marschall H. R., Wanless V. D., Shimizu N., Pogge von Strandmann P. A. E., Elliott T. & Monteleone B. D., 2017 – The boron and lithium isotopic composition of mid-ocean ridge basalts and the mantle. *Geochimica et Cosmochimica Acta*, 207: 102-138.

Mercadier J., Richard A. & Cathelineau M., 2012 – Boron- and magnesium-rich marine brines at the origin of giant unconformity-related uranium deposits: $\delta^{11}B$ evidence from Mg-tourmalines. *Geology*, 40: 231-234.

Míková J., Košler J. & Wiedenbeck M., 2014 – Matrix effects during laser ablation MC-ICP-MS analysis of boron isotopes in tourmaline. *Journal of Analytical and Atomic Spectrometry*, 29: 903-914.

Nie N. X., Dauphas N., Esen E. A., Zeng H., Corliss K. S., Hu J. Y., Chen X., Aarons S. M., Zhang Z., Tian H.-C., Wang D., Prissel K. B., Greer J., Bi W., Hu M. Y., Zhao J., Shahar A., Roskosz M., Teng F.-Z., Krawczynski M. J., Heck P. R. & Spear F. S., 2021 – Iron, magnesium, and titanium isotopic fractionations between garnet, ilmenite, fayalite, biotite, and tourmaline: Results from NRIXS, ab initio, and study of mineral separates from the Moosilauke metapelite. *Geochimica et Cosmochimica Acta*, 302: 18-45.

Pogge von Strandmann P. A. E., Dohmen R., Marschall H. R., Schumacher J. C. & Elliott T., 2015 – Extreme magnesium isotope fractionation at outcrop scale records the mechanism and rate at which reaction fronts advance. *Journal of Petrology*, 56: 33-58.

Su Z. K., Zhao X. F., Zeng L. P., Zhao K. D. & Hofstra A. H., 2019 – Tourmaline boron and strontium isotope systematics reveal magmatic fluid pulses and external fluid influx in a giant iron oxide-apatite (IOA) deposit. *Geochimica et Cosmochimica Acta*, 259: 233-252.

Trumbull R. B. & Chaussidon M., 1999 – Chemical and boron isotopic composition of magmatic and hydrothermal tourmalines from the Sinceni granite–pegmatite system in Swaziland. *Chemical Geology*, 153: 125-137.

Trumbull R. B., Codeço M. S., Jiang S. Y., Palmer M. R. & Slack J. F., 2020 – Boron isotope variations in tourmaline from hydrothermal ore deposits: A review of controlling factors and insights for mineralizing systems. *Ore Geology Reviews*, 125: 103682.

Wiedenbeck M., Trumbull R. B., Rosner M., Boyce A., Fournelle J. H., Franchi I. A., Halama R., Harris C., Lacey J. H., Marschall H., Meixner A., Pack A., Pogge von Strandmann P. A. E., Spicuzza M. J., Valley J. W. & Wilke F. D.H., 2021 – Tourmaline reference materials for the in situ analysis of oxygen and lithium isotope ratio compositions. *Geostandards and Geoanalytical Research*, 45: 97-119.

Xiang L., Romer R. L., Glodny J., Trumbull R. B. & Wang R., 2020 – Li and B isotopic fractionation at the magmatic-hydrothermal transition of highly evolved granites. *Lithos*, 376-377: 105753.

The "Elbana" mineralogical collection of the Natural History Museum of the University of Florence, Italy

Vanni Moggi Cecchi[1]*, Lucilla Fabrizi[1], Luciana Fantoni[1], Marco Benvenuti[1,2]

INTRODUCTION

Elba Island has been known since ancient times for its deposits of iron and granite quarries and only since the end of the 18th century the passion for collecting minerals gradually developed. This activity was first moved by the aesthetic value of the crystals and the specimens but soon it became the basis for great scientific researches.

After the discovery of ilvaite at Torre di Rio (in the first times named "ienite", an than "lievrite", and finally ilvaite from the old latin name of Elba Island: Ilva), on early nineteenth century, several documents published by Ottaviano Targioni Tozzetti and other authors, confirmed and promoted the great interest for the island and its minerals (Fantoni & Poggi, 2014, Tanelli *et al*., 2014).

Due to the special attention to the mineralogy of the Island devoted by curators and directors since the foundation of the Museum, the Natural History Museum - Sistema Museale di Ateneo of the University of Florence, contains today by far the most important and comprehensive collection of minerals from Elba. Such collection, named "Collezione Elbana", is mainly resulting from the merging of the Raffaello Foresi and the Giorgio Roster collections, described below.

THE "5000 ELBANI" AND THE "COLLEZIONE ELBANA"

Federico Millosevich (1875-1942) came to Florence as Professor of Mineralogy, after the death of Grattarola. He devoted most of his attention to Elba minerals, addressing his study from both scientific and museological perspective. The synthesis of his work is his publication titled: "I 5000 Elbani" (Millosevich, 1914).

This is a complete catalogue with precise bibliographic citations updated with the most recent studies about Elba, at the time.

[1] Collezione Lito-Mineralogica - Sistema Museale di Ateneo, Università degli Studi di Firenze, 50121 Firenze, Italia.
[2] Dipartimento di Scienze della Terra, Università degli Studi di Firenze, Via La Pira, 4, 50121 Firenze, Italia.

* Corresponding author: vanni.moggicecchi@unifi.it

He also produced the precious "Catalogues of Elba collections", a manuscript containing extremely detailed descriptions and comprehensive reports of the crystalline forms and their combinations., as well as locations and collection of origin of the specimens from the Island. Finally, he also produced, for each mineral of the new and the old collections, a catalogue card with a consecutive numbering. The number of specimens described in the catalogue is in fact 4966, subdivided into: Foresi (2553 specimens), Roster (1467), Antico Magazzino (717), Pisani (151), other (67).

The so-called "Antico Magazzino" consists in specimens already present at the founding of the Museo di Fisica e Storia Naturale (1775). The name "Pisani" has to be referred to Spirito Pisani and Capt. Giuseppe Pisani, who sold and donated to the museum a group of samples in the first half of the nineteenth century and was the former owner of "Cava Pisani", also known as "Fonte del Prete" or "Filone della Speranza" (Orlandi & Pezzotta, 1996).

The few specimens labeled "Ammannati" should be those belonging to the lieutenant Giovanni Ammannati, whose collection is cited by Targioni Tozzetti in his documents.

THE FORESI COLLECTION

Raffaello Foresi (1820-1876) collected minerals, rocks and paleo-ethnological artifacts. The collection was formed by: a) more than 1000 specimens of rocks and fossils of Elba, Pianosa and Montecristo, with labels informing about the locality, even if not certain; b) 4500-5000 mineral specimens not determined and without a specification of the locality; c) about 2900 paleo-ethnological pieces. These collections formed the "Museum Foresi" of Portoferraio, which remained open until Christmas Eve 1876, a few months after Foresi's sudden death. It was visited by the illustrious names for the mineralogy and geology of the time.

In 1878 Foresi's heirs sold the collection to the Natural History Museum of the Istituto di Studi Superiori, progenitor of the University of Florence, dealing with the museum's director G. Grattarola. The transfer of the collection to Florence, in March 1877, was quite complex. Right after the acquiring, it was exhibited in the Poccianti gallery at "La Specola", in special showcases built for the occasion.

Unfortunately, there was very poor documentation associated with this collection, such as very few labels and excursions notes written by Foresi. Giuseppe Grattarola, with the help of Giorgio Roster wrote a list of the specimens with some additional information about localities.

Most of the mineralogical collection consists of specimens from the iron ore mines, but the most famous part of the collection are the specimens of tourmaline, beryl, orthoclase, garnet and others collected in the pegmatite localities of the S. Piero area, among which four large blocks of rocks covered by drusy feldspars and quartz, with tourmalines, beryls, petalite and pollucite, covered by zeolites, discovered at Masso Foresi and called "four Evangelists". Indeed, Foresi was the owner of some of the most famous mines (known at that time as "caves") of pegmatite minerals and he was helped by Luigi Celleri (1828-1900), a famous miner who worked for him and, later, for Giorgio Roster, for Pilade del Buono and also for Giovanni D'Achiardi.

THE ROSTER COLLECTION

Giorgio Roster (1843-1927) played a key role in the increase of the "Elbana" collection. Professor of hygiene at the Istituto di Studi Superiori in Florence, Roster was a keen botanist and mineralogist who found in the island of Elba the perfect setting for his research. He put together a mineralogical collection of about 1500 specimens, 1150 of which were result of hiking or excavations, about one hundred were the result of purchases from miners Spirito Pisani and Luigi Celleri, about one hundred were donated by friends and acquaintances (such as Mellini and Toscanelli), and about one hundred more were the result of exchanges with other collectors such as Foresi and Corsi.

In fact, besides the unquestionable aesthetic and scientific value, the existence of collection notebooks, catalogue cards, tags, labels and a catalogue in six manuscripts volumes with all the relevant information, make this collection a perfect collection to be stored in a museum.

The very beginning of the collection was in 1869 even if the Roster's collecting activity continued intensively until 1884. Most of the mineral specimens present in the Roster collection are tourmalines and other pegmatite minerals from the area of M. Capanne; nevertheless, significant specimens of the ore-mines and other mineralized outcrops of the island are also present. Roster sold his collection to the Natural History Museum of Florence in 1888.

SOME HIGHLIGHTS OF THE "ELBANA" COLLECTION

Several specimens of crystallized hematite from the ore mines in Rio Marina are considered among the best crystallized pieces ever found in Elba. Moreover, a giant specimen of ilvaite, from the type locality of Torre di Rio, in Rio Marina, is among the largest crystallized pieces of the species. The most important specimens are represented by the tourmalines: the most famous pieces are the "Four Evangelists" and two spectacular large drusy tourmaline pieces, also containing beryls, sold to the Museum in 1881 by Giorgio Roster, and found in a large cavity at Grotta d'Oggi. The largest of the two pieces is probably the most famous from Elba (Fig. 1).

FROM THE MILLOSEVICH TIMES TO PRESENT DAYS

In the following decades of the twentieth century the number of specimens in the "Elbana" collection has markedly increased, up to the present number of about 6000 (Tanelli & Poggi, 2012). Part of the most important specimens are presently exposed in the exhibition hall of the lithological and mineralogical collection of the University's Museum System at Via La Pira, Florence, in a showcase specifically dedicated to the "Elbana" (Fig. 2). Nevertheless, a project of exhibiting many more specimens at the "La Specola" Museum, in Via Romana, is in progress.

Fig. 1 - A beautiful specimen of the Elba collection with 132 tourmaline crystals. Grotta d'Oggi, S.Piero, Elba Island. Size: 38 x 30 x 25 cm. Spec. n. 4973E. (Museo di Storia Naturale – Sistema Museale di Ateneo, Università di Firenze. Photo: S. Bambi).

Fig. 2 - View of the display case dedicated to the Elba collection in the La Pira exhibition course of the Museo di Storia Naturale - Sistema Museale di Ateneo, Firenze. (Photo: S. Bambi).

REFERENCES

Fantoni L. & Poggi L., 2014 − Ottaviano Targioni Tozzetti: interessi mineralogici di un naturalista visti attraverso i suoi corrispondenti. *Atti e Memorie Accademia "La Colombaria"*, 78: 217-255.

Millosevich F., 1914 − I 5000 Elbani del Museo di Firenze. Contributo alla conoscenza della mineralogia dell'Isola d'Elba. *Regio Istituto di Studi Superiori*, Firenze.

Orlandi P. & Pezzotta F., 1996 − Minerali dell'Isola d'Elba. *Novecento Grafico*, Bergamo.

Tanelli G. & Poggi L., 2012 − La Collezione elbana. In: Il Museo di Storia Naturale dell'Università degli Studi di Firenze. Volume IV. Le collezioni mineralogiche e litologiche. G. Pratesi (a cura di). *Firenze University Press*, Firenze.

Tanelli G., Poggi L. & Fantoni L., 2014 − La miniera di Rio e i minerali dell'Isola d'Elba: corrispondenza inedita fra Antonio e Ottaviano Targioni Tozzetti, Giacomo Mellini e Giovanni Fabbroni i tempi della Regia Mista (1816-1818). *Atti e Memorie Accademia "La Colombaria"*, 78:155-179.

Preliminary results of electron microprobe quantification of the Fe oxidation state in tourmalines

Eva Mrkusová, Radek Škoda*

Oxidation state of Fe in natural glasses, crystalline rocks and their minerals reflects the local redox conditions and the crystal-structural constrains of the minerals. It makes the determination of the oxidation state of Fe highly important in geological sciences.

Various analytical methods have been developed for the $Fe^{3+}/\sum Fe$ determination in solids. However, most of them represent a bulk analysis, e.g. Mössbauer spectroscopy (MS), volumetric and colorimetric methods, electrochemical cells method, and crystal field absorption spectroscopy. The major disadvantages of the bulk methods concern the purity and homogeneity of the sample. To avoid contamination of the measured phase the microbeam techniques have been developed (micro MS, micro-XANES, XPS). These techniques require either long-time exposition, synchrotron source, or have a problematic interpretation, respectively. Electron-beam micro techniques include TEM based EELS allowing the determination of the $Fe^{3+}/\sum Fe$ in a nanometre scale and EPMA based technique developed mostly by Höfer *et al.* (1994, 2000), and Fialin *et al*. (2001, 2004). Different approach of Fe valence estimation exploits the bond-valence method (Brown & Altermatt, 1985). The use of the EPMA for quantification of the $Fe^{3+}/\sum Fe$ is essentially associated with the $L_{2,3}$ absorption and these spectra fingerprints Fe electronic state.

The relative positions of the Fe *L*α and *L*β peak maxima and their shapes are functions of coordination, nearest neighbour occupation, oxidation state, and the Fe content (e.g. de Groot *et al*., 1992).

The differences in Fe *L*α and *L*β X-ray spectra can be detected by thorough wavelength angle scans collected by TAP monochromator of the EPMA, and the systematic shift and intensity variation with respect to the Fe^{2+} and Fe^{3+} oxidation state are clearly visible. The calibration of the peak shift and the intensity change in the Fe *L* region, based on the measurement of the standards with known and variable Fe_{tot} content and $Fe^{3+}/\sum Fe$ value, can be used for determination of the $Fe^{3+}/\sum Fe$ value in the unknown.

Flank method developed by Höfer *et al.* (1994, 2000), Höfer & Brey (2007) combines the peak shift and the differences of the Fe *L*α and Fe *L*β intensities as a function of the Fe content and $Fe^{3+}/\sum Fe$ value. The method is based on the measurement of the X-ray intensities at the specific positions on the flanks of the Fe *L*α and Fe *L*β peaks and has been proven to obtain higher sensitivity and better accuracy when compared to the peak-shift method used by *e.g.* Fialin *et al*. (2001, 2004).

Up to date, the EPMA-based $Fe^{3+}/\sum Fe$ determination methods were developed for silicate glasses, garnet supergroup, amphibole supergroup, micas, spinels and olivines.

For the quantitative estimation of the Fe valence in tourmaline we adopted the flank method. For preliminary calibration schorl-dravite from Hodíškov, Czech Republic (Gadas *et al.* 2012), with ~9-11 wt.% FeO_{tot} and fluor-schorl from Erongo, Namibia, with ~20 wt.% FeO_{tot} were selected; MS revealed <0.03 and 0 of $Fe^{3+}/\sum Fe$ in these tourmalines, respectively. The tourmalines are chemically homogeneous, although small (chemically slightly different) core was observed. Tourmaline crystals from both localities were cut into two equal parts and one half of each sample was annealed at 700°C for 100 hours in a furnace in order to oxidation of the Fe^{2+} into Fe^{3+} (Filip *et al*., 2012). This way, we obtained pairs of tourmalines with similar composition differing in Fe oxidation state. Tests of the $Fe^{3+}/\sum Fe$ determination were performed on CAMECA SX100 electron microprobe. Comparison of thorough wavelength angle scans (using TAP monochromator) on tourmaline with Fe^{2+} and Fe^{3+} at the Fe *L*α and *L*β region leads to determination of the flank positions as parts of the X-ray spectra where maximal differences between Fe^{3+} and Fe^{2+} X-ray distribution occur. The maximal difference was obtained at 10 kV. The beam current of 100 nA, and 20 μm beam diameter provided reasonable count rate and no changes of the analysed spot was observed at these conditions after the measurement. The X-ray counts at Fe *L*α and *L*β flank positions were recorded at the same conditions for 240s at each flank position. The flank intensities were collected on natural tourmalines and their annealed counterparts and the calibration of the method

Department of Geological Sciences, Faculty of Science, Masaryk University, Kotlářská 2, CZ-61137 Brno, Czech Republic.
E-mail: 484435@mail.muni.cz

* Corresponding author: rskoda@sci.muni.cz

was done on the basis of Fe *Lα*/*Lβ* flank count ratio and the amount of FeO_{tot}. The quantification of the oxidation state on the test sample form Cancrinite Hill, Bancroft Canada gave reasonable match with the MS data (Filip *et al*., 2012), 0.50±3% and 0.44, respectively, however the EPMA and MS analysed samples slightly differ in composition (~18 and ~20 FeO_{tot}, respectively).

Further calibration and verification using other well-characterized samples is planned to obtain more reliable results. However, preliminary data show a great potential of this method to determine Fe oxidation state in a micrometre scale.

REFERENCES

Brown I. D. & Altermatt D., 1985 – Bond-valence parameters obtained from a systematic analysis of the inorganic crystal structure database. *Acta Crystallographica Section B: Structural Science*, 41 (4), 244-247.

Fialin M., Wagner C., Métrich N., Humler E., Galoisy L. & Bézos A., 2001 – $Fe^{3+}/\sum$ Fe vs. Fe L α peak energy for minerals and glasses: Recent advances with the electron microprobe. *American Mineralogist*, 86 (4), 456-465.

Fialin M., Bézos A., Wagner C., Magnien V. & Humler E., 2004 – Quantitative electron microprobe analysis of Fe3+/∑ Fe: Basic concepts and experimental protocol for glasses. *American Mineralogist*, 89 (4), 654-662.

Filip J., Bosi F., Novák M., Skogby H., Tuček J., Čuda J. & Wildner M., 2012 – Iron redox reactions in the tourmaline structure: High-temperature treatment of Fe^{3+}-rich schorl. *Geochimica et Cosmochimica Acta*, 86: 239-256.

Gadas P., Novák M., Staněk J., Filip J. & Vašinová Galiová M., 2012 – Compositional Evolution of Zoned Tourmaline Crystals from Pockets in Common Pegmatites of the Moldanubian Zone, Czech Republic. *The Canadian Mineralogist*, 50, 895-912.

de Groot F. M. F., Figueiredo M. O., Basto M. J., Abbate M., Petersen H. & Fuggle J. C., 1992 – 2 p X-ray absorption of titanium in minerals. *Physics and Chemistry of Minerals*, 19 (3), 140-147.

Höfer H. E. & Brey G. P., 2007 – The iron oxidation state of garnet by electron microprobe: Its determination with the flank method combined with major-element analysis. *American Mineralogist*, 92 (5-6), 873-885.

Höfer H. E., Brey G. P., Schulz-Dobrick B. & Oberhaensli R., 1994 – The determination of the oxidation state of iron by the electron microprobe. *European Journal of Mineralogy*, 407-418.

Höfer H. E., Weinbruch S., Mccammon C. A. & Brey G. P., 2000 – Comparison of two electron probe microanalysis techniques to determine ferric iron in synthetic wustite samples. *European Journal of Mineralogy*, 12 (1), 63-71.

Tourmalines and pegmatites

Milan Novák

Granitic pegmatites and their exocontacts are geological systems with evidently the largest number of mineral species of the tourmaline supergroup. It is constrained by the availability of B, Al, cations compatible with the tourmaline crystal structure (Na, Ca, Mg, Fe^{2+}, Fe^{3+}, Mn^{2+}, Li, Ti) and F in pegmatite melts as well as by highly variable PT conditions from magmatic stage (~700-400 °C) via early subsolidus (~400-300 °C) to late subsolidus stage down to ~100-200 °C, and P from ~0.5 to ~5 kbar.

Tourmalines exhibit a wide spectrum of chemical compositions and compositional trends studied typically in the pegmatites affiliated to the LCT (Li-Cs-Ta) petrogenetic family including simple barren, beryl-columbite ± phosphate, Li-rich lepidolite-, elbaite-, petalite- and spodumene- subtype, and miarolitic pegmatites (e.g., Jolliff *et al*., 1986; Novák & Povondra, 1995; Selway *et al*., 1999; Tindle *et al*., 2002). Tourmalines from NYF (Nb-Y-F) pegmatites (Novák *et al*., 2011), and primitive anatectic pegmatites (Gadas *et al*., 2012; Fig. 1) have been only sporadically examined mainly due to scarcity of tourmalines in these types of pegmatites. Majority of studies was focused on behaviour of major and minor elements (see the citations above); concentrations of light elements (Li, B, H), trace elements, Fe^{2+}/Fe^{3+}, B-isotopes and Li-isotopes were studied mainly in the last decade (e.g., Novák *et al*., 2011; Siegel *et al*., 2016; Maner & London, 2017; Trumbull & Slack, 2018; Sunde *et al*., 2020).

Due to highly variable chemical composition including B-isotopes and refractory behavior, tourmaline is considered a very useful indicator of a variety of geological processes. Most studies in granitic pegmatites have been focused on primary (solidus) tourmaline, tourmalines from pocket and on tourmalines from endocontact and exocontact zones whereas tourmalines filling late fractures and from subsolidus replacement assemblages were examined rather sporadically. However, large number of paragenetic, textural, morphological, and compositional types of tourmalines in granitic pegmatites requires very careful approach to sampling and thorough study of mineral assemblages, textural relations and mainly internal zoning in BSE images to get reliable conclusions.

Early studies, in part those cited above, as well as some recent studies did not described adequately internal zoning of tourmaline crystals, their position in pegmatite evolution and overall mineral assemblages of the host textural-paragenetic unit. In order to better understand position of tourmaline in the pegmatite evolution, several basic textural-paragenetic types were defined below to be comparable among the individual pegmatite localities. The following types were recognized for Li-poor pegmatites in the first step because complex Li-rich pegmatites typically show more complicated internal structure, richer mineral assemblages, and larger number of tourmaline species. Textural-paragenetic types are highly variable including common pockets and mainly presence of replacement (metasomatic) units. Where appropriate, abundant tourmaline types, characteristic for Li-pegmatites are given as well.

The following tourmaline environments were defined in granitic pegmatites including primary (magmatic) minerals, secondary tourmalines originated by replacement of variety of primary minerals both situated within pegmatite bodies as well as the mineral assemblages with tourmaline from exocontacts of pegmatite bodies.

A. PRIMARY TOURMALINES

(i) Multi-mineral assemblages (Kf+Pl/Ab+Qz±Bt,Ms) with subhedral to euhedral tourmaline (dravite to schorl) occur mainly in border and wall units. It is less common in graphic, blocky and intermediate units where the next defined bi-mineral assemblage (Qz+Tur) is more common. Tourmaline is typically in a direct contact with all minerals within a single pegmatite unit. In Li-pegmatites these assemblages occur in Li-poor units (Kfs+Ab+Qz+Ms+Tur). Lithium-rich units show more variable assemblages (Lpd+Ab+Qz+Elb ± Spd, Ptl, Amb) and the associated Li-rich mineral (lepidolite or petalite/spodumene /amblygonite) influences availability of Li in the parental medium; hence, Li-rich tourmalines are more common in lepidolite- and elbaite-subtype pegmatites characterized also by elevated activity of F.

Department of Geological Sciences, Masasaryk University, Brno, Czech Republic.
E-mail: mnovak@sci.muni.cz

(ii) Bi-mineral assemblage typically Qz+Tur (schorl) with anhedral to euhedral tourmaline and graphic intergrowths with quartz is common in graphic unit, blocky unit, intermediate unit, and massive quartz of the quartz core. Careful study of tourmalines revealed that this type is very common as quartz + tourmaline aggregates (including graphic intergrowths) often enclosed within the pegmatite unit (Fig. 2a) with the multi-mineral assemblage (feldspars + quartz + micas ± garnet, andalusite), where tourmaline is mostly absent or rare; also, their compositions may be distinct. Tourmaline grains are in a direct contact only with quartz which separates tourmaline from other minerals or tourmaline evidently overgrown as a later mineral mostly crystals of blocky K-feldspar (Fig. 2b). Less common bi-mineral assemblages Kfs+Tur and Ab+Tur are mostly part of multi-mineral assemblages in a single pegmatite unit; in Li-pegmatites, the assemblages Ms+Tur (Fe-elbaite) and Lpd+Tur (e.g., elbaite, rossmanite) are common.

(iii) Mono-mineral assemblage where tourmaline crystallized as a sole mineral in open pockets after crystallization of early quartz and feldspars is very rare but present in both Li-poor (schorl, dravite) and Li-rich (elbaite, liddicoatite) pegmatites.

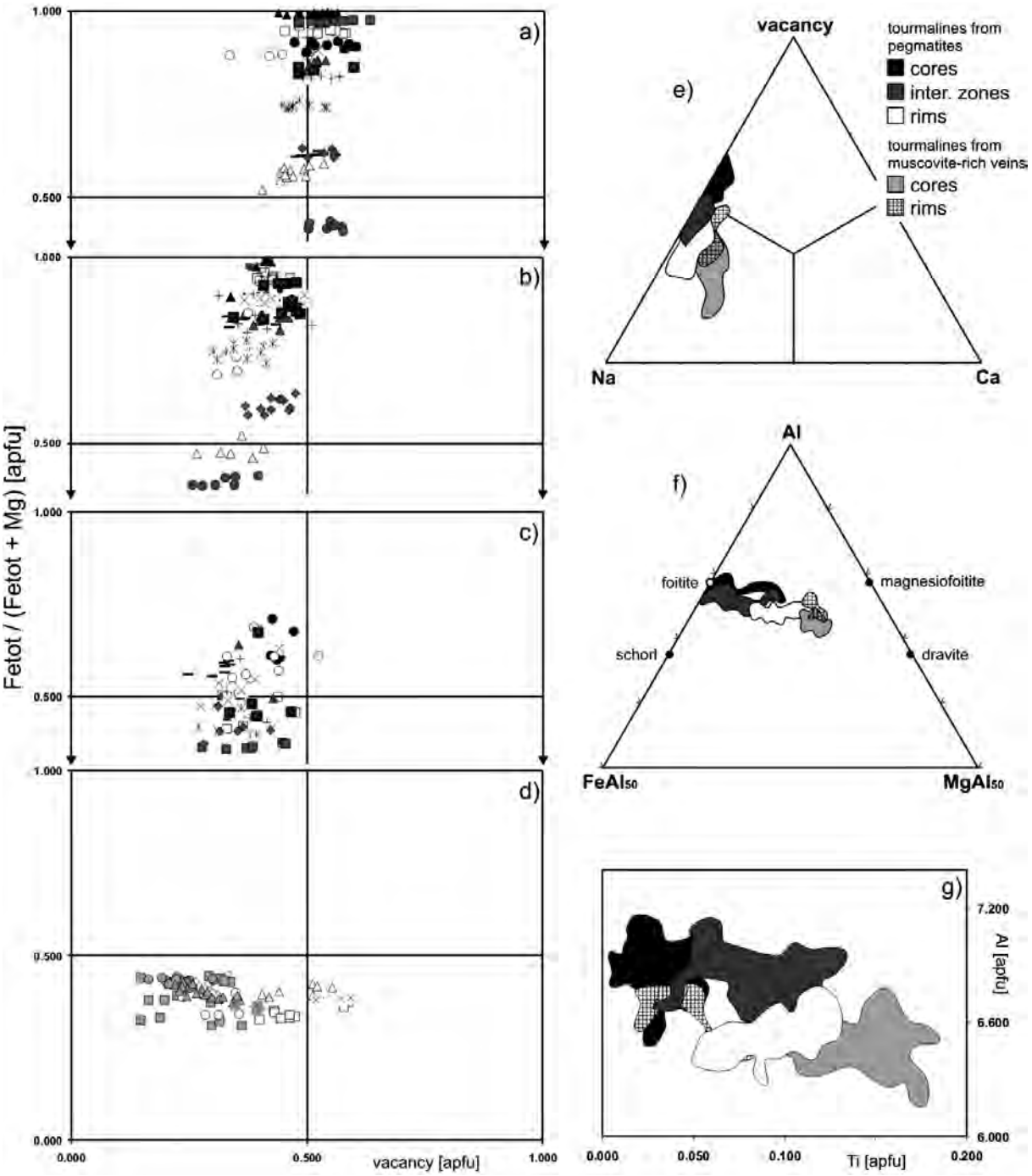

Fig. 1 - Compositional trends of tourmalines from anatectic pegmatites and associated muscovite veins illustrated by various types of diagrams (Gadas *et al*., 2012).

(iv) Fracture-filling tourmaline in thick veins to thin veinlets cutting a massive pegmatite (Fig. 2c) is often primary because it does not replace host minerals typically quartz. However, tourmalines may have partly replaced feldspar of host pegmatite unit at some pegmatites. In this case, it belongs to the next defined type (v) of secondary tourmalines. Both latter types of primary tourmaline (iii) and (iv) evidently crystallized from hydrothermal fluids.

B. SECONDARY TOURMALINES

(v) Tourmaline replacing other primary minerals (e.g., biotite, cordierite) is rather rare in outer units of Li-poor pegmatites (Novák *et al*., 2011); however, this type is more abundant in complex Li-pegmatites and number of replaced minerals is larger (e.g., garnet, primary Fe,Mn-phosphates, borosilicates; e.g., Felch *et al*., 2016). They also include tourmalines veins cutting pegmatite and replacing feldspars from the host pegmatite unit.

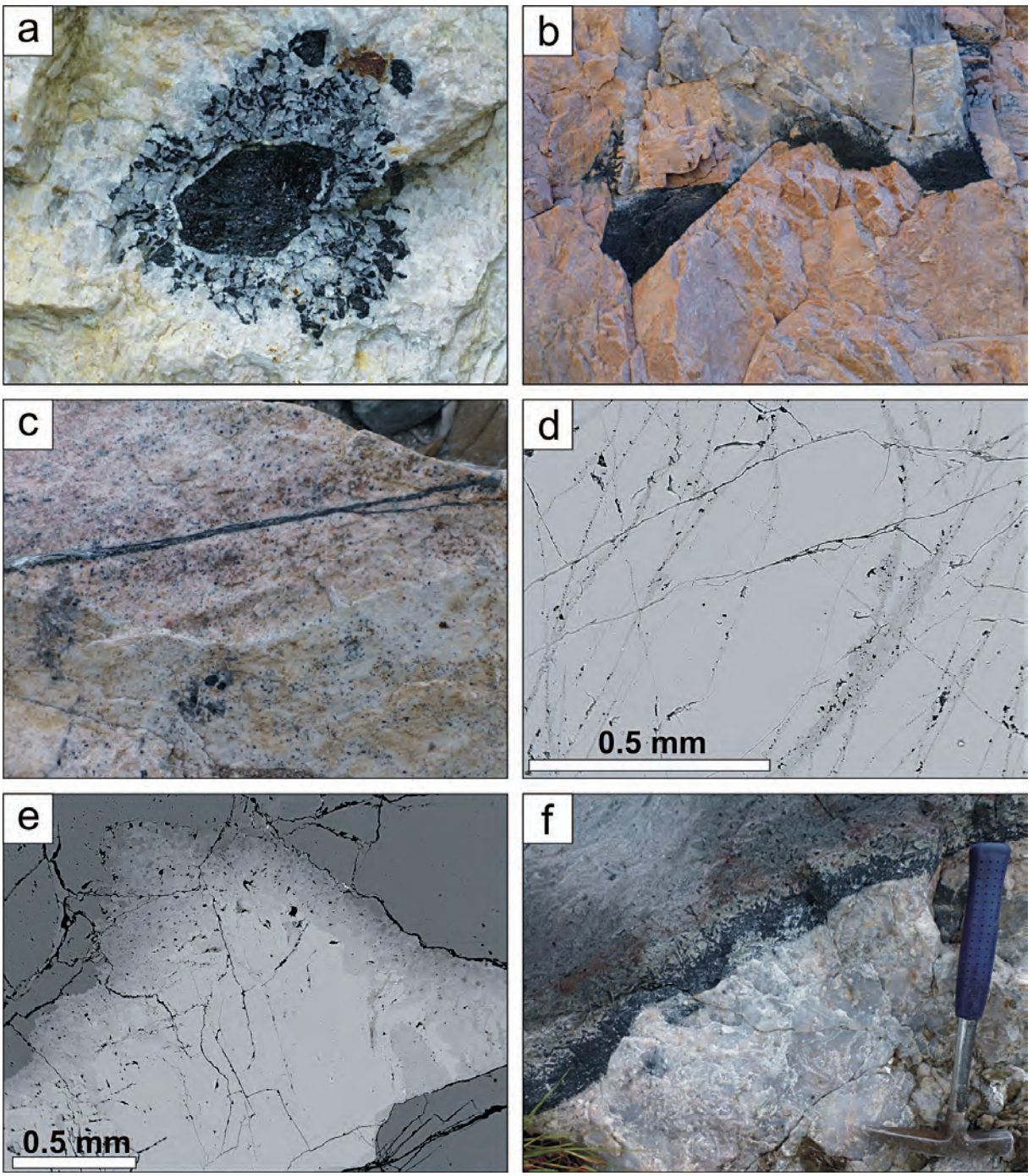

Fig. 2 - Examples of the individual types of tourmaline: a) (ii) bi-mineral assemblage quartz + tourmaline enclosed in feldspars-rich unit, Mt. Mica, Maine, USA; b) (ii) bi-mineral assemblage quartz + tourmaline in quartz core adjacent to blocky K-feldspar, Rancul, San Luis, Argentina; c) (iv) tourmaline veinlet ~ 1 cm thick, cutting pegmatite, Las Cuevas, San Luis, Argentina; d) (vi) BSE image of late veining of tourmaline II in tourmaline I, Puklice, Czech Rep.; e) (vi) BSE image of metasomatic tourmaline II with inclusions of quartz after albite, note weak reaction with quartz, Tamponilapa, Madagascar; f) (vii) exocontact tourmaline-rich zone, Las Cuevas, San Luis, Argentina.

(vi) Tourmaline II replacing early tourmaline I is very common. Late veining and complex replacement textures mostly visible only in BSE images (Fig. 2d,e) are common and may be easily overlooked. Also, it forms fibrous aggregates as replacing terminations of large crystals close to the type (iii).

C. EXTERNAL TOURMALINES

(vii) Tourmalines from exocontact zones are developed mainly along contacts of more evolved pegmatites, typically Li-rich. They occur on the contact with pegmatite mostly as tourmaline-dominant zones (Fig. 2f) of different thickness, textures and mineral assemblages which reflect compositions of host rock and of residual fluids released from pegmatite.

(viii) Tourmaline from external quartz veins released from pegmatite body are rather rare; however, they manifest output of B from pegmatite. The occurrence of external types (vii) and (viii) at the pegmatite is crucial for isotopic studies.

Definition of the individual textural-paragenetic types of tourmaline is certainly accompanying with some degree of simplification. It is evident mainly in Li-pegmatites; however, this approach seems to me better than absence such information in scientific studies. This approach is descriptive and does not require declaration of origin (e.g., magmatic *versus* hydrothermal) of the individual basic types of tourmalines.

CONCLUSIONS

The following information about tourmaline and its mineral assemblages should be given in the studies (e.g., B-isotopes; trace-elements – LA-IC-MS, SIMS; fluid inclusions; spectroscopic studies) to enable comparative study of variety of analytical data from different granitic pegmatites.

1. List of textural-paragenetic types of tourmaline from the particular pegmatite body and which type(s) was examined in detail.

2. Overall mineral assemblage of a single tourmaline sample and potential replacement textures, if needed list of the minerals associated with tourmaline mainly the minerals compatible with B (muscovite, borates, dumortierite, axinite, borosilicates) as well as abundances of the relevant minerals.

3. Size and shape of tourmaline grains, texture of aggregates including their preferential orientation, intergrowths with other minerals or replacement textures.

4. Detailed description of internal zoning of the individual crystals/grains mostly based on BSE study (homogeneous, oscillatory, sectorial, late veining, replacement textures).

5. Presence/absence of microscopic mineral inclusions (mainly quartz) and their distribution (random, oriented) within the examined grains.

6. If tourmaline is developed in pocket its textural paragenetic position – tourmaline crystal is growing from host massive pegmatite unit into open pocket (typically zoned) or crystals are overgrowing early pocket minerals (Kfs, Ab, Qz) (typically homogeneous).

In the case that such detailed information about tourmaline is provided in the paper (including supplements), the analytical results from various localities could be much more easily and more effectively compared and adequately discussed.

REFERENCES

Felch M., Falster A. U. & Simmons W. B., 2016 – Iron-bearing pollucite and tourmaline replacement of garnet in the garnet line in the Mt. Mica and Havey pegmatites, Western Maine. *The Canadian Mineralogist*, 54 (4): 1071-1086.

Gadas P., Novák M., Staněk J., Filip J. & Vašinová Galiová M., 2012 – Compositional evolution of zoned tourmaline crystals from pockets in common pegmatites, the Moldanubian Zone, Czech Republic. *The Canadian Mineralogist*, 50: 895-912.

Jolliff B. L., Papike J. J. & Shearer C. K., 1986 – Tourmaline as a recorder of pegmatite evolution: Bob Ingersol pegmatite, Black Hills, South Dakota. *American. Mineralogist,* 71: 472-500.

Maner IV J. L. & London D., 2017 – The boron isotopic evolution of the Little Three pegmatites, Ramona, CA. *Chemical Geology*, 460: 70-83.

Novák M. & Povondra P., 1995 – Elbaite pegmatites in the Moldanubicum: a new subtype of the rare-element class. *Mineralogy and. Petrolology*, 55: 159-176.

Novák M., Škoda R., Filip J., Macek I. & Vaculovič T., 2011 – Compositional trends in tourmaline from the intragranitic NYF pegmatites of the Třebíč Pluton, Czech Republic; electron microprobe, LA-ICP-MS and Mössbauer study. *The Canadian Mineralogist*. 49: 359-380.

Selway J. B., Novák M., Černý P. & Hawthorne F. C., 1999 – Compositional evolution of tourmaline in lepidolite-subtype pegmatites. *European Journal of Mineralogy,* 11: 569-584.

Siegel K., Wagner T., Trumbull R. B., Jonsson E., Matalin G., Wälle M. & Heinrich C. A., 2016 – Stable isotope (B, H, O) and mineral-chemistry constraints on the magmatic to hydrothermal evolution of the Varuträsk rare-element pegmatite (Northern Sweden). *Chemical Geology*, 421: 1-16.

Sunde Ø., Friis H., Andersen T., Trumbull R. B., Wiedenbeck M., Lyckberg P., Agostini S., Casey W. H. & Yu P., 2020 – Boron isotope composition of coexisting tourmaline and hambergite in alkaline and granitic pegmatites. *Lithos*, 352: 105293.

Tindle A. G., Breaks F. W. & Selway J. B., 2002 – Tourmaline in petalite-subtype granitic pegmatites: evidence of fractionation and contamination from the Pakeagama Lake and Separation Lake areas of northwestern Ontario, Canada. *The Canadian Mineralogist*, 40 (3): 753-788.

Trumbull R. B. & Slack J. F., 2018 – Boron isotopes in the continental crust: granites, pegmatites, felsic volcanic rocks and related ore deposits. In: Boron Isotopes. The Fifth Element, Advances. Marschall H. R. & Foster G. L. (eds.). *Geochemistry*, *Springer*, Heidelberg, 7: 249-272.

Tourmaline evolution in a P, F-rich elbaite-subtype pegmatite

František Novotný*, Jan Cempírek

The elbaite subtype of granitic pegmatites is represented by rather diverse group of localities with both regionally (e.g. Ca-rich pegmatites in Madagascar) and locally distinct geochemical and mineralogical signatures. The P,F-rich elbaite-subtype granitic pegmatite at Dolní Rožínka shows complex magmatic and metasomatic/hydrothermal history of crystallization from early (potassic) and late (sodic) pegmatitic melt followed by hydrothermal overprint, well recorded by tourmaline compositional and textural evolution. The pegmatite minerals include dominant quartz, K-feldspar and albite (in center as cleavelandite zone with pockets), with common tourmaline, garnet (up to 0.5 wt.% P_2O_5), beryl, and apatite; minor and accessory minerals include polylithionite, manganocolumbite, ixiolite, and zircon (up to 3 wt.% HfO_2). Tourmalines are usually black in less evolved units, whereas near pockets they are pink, purple or rarely blue.

Primary magmatic tourmaline (Fig. 1) shows a gradual enrichment in Al+Li and Mn and decrease of Fe+Mg. The early magmatic tourmalines that crystallized from potassic melt are Mg-bearing; last Mg is removed from the melt by the F-poor schorl intergrown with quartz (Tur 1a2). Crystallization of tourmalines in pockets is dominated by fractionation of Mn, and Al+Li – cores (Tur 2a1) are formed by Li-rich schorl whereas rims (Tur 2a2) by Mn-rich elbaite. The zoned crystals from pockets are sometimes overgrown by acicular **hydrothermal tourmaline** (Tur 2c) with heterogeneous composition corresponding to (fluor-)elbaite, locally with elevated Ca, similar to acicular tourmaline in pockets (Tur 2d) that is Ca,F-rich, with peculiar sector zoning and extreme variation of F.

Very abundant **metasomatic tourmaline** after biotite (Tur 1b) is typically Al-deficient Mg-enriched schorl, with clear trend towards bosiite. Metasomatic tourmaline (Tur 1c, Tur 1d) that rims and replaces garnet and tourmaline in early units has very heterogeneous chemical composition dependent on the composition of replaced phase. It is enriched in F, Ca, and Mn, corresponding to either F- or OH-dominated schorl, elbaite, and liddicoatite.

Primary magmatic tourmaline shows a gradual change from Mg+Fe to Mn-enriched and Al+Li-dominant compositions; this change is strikingly different from the abrupt change observed in lepidolite-subtype pegmatites (Skřápková & Cempírek, 2021), as well as the weaker variation of X-site occupancy (e.g. Selway *et al*., 1999).

Transition to the hydrothermal stage caused change of tourmaline habitus to fibrous (e.g. Dutrow & Henry, 2018). The fluids metasomatically reacted with early minerals and are strongly enriched in F, Li, and Ca. Due to absence of Mg in the late stage (cf. Novák *et al*., 2017), we interpret the Ca,Li,F-enrichment as a result of fractionation of late P, F-rich sodic melt followed by exsolution of hydrothermal fluid from the melt in the late stage of albite zone and pockets crystallization.

Rather unclear is the source of B-rich, Li-poor fluid that replaced biotite and produced Al-deficient tourmaline close to bosiite. This secondary tourmaline is later replaced by the omnipresent secondary Li,Ca,F-rich tourmaline (F-rich elbaite and fluor-elbaite). Presence of two secondary tourmalines might indicate two stages of fluid exsolution (B-rich and Li,B,F-rich) during the pegmatite formation.

In general, influence of external contamination from the host rock seems to be very low or none, as the hydrothermal stage is missing Mg-enrichment typical elsewhere (e.g. Novák *et al*., 2017). Early in-situ contamination does not seem to be significant either, as no signs of contact metasomatism (skarn) were observed and the Mg content in in the early pegmatite minerals is not unusually high.

Department of Geological Sciences, Faculty of Science, Masaryk University, Kotlářská 2, 611 37 Brno, Czech Republic.
E-mail: jan.cempirek@gmail.com

* Corresponding author: fk.novotny@seznam.cz

This work was supported by the research projects GAČR 19-05198S and MUNI/A/1594/2020.

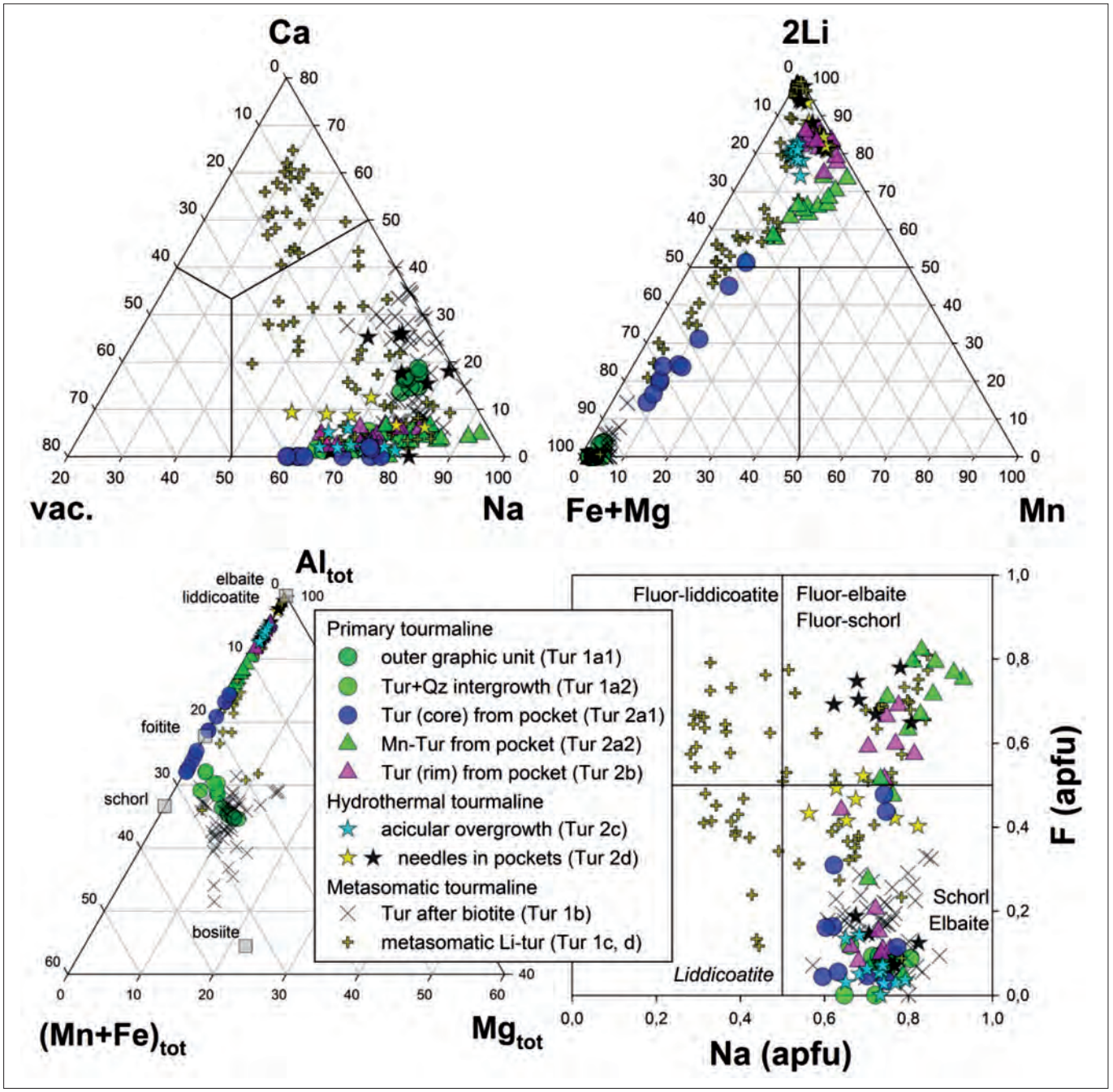

Fig. 1 - Composition of tourmaline from the Dolní Rožínka elbaite-subtype pegmatite.

REFERENCES

Dutrow B. L. & Henry D. J., 2018 − Tourmaline compositions and textures: reflections of the fluid phase. *Journal of Geosciences*, 63: 99-110.

Novák M., Prokop J., Losos Z. & Macek I., 2017 − Tourmaline, an indicator of external Mg-contamination of granitic pegmatites from host serpentinite; examples from the Moldanubian Zone, Czech Republic. *Mineralogy and Petrology*, 111: 625-641.

Selway J. B., Novák M., Černý P. & Hawthorne F. C., 1999 − Compositional evolution of tourmaline in lepidolite-subtype pegmatites. *European Journal of Mineralogy*, 11: 569-584.

Skřápková L. & Cempírek J., 2021 − The role of oxy-tourmalines and metasomatic mixing in evolution of lepidolite-subtype pegmatites. In: TUR2021, 3rd International Conference on Tourmaline, Elba Island, Italy, September 9-11, 2021. Bosi F., Pezzotta F. & Andreozzi G. B. (eds.). *Natura*, 111 (1): 99-100.

Remobilization of B, Be and REE in Veporic granites: late-magmatic formation of tourmaline and neoblastic development of hellandite-(Y) + hingganite-(Y) reaction coronae around xenotime-(Y) during granite mylonitization

Martin Ondrejka[1]*, Peter Bačík[1,2], Igor Broska[2], Pavel Uher[1], Alexandra Molnárová[1], Marián Putiš[1]

This contribution describes late-magmatic tourmaline formed in the Permian Klenovec-type granite and reaction coronae of Y-B-Be silicate minerals developed in Variscan (Carboniferous) metagranites overprinted by Alpine (Cretaceous) blastomylonitization of the Fabova Hoľa Complex, both in the Veporic Unit, Slovakia.

The accumulation of tourmaline in the Klenovec granite developed as large radial aggregates or solitary crystals scattered in the rock. However, Variscan arc granites are not a favorable environment for magmatic borosilicate minerals and high B activity was recognized only in Alpine overprinted rocks. Here, the alteration of primary magmatic xenotime-(Y) produced a novel type of secondary corona consisting of fluorapatite-hellandite-(Y)-hingganite-(Y) and clinozoisite mineral zones.

The tourmaline from the Klenovec granite has mostly schorlitic, rarely oxy-schorlitic composition (Fig. 1A) and a relatively limited chemical variability with Si = 5.9–6.1 apfu, Al = 5.8–6.8, Fe^{2+} = 1.35–2.0, Mg = 0.28–0.98, Ca = 0.0–0.17, Na = 0.61–0.84, and *X*-site vacancies of 0.01–0.37 (Fig. 1B). The composition of hellandite-(Y) and hingganite-(Y) from metagranites of the Fabova Hoľa Complex reflects the Y-dominance over REE (Y = 2.1–2.5 vs. 1.0–1.3, respectively) and a strong Al-Fe distinction, whereby Al dominates over Fe^{3+} in hellandite-(Y): (Al = 0.7–1.0, Fe^{3+} = 0.0–0.26) and vice versa in hingganite-(Y): (Al = 0.0–0.01, Fe^{2+} = 0.34–0.5).

While late-magmatic tourmaline in the Permian Klenovec granite crystallized from a B-rich melt, the localized occurrence of Y-B-Be silicate minerals in the Variscan metagranites, which formed in reaction coronae during post-peak Alpine metamorphism along with other secondary minerals, suggests a high activity of light elements (B and Be) in the transformations. Moreover, this could be also suggested in the surrounding Paleozoic micaceous metapelites of the Veporic Unit, which are rich in tourmaline neoblasts (cf. Jeřábek *et al*., 2008).

Boron and Be were probably mobilized during the Alpine mylonitization from common rock-forming minerals, especially muscovite and plagioclase, which are the principal host phases for B and also Be, considering their relatively low B, Be contents but high modal abundance (cf. Domanik *et al*., 1993; Leeman & Sisson, 1996; London *et al*., 1996). Alternatively, or additionally, a possible source of B could be the altered xenotime-(Y) itself, which contains traces of B (Fig. 2). The incorporation of B into the xenotime-(Y) structure is most probably controlled by coupled heterovalent substitution $(Nb,Ta)BY_{-1}P_{-1}$ (Nb^{5+}, $Ta^{5+} + B^{3+} \leftrightarrow Y^{3+} + P^{5+}$). The natural occurrences of Nb-Ta orthoborates with zircon-xenotime type crystal structure: schiavinatoite $NbBO_4$ and béhierite $TaBO_4$ (Mrose & Rose, 1962; Demartin *et al*., 2001), together with previous indications of B replacing P in xenotime (Oftendal, 1964), support the observation of boron in xenotime-(Y) and the existence of a possible xenotime-(Y)–schiavinatoite–béhierite solid solution. However, this substitution is limited due to very low Nb content in xenotime (~0.1 wt.%), close to detection limit. Consequently, the principal source of B in the studied metagranites is external, most probably from widespread Permian magmatic rocks in the area, e.g., tourmaline-rich Klenovec granite and/or other volcanic rocks (cf. Kotov *et al*., 1996; Vozárová *et al*., 2016).

[1] Comenius University, Ilkovičova 6, 842 15 Bratislava, Slovakia.
[2] Earth Science Institute of the Slovak Academy of Sciences, Dúbravská cesta 9, P.O. BOX 106, 84005 Bratislava, Slovakia.

* Corresponding author: martin.ondrejka@uniba.sk

REFERENCES

Demartin F., Diella V., Gramaccioli C. M. & Pezzotta F., 2001 – Schiavinatoite, $(Nb,Ta)BO_4$, the Nb analogue of behierite. *European Journal of Mineralogy*, 13 (1): 159-165.

Domanik K. J., Hervig R. L. & Peacock S. M., 1993 – Beryllium and boron in subduction zone minerals: An ion microprobe study. *Geochimica et Cosmochimica Acta*, 57: 4997-5010.

Jeřábek P., Janák M., Faryad S. W., Finger F. & Konečný P., 2008 – Polymetamorphic evolution of pelitic schists and evidence for Permian low-pressure metamorphism in the Vepor Unit, West Carpathians. *Journal of Metamorphic Geology*, 26 (4): 465-485.

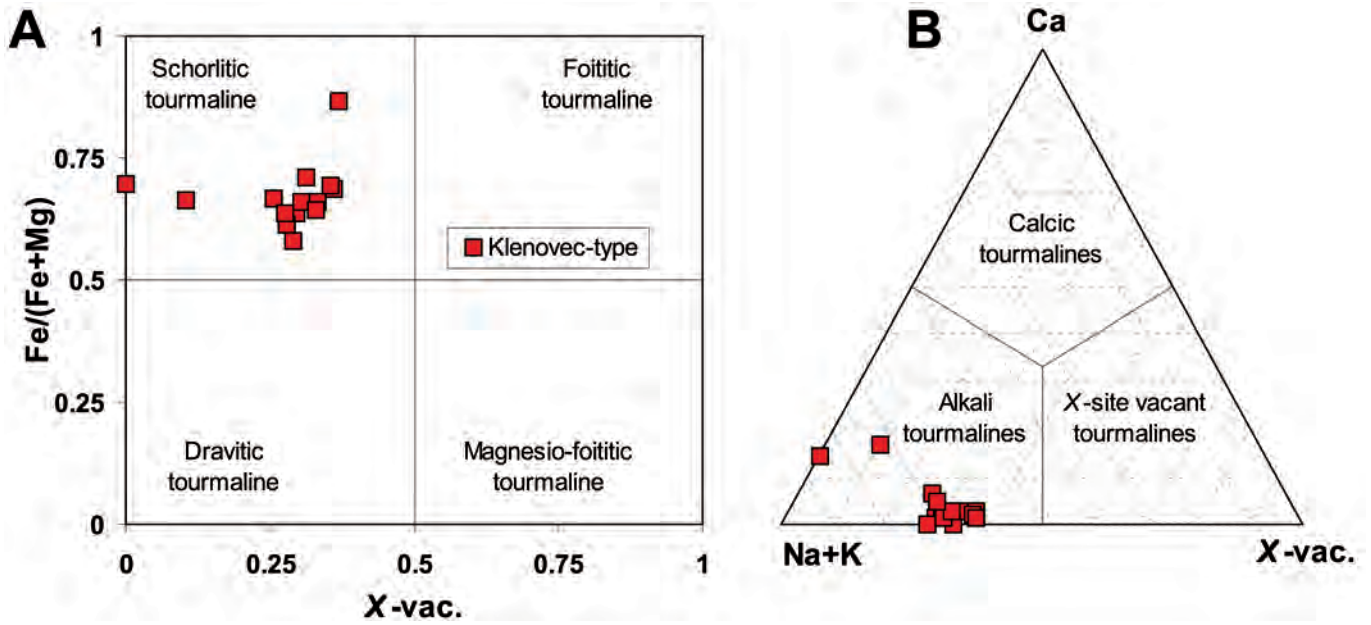

Fig. 1 - Observed tourmaline compositions plotted in (A) the Fe/(Fe+Mg) vs. *X*-vac diagram of the tourmaline group, and (B) the ternary diagram Na+K vs. *X*-vac vs. Ca of tourmaline group.

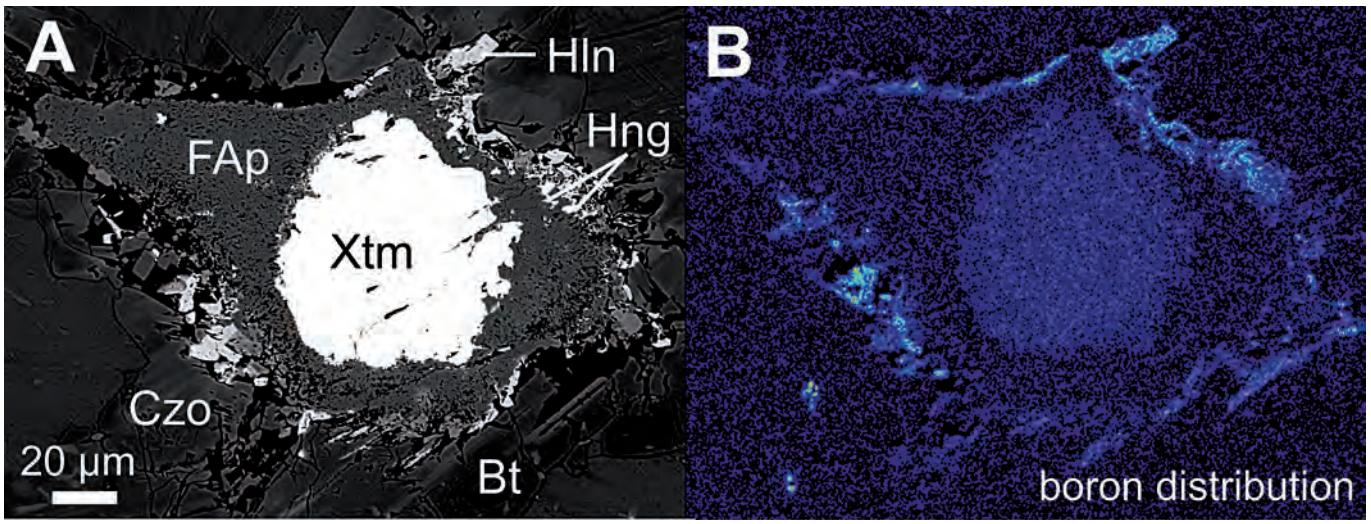

Fig.2 - A: BSE image of the retrograde reaction corona around primary magmatic xenotime-(Y) from the Fabova Hoľa Complex. B: False-coloured X-ray map of boron distribution within the corona assemblage. Mineral abbreviations are as follows: Bt) biotite, Czo) clinozoisite, FAp) fluorapatite, Hln) hellandite, Hng) hingganite, Xtm) xenotime.

Kotov A. B., Miko O., Putiš M., Korikovsky S. P., Salnikova E. B., Kovach V. P., Yakovleva S. Z., Bereznaya N. G., Kráľ J. & Krist E., 1996 – U/Pb dating of zircons of postorogenic acid metavolcanics and metasubvolcanics: A record of Permian-Triassic taphrogeny of the West-Carpathian basement. *Geologica Carpathica*, 47: 73-79.

Leeman W. P. & Sisson V. B., 1996 – Geochemistry of boron and its implications for crustal and mantle processes. In: Boron: Mineralogy, petrology and geochemistry. Grew E. S. & Anovitz L. M. (eds.). *Reviews in Mineralogy & Geochemistry*, *Mineralogical Society of America*, Washington, DC, USA, 33: 645-708.

London D., Morgan VI G. B. & Wolf M. B. 1996 – Boron in granitic rocks and their contact aureoles. In: Boron: Mineralogy, petrology and geochemistry Grew E. S. & Anovitz L. M. (eds.) *Reviews in Mineralogy& Geochemistry*, *Mineralogical Society of America*, Washington, DC, USA, 33: 299-330.

Mrose M. E. & Rose H. J., 1962 – Behierite (Ta,Nb)BO_4, a new mineral from Manjaka, Madagascar. *Geological Society of America*, *Annual Meeting Abstract*, 68: 235.

Oftendal I., 1964 – On the occurrence and distribution of boron in pegmatite. *Norsk Geologisk Tidsskrift*, 44: 217-225.

Vozárová A., Rodionov N., Vozár J., Lepekhina E. & Šarinová K., 2016 – U–Pb zircon ages from Permian volcanic rocks and tonalite of the Northern Veporicum (Western Carpathians). *Journal of Geosciences*, 61: 221-237.

Elba tourmalines, over two centuries of collecting and scientific research

Federico Pezzotta

Elba tourmalines are worldwide known for their long collecting and scientific history, for their rarity, and for the intrinsic beauty and elegance of the crystals, despite their limited size. The most unusual and famous Elba tourmaline variety is represented by the "black cap" (*testa di moro*, in Italian), characterized by transparent (yellow-green, olive-green, colorless, or pink) crystals with a sharp transition to black at the analogous termination.

THE EARLY TIMES

It is possible that in the long Elba history somebody found and collected some gem-quality tourmaline crystals. However, the first information about the potential occurrence of some gem minerals in the area is reported in Pini (1777). In 1784 the famous French geologist Deodat Gratet de Dolomieu (1750-1801) provided the first confirmation of the occurrence of unusual multicolored tourmaline crystals. In the following years, more and more mineral specimens of pegmatitic origin started to be distributed to museum collections across the Europe (such as the École des Mines in Paris, and the Geneva Museum) and several naturalists visiting Elba gave the first descriptions of the localities (e.g. Claude Hugues Le Lièvre, Arsène Thiébaut deBerneaud, and Eduard Rüppel) (Pezzotta, in press).

1825: THE FIRST DOCUMENTED GREAT DISCOVERY

Tuscan naturalist Ottaviano Targioni Tozzetti (1755-1829) reported in 1825 (Targioni Tozzetti, 1825) that in the same year Lieutenant Giovanni Ammannati, after buying a property in San Piero in Campo, known as Grotta d'Oggi, mined a large granite outcrop discovering a number of magnificent mineral specimens. Targioni Tozzetti gave a detailed description of the Ammannati collection. Thanks to this publication, the discovery become very famous as nobody had ever reported anything similar from Elba or from other localities in the world.

Museo di Storia Naturale di Milano, Corso Venezia 55, 20121 Milano, Italia.
E-mail: fpezzotta@yahoo.com

"CERVELLOFINE" AND THE GIULJ EVALUATION OF THE GEM-POTENTIAL OF ELBA

After the Ammannati's discovery, Elba Island started becoming the place of visit of many eminent European mineralogists and geologists, and San Piero in Campo and Grotta d'Oggi became well-known locality names. Several local touristic guides, such as Giuseppe Lazzerini and Pietro Pinotti, specialized in mineralogical and geological localities and, in some cases, also become expert miners in finding mineral specimens for selling. Both Giuseppe and Pietro got the nick-name of "Cervellofine" (smart-brain). On the early 1830th, the Grand Duke of Tuscany charged Giuseppe Giulj to evaluate the potential of some localities in Elba for the production of gem and ornamental stones. In his report of 1835, Giuseppe (Giulj, 1835) described as gem-rich localities Grotta d'Oggi and Fonte del Prete. There are evidences in literature that Elba tourmalines, beryls, and garnets have been used to be included in jewels, faceted or as single crystals; nevertheless, this use remained sporadic and never become a common use.

Fig. 1 - San Piero in Campo village in 1910.

Fig. 2 - Grotta d'Oggi at the end of the 19th Century (D'Achiardi, 1910b).

CAPITAN GIUSEPPE PISANI

Giuseppe Pisani (1808-1885), from San Piero in Campo, made a military carrier and devoted most of his mineral-research activity to the locality named "Fonte del Prete" (Priest's Spring), also known as "Filone della Speranza" (Hope Vein) and "Cava Pisani" (Pisani Quarry). He assembled several collections which were the objects of several donation and sales starting from the period 1939-1941 to the University of Florence. A very large collection rich in magnificent specimens was sold to the Ministry of Education in 1861. In 1883 he sold his last mineral collection to the Natural History Museum of Milano.

NOBLEMAN RAFFAELLO FORESI

Around 1850, the nobleman Raffaello Foresi (1820-1876) from Portoferraio, Elba, started collecting minerals. Raffaello was a self-taught and dedicated much of his time to the study of natural sciences, literature, archeology, art and music. On February 1873, Raffaello succeeded in opening to the public a museum in Portoferraio to exhibit his huge mineral collection. Pullé & Capacci (1874) published a description of the collection in the Museum and reported several anecdotes. A famous one is about a monk who, in front of the four largest and best blocks mined in Masso Foresi, "was so amazed and astonished that in the enthusiasm of admiration, throwing himself on his knees, he proclaimed them to be the Four Evangelists". In 1876, Raffaello Foresi prematurely died at the age of 56. His Museum closed. The entire collection, including the "four evangelists", was sold by the heirs to the Institute of Higher Studies (today University) of Florence in 1877.

MINER LUIGI CELLERI

Around 1860, the bricklayer Luigi Celleri (1828-1900) from San Piero in Campo, took a keen interest in researching and digging of minerals, and he started his activity working for Raffaello Foresi (D'Achiardi, 1910a). For about a decade this relationship has continued to be a strong and efficient collaboration. Luigi Celleri was enthusiastic and full of energy, but he was also a careful observer of minerals and he liked to learn from the mineralogists that from time to time visited Elba, and whom he took to the tourmaline localities. He was also proud of having discovered the tourmaline locality of Facciatoia, and in 1872 he mined the "Masso Foresi" (Foresi's boulder), in which the famous "Four Evangelists" were extracted (Pezzotta, in press). Luigi Celleri broke his relationship with Raffaello Foresi in 1874, and the same year he started a new relationship with Prof. Giorgio Roster (1843-1927) from Florence. After Giorgio Roster sold his collection, around 1888, Pilade del Buono (1852-1930), industrialist, business-man and politician of Elba, agreed to help him and decided to build a mineralogical museum in his house in Villa San Martino. Many new and nice specimens were recovered during this project, and a significant collection was assembled. On July 1900, while mining at Grotta d'Oggi, Luigi Celleri had a sudden illness and died.

Fig. 3 - Drawings made by prof. Luigi Bombicci of Elba pegmatite specimens, on late 19th Century. (Mineralogical Museum L. Bombicci, University of Bologna).

GIORGIO ROSTER AND BISTA TOSCANELLI

In 1875 Prof. Giorgio Roster from Florence, together with his young friend Giovanni Battista (Bista) Toscanelli (1857-1882), started an intense mineral collecting activity in Elba. He built an incredibly well selected and documented collection, but he also sold many important specimens to several worldwide mineral and gemstones dealers, including Tiffany in New York. After the premature death of Bista at the age of only 25, Giorgio Roster, in 1887, decided to sell his collection (completed with rich in notes catalogues) to the University of Florence.

THE GIOVANNI D'ACHIARDI STUDIES

Mineralogists of the 19th century tried to classify different Elba tourmaline varieties by their dominant color, or by the color occurring at the termination of the crystals. The extensive studies published in 1894 and in 1897 by Giovanni D'Achiardi (1872-1944), were based on a collection of several thousand loose crystals and a number of crystals on matrix, belonging to the University of Pisa, and reviewed all the previous information on this subject, adding many new information about crystal morphologies and physical properties.

Fig.4 - Multicolored tourmaline crystals up to 2.5 cm, on matrix from Grotta d'Oggi. (Private collection. Photo: A. Miglioli).

ELBAITE: A MINERAL SPECIE ESTABLISHED BY W. VERNADSKY

Vernadsky (1913) set a species distinction in tourmalines choosing the name "elbaite" for the most recurrent composition that he obtained analyzing a series of multicolored tourmalines from various localities, and in particular from Elba island.

THE FIRST DECADES OF THE 20TH CENTURY AND THE MODERN TIMES

Despite the several attempts made by Count Giulio Pullé and mostly Dutch geologist and mining engineer John Adam (1884-1971), not much was found after the death of Celleri in 1900. Andreani (1935) reported that all excavations were almost totally abandoned and that senator Prof. Giovanni D'Achiardi (1872-1944) said that most likely there were no more pegmatite veins to be discovered, and that the old quarries were probably completely exhausted. After World War II, some researches for pegmatites and tourmaline gems and specimens started again. A mining-research permit was released for a few years for the research of lithium to the Larderello Company in the 1960th and a second one to Gianni la Torre (grandson of John Adam) at the end of the 1970th. A number of mineral collectors dig mostly in the 1980th in the locality of Facciatoia where a new series of nice discoveries of pink tourmalines was made. Some more discoveries were made in the following years in the localities of Catri and Forcioni (Pezzotta, 2021 in press). The author, together with mineral collector Klaus Wirth, discovered in 1991 a new important pegmatite which he named "Rosina Pegmatite", where several nice specimens have been recovered and in which many samples for scientific research have been collected. Since 2013 this pegmatite become also the object of a mining-research permit.

Fig. 5 - Gianni la Torre in a pegmatite prospect near Grotta d'Oggi, around 1965.

MUM, A MINERALOGICAL MUSEUM DEDICATED TO LUIGI CELLERI

In January 2014, the Mineralogical and Gemological Museum "Luigi Celleri" ("MUM", acronym for *MUseo Mineralogico*) was opened to the public at San Piero in Campo. Several persons and mostly Fausto Carpinacci, were instrumental in carrying out this project. MUM belongs to the local township of Campo nell'Elba, and the exhibits are mostly based on the private Elba collection of the author. MUM (www.museomum.it) is today also the center for touristic and didactic excursions devoted to the nature, mineralogy, and history of the San Piero in Campo area.

THE RECENT SCIENTIFIC RESEARCHES ON ELBA TOURMALINES

Scientific studies performed in the last 25 years, coupled with the development of the nomenclature of the tourmaline supergroup (Henry *et al*., 2011), revealed a wide variety of chemical compositions and the discovery of several new species in the Elba tourmalines. Foitite and rossmanite were identified by Pezzotta. *et al*., (1996) and Pezzotta *et al*., (1998), respectively. Bosi *et al*., (2012) and Bosi *et al*., (2015) described the new Mn-rich, sodic species as tsilaisite and fluor-tsilaisite. A recent systematic investigation of the composition of the dark termination of several tourmaline crystals from different localities and cavities, allowed the discovery of an additional new X-vacant Mn-rich species, named celleriite in honor of Luigi Celleri (Bosi *et al*., 2021 in press). Two more new species found in the San Piero area, occurring not in pegmatites but in metabasic hornfels, were recently approved: uvite and magnesio-lucchesiite (Biagioni *et al*., 2021 in press). To date, the tourmaline-group minerals for which Elba is the type locality are six: elbaite, tsilaisite, fluor-tsilaisiate, celleriite, uvite, and magnesio-lucchesiite.

Fig. 6 - Elbaite and fluor-elbaite crystal with a dark termination of celleriite. Filone Rosina. (Natural History Museum of Milan. Photo: F. Picciani).

REFERENCES

Andreani D., 1935 – Note di mineralogia elbana. II, zona centrale e occidentale. *Il Polopano*, Portoferraio, anno XIII, n. 1800 del 19 ott. 1935.

Biagioni. C., Mauro D., Dottorini V., Dini A., Orlandi P., Pezzotta F. & Bosi F., 2021 in press – Magnesio-lucchesiite, i cristalli delle metabasiti di San Piero in Campo. *Rivista Mineralogica Italiana*, 45 (3).

Bosi F., Skogby H., Agrosi G. & Scandale E., 2012 – Tsilaisite, $NaMn_3Al_6(Si_6O_{18})(BO_3)_3(OH)_3OH$, a new mineral of the tourmaline supergroup from Grotta d'Oggi, San Piero in Campo, Island of Elba, Italy. *American Mineralogist*, 97: 989-994.

Bosi F., Skogby H., Agrosi G. & Scandale E., 2015 – Fluor-tsilaisite, $NaMn_3Al_6(Si_6O_{18})(BO_3)_3(OH)_3F$, a new mineral from San Piero in Campo (Elba, Italy) and new data on tsilaisitic tourmaline from the holotype specimen locality. *Mineralogical Magazine*, 79: 89-101.

Bosi F., Pezzotta F., Altieri A., Andreozzi G. B., Ballirano P., Tempesta T., Cempírek J., Škoda R., Filip J., Čopjaková R., Novák M., Kampf A. R., Scribner E. D., Groat L. A. & Evans R. J., 2021 in press − Celleriite, $\square(Mn^{2+}_2Al)Al_6(Si_6O_{18})(BO_3)_3(OH)_3(OH)$, a new mineral species of the tourmaline supergroup. *American Mineralogist*. <doi.org/10.2138/am-2021-7818>

D'Achiardi G., 1910a – Luigi Celleri. *Bollettino della Società Geologica Italiana*, 29: 233-239.

D'Achiardi G., 1910b – Guida al Corso di Mineralogia. Mineralogia Speciale. *Enrico Spoerri Libraio-Editore*, Pisa.

Giulj G., 1835 – Progetto di una carta geognostica e orittognostica della Toscana. *Presso Onorato Porri*, Siena, 23.

Henry D. J., Novak M., Hawthorne F., Ertl A., Dutrow B. L., Uher P. & Pezzotta F., 2011 – Nomenclature of the tourmaline supergroup-minerals. *American Mineralogist*, 96: 895-913.

Pezzotta F., 2021 in press – Tourmalines of Elba Island (Tuscany, Italy) from discovery to present days. *The Mineralogical Record*.

Pezzotta F., Hawthorne F. C., Cooper M. A. & Teerstra D. K., 1996 – Fibrous foitite from San Piero in Campo, Elba, Italy. *The Canadian Mineralogist*, 34: 741-744.

Pezzotta F., Guastoni A. & Aurisicchio C., 1998 – La rossmanite di Roznà e dell'Elba. *Rivista Mineralogica Italiana*, 22 (1): 46-50.

Pini E., 1777 – Osservazioni mineralogiche sopra le miniere di ferro e di altre parti dell'Isola d'Elba. *Presso Giuseppe Marelli*, Milano.

Pullé G. & Capacci W. C., 1874 – Un viaggio nell'arcipelago toscano. *Estratto da "La Nazione"*: 49-52.

Targioni Tozzetti O., 1825 – Minerali particolari dell'Isola d'Elba ritrovati e raccolti dal signor Giovanni Ammannati. *Tip. Tofani*, Firenze.

A thermodynamic model for Li-free tourmaline

Stan Roozen[1]*, Vincent J. van Hinsberg[1], Edgar Dachs[2], Günter Redhammer[2], Artur Benisek[2], Xiaofeng Guo[3], Dominic H. Ryan[4], Klaus-Dieter Grevel[5]

Tourmaline is the most common borosilicate in crustal settings, with unprecedented potential for metamorphic petrology. In its mineral chemistry, tourmaline captures a record of its phase relations and its surroundings, including different mineral assemblages during pro- or retrograde metamorphism, as well as internally or externally buffered fluids. Due to its high stability range in the crust and negligible static diffusional reequilibration, this record is preserved in space and time, commonly in the form of compositional zoning. In order to understand and model tourmaline's stability and phase relations, and read the record contained in tourmaline's chemistry, we need an internally consistent set of thermodynamic properties and a solution model. Indeed, lack of thermodynamic data was highlighted as one of the main challenges in tourmaline research in the introduction of the Canadian Mineralogist 2011 special issue on tourmaline (van Hinsberg *et al.*, 2011).

An ordinary tourmaline already requires 7 endmembers to describe its composition, and constructing a full solid solution model for its thermodynamic properties is a challenge. This is a problem for multi-component solid solutions in general. Such complex multi-component systems need a vast amount of caloric and volumetric measurements to quantify all the inter-component mixing parameters. A solution is to obtain (part of) these parameters by thermodynamic analysis of natural assemblages (e.g. Green *et al*., 2016). There is nothing inherently wrong with the 'fitting the rock' methodology; however, these empirically fitted thermodynamic parameters often have lost their physical significance and become highly correlated, with limited predictive power outside the rock chemistries used for calibration.

In this study, we combine direct measurements with *ab-initio* computational techniques to obtain the many data points statistically necessary to fit and anchor a thermodynamic model for the Li-free tourmalines.

The sample-set that we use to fit the thermodynamic model consists of synthesized and natural intermediate compositions of Li-poor tourmaline within the Na-Ca-Mg-Fe^{2+}-Fe^{3+}-Ti-Al-B-O-H-F chemical system. Most tourmalines are within the dravite-schorl-olenite-uvite-feruvite-magnesiofoitite-foitite endmember space, with small extensions towards their oxy and F equivalents. Ti, Al^{IV}, and Fe^{3+} are common. Mn, K, Zn, Cr, and V are important minor elements. No true endmember has ever been synthesized due to tourmaline's nonstoichiometric nature (e.g., its ability to contain vacancies), and the same is true for natural tourmalines, meaning that many endmembers are hypothetical (Bosi, 2018) and we are forced to use intermediate compositions.

All samples have been characterized in detail using WDS-EPMA for major elements, LA-ICP-MS for minor elements, Mössbauer for Fe-valence, Karl Fisher titration for H_2O content, and single crystal-XRD for long-range order. We measured low-T heat capacities (C_p) by relaxation calorimetry and extracted absolute entropies from these data (see Dachs & Bertoldi, 2005). We measured high-T C_p with differential scanning calorimetry (DSC), and we obtained molar volumes from the refinement of single-crystal XRD data. We constrained enthalpies for a select set by solution calorimetry and are in the process of extending this set with ab-initio density functional theory (DFT) computational modeling. These results are combined with infrared and Raman spectroscopy to explore excess enthalpy, given the correlation between line broadening and excess enthalpy due to lattice strain (Ballaran, 2003).

As tourmaline exist solely as a solid solution, the main function of hypothetical endmember data is to anchor the closed-form analytical expressions such that they go through the experimentally measured natural dataset. We acquire the endmember data by using a stepwise least square procedure on the sample set which separates endmember

[1] Department Earth and Planetary Sciences, McGill University, Montreal, Canada.
[2] Department Chemistry and Physics of Materials, University of Salzburg, Salzburg, Austria.
[3] Department of Chemistry, Washington State University, Pullman, USA.
[4] Physics Department, McGill University, Montreal, Canada.
[5] Institut für Geowissenschaften, Bereich Mineralogie, Friedrich-Schiller-Universität Jena, Jena, Germany.

* Corresponding author: stanroozen@gmail.com

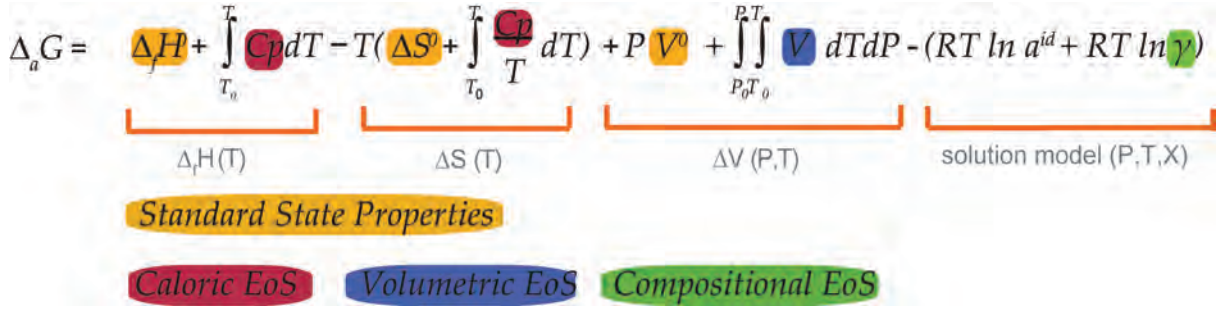

Fig. 1 - The key thermodynamic parameters color coded.

from excess mixing properties. In addition, we compute the standard state properties of ideal endmembers with *ab-initio* DFT calculations. DFT is especially good at predicting energy differences (Benisek & Dachs, 2018). The single defect method can be used to obtain mixing parameters in the dilute limits where order/disorder would not have an influence (Sluiter & Kawazoe, 2002). The double defect method can be used to constrain coupled substitutions and give estimates of the ordering effect at more intermediate compositions (Vinograd *et al*., 2009). Combining these with my direct measurements permits "calibrating" the DFT results and constructing an internally consistent thermodynamic model for the full tourmaline compositional space of interest. The resulting model will then be tested against a database of phase assemblages containing tourmaline in nature and experiments and well-constrained natural and experimental tourmaline-mineral Fe-Mg K_D values (see van Hinsberg *et al.* 2011, for a list of references of these synthetic/natural data).

The resulting tourmaline thermodynamic model can be used in petrological software, e.g. PerpleX (Connolly, 2005) to model the formation of tourmaline and its exchange with other phases, including fluid (e.g. Connolly & Galvez, 2018). Given how common tourmaline is as an accessory phase, this model will benefit the metamorphic, igneous, and hydrothermal communities and will permit thermobarometry, provenance studies, mineral exploration, and rock process identification.

REFERENCES

Ballaran T. B., 2003 – Line broadening and enthalpy: some empirical calibrations of solid solution behaviour from IR spectra. *Phase Transitions: A Multinational Journal*, 76 (1-2): 137-154. <doi:10.1080/01411590310000761 01>

Benisek A. & Dachs E., 2018 – The accuracy of standard enthalpies and entropies for phases of petrological interest derived from density-functional calculations. *Contributions to Mineralogy and Petrology*, 173 (11): 1-11. <doi:10.1007/s00410-018-1514-x>

Bosi F., 2018 – Tourmaline crystal chemistry. *American Mineralogist: Journal of Earth and Planetary Materials*, 103 (2): 298-306. <doi:10.2138/am-2018-6289>

Connolly J. A., 2005 – Computation of phase equilibria by linear programming: a tool for geodynamic modeling and its application to subduction zone decarbonation. *Earth and Planetary Science Letters*, 236 (1-2): 524-541. <doi:10.1016/j.epsl.2005.04.033>

Connolly J. A. & Galvez M. E., 2018 – Electrolytic fluid speciation by Gibbs energy minimization and implications for subduction zone mass transfer. *Earth and Planetary Science Letters*, 501: 90-102. <doi:10.1016/j.epsl.2018.08.024>

Dachs E. & Bertoldi C., 2005 – Precision and accuracy of the heat-pulse calorimetric technique: low-temperature heat capacities of milligram-sized synthetic mineral samples. *European Journal of Mineralogy*, 17 (2): 251-261. <doi:10.1127/0935-1221/2005/0017-0251>

Green E. C. R., White R. W., Diener J. F. A., Powell R., Holland T. J. B. & Palin R. M., 2016 – Activity–composition relations for the calculation of partial melting equilibria in metabasic rocks. *Journal of Metamorphic Geology*, 34 (9): 845-869. <doi:10.1111/jmg.12211>

Sluiter M. H. & Kawazoe Y., 2002 – Prediction of the mixing enthalpy of alloys. *EPL* (*Europhysics Letters*), 57 (4): 526. <doi:10.1209/epl/i2002-00493-3>

van Hinsberg V. J., Henry D. J. & Marschall H. R., 2011 – Tourmaline: an ideal indicator of its host environment. *The Canadian Mineralogist*, 49 (1): 1-16. <doi:10.3749/canmin.49.1.1>

Vinograd V. L., Sluiter M. H. & Winkler B., 2009 – Subsolidus phase relations in the CaCO3–MgCO3 system predicted from the excess enthalpies of supercell structures with single and double defects. *Physical Review B*, 79 (10): 104201. <doi:10.1103/PhysRevB.79.104201>

Inner structures of tourmaline crystals

Paul Rustemeyer

Surprisingly, slices of "black" tourmalines are not only colored when ground thin enough, they also may contain an incredible variety of fine structures. In 1994 this "discovery" was the starting point of an intense screening made by the author of the inner structures of thousands of dark tourmaline crystals. Quite astonishing new tourmaline worlds opened up with phenomena never documented before (Rustemeyer, 2003; 2012; 2015; 2018).

The new methodical approach for this research of phenomena and structures in the "black" tourmalines was a combination of three lines of action:

1) the thickness of the slices is defined as optimum color saturation and varies individually between 1 mm and 10 micrometers;

2) the whole crystal is cut into a series of slices. This allows documenting the entire internal three-dimensional structure of a tourmaline crystal. Third, processing of several crystals from the same location often shows an interesting variety of structures.

Most of the slices have been cut perpendicular to the *c*-axis. The cuts made along the *c*-axis reveal growth structures very well - however, because of the strong dichroism, these are predominantly brown-colored. Thus slices along the *c*-axis are less attractive in color and they have a lower color density.

This paper provides a short review of the different types of structures within tourmaline crystals, using some examples of slices, out of the author's collection, which is composed by more than 30,000 slices.

Two zoning types commonly occur together in tourmaline slices: **sector zoning** and **concentric growth zoning**. Sectoral zoning arises from differences in the incorporation of elements at symmetrically nonequivalent crystal faces during growth, expressed as compositionally distinct growth sectors (Reeder & Rakovan, 1999). In the case of most tourmalines the sectoral zoning is superimposed by with a concentric growth zoning, as the tourmaline slices perpendicular to the *c*-axis cut through the consecutive color zones, which are often shaped as trigonal pyramids (van Hinsberg *et al*., 2006; Fig. 1). A series of consecutive slices gives a holistic view about the evolution of the crystal morphology of the growing crystal and the sequence of color zones. The perspective view of a staple of tourmaline slices offers an easy insight of the three-dimensional inner structure of the crystal and allows the reconstruction of the vertical structure, parallel to the *c*-axis (Fig. 1).

The rim zones in many tourmaline slices are the sector zones of the prism layers. They often contain a series of narrow concentric colored bands. Very often in the last stage of crystallization there is no more rim-zone. This means, that the tourmaline crystal is only growing in the direction of its *c*-axis (Fig. 5).

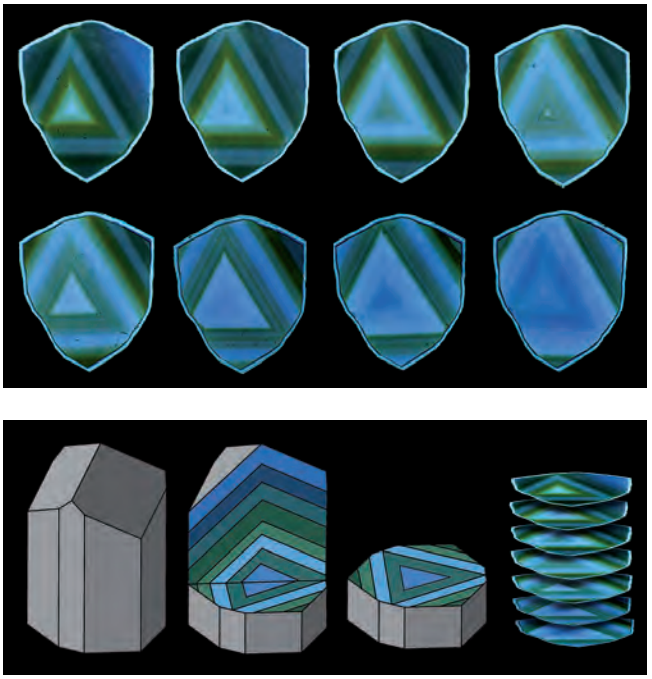

Fig. 1 - Above: eight consecutive tourmaline slices. Bottom right: the view of a staple of tourmaline slices offers an easy insight in the three-dimensional inner structure of the crystal and allows the construction of the plane parallel to the *c*-axis.

Waldackerweg 7, 79194 Gundelfingen, Germany.
E-mail: rustemeyer-gundelfingen@t-online.de

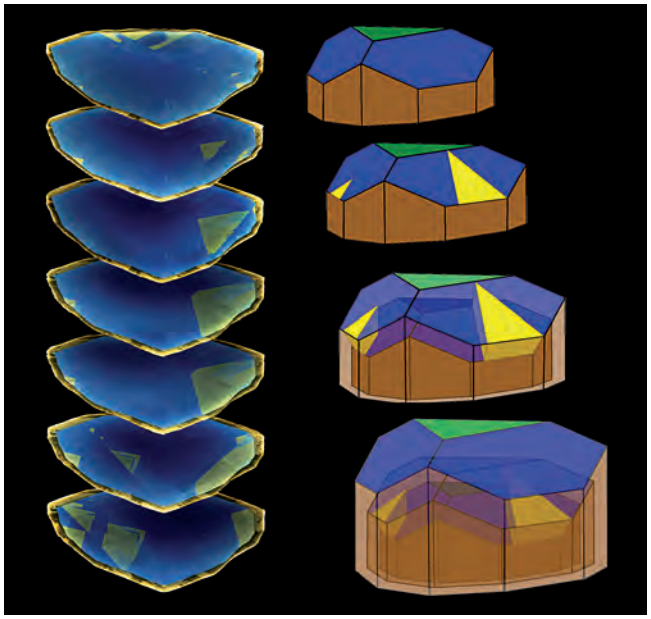

Fig. 2 - Left side: staple of tourmaline slices with yellowish delta structures, (Skardu, Pakistan, 28 mm in diameter). Right side: development of the Delta-structure as triangular second color phase within the face trigonal pyramid. The delta structures form layer packages that are arranged in the crystal like inclined triangular pieces of cake (parallel to the pyramid surface).Often the horizontal slice exhibits only a part of the inclined delta structure.

DELTA STRUCTURES

Interestingly, a second differently tourmaline "color-phase" is able to grow simultaneously within the faces of trigonal pyramids. Because of its mostly triangular shape, this type of color zone was called "delta structure" (Rustemeyer, 2003; 2012; 2015; Figs. 3-5). The most common delta structures start at a seed point in the sector of a trigonal pyramid and spread downwards towards the edges of the pyramid faces with the prism faces, shaped as triangle (Figs. 2-3). The development of delta-structures is still under investigation by the author. A big variety of shapes of delta structures has been discovered (Figs. 3-5).

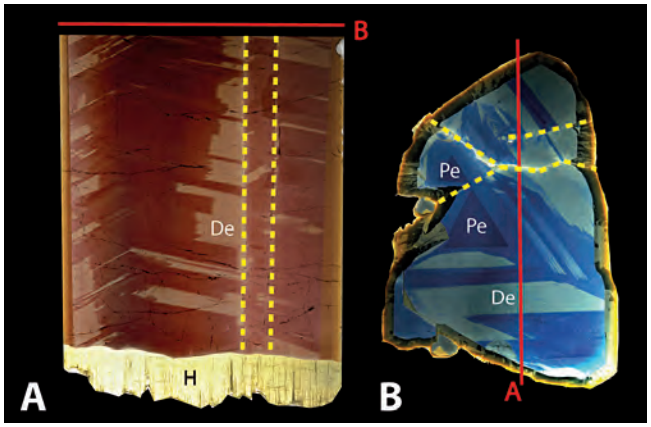

Fig. 3 - Slice A parallel (brown) and slice B perpendicular to the *c*-axis from the same Schorl crystal with delta structures (different colors due to dichroism) Kunar Valley, Afghanistan, width of the slices 3.5 cm, (the red lines indicate the orientations of the slices).
The two sector zones from pedion faces Pe and the border lines (reinforced with dotted yellow lines) indicate that the crystal consists of three parallel crystals. In slice A delta structures can be seen as light brown colored areas that slope upwards from the edges, in slice B as yellowish areas.
The horizontal slice B cuts through several of the inclined delta structures. At the bottom the red-brown area ends with an irregular border, which is typical for a fractured surface. This was later overgrown by numerous fibrous yellowish tourmalines (H).

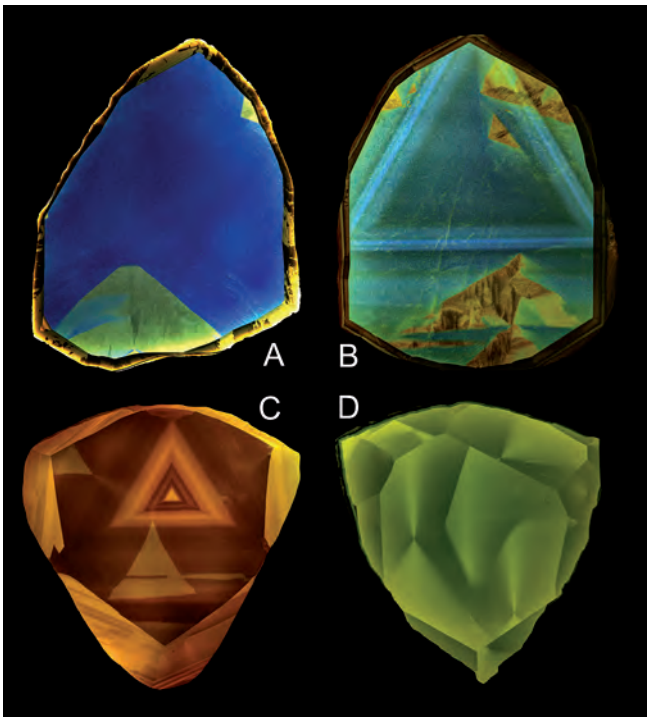

Fig. 4 - These four slices illustrate the variety of shapes of delta-structures. A) Simple shape Skardu, Pakistan, diameter 28 mm. B) Wildly disrupted delta structures, Minas Gerais, diameter 18 mm. C) Delta-structure with "ash-cloud", Uvite from Madagascar, diameter 35 mm. D) Delta-structure with "ash-cloud", Minas Gerais, diameter 20 mm.

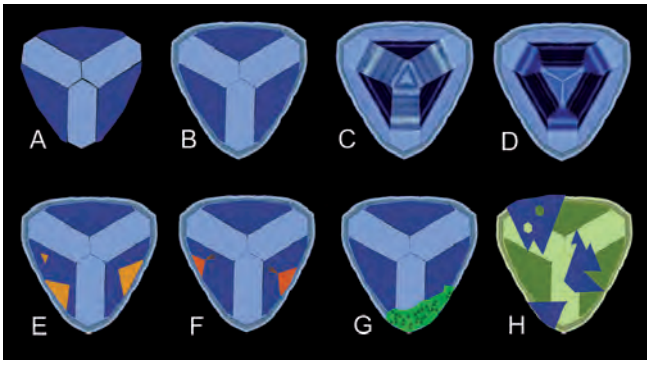

Fig. 5 - Overlook on some features of tourmaline slices. A) sector zoning of the two trigonal pyramids r (10.1) and o (021). B) is A with an additional rim zone (layers from the prim faces). C) the sectoral zoning is superimposed by with a concentric growth zoning. D) is C with an abrupt change of the relative growth rate of the trigonal pyramids. E-F) are B with additional brownish Delta structures. G) is B with a green "healing" area, which broke off and recrystallized later with a superposition of many pyramidal sector zones and prismatic layers. H) is B, with blue "healing" areas, which first corroded and then recrystallized (healed) with a superposition of many pyramidal sector zones and prismatic layers.

HEALING PHENOMENA AFTER FRACTURATION

Sometimes parts of the original tourmaline crystal are broken off due to tectonic events. Often the missing parts of the crystal then recrystallize in a different color, and thus indicate, that new elements came into the pocket (Fig. 2). These healing areas are frequently strongly structured (Rustemeyer, 2003; 2015). They show different ways of how the fractured surface offers germination points for many small, needle shaped crystals, which then more and more unify. Often an irregularly shaped borderline between original crystal and healing area indicates a fracturation (Fig. 6).

HEALING PHENOMENA AFTER CORROSION

When the fluid in the pocket with the growing tourmalines passes through a period of undersaturation, the crystals are partially dissolved again (Rustemeyer, 2003; 2015; London, 2016). This corrosion often takes place along faulty areas in the crystal and it leads to an enormous variety of shapes and forms. Often the crystals recrystallize on the etched surface in different, face specific colors. Additional oriented overgrowth with needle shaped crystals makes the structures in the healing areas quite complex (Fig. 7).

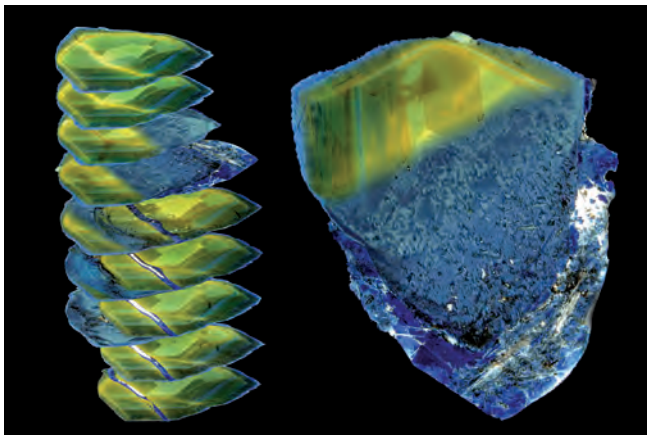

Fig. 6 - Example of a fractured and healed tourmaline from Minas Gerais, diameter 2.5 cm.

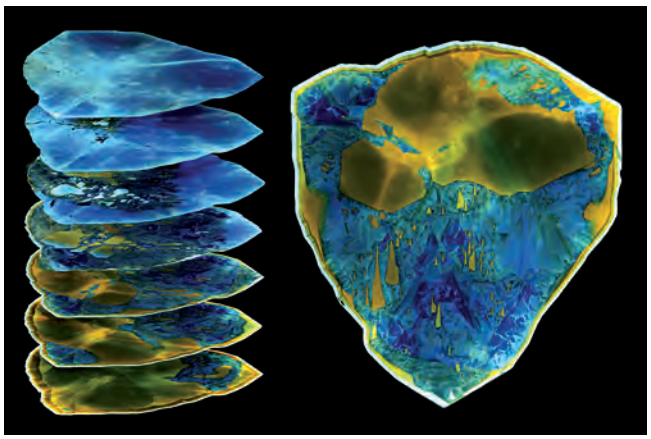

Fig. 7 - Example of a corroded and healed tourmaline from Minas Gerais, diameter 2 cm. A regular crystallographic shape of the borderline between original yellow crystal and the dark olive and blue healing areas indicates the former corrosion.

"DIVISION" PHENOMENA

There are tourmalines, in which a single crystal develops into a bunch of parallel or subparallel sub-individuals. The author proposes to classify this as: "division" phenomena. Different cases can be observed: first, a basic single crystal is overgrown with many needle shaped crystals; second, the crystal divides itself due to a high number on lattice defects gradually into sub-individuals; third, the tourmaline develops dislocations and crevasses with trigonal orientation. In all these cases slices show a specific mosaic-structure (Figs. 8-9).

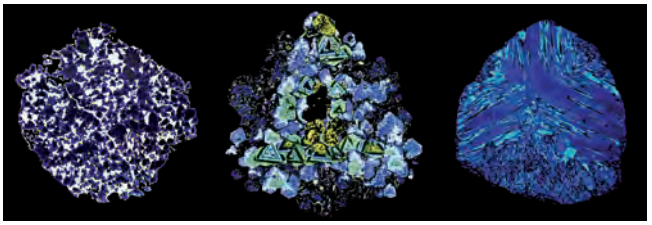

Fig 8 - "Division" structures, left: needle shaped overgrowth (Elba), middle: gradual division into sub-individuals (Erongo, Namibia), right: trigonal dislocations (Minas Gerais, Brazil).

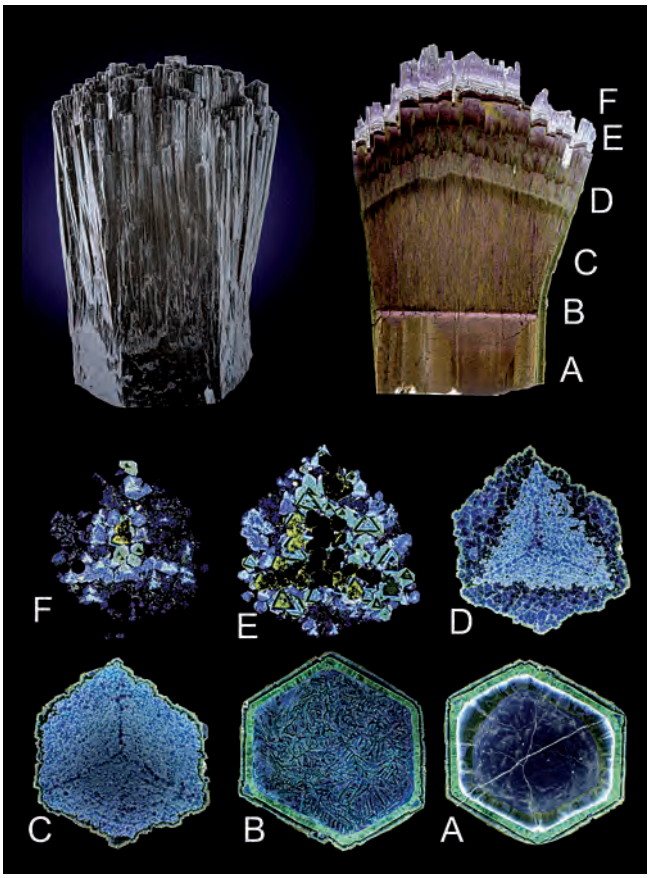

Fig. 9 - Tourmaline with "division" phenomena from Erongo, Namibia, 4 cm wide. The crystal on the top was cut into a series of 25 slices, from which six are shown here. From a second crystal of the same pocket a slice parallel to the *c*-axis was produced. The letters indicate the level of the cross-slices in the corresponding slice along the *c*-axis.
A) initial single crystal. B) dark skeleton structure. C) mosaic structure of hundreds of parallel crystals. D) collective of parallel crystals forming joint concentric growth zones. E-F) some subindividuals prevail and become wider.

SKELETON AND DENDRITIC GROWTH

Parallel aggregates of tourmalines from many locations have been sliced. Often they have a surprisingly complex inner structure: In the center of these tourmalines there is a skeletal structure of a hollow tubular tourmaline crystal which widens towards the top. In addition, dendrites in the form of lamellae arms have grown on the inner and outer wall side of that pipe. At the outside these arms often are germination points for a wreath of parallel satellite crystals, which sometimes in turn form further satellite crystals on their own dendritic arms. In the late stage this fragile framework structure is overgrown with a more or less massive tourmaline layer (Fig. 9; Rustemeyer, 2018).

Skeletal and dendritic tourmaline structures are often found as graphic intergrowth of tourmaline, quartz and sometimes feldspar (Figs. 10-12).

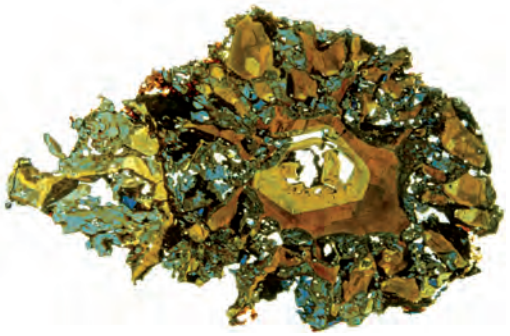

Fig. 10 - From the hollow Skeleton crystal in the center brownish dendritic arms have grown on which a wreath of satellite crystals has been formed. In later growth periods the structure was overgrown with blue tourmaline. "Apatite"-pocket, Amerika-quarry, Penig, Saxony, Germany, diameter 2 cm.

Fig. 11 - Crystallization shifted from skeleton growth forming the hollow center to dendritic growth (intergrowth with quartz). Finally the satellite crystals in the rim and on the top grew in normal mode. Crystal from Minas Gerais, diameter 2.5 cm.

Interestingly dendritic parallel aggregates and massive single crystals with an identic sequence of color zones can be found in the same pocket. This could be seen as consequence of a phase separation into a supercritical aqueous phase producing compact crystals and a high viscosity melt phase, in which the dendrites grow.

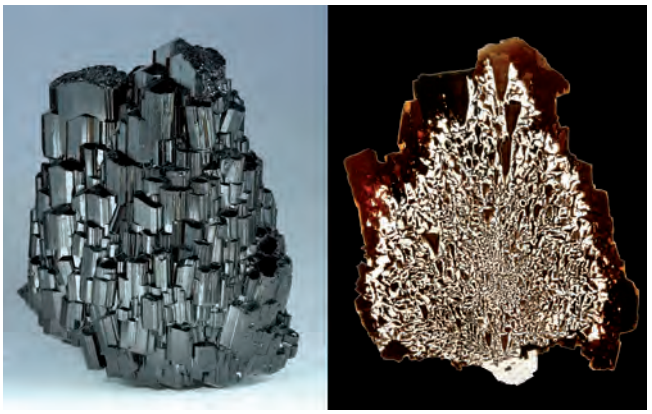

Fig. 12 - Parallel tourmaline aggregate and a slice parallel to its *c*-axis; Minas Gerais, height: 7 cm, Brazil. In the center there is a typical monocrystalline dendritic tourmaline, intergrown with quartz. At the outcrops of the dendritic arms many parallel compact tourmalines crystallized.

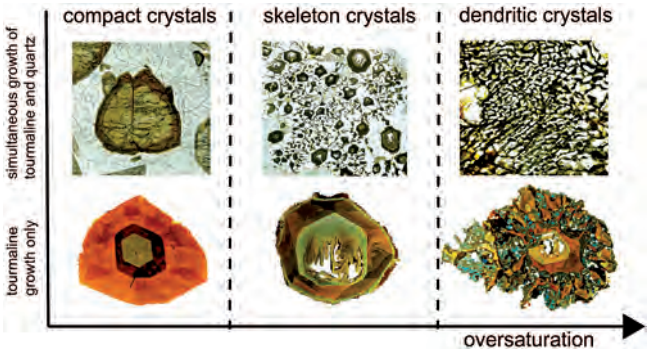

Fig. 13 - Typical structures of cross sections of tourmalines with skeletal and dendritic growth, with and without simultaneous growth of quartz.

REFERENCES

London D., 2016 − Reading Pegmatites – Part 2: What Tourmaline says. *Rocks & Minerals*, 91 (2): 132-149.

Reeder R. J. & Rakovan J., 1999 − Surface Structural Controls on Trace Elements Incorporation during Crystal Growth. In: Growth, Dissolution and Pattern Formation in Geosystems. Jamtveit B. & Meakin P. (eds.). *Kluwer Academic Publisher*, Dordrecht, The Netherlands: 143-162.

Rustemeyer P., 2003 − Faszination Turmalin. Spektrum. Formen, Farben, Strukturen. *Spektrum Akademischer Verlag*, Heidelberg, Germany.

Rustemeyer P., 2012 − Turmalin II. *extraLapis*, 41.

Rustemeyer P., 2015 – Tourmaline. Fascinating Crystals with Fantastic Inner Worlds. *Verlag Dr. Friedrich Pfeil*.

Rustemeyer P., 2018 − Kristall Phänomene. *extraLapis*, 54.

van Hinsberg V. J., Schumacher J. C., Kearns S., Mason P. R. D. & Franz G., 2006 − Hourglass sector zoning in metamorphic tourmaline and resultant major and trace-element fractionation. *American Mineralogist*, 91: 717-28.

About the aesthetics of tourmaline slices and "TourmalineArt"

Paul Rustemeyer

After the first mention of the inner beauty of tourmaline slices cut across the **c**-axes from Madagascar reported in Lacroix (1908), several natural history museums acquired tourmaline slices for their highly decorative qualities. After the two world wars, the pegmatite of Anjanabonoina was rediscovered, and in 1960 (Petsch, 2011) started delivering numerous large zoned tourmaline crystals, which were mostly sliced in Germany. Some members of the anthroposophical community started to collect such crystal slices, as they were seen as gemstones of Jesus Christ and as symbols of metamorphosis. Highlights of this movement were the special exhibitions at the Munich Show in 1985 and the large sized book "Der Turmalin" (Benesch, 1990), which helped a lot to bring the beautiful phenomena to the public awareness. The hype around the Madagascar slices was one of the motivators to look "deeper" into the dark tourmalines, to grind them thin enough to make their fantastic structures visible. These discoveries have been presented in the 2003 Munich Show, and in the book "Faszination Turmalin" (Rustemeyer, 2003).

The feedback from people was so encouraging, that from 2007 on, the temporary exhibition "Crystal Magic – fascinating structures in dark tourmaline crystals" was created. It combines an aesthetic view of tourmaline slices, crystals and "TourmalineArt" pictures with a holistic view on crystal growth phenomena. Art arouses curiosity about earth science - and vice versa. By now the exhibition was shown in more than twenty natural history museums in Europe. Until August 2022 it is exhibited in Salzburg (Austria).

There are different approaches to transform the structures of tourmaline slices into a "feast for the eyes".

1. CHOICE OF MOST BEAUTIFUL SLICES

Among the most expressive slices are those with perfect trigonal symmetric sector and growth zoning. Triangles and tree-ailed stars are strong symbols. And sometimes the sequences of colors are overwhelming.

Sometimes the picture in the slice reflects the stress field, in which, on one hand, the tourmaline is striving to obtain its natural perfect symmetric structure. On the other hand the growing crystal is often faced with external events, to which it reacts sensitively changing its color and shape. Such "strokes of fate" are i.e. other minerals growing on the crystal, breakage events, natural corrosion, and healing processes. They cause a disruption of the exact symmetry of the crystal structure and enrich the pictures of the tourmaline slices with a multitude of new forms.

2. CHOICE OF THE MOST ATTRACTIVE DETAIL

At best the whole slice is well proportioned and attractive like a small mandala. But there are more tourmaline slices with confusing patterns. Those are shifted and turned under the microscope until an interesting structure appears. An idea of a detailed picture and how to show it to its best

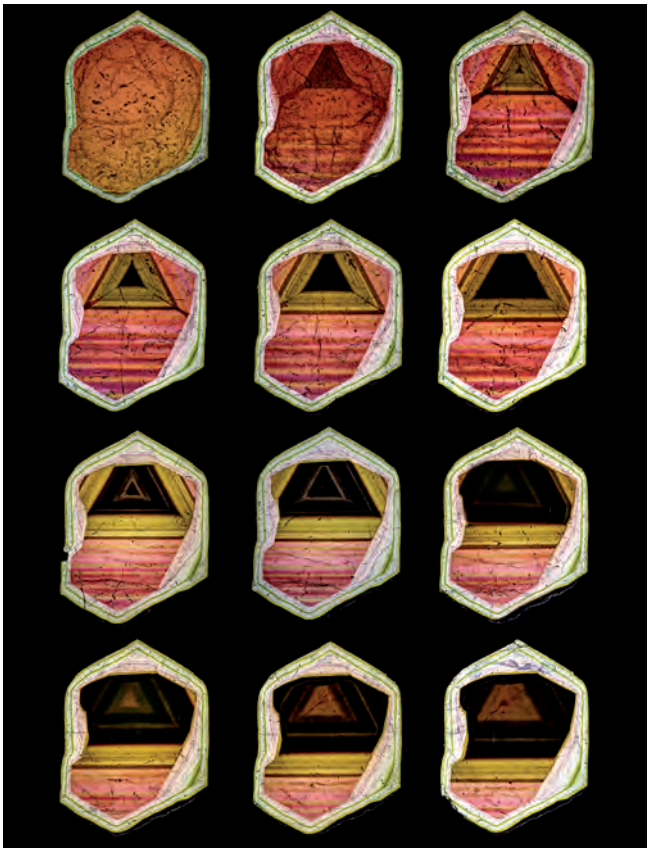

Fig. 1 - A Series of tourmaline slices from Madagascar, height 18 cm. (Federico Pezzotta collection).

Waldackerweg 7, 79194 Gundelfingen, Germany.
E-mail: rustemeyer-gundelfingen@t-online.de

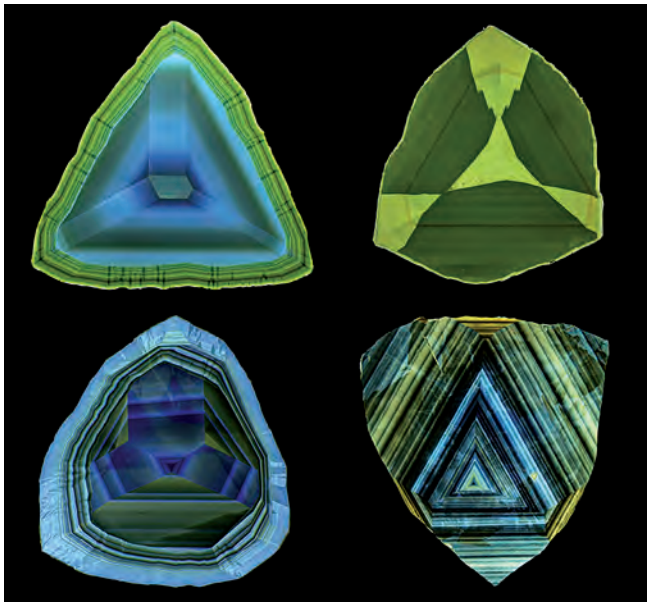

Fig. 2 - Schorl-slices with nearly perfect trigonal symmetric sector and concentric growth zoning, Minas Gerais, 2-3 cm in diameter.

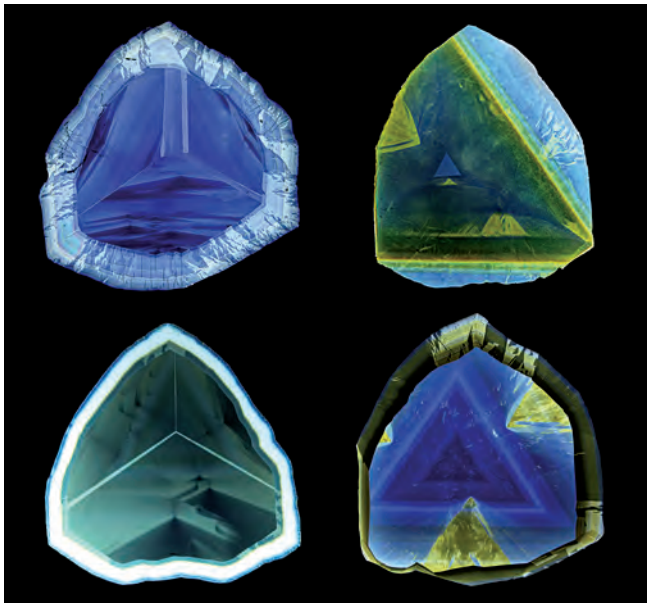

Fig. 3 - Schorl-slices with Delta-structures, Minas Gerais, 2-4 cm in diameter. (Paul Rustemeyer collection).

advantage is developed and documented with micro-photographic tools as "TourmalineArt" (Rustemeyer, 2015).

In a projection, a zoom tacking shot into the most fascinating area of the slice provides attractive effects.

3. "FLIGHT" THROUGH A TOURMALINE CRYSTAL

To project the pictures of a series of tourmaline slices using the dissolve technique enables the unique adventure to "fly" through the crystal.

4. CRYSTAL GROWTH ANIMATION

A picture of a slice can be processed into a series of photos cut along the concentric growth zones stepwise from the outer to the inner zone. Projecting this series of photos using the dissolve technique shows in a quite impressive manner, how the crystal grew.

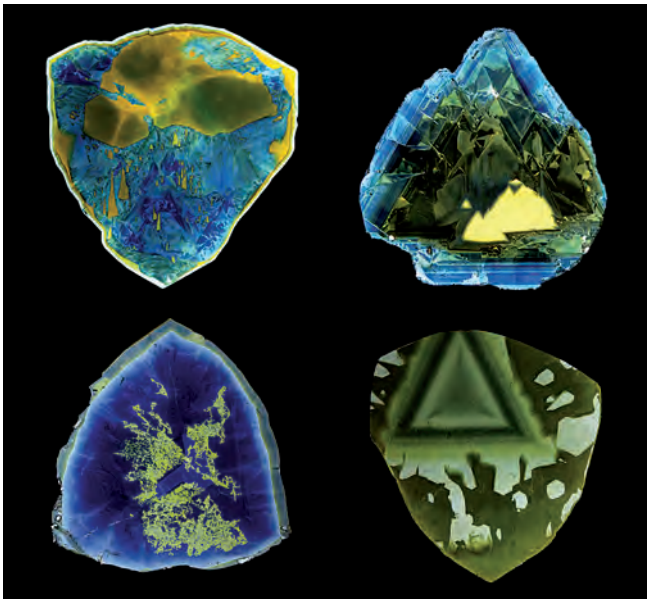

Fig. 4 - Schorl-slices with Delta-structures, Minas Gerais, 2-4 cm in diameter. (Paul Rustemeyer collection).

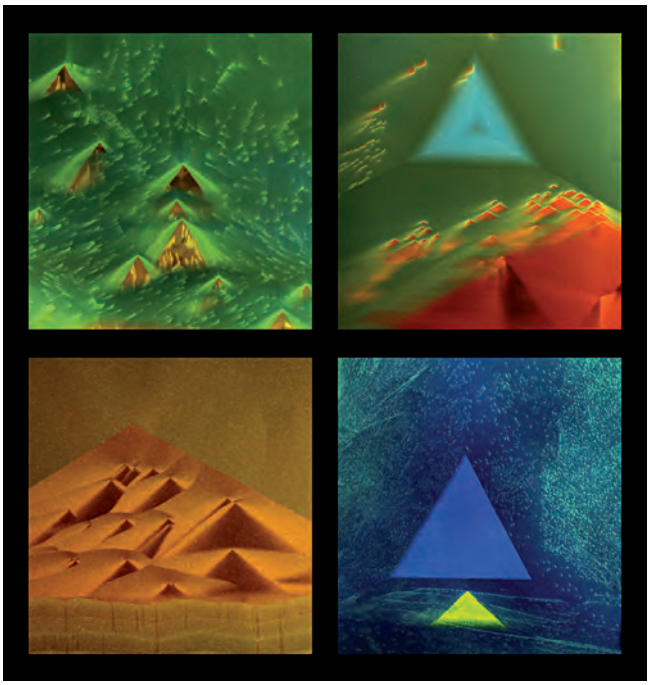

Fig. 5 - "TourmalineArt": aesthetic detailed pictures from schorl slices, 1-5 mm wide. (Photos: Paul Rustemeyer).

REFERENCES

Benesch F., 1990 − Der Turmalin. *Urachhaus*, Stuttgart.

Lacroix M. A., 1908 − Les minéraux des filons de pegmatite à tourmaline lithique de Madagascar. *Bulletin de la Société française de Minéralogie*, 31 (6): 218-247.

Petsch J., 2011 − Madagaskar: Die Wiederentdeckung einer Turmalinmine. In: Turmalin II. Rustemeyer (ed.). *extraLapis*, 41.

Rustemeyer P., 2003 − Faszination Turmalin. Spektrum. Formen, Farben, Strukturen. *Spektrum Akademischer Verlag*, Heidelberg, Germany.

Rustemeyer P., 2015 − Tourmaline. Fascinating Crystals with Fantastic Inner Worlds. *Verlag Dr. Friedrich Pfeil*.

Tourmalines from the eastern metamorphic cover of the Karkonosze granite: an evolution model

Mateusz Przemysław Sęk

Tourmalines from the eastern cover of the Karkonosze granite crystallized as multi-zoned crystals during the Variscan metamorphic events and the contact metamorphism event. The study is aimed at determination of a protolith and processes, which resulted in the final composition of the tourmalines.

The eastern cover of the Karkonosze granite, a part of the Karkonosze–Izera Massif (NE part of the Bohemian Massif), consists of Neoproterozoic-Paleozoic metamorphic rocks, and is divided into four lithostratigraphic units (Kryza & Mazur, 1995); Kowary Gneiss Group and Czarnów Schist formation (merged to Kowary-Czarnów unit) closer to the Karkonosze granite, and more distal Niedamirów Schist formation and Leszczyniec meta-igneous complex. The Kowary-Czarnów unit is interpreted as a unit composed of the nappe structure elements metamorphosed regionally under medium P-T conditions in the Upper Devonian (Kryza & Mazur, 1995). The structure was modified in the Lower Carboniferous and intruded by the Karkonosze granite ~320 Ma. The intrusion formed a contact aureole several hundred metres up to 2 km in width (Mierzejewski & Oberc-Dziedzic, 1990).

Tourmalines are accessory mineral components in granitic gneisses of the Kowary Gneiss unit, occurring in quartz-chlorite-tourmaline veins, e.g. in a milky quartz vein with brannerite at the Wołowa Mt. (Pieczka *et al.*, 2018), in quartz veins cutting a metabasite (amphibolitic) body with Ti-oxide/Fe-Cu-Ni-Co-Zn-Pb sulphide-sulphoarsenide mineralization at Budniki near Kowary, in Tu+Qtz+Ms+Chl±Grt veins near Malá Úpa Mt. (Čopjaková *et al.*, 2012), and as accessory minerals in a hornfels body cropping out in the Rędziny dolostone quarry (Majka *et al.*, 2018). This study is focused on yellowish and greenish crystals from the qtz-tur-chl vein from Wołowa Mt., black crystals from quartz veinlets cutting the metabasite body at Budniki, and tourmaline from hornfelses from Rędziny. Crystal chemistry of tourmalines was studied based on electron-probe microanalysis (EPMA).

Crystal chemistry of the tourmalines from all mentioned localities revealed that they are formed generally in two main stages; the first generation grown as multi-zoned crystals, and the second one forms rims on the crystals or fillings of cracks within them.

The first generation is represented by species of the alkali series (rarely the X-vacant series) with a variable $Mg/(Mg+Fe_{tot})$ ratio from 0.47-0.58 at Rędziny, 0.46-0.63 at Budniki, and up to 0.99 in the Wolowa Mt. area. In general, the first generation of all the tourmalines is characterized by relatively low content of ^{X}Ca and ^{W}F and variable Ti content. The presence of Ti-bearing minerals (like ilmenite) in the tourmaline crystals is responsible for the formation of Ti-rich zones in the core or mantle of the first-generation tourmaline. The Rędziny tourmalines, with the Ti content up to 0.30 apfu, have been classified as dutrowite (~60 mol.%). In most cases, the W site is occupied by OH with increasing amounts of $^{W}O^{-}$. Generally, the tourmalines of the first generation are represented by oxy-dravite, Fe-rich dravite, dravite, and rarely foitite.

The second generation is marked by increasing role of Ca, F and, in some cases, Ti. The increasing ^{X}Ca evolves up to compositions corresponding to uvite (0.60 apfu) in crystals hosted by the Budniki metabasites, and Ca-rich dravite and fluor-dravite (0.32 apfu) in crystals from the Wołowa Mt. area. The $Mg/(Mg+Fe_{tot})$ ratio is similar to the older generation, except crystal rims and crack fillings in yellowish crystal of oxy-dravite from Wołowa Mt. In the last crystals an increasing content of Fe (up to 1.72 Fe^{2+} apfu) could be noticed as well. Tourmaline group members from the second generation are represented mainly as fluor-dravite, F-rich dravite and F-rich uvite.

The W-site occupancy suggests that the first generation of tourmalines grew from fluids depleted in F, whilst the presence of F in the second generation could be caused by a change of external factors, including the fluid composition (Henry & Dutrow, 2011).

The increasing role of ^{X}Ca should be related to decomposition of Ca-plagioclase and calcic amphibolite-group members at decreasing temperature of the late phase of Variscan regional metamorphism and decomposition of

AGH University of Science and Technology, Department of Mineralogy, Petrography and Geochemistry, Mickiewicza 30, 30-059 Cracow, Poland.
E-mail: msek@agh.edu.pl

Ca-plagioclases during the late phase of the contact metamorphism. The formation of Ca-poor tourmalines of the first generation in a relatively Ca-rich environment of metabasites could be caused by crystallization under relatively high pressure during the prograde metamorphism with the peak conditions (7.3 kbar at 620-630ºC – Ilnicki, 2011). Formation of the second generation of Ca-rich tourmaline could have started during the retrogression ± contact metamorphism under decreasing pressure and increasing temperature (Berryman *et al.,* 2016). In metabasite body from Budniki Ca-rich tourmaline coexists with Al-rich titanite that is explained as a product of retrogression (635–470 ºC) (Mochnacka *et al.*, 2008). The Ti content range is strictly connected with co-occurrence of ilmenite and other Ti-bearing mineral inclusions interacting with B-, H_2O-, F-bearing fluids, which mobilized Ti^{4+} from the inclusions.

Crystallization of the tourmalines is generally connected with remobilization of some protolith [mixed sedimentary and bimodal, pre-Variscan volcanism products (Oberc-Dziedzic *et al.*, 2010)] components by B-, H_2O- and F-bearing fluids during the prograde regional metamorphism, and the contact metamorphism that could overlap a retrograde event. The diversified crystal chemistry of the tourmalines analysed, sampled from various localities of the Kowary-Czarnów unit, may be interpreted as a result of similar geological processes that transformed more or less differentiated local protoliths.

The study was supported by the National Science Centre (Poland) grant 2017/27/N/ST10/01579 to M.S.

REFERENCES

Berryman E. J., Wunder B., Rhede D., Schettler G., Franz G. & Heinrich W., 2016 − *P–T–X* controls on Ca and Na distribution between Mg–Al tourmaline and fluid. *Contributions to Mineralology and Petrology*, 171 (31). <https://doi.org/10.1007/s00410-016-1246-8>

Čopjaková R., Škoda R. & VaŠinová Galiová M., 2012 − „Oxy-dravit“ z turmalinitů krkonošsko-jizerského krystalinika. *Bulletin mineralogicko-petrologického Oddělení Národního Muzea*, Praha, 20 (1): 37-46.

Henry D. J. & Dutrow B. L., 2011 − The incorporation of fluorine in tourmaline: internal crystallographic controls or external environmental influences?. *The Canadian Mineralogist,* 49 (1): 41-56. <https://doi.org/10.3749/canmin.49.1.41>

Ilnicki S., 2011 − Variscan prograde PT evolution and contact metamorphism in metabasites from the Sowia Dolina, Karkonosze-Izera massif, SW Poland. *Mineralogical Magazine*, 75 (1): 185-212.

Kryza R. & Mazur S., 1995 − Contrasting metamorphic paths in the SE part of the Karkonosze-Izera block (Western Sudetes, SW Poland). *Neues Jahrbuch Fur Mineralogie-Abhandlungen*, 169 (2): 157-192.

Majka J., Sęk M., Mazur S., Gołębiowska B. & Pieczka A., 2018 − Polymetamorphic evolution of pelites inferred from tourmaline zoning – the Rędziny hornfels case study at the eastern contact of the Karkonosze Granite, Sudetes, Poland. *Mineralogia*, 49 (1-4): 17-34. <https://doi.org/10.2478/mipo-2018-0003>

Mierzejewski M. & Oberc-Dziedzic T., 1990 − The Izera-Karkonosze block and its tectonic development (Sudetes, Poland). *Neues Jahrbuch für Geologie und Paläontologie, Abhandlungen*, 179 (2/3): 197-222.

Mochnacka K., Oberc-Dziedzic T., Mayer W. & Pieczka A., 2008 − Ti remobilization and sulphide/sulphoarsenide mineralization in amphibolites: effect of granite intrusion (the Karkonosze–Izera Massif, SW Poland). *Geological Quarterly*, 52: 349-349.

Oberc-Dziedzic T., Kryza R., Mochnacka K. & Larionov A., 2010 − Ordovician passive continental margin magmatism in the Central-European Variscides: U-Pb zircon data from the SE part of the Karkonosze-Izera Massif, Sudetes, SW Poland. *International Journal of Earth Sciences*, 99 (1): 27-46. <https://doi.org/10.1007/s00531-008-0382-4>

Pieczka A., Ertl A., Sęk M. P., Twardak D., Zelek S., Szełęg E. & Giester G., 2018 − Oxy-dravite from Wołowa Góra Mountain, Karkonosze massif, SW Poland: Crystallochemical and structural studies. *Mineralogical Magazine*, 82 (4): 913-928.

Crystal growth and Raman spectroscopy of Ga, Ge-rich tourmaline

Tatiana Setkova[1]*, Elena Borovikova[2], Anna Spivak[1], Vladimir Balitsky[1]

Tourmaline crystals have unique physical properties, such as piezo- and pyroelectricity, permanent spontaneous polarization, infrared radiation water electrolysis, anion releasing and other (Pandey & Schreuer, 2012). The currently researchers partially solved the problem of tourmaline crystals growth on seed crystals (Setkova *et al*., 2019).

Incorporation of large cations into the tourmaline structure has significance in the crystal chemistry of the tourmaline supergroup minerals. Ga, Ge-rich tourmalines with larger cations in *Y*, *Z*- and *T*-sites can be considered as the potential structural analogue models of tourmalines at high pressure, with corresponding compression of the structure (Pushcharovsky *et al*., 2020). Crystal growth and characterization of novel tourmaline compounds is an important field of research from both fundamental and applied points of view.

In the present work, we carried out experiments in order to find crystallization conditions for Ga, Ge-rich tourmaline at hydrothermal condition of 600/650 °C and 100 MPa. Single crystals were grown in Ni–Cr alloy high-pressure autoclaves using either boric, boron-alkaline, boron-fluoride solutions as the solvent. The seeds from natural elbaite were cut perpendicular to the c-axis (0001). We applied two growth schemes: i– (direct solubility factor) nutrients containing germanium and gallium oxides with mixture of quartz and corundum were located in the lower hotter zone (650 °C), the seeds were fixed in the upper colder zone (600 °C); ii– (reverse solubility factor) seeds and germanium and gallium oxides were located in the lower hotter zone, and the powdered mixture consisting of crystalline topaz and quartz was placed in the upper colder zone of autoclave.

The composition of the new formed crystals were determined by electron microprobe analysis (Tescan Vega II XMU). Raman spectra excited by the monochromatic radiation with the wavelength 532 nm were obtained using a JY Horiba XPloRA Jobin confocal Raman microscope attached to an Olympus BX41 polarizing microscope to characterize the tourmaline.

Overgrowths of Ga, Ge-rich tourmaline on seed crystals were obtained in all solutions. Depending on the growth conditions, solution and nutrient composition, the growth rate can vary from 9 to 60 μm per day (Fig. 1). The maximum growth on the seed was 1.2 mm according to growth scheme ii in boron-fluoride solution. The color of the overgrown layers is varied (black, brown, green), depending on the new tourmaline composition. In some experiments, simultaneously with the tourmaline crystal growth, spontaneous nucleation tourmaline crystals were formed on the surface of the seeds and nutrient.

The maximum gallium and germanium content in grown tourmaline crystals reaches 20.8 wt% Ga_2O_3 and 12.4 wt.% GeO_2. Iron, nickel and titanium are also abundantly observed in the grown crystals. High content of these elements in tourmaline is associated with insignificant corrosion of the walls of the autoclave and internal

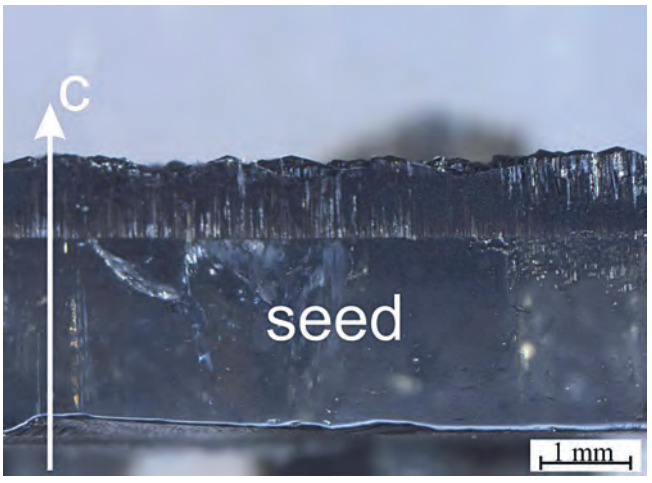

Fig. 1 - Overgrown layer of Ga, Ge-rich tourmaline on elbaite seed.

[1] D.S. Korzhinskii Institute of Experimental Mineralogy RAS, 142432, Chernogolovka, Russia.
E-mail: spivak@iem.ac.ru
balvlad@iem.ac.ru
[2] Faculty of Geology, Moscow State University, Vorobievy Gory, 119991, Moscow, Russia.
E-mail: alena.amurr@gmail.com

* Corresponding author: setkova@iem.ac.ru

equipment (wire, frame). In boric, fluoride and alkaline solutions, the iron, nickel and titanium solubility is different; therefore, their content varies depending on the solution composition and autoclaves deterioration. The FeO content varies 3.1 – 14.68 wt.%. and NiO – 0.27 – 9.55 wt.%. Titanium up to 1.51 wt.%. (TiO_2) was found mainly in tourmalines grown in boron and boron-alkaline solutions.

For boron-alkaline solutions, the Na contents in analyzed tourmalines ranging from 1.11 wt.% of Na_2O up to 1.92 wt.%, which is evidence for the role of Na during the crystallization process. However, according to the X-site occupancy we cannot classify those synthetic tourmalines as alkali group members, only as X-vacant.

In the Raman spectra of Ga, Ge-rich tourmaline with high Ge content, the elbaite band at 976 cm^{-1} almost disappears and new band of Ge – O vibrations at 869-875 cm^{-1} appears (Fig. 2). Its intensity correlates with Ge content in the sample. This band shifts to the higher frequencies for 25-30 cm^{-1} in comparison with cyclogermanates Raman spectra (Sitarz *et al*., 2002). The stretching Si – O vibrational bands shift toward the lower wavenumbers in comparison with natural tourmaline spectra (Hoang *et al*., 2011). The band's shifts indicate the longer Si – O bonds in Ge-bearing tourmalines relative to those in elbaite, and the shorter Ge – O bonds than in cyclogermanates. Ga^{3+} ions, could occupy both *Y* and *Z* octahedral sites (Vereshchagin *et al*., 2016).

The high-frequency O–H stretching modes (3300–3900 cm^{-1}) can provide important information about ionic substitutions in the different types of tourmaline, because OH vibration frequencies will be modified by the ion substitution in the *X*, *Y* and *Z* sites. The previous investigations of natural tourmalines revealed ^{V}OH stretching modes in the region between 3400 and 3615 cm^{-1} and ^{W}OH stretching modes have been found above ~3615 cm^{-1} (Watenphul *et al*., 2016). In the region of ^{V}OH stretching vibrations, we observed the broad overlapping bands, indicating the wide range of isomorphic substitutions. The preliminary Mössbauer spectroscopy data suggests that the prevalent iron is in Fe^{2+} form in the *Y* sites. Taking into account the fact that the Z site in grown tourmaline is predominantly occupied by trivalent cations, we suggest the deconvolution of Raman spectra in the region of ^{V}OH vibrations for four bands, corresponding the different combination of di- and trivalent cations in *Y* sites of *YZZ-YZZ-YZZ* triplet in the unit cell. The bands at 3430 – 3450 cm^{-1} correspond to ^{v}OH group surrounded by only trivalent ions, the band at 3470 – 3500 cm^{-1} - by one divalent and two trivalent *Y* cations in unit cell, the bands at 3530 – 3550 cm^{-1} characterize $2Y^{2+}Y^{3+}$ combination, and high frequency bands at 3560-3590 cm^{-1} were assigned to the local configuration of only divalent cations in 3*Y* sites.

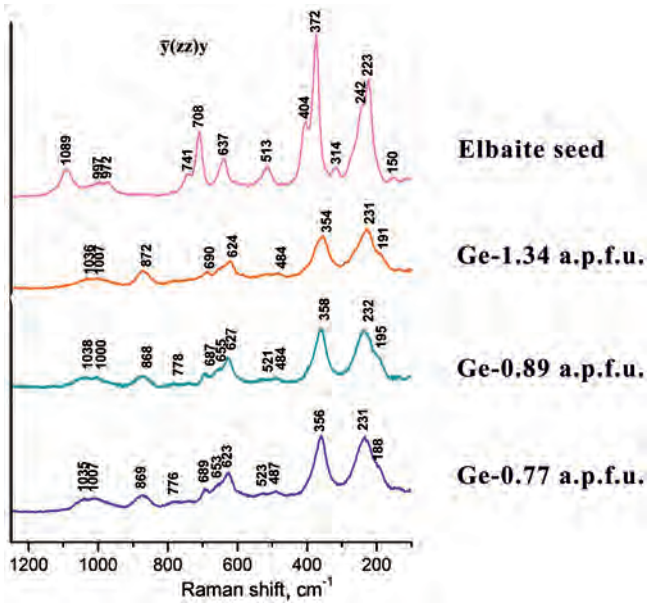

Fig. 2 - Polarized Raman spectra Ga, Ge-rich tourmaline in y(zz)y scattering geometry.

We also observed the weak bands in the region 3615 – 3645 cm^{-1}. This suggests that there is a small amount of OH in ^{W}OH position and that the OH groups are present only in local combination with an *X*-vacancy.

The overgrown layer of Ga, Ge-rich tourmaline obtained was of sufficient size to establish the piezoelectric characteristics, which will be determined in the near future.

This work is fulfilled under the Research Program AAAA-A18-118020590150-6 of the IEM RAS.

REFERENCES

Hoang L. H., Hien N. T. M., Chen X. B., Minh N. V. & Yang I.-S., 2011 – Raman spectroscopic study of various types of tourmalines. *Journal of Raman Spectroscopy*, 42: 1442-1446. <doi.org/10.1002/jrs.2852>

Pandey S. & Schreuer J., 2012 – Elastic and piezoelectric constants of tourmaline single crystals at non-ambient temperatures determined by resonant ultrasound spectroscopy. *Journal of Applied Physics*, 111 (1). <doi.org/10.1063/1.3673820>

Pushcharovsky D. Y., Zubkova N. V., Setkova T. V., Balitsky V. S., Nekrasov A. N. & Nesterova V. A., 2020 – (Ga, Ge)-analogue of tourmaline: crystal structure and composition, *Crystallography Reports*, 65: 849-856. <doi.org/10.1134/S1063774520060279>

Setkova T. V., Balitsky V. S. & Shapovalov Y. B., 2019 – Experimental study of the stability and synthesis of the tourmaline supergroup minerals. *Geochemistry International*, 57: 1082-1094.

Sitarz M., Handke M. & Otto H. H., 2002 – FT-IR studies of cyclogermanates. *Vibrational Spectroscopy*, (29): 45-51. <doi.org/10.1016/S0924-2031(01)00176-X>

Vereshchagin O. S., Setkova T. V., Rozhdestvenskaya I. V., Frank-Kamenetskaya O. V., Deyneko D. V. & Pokholok K. V., 2016 – Synthesis and crystal structure of Ga-rich, Fe-bearing tourmaline. *European Journal of Mineralogy*, 28 (3): 593-599. <doi.org/10.1127/ejm/2016/0028-2542>

Watenphul A., Burgdorf M., Schlüter J., Horn I., Malcherec T. & Mihalova B., 2016 – Exploring the potential of Raman spectroscopy for crystallochemical analyses of complex hydrous silicates: II. Tourmalines *American Mineralogist*, 101 (4): 593-599. <doi.org/10.2138/am-2016-5530>

NATURA 111 (1): 99-100, 2021 - TUR2021 3rd International Conference on Tourmaline

The role of oxy-tourmalines and metasomatic mixing in evolution of lepidolite-subtype pegmatites

Lenka Skřápková*, Jan Cempírek

The lepidolite-subtype Lhenice pegmatite is a member of the South Bohemian pegmatite field in the is located in the southern part of the Moldanubian Zone of the Bohemian Massif, Czech Republic (Novák & Cempírek, 2010). It forms a flat tabular body ca. 4 m thick and 20 m long in its most fractionated part. The dike has concentric zoning with (from border to center) graphic zone, granitic zone, Qtz-Ms-Ab zone and Ab-Lpd zone. We present results of textural and mineralogical analysis combined with data acquired using electron microprobe and LA-ICP-MS.

Primary tourmaline that originated from melt(s) evolved in several generations in the pegmatite. The crystallization trend of primary generation in early pegmatite zones is (Fig. 1): Mg-bearing Al-rich schorl → foitite to schorl (up to 0.52 ^{W}O) → foitite to F-rich schorl (up to 0.51 ^{W}O). Primary generations of tourmaline and other minerals like biotite, primary muscovite, K-feldspar crystallized from potassic melt and were later affected by albitization. In the inner Ab-Lpd zone, primary tourmaline crystallized from residual albite melt and is characterized by zoning and variable contents of F (and Na); evolutional trend is Ca-bearing fluor-elbaite → Mn-bearing darrellhenryite-rossmanite (up to 0.65 apfu ^{W}O) → fluor elbaite (Fig. 1).

Metasomatic tourmaline partly replaced the primary generations in all pegmatite zones mainly at the rims and along fractures, and in some cases replaced it completely. Its composition is quite similar in all zones and depends on the composition of replaced mineral: Li-rich schorl to Fe-rich elbaite → fluor-elbaite → fluor-elbaite → Fe-bearing fluor-elbaite.

Our data show contrasting compositions of primary tourmaline generations from early units and from albite-lepidolite zone, both with medium to elevated contents of F and Na. The textural-paragenetic evidence shows that all compositions with very high F and Na contents belong to secondary tourmalines, formed by metasomatic or hydrothermal replacement of earlier generations (Fig. 1).

The most pronounced process in the Lhenice I pegmatite is the **albitization** that took place in all early-crystallized units and almost completely replaced the K-feldspar in the blocky unit and allowed crystallization of muscovite I in coarse crystals. Most notably, it caused partial or complete recrystallization of primary tourmaline generations, resulting in Fe-enrichment of the sodic melt and formation of green Li,Fe-tourmaline (Fig. 1 - green triangles). Albitization of the K-feldspar of the blocky zone raised the K_2O content in the melt and allowed formation of micas in the Qtz-Ms-Ab and Ab-Lpd zones.

The Ab-Lpd zone contains primary euhedral and fibrous tourmaline (as well as cassiterite, Nb,Ta-oxides, and muscovite I) that formed in albite. The euhedral tourmaline crystallized together with albite, rarely likely in albite pockets subsequently filled by quartz; the fibrous tourmaline could have formed in pockets at the end of the euhedral tourmaline crystallization. The change of the crystal habitus could indicate the beginning of the hydrothermal stage (Dutrow & Henry, 2016). All minerals were fractured before (or during) formation of lepidolite. In this context, the exact cause of the temporary decrease in F reflected in the "darellhenryite-rossmanite loop" remains an open question; the most significant process that removes F from the albitic melt is most likely the onset of crystallization of lepidolite.

K,Li-metasomatism took place along with solidification of the two albite-rich zones. Crystallization of lepidolite in Ab-Lpd zone was associated with K,Li-metasomatism (formation of lepidolite rims around muscovite I in Qtz-Ms-Ab zone).

In early zones it affected especially garnet and partially also the associated primary tourmaline that were both altered by metasomatic assemblage zinnwaldite ± muscovite.

Late hydrothermal processes altered all earlier micas, K-feldspar, primary tourmaline, and even the metasomatic Fe-enriched tourmaline to a fine-grained muscovite III and Fe-enriched lepidolite II.

Department of Geological Sciences, Faculty of Science, Masaryk University, Kotlářská 2, 611 37 Brno, Czech Republic.
E-mail: jan.cempirek@gmail.com

* Corresponding author: lenka.skrapkova@gmail.com

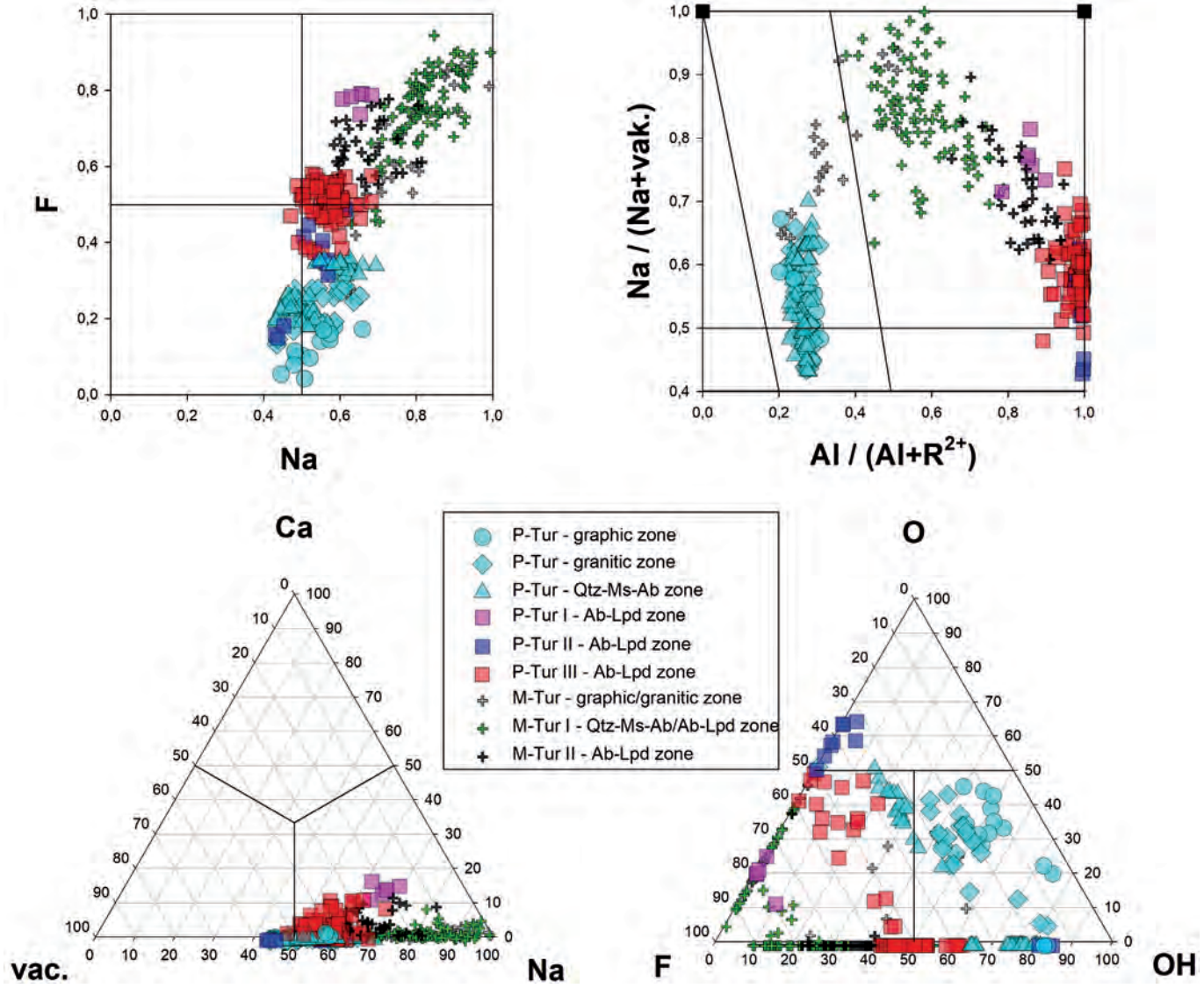

Fig. 1 - Composition of tourmaline generations.

The tourmaline in the Lhenice pegmatite shows apparently gradual evolution from the pegmatite border to its core from the most primitive to the most fractionated, with significant presence of oxy-tourmaline in all pegmatite zones. Tourmaline evolution is characterized by the crystallization of two primary tourmaline groups that, together with metasomatic generations, form the apparently continuous trend described by Selway *et al*. (1999).

Study of the Lhenice pegmatite revealed complex evolution of tourmaline, mica and other accessory minerals that were very significantly affected by metasomatic and hydrothermal processes.

REFERENCES

Dutrow B. L. & Henry D. J., 2016 − Fibrous tourmaline: A sensitive probe of fluid compositions and petrologic environments. *The Canadian Mineralogist*, 54: 311-335.

Novák M. & Cempírek J., 2010 − Granitic pegmatites and mineralogical museums in the Czech Republic. *IMA2010. Acta Mineralogica-petrographica, Field guide series*, 6: 1-56.

Selway J. B., Novák M., Černý P. & Hawthorne F. C., 1999 − Compositional evolution of tourmaline in lepidolite-subtype pegmatites. *European Journal of Mineralogy*, 11: 569-584.

New perspectives on the origins of stratiform tourmalinites

John F. Slack

Stratiform tourmalinites are rocks concordant with the compositional layering of host lithologies and contain more than 15 volume percent tourmaline. These distinctive rocks are metallogenically important in locally having a spatial association with a variety of metal deposits including Cu, Pb, Zn, Ag, Au, W, Co, and U (e.g., Slack, 1996). Syngenetic or diagenetic origins for stratiform tourmalinites have been proposed from myriad geological, structural, and geochemical studies. However, detailed field-based textural studies have also documented epigenetic origins involving metamorphic or magmatic processes. Such discordant and epigenetic tourmalinites are generally distinguished by a lack of lateral continuity (<10 m) along strike, and by proximity to shear zones, veins, or the margins of granitic intrusions. This paper is not concerned with epigenetic varieties of hydrothermal, metamorphic, or magmatic origin, but is focused on stratiform tourmalinites.

Importantly, some stratiform tourmalinites can be misidentified as compositionally different rock types. For example, in weakly metamorphosed terranes, very fine-grained tourmalinite may superficially resemble carbonaceous argillite, siltstone, or chert. In highly metamorphosed terranes, coarse-grained tourmalinite has been mistaken for hornblende amphibolite. Because of the potential for associated mineral deposits, it is thus crucial during field work and later laboratory studies that stratiform tourmalinites not be overlooked or misidentified.

Host lithologies are typically dominated by siliciclastic metasedimentary rocks with locally important felsic metavolcanics. Meta-carbonates, meta-basalts, and other lithologies are less common. Some tourmalinites are interbedded with iron formation or coticule (fine-grained Mn-garnet-quartz rock). Thicknesses of tourmalinites range from <1 cm up to several meters and include interlaminations of siltstone, argillite, or chert, and their metamorphosed equivalents. Characteristically, only tourmaline and quartz are essential constituents, together making up >90 vol % of the rock in most cases. Textural studies indicate that the tourmaline can be randomly oriented, especially in weakly deformed sequences, or strongly aligned in highly deformed metamorphic terranes.

The dominant deposit type associated with stratiform tourmalinites is sediment-hosted, stratiform (SEDEX) Zn-Pb-Ag ores. Less common are occurrences with Cu- or Zn-rich volcanogenic massive sulphide (VMS) deposits. These and many other metallogenic associations are summarized in Slack (1996). Tourmalinites commonly form beds or lenses <1 m thick in the hanging wall of the ore deposits, or lateral equivalents along strike. Although not wholly stratiform, alteration zones in both sediment- and volcanic-hosted deposits may contain abundant tourmaline, such as in the footwall tourmalinite pipe of the large Sullivan Pb-Zn-Ag deposit (British Columbia) in which very fine-grained (<10 μm) tourmaline makes up 20 to 60 vol % of the rock over 450 m of vertical extent.

Many studies have reported on bulk compositions of tourmalinites including data for major elements (ME), trace elements (TE), and rare earth elements (REE). Contents of ME largely record the composition and proportion of tourmaline, whereas TE and REE contents mainly reflect accessory detrital minerals such as monazite, ilmenite, rutile, and zircon. In hydrothermal systems with relatively low fluid/rock ratios (i.e., rock-buffered), as recorded in many tourmalinites like those from the Broken Hill district, ME can be enriched or depleted relative to unaltered host metasedimentary rocks, whereas TE and REE contents tend to be broadly similar (Slack *et al.*, 1993). However, in high fluid/rock systems, as shown by footwall tourmalinites in the Sullivan deposit, ME can be both enriched and depleted, and TE and REE differ greatly due to preferential mobility of some elements, especially light REE, during metasomatic formation of tourmaline within precursor aluminous sediments (Slack, 1996).

Tourmaline is especially valuable in typically retaining original chemical and isotopic compositions, even in metamorphosed terranes, thus providing a potential record of primary fluid chemistry (Slack & Trumbull, 2011). Among stable isotope systems, boron isotopes have been widely applied to tourmaline and tourmalinites (Palmer & Slack, 1989; Trumbull *et al.*, 2020). Tourmalines in most

Department of Earth Sciences, Memorial University of Newfoundland, St. John's, NL A1B 3X5, Canada.
U.S. Geological Survey (Emeritus), National Center, MS 954, Reston, VA 20192, USA.
E-mail: jfslack7@gmail.com

tourmalinites have $\delta^{11}B$ values from -16 to 5 ‰ that reflect boron sourced chiefly from marine sediments, felsic volcanics, or basement rocks. Early work suggested that isotopically light boron in tourmaline, lower than ca. -17 ‰, records a predominantly non-marine evaporite source. However, results of more recent studies cast doubt on this interpretation, due to the recognition that some normal marine sedimentary rocks also have very light isotopic boron, as low as -24.9 ‰ (Trumbull *et al.*, 2020, and references therein). Based on currently available data, only tourmaline with $\delta^{11}B$ values higher than ca. +10 ‰ can be confidently assigned to have a major B component from a marine source, either evaporites or carbonates.

High alumina contents of tourmaline (~28-35 wt % Al_2O_3) greatly limit models of tourmalinite formation. The precipitation of tourmaline directly from an aqueous phase, such as metalliferous hydrothermal fluids, requires the transport of significant Al in solution. However, in hydrothermal fluids with temperatures of less than 300°C, Al has appreciable solubility under low or high pH conditions, and with high contents of fluoride, sulphate, or organic acids. In modern seafloor-hydrothermal systems, Al contents are very low (<0.02 mmol/kg) and hence probably insufficient to permit tourmaline saturation within vent fluids. In contrast, in high-temperature Si- and Cl-bearing metamorphic and magmatic fluids, Al solubility can be very high (up to ~80 mmol/kg), thus explaining the presence of abundant tourmaline in such settings where fluid B concentrations are also relatively high.

The minimum temperature of tourmaline stability is a further constraint. Although the lowest possible formational temperature is unknown, a reasonable estimate is 100 to 150°C, based on data for diagenetic tourmaline overgrowths in sandstones and authigenic grains in the cap rocks of salt domes. In modern seafloor-hydrothermal systems distal (>100 m) from vent sites, temperatures at or near the sediment-seawater interface are generally <50°C. These and other considerations led to early suggestions that tourmaline does not form in modern seafloor environments, instead being derived from an original B-rich gel or colloid precursor (Slack, 1996).

Importantly, modern analogs of tourmalinites are unknown. However, in seafloor environments there appears to be a general affinity of B for Mn, such as on the East Pacific Rise where 300 to 800 ppm B (carbonate-free basis) is preferentially associated with Al-poor Fe-Mn sediments. In this setting, B-rich precursors to tourmaline may exist, a possibility supported by the interbedded nature of tourmalinites and coticules in numerous metamorphosed metasedimentary and metavolcanic terranes. Overall, tourmalinite components that formed at or near the seafloor had sources from (1) hydrothermal plumes: Fe, Mn, Si, B; (2) sediments and felsic volcanics: B, Al, Si, Mg, Ca, Na; and (3) seawater: Si and B. In the Red Sea, metalliferous brines in several deep basins have temperatures and B concentrations up to 68°C and 4580 µmol/kg, respectively. Although probably too low for tourmaline growth on the seafloor, such elevated temperatures may permit the formation of a B-rich gel or colloid.

The importance of precursor aluminous sediments or felsic volcanic rocks in the formation of stratiform tourmalinites supports a diagenetic origin involving the influx of B-rich hydrothermal fluids. This model is consistent with numerous observations of tourmalinites that preserve sedimentary structures such as graded beds, cross-laminations, and rip-up clasts (Slack, 1996). Within these structures, tourmaline shows preferential replacement of the clay and/or feldspar matrix. A preferred origin involves the migration of B-rich hydrothermal fluids along permeable, sandy beds and the selective replacement of argillaceous beds or laminae. This replacement may occur at or near the sediment-water interface, or tens to hundreds of meters below. Such a model is also applicable to permeable felsic volcanics, especially volcaniclastic rocks. The timing of the proposed replacement most likely is during sedimentation or early diagenesis, but a much later timing (e.g., metamorphic) is also possible, if sufficient permeability is maintained for fluid transport over large distances within individual beds or laminae.

REFERENCES

Palmer M. R. & Slack J. F., 1989 – Boron isotopic composition of tourmaline from massive sulfide deposits and tourmalinites. *Contributions to Mineralogy and Petrology*, 103: 434-451.

Slack J. F., 1996 – Tourmaline associations with hydrothermal ore deposits. In: Boron: mineralogy, petrology and geochemistry. Grew E. S. & Anovitz L. M. (eds.). *Reviews in Mineralogy*, 33: 559-643.

Slack J. F. & Trumbull R. B., 2011 – Tourmaline as a recorder of ore-forming processes. *Elements*, 7: 321-326.

Slack J. F., Palmer M. R., Stevens B. P. J. & Barnes R. G., 1993 – Origin and significance of tourmaline-rich rocks in the Broken Hill district, Australia. *Economic Geology*, 88: 505-541.

Trumbull R. B., Codeço M. S., Jiang S.-Y., Palmer M. R. & Slack J. F., 2020 – Boron isotope variations in tourmaline from hydrothermal ore deposits: a review of controlling factors and insights for mineralizing systems. *Ore Geology Reviews*, 125. <doi.org/10.1016/j.oregeorev.2020.103682>

A simplified species classification for gem quality tourmaline by LA-ICP-MS

Ziyin Sun[1], Aaron C. Palke[1]*, Christopher M. Breeding[1], Barbara L. Dutrow[2]

In the gem and jewelry trade, tourmaline species are typically made by sight-identification based on the typical colors of the various species rather than on accurate chemical analyses. However, the same color can be exhibited by several species because color is not species specific. Electron Probe MicroAnalysis (EPMA) is the most widely accepted method to determine tourmaline species. Unfortunately, EPMA is expensive and time consuming, requiring considerable sample preparation. Most gemological laboratories do not have EPMA instruments and cannot justify the overhead costs associated with outsourcing this analysis. Therefore, EPMA is not a practical everyday tool for a gemological laboratory. Here, we present a comprehensive method for using LA-ICP-MS analyses to accurately determine (most) tourmaline species. The new method allows for inexpensive, clean, fast, and largely non-destructive analysis of tourmaline chemistry by LA-ICP-MS.

With adequate standards (GSD-1G, GSE-1G and NIST 610) and calibration, this technique can measure six common major elements (Na, Mg, Al, Si, Ca and Fe) in tourmaline as well as trace elements. Analyses of the fourteen tourmalines by both the EPMA (Electron Probe MicroAnalysis) and LA-ICP-MS for major elements demonstrates that an LA-ICP-MS system with proper calibration, standardization and normalization procedures is capable of accurate measurements of six major elements in tourmalines generally within ±10% error (Sun *et al*., 2019).

The species classification presented here is a simplified version of Henry *et al*. (2011) necessary for the limitations of LA-ICP-MS analysis. Our inability to measure F or transition metal oxidation states by LA-ICP-MS means that we are unable to determine the occupancy of the V-site and W-sites; therefore we cannot determine the flour- or oxy species. Consideration of these limitations provides the following groups of 11 tourmaline species (below). If the tourmaline data falls outside these simplified classification categories, the tourmaline is assigned to Alkali-subgroup 3, 4 and 5, or Calcic-subgroup 3 and 4, or Vacant-subgroup 3 (Henry *et al*., 2011, Tab. 1). None of these tourmaline species are considered in this method as they are rarely encountered as gem quality specimens.

1. Dravite
   $^{X}Na^{Y}Mg_3{}^{Z}Al_6{}^{T}Si_6O_{18}(BO_3)_3(OH)_3(OH)$
2. "Vanadium-dravite"
   $^{X}Na^{Y}Mg_3{}^{Z}V_6{}^{T}Si_6O_{18}(BO_3)_3(OH)_3(OH)$
3. Chromium-dravite
   $^{X}Na^{Y}Mg_3{}^{Z}Cr_6{}^{T}Si_6O_{18}(BO_3)_3(OH)_3(OH)$
4. Schorl
   $^{X}Na^{Y}Fe^{2+}{}_3{}^{Z}Al_6{}^{T}Si_6O_{18}(BO_3)_3(OH)_3(OH)$
5. Elbaite
   $^{X}Na^{Y}(Li_{1.5}Al_{1.5})^{Z}Al_6{}^{T}Si_6O_{18}(BO_3)_3(OH)_3(OH)$
6. Uvite
   $^{X}Ca^{Y}Mg_3{}^{Z}(MgAl_5)^{T}Si_6O_{18}(BO_3)_3(OH)_3(OH)$
7. Feruvite
   $^{X}Ca^{Y}Fe^{2+}{}_3{}^{Z}(MgAl_5)^{T}Si_6O_{18}(BO_3)_3(OH)_3(OH)$
8. "Liddicoatite"
   $^{X}Ca^{Y}(Li_2Al)^{Z}Al_6{}^{T}Si_6O_{18}(BO_3)_3(OH)_3(OH)$
9. Foitite
   $^{X}\square^{Y}(Fe^{2+}{}_2Al)^{Z}Al_6{}^{T}Si_6O_{18}(BO_3)_3(OH)_3(OH)$
10. Magnesio-foitite
    $^{X}\square^{Y}(Mg_2Al)^{Z}Al_6{}^{T}Si_6O_{18}(BO_3)_3(OH)_3(OH)$
11. Rossmanite
    $^{X}\square^{Y}(LiAl_2)^{Z}Al_6{}^{T}Si_6O_{18}(BO_3)_3(OH)_3(OH)$

Many gem quality tourmaline have unusal and interesting chemical composition, such as Paraiba "liddicoatite" tourmaline (Katsurada & Sun, 2017, Fig. 1, bottom row) and the high Pb (17400 ppmw) and Mn (23400 ppmw) "liddicoatite" tourmaline shown in Fig. 2. Many large complexly set stones, such as the rainbow tourmaline bracelet (Fig. 3) mounted with 33 square step cut stones, can be easily analyzed with good precision and accuracy.

[1] Carlsbad laboratory, Gemological Institute of America, 5345 Armada Drive, Carlsbad, CA 92008, USA.
E-mail: zsun@gia.edu
mbreeding@gia.edu
[2] Department of Geology and Geophysics, Louisiana State University, Baton Rouge, Louisiana, USA.
E-mail: dutrow@lsu.edu

* Corresponding author: apalke@gia.edu

The ability to accurately measure the range of chemical compositions found in gem tourmaline using LA-ICP-MS allows GIA to help the colored stone industry better understand the varieties of tourmaline being bought and sold and to ensure that all stones are tourmaline.

Fig. 1 - "Liddicoatite" tourmaline. Top three red stones from left to right: 7.54 ct purple-red "liddicoatite", 3.57 ct purple-red "liddicoatite", 4.60 ct purple-red "liddicoatite", courtesy of GIA museum; Bottom row two pear shaped stones from left to right: 3.80 and 4.14 ct blue-green cuprian "liddicoatite", courtesy of Hubert Gesser at Hubert Inc.. Bottom center stone: 3.16 ct bluish-green cuprian "liddicoatite", courtesy of John R. Evans. Photo © GIA.

Fig. 2 - 3.34 ct colorless "liddicoatite" with extremely high Pb (17400 ppmw) and Mn (23400 ppmw) concentration, courtesy of Bruce A. Fry. Photo © GIA.

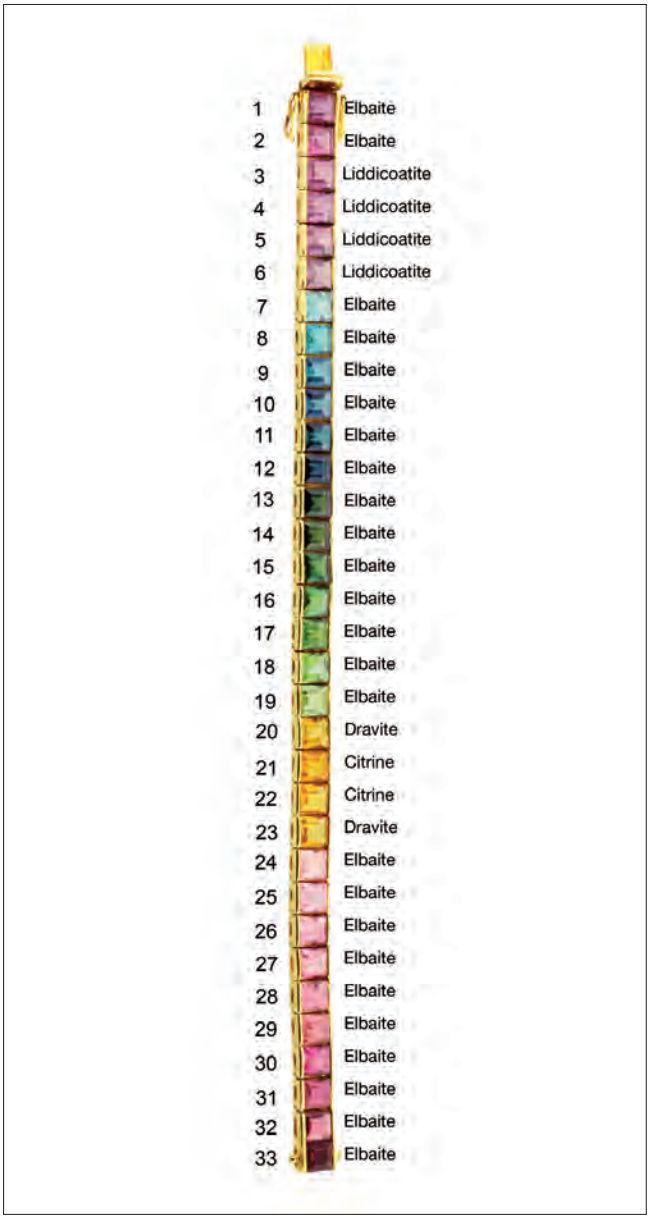

Fig. 3 - This rainbow-colored tourmaline bracelet was examined for identification and species classification in GIA Carlsbad, USA, Laboratory. The tourmaline species are from red -pink elbaite and orange dravites, to green-blue elbaites and violet-purple "liddicoatites". Stone 21 and 22 were two citrines that had been mixed with other two orange dravites, courtesy of Barbara L. Dutrow.

REFERENCES

Henry D. J., Novák M., Hawthorne F. C., Ertl A., Dutrow B. L., Uher P. & Pezzotta F., 2011 − Nomenclature of the tourmaline-supergroup minerals. *American Mineralogist*, 96 (5-6): 895-913.

Katsurada Y. & Sun Z., 2017 − Cuprian liddicoatite tourmaline. *Gems & Gemology*, 53 (1): 34-41. <http://dx.doi.org/10.5741/GEMS.53.1.34>

Sun Z., Palke A. C., Breeding C. M. & Dutrow B. L., 2019 − A new method for determining gem tourmaline species by LA-ICP-MS. *Gems & Gemology*, 55 (1): 2-17. <http://dx.doi.org/10.5741/GEMS.55.1.2>

Petrogenesis of tourmaline-bearing NYF, LCT, and mixed NYF-LCT granitic pegmatites of the Peninsular Ranges Batholith, southern California, USA

Matthew C. Taylor

Granitic pegmatites of NYF, LCT, and mixed NYF-LCT families are found throughout the Peninsular Ranges Batholith (PRB), an assemblage of Mesozoic subduction-derived early arc volcanics and gabbros (western zone) followed by I-type tonalites and monzogranites that intruded Paleozoic metasediments and older Mesozoic S-type granitic gneisses. Black tourmaline is common in pegmatites of all families, which span the entire length and width of the PRB; however, only LCT and mixed families may have polychrome varieties. Locally, PRB pegmatites are the last intrusive rocks, becoming younger with the eastward movement of the center of arc magmatism with time. Hydrous (i.e., hornblende + biotite-bearing) tonalites are parental to NYF pegmatites when shear of the mostly brittle outer parts of crystal-rich mushes suddenly opened fissures for hydrous fractionated, intergranular fluids to rapidly fill. These NYF pegmatites lack fluorine (i.e., no topaz or fluoride minerals) through its probable removal by abundant hornblende and biotite in their tonalitic parents.

Tectonic squeezing of larger hydrous tonalitic crystal-rich mushes (*e.g.*, La Posta-type tonalites of the eastern zone) extracts more hydrous and aluminous intergranular melts that accumulate and crystallize peripheral to these tonalites as monzogranitic satellites (biotite- or biotite + muscovite ± garnet-bearing) that due to their very hydrous nature become locally contaminated by partially assimilating their metamorphic sidewalls. Quartz-tourmaline clots and nodules and tourmaline replacing biotite may occur locally within monzogranites, and local tourmalization of the exocontact can extend outward for several meters. Through shear, fissures develop in the mostly brittle carapaces of crystal-rich mushes and their brittle host rocks for the most fractionated, hydrous intergranular fluids to flow into and to crystallize to become LCT to mixed NYF-LCT pegmatites. The degree of mixed family affiliation appears related to the amount of titanite present in the larger tonalitic sources regulating Ti and REE available for monzogranitic parents of mixed pegmatites.

The process of fissuring the brittle parts of crystal-rich (90-99 vol%) mushes from hydrous melts regardless of their bulk compositions generates seismic waves and the resulting drop in pressure induces the intergranular melt within the sidewalls of fissures to suddenly boil (*i.e.*, spontaneously exsolve copious vapor) and to travel towards these areas of extreme low pressure. This process breaks up the supersaturated melt into droplets that must travel through a network of irregular gaps and orifices between crystals of the mush to be sprayed, likely with supersonic flow, from the sidewalls into the newly created void spaces. During their travel, the impact upon numerous surfaces of crystals of the mush reduces the melt droplets in size and makes them spherical in shape in the expanding vapor-propelled spray. The drop in pressure also causes a drop in the vapor's temperature, the suspended melt nanospheres becoming undercooled, conceivably at times to glass, while traveling to and within fissures. The complete process causes a typical melt-vapor system (i.e., vesiculated melt) to transform into a pegmatitic fluid: undercooled silicate melt/glass nanospheres that are suspended in their exsolved supercritical aqueous fluid. This process is akin to techniques used in the commercial manufacturing of nanospheres whereby liquid is drawn from a reservoir through the expansion of an exsolving gas whose spray is directed upon a plate to break-up the droplets further, producing spherical nanoparticles of uniform size after rapid cooling or drying (e.g., Biskos *et al*., 2008; Charitidis *et al*., 2014).

Once at rest, short-range attraction and spinodal decomposition (e.g., spontaneous melt-vapor phase separation) of the undercooled nanospheres leads to networks developing between particles, sticking them together to form a particle gel (Lu *et al*., 2008) that supports the growth of giant crystals, pegmatitic textures, and replacement phenomena. Gel ageing (i.e., long-range ordering and the expulsion of hydrous fluid) causes dikes to shrink during consolidation, at times fracturing and displacing primary minerals (e.g., blocky K-feldspar, black and polychrome tourmaline) found in massive quartz (i.e., crystallized silica gel), and generates the hydrothermal fluids that cause autometasomatism and clay mineralization.

3744 Blue Bird Canyon Road, Vista, California (CA), 92084, USA.
E-mail: pegmatologist@yahoo.com

The processes of forming pegmatitic fluids and particle gels depend only on the exsolution of a supercritical aqueous vapor phase and are not dependent on the presence of fluxes that lower the solidi and viscosities of granitic melts (e.g., Li, B, P, F); pegmatites typically show trace amounts of these components. The occurrences of tourmaline are a consequence of the strong partitioning of boron into the vapor phase of hydrous intergranular melts within crystal-rich mushes.

REFERENCES

Biskos G., Vons V., Yurteri C. U. & Schmidt-Ott A., 2008 – Generation and sizing of particles for aerosol-based nanotechnology. *KONA Powder and Particle Journal*, 26: 13-35. <doi: 10.14356/KONA.26.2008006>

Charitidis C. A., Georgiou P., Koklioti M. A, Trompeta A-F. & Markakis V., 2014 – Manufacturing nanomaterials: from research to industry. *Manufacturing Review*, 1 (11): 1-19. <doi: 10.1051/mfreview/2014009>

Lu P. J., Zaccarelli E., Ciulla F., Schofield A. B., Sciortino F. & Weitz D. A., 2008 – Gelation of particles with short-range attraction. *Nature*, London, 453: 499-503. <doi: 10.1038/nature06931>

Rare lithophile elements (Zr, Hf, Nb, Ta) in tourmalines from granite-pegmatite suites

Pavel Uher[1]*, Peter Bačík[1,2], Martin Ondrejka[1]

Tetravalent and pentavalent rare litophile elements: Zr, Hf, Nb and Ta (also HFSE – High Field Strength Elements), represent very important markers of magmatic fractionation in granite-pegmatite suites as well as essential elements of rare and economic important minerals (zircon to hafnon, Nb-Ta oxide minerals). However, these elements occur in trace contents in many other rock-forming and accessory minerals of evolved granites and pegmatites (e.g., micas, garnet, phosphate phases).

Concentrations of Zr, Hf, Nb and Ta in tourmaline-supergroup minerals (dravite, schorl, fluorschorl, fluorelbaite) were investigated in various suites of tourmaline-bearing granites, LCT and NYF granitic pegmatites without or with Li mineralization worldwide, determined by in-situ LA-ICP-MS method (e.g., Roda-Robles *et al.*, 2004, 2015; Peretti *et al.*, 2009; Bačík *et al.*, 2012; Čopjaková *et al.*, 2013; Marks *et al.*, 2013; Hong *et al.*, 2017; Breiter *et al.*, 2018; Sciuba *et al.*, 2021; Zhao *et al.*, 2021; unpublished data of authors). The contents of Nb and Ta in tourmalines are generally 5−10 times higher than their Zr and Hf counterparts; they reach ≤30 ppm Nb (usually 1−15 ppm), ≤25 ppm Ta (0.2−5), ≤7 ppm Zr (0.1−1), and ≤0.4 ppm Hf (0.02−0.2). The atomic Hf/(Hf+Zr) = 0.01−0.41 and Ta/(Ta+Nb) = 0.07−0.83 in the studied tourmalines. There are usually missing any systematic relationships between concentration of Zr, Hf, Nb and Ta in tourmalines and parental rocks (granites versus pegmatites), between barren (Li-poor) and Li-rich pegmatites, or between LCT and NYF pegmatites. However, some (fluor)elbaite (including Cu-rich compositions) show local enrichment in Ta. Some positive Hf−Zr, Ta−Nb and Hf/(Hf+Zr) versus Ta/(Ta+Nb) correlations were observed rather in regional than general scale (within granite batholith or pegmatite field).

[1] Department of Mineralogy, Petrology and Economic Geology, Faculty of Natural Scieces, Comenius University, Ilkovičova 6, 842 15, Bratislava, Slovakia.
[2] Earth Science Institute, the Slovak Academy of Sciences, Dúbravská cesta 9, P.O. BOX 106, 840 05 Bratislava, Slovakia.

* Corresponding author: pavel.uher@uniba.sk

Effective ionic radii of the investigated cations in six-fold (octahedral) coordination (Shannon, 1976) are similar to dominant octahedral cations in *Y* and *Z* sites of tourmalines: Zr^{4+} (0.72 Å) and Hf^{4+} (0.71) are close to Mg^{2+} (0.72), Sn^{4+} (0.69), Li^{+} (0.76) and Fe^{2+} (0.78), whereas smaller Nb^{5+} and Ta^{5+} (both 0.64 Å) are analogous to Fe^{3+} (0.645) and Ti^{4+} (0.605). Consequently, Zr^{4+}, Hf^{4+}, Nb^{5+} and Ta^{5+} are most probably located in the octahedral *Y* and *Z* sites of tourmalines.

This assumption is also supported by the bond length calculation constraints. Calculated bond length parameters of Zr^{4+}, Hf^{4+}, Nb^{5+} and Ta^{5+} in tourmalines were compared to bond lengths typical for the *T*, *Y* and *Z* sites defined as the "Goldilocks zone" of stable bond lengths for each site (Gagné & Hawthorne, 2015; Bačík & Fridrichová, 2021).

All studied cations have very similar calculated bond length with O^{2-} for both tetrahedral and octahedral coordination. For tetrahedral coordination, it varies between 1.909 Å (Nb^{5+}) and 1.923 Å (Hf^{5+}). However, this is significantly larger than upper limit of the "Goldilocks zone" for the tourmaline *T* site. Therefore, it is extremely unlikely that these cations despite their high charge occupy the *T* site substituting for Si^{4+}. In the octahedral coordination, studied elements split into two pairs. Four-valent Zr and Hf have slightly longer bonds of 2.075 Å (Zr^{4+}) and 2.078 Å (Hf^{4+}), while Ta^{5+} forms 2.055 Å and Nb^{5+} 2.059 Å long bonds. These values are situated perfectly in the middle of the "Goldilocks zone" for the octahedral sites in tourmalines. Since it is slightly lower than ideal Mg^{2+}–O bond length and higher than Fe^{2+}–O bond length, it cannot be strictly defined if these cations would prefer *Z* or *Y* site.

However, high charge of Zr^{4+}, Hf^{4+}, Nb^{5+} and Ta^{5+} for the octahedral sites compared to their most usual occupants (Al^{3+}, Fe^{2+}, Mg^{2+}) limits the possible substitutional mechanisms allowing the incorporation of these four- and five-valent cations in the tourmaline octahedral sites. The charge balancing can be achieved by subsequent substitution of Li^{+} at the *Y* site, divalent cations for Al^{3+} at the *Z* site, vacancy at the *X* site, and deprotonation of the W or V site.

This research was funded by the projects APVV-18-0065, APVV-19-0065, VEGA-1/0137/20, VEGA 1/0467/20, and VEGA 1/0151/19.

REFERENCES

Bačík P. & Fridrichová J., 2021 – Cation partitioning among crystallographic sites based on bond-length constraints in tourmaline-supergroup minerals. *American Mineralogist*, 106: 851-861.

Bačík P., Uher P., Ertl A., Jonsson E., Nysten P., Kanický V. & Vaculovič T., 2012 – Zoned REE-enriched dravite from a granitic pegmatite in Forshammar, Bergslagen Province, Sweden: An EMPA, XRD and LA-ICP-MS study. *The Canadian Mineralogist*, 50: 825-841.

Breiter K., Ďurišová J., Hrstka T., Korbelová Z., Vašinová Galiová M., Müller A., Simons B., Shail R. K., Williamson B. J. & Davies J. A., 2018 – The transition from granite to banded aplite-pegmatite sheet complexes: An example from Megiliggar Rocks, Tregonning topaz granite, Cornwall. *Lithos*, 302-303: 370-388.

Čopjaková R., Škoda R., Vašinová Galiová M. & Novák M., 2013 – Distribution of Y + REE and Sc in tourmaline and their implications for the melt evolution; examples from NYF pegmatites of the Třebíč Pluton, Moldanubian Zone, Czech Republic. *Journal of Geosciences*, 58: 113-131.

Gagné O. C. & Hawthorne F. C., 2015 – Comprehensive derivation of bond-valence parameters for ion pairs involving oxygen. *Acta Crystallographica B*, 71: 562-578.

Hong W., Cooke D. R., Zhang L., Fox N. & Thompson J., 2017 – Tourmaline-rich features in the Heemskirk and Pieman Heads granites from western Tasmania, Australia: Characteristics, origins, and implications for tin mineralization. *American Mineralogist*, 102: 876-899.

Marks M. A. W., Marschall H. R., Schühle P., Guth A., Wenzel T., Jacob D. E., Barth M. & Markl G., 2013 – Trace element systematics of tourmaline in pegmatitic and hydrothermal systems from the Variscan Schwarzwald (Germany): The importance of major element composition, sector zoning, and fluid or melt composition. *Chemical Geology*, 344: 73-90.

Peretti A., Bieri W. P., Reusser E., Hametner K. & Günther D., 2009 – Chemical variations in multicolored "Paraiba"-type tourmalines from Brazil and Mozambique: Implications for origin and authenticity determination. *Contributions to Gemology*, 9: 1-77.

Roda-Robles E., Pesquera A., Gil P. P., Torres-Ruiz J. & Fontan F., 2004 – Tourmaline from the rare-element Pinilla pegmatite, (Central Iberian Zone, Zamora, Spain): chemical variation and implications for pegmatitic evolution. *Mineralogy and Petrology*, 81: 249-263.

Roda-Robles E., Simmons W., Pesquera A., Gil-Crespo P. P., Nizamoff J. & Torres-Ruiz J., 2015 – Tourmaline as a petrogenetic monitor of the origin and evolution of the Berry-Havey pegmatite (Maine, U.S.A.). *American Mineralogist*, 100: 95-109.

Sciuba M., Beaudoin G. & Makvandi S., 2021 – Chemical composition of tourmaline in orogenic gold deposits. *Mineralium Deposita*, 56: 537-560.

Shannon R. D., 1976 – Revised effective ionic radii and systematic studies of interatomic distances in halides and chalcogenides. *Acta Crystallographica* A, 32: 751-767.

Zhao Z., Yang X., Liu Q., Lu Y., Chen S., Sun C., Zhang Z., Wang H. & Li S., 2021 – In-situ boron isotopic and geochemical compositions of tourmaline from the Shagbao Nb-Ta bearing monzogranite, Nanling Range: Implication for magmatic-hydrothermal evolution of Nb and Ta. *Lithos*, 386-387: 106010.

Evolution of tourmaline from Li-poor, F-rich pegmatites at the SE border of the Moldanubian Zone, Bohemian Massif

Scarlett Urbanová*, Jan Cempírek

Eastern margin of the Moldanubian Zone is characterized by common occurrences of rare-element pegmatites, loosely grouped in two large pegmatite fields (Strážek and Vratěnín-Radkovice; Fig. 1). The area is characterized by presence of S-type granites and leucogranites in the thermal aureole of the Třebíč durbachite pluton, and various metamorphosed, strongly migmatized paragneiss to migmatites of the Gföhl Unit of the Moldanubian Zone.

The two pegmatite fields include ca. 15 fractionated pegmatite dikes containing rare elements such as Li, Rb, Be, Cs, Nb, Ta, Sn and W. The pegmatites range from lepidolite subtype to elbaite subtype of the complex type of the rare-element class of granitic pegmatites, with thickness from 10 cm to more than 20 m. We studied mineralogy and tourmaline evolution in three highly to moderately fractionated elbaite-subtype pegmatites – Ctidružice, Hrotovice and Křižínkov.

The most evolved elbaite-subtype pegmatite is the Ctidružice dike (e.g. Buřival & Novák 2018), which contains common fine-grained greenish cleavelandite, tourmaline, garnet and accessory Mn-rich polylithionite-masutomilite, fluorapatite, topaz, zircon, W-rich ixiolite, columbite, cassiterite, monazite, and secondary stokesite and Be,B-minerals (e.g. hambergite, bertrandite). Tourmaline evolves from vacant, Fe,Mg-rich composition (foitite to schorl) → Mn-rich compositions (Mn-rich schorl, tsilaisite) → fluor-elbaite Intense metasomatic processes are present in all units, with variable F and Na contents (Fig. 2a).

The pegmatite from Hrotovice in relatively poor in rare-element mineralization which, however, locally reaches a high degree of fractionation. Besides F-rich tourmaline in contains minor lepidolite with unusual composition (polylithionite and sokolovaite), accessory topaz, Be-rich cordierite, W-rich Nb-Ta oxides with strong Mn/(Mn+Fe) fractionation (columbite ixiolite, qitianlingite), fluorapatite, cassiterite, uranmicrolite, xenotime, and monazite. The evolution of tourmaline is rather simple, from primary Mg,Fe-tourmalines with lower amounts of F to late (dark green) tourmaline (fluor-elbaite) with high content of Na, F and Li. Metasomatic and recrystallized tourmalines are affected by composition of the replaced tourmaline (Fig. 2b).

In the Křižínkov pegmatite group, pegmatite albite-rich zones are characterized by presence of fine-grained

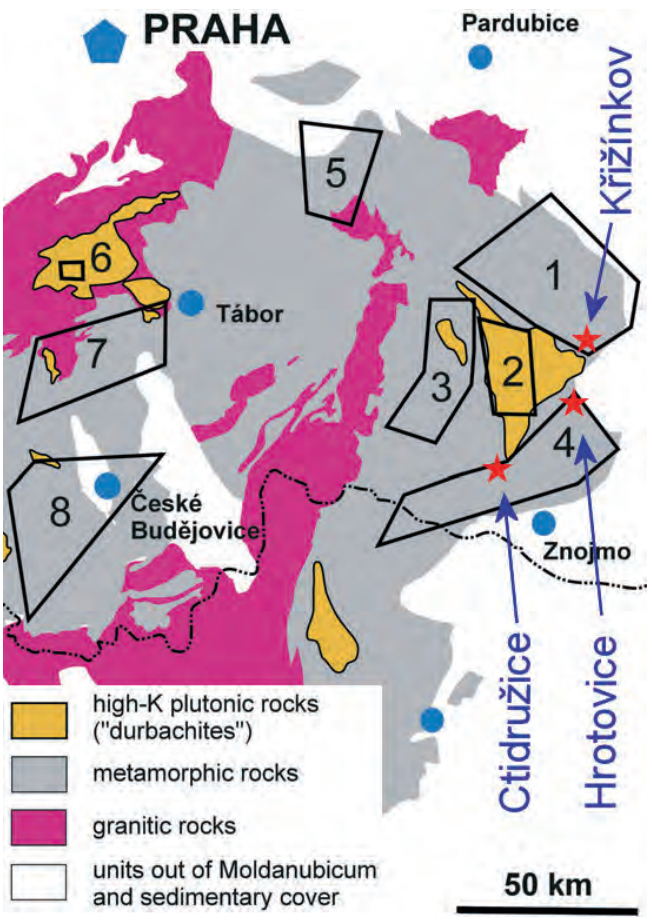

Fig. 1 - Studied localities and the pegmatite fields in the eastern part of the Moldanubian Zone (after Novák & Cempírek, 2010). Names of the pegmatite fields: 1) Strážek, 2) Třebíč, 3) Jihlava, 4) Vratěnín-Radkovice, 5) Vlastějovice, 6) Vepice, 7) Písek, 8) South Bohemian pegmatite field.

Department of Geological Sciences, Faculty of Science, Masaryk University, Kotlářská 2, 611 37 Brno, Czech Republic.
E-mail: jan.cempirek@gmail.com

* Corresponding author: scarlett.scala@gmail.com

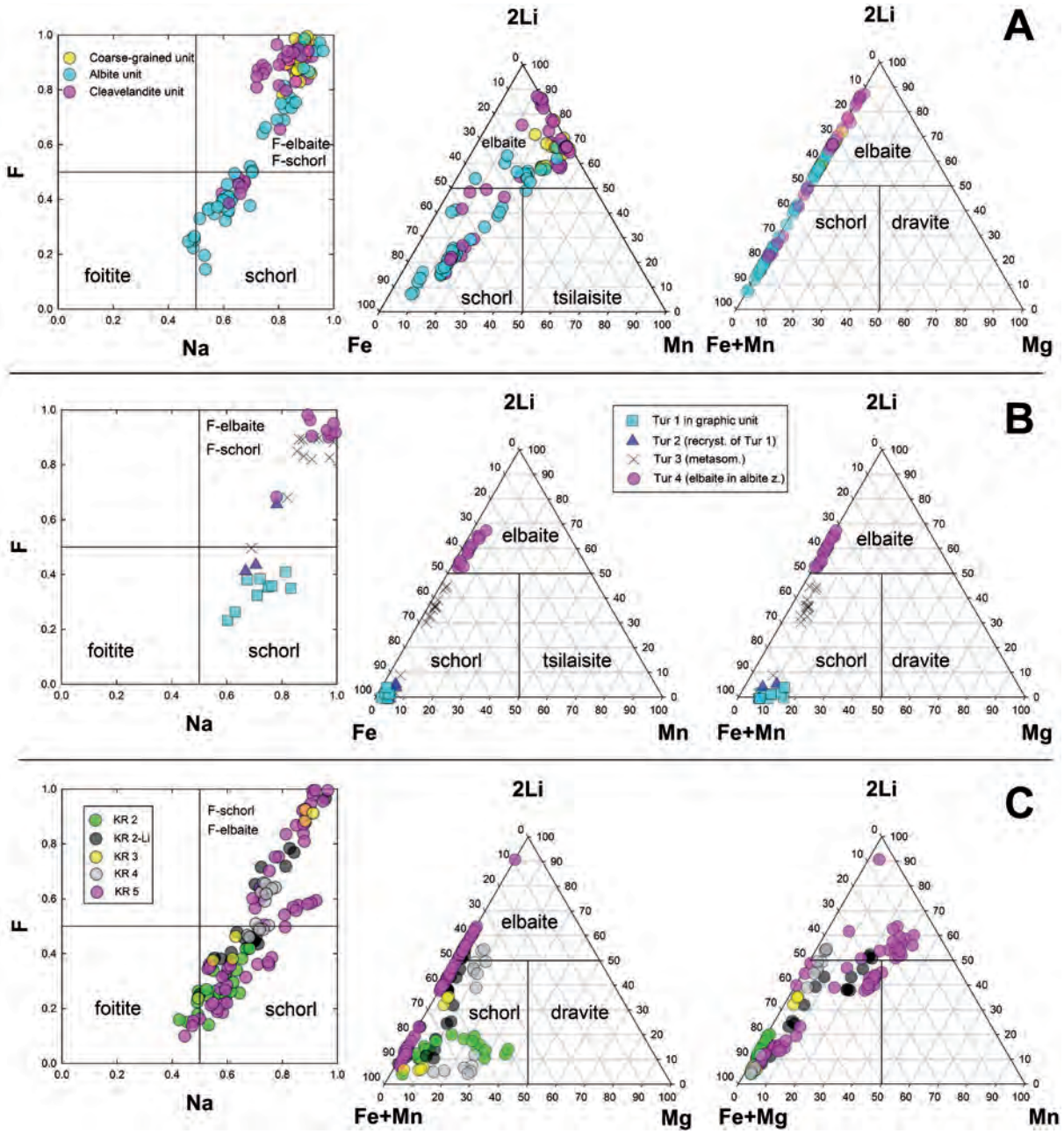

Fig. 2 - Evolution of tourmaline from Ctidružice (A), Hrotovice (B) and Křižínkov (C) pegmatites.

greenish cleavelandite that contains the lithium mineralization, topaz, tourmaline, fluorapatite, cassiterite, wodginite, ixiolite, Nb-rutile, zircon, xenotime. masutomilite and garnet. Tourmaline evolution (foitite → schorl → fluor-schorl → fluor-elbaite) documents an increase of Na, F, Li, and Mn (Fig. 2c).

The three localities show several common features such as F-rich mineral assemblages (topaz, F-rich tourmaline), metasomatic micas with locally very high fractionation of Cs and Mn (sokolovaite, masutomilite), and high contents of W present in Nb,Ta-oxides (W-rich columbite, ixiolite, qitianlingite).

The observed evolution of tourmaline with high initial contents of Fe and high Na,F-contents corresponds to relatively high initial fractionation of the melt. The tourmaline composition and presence of HFSE such as Nb, Ta and W in combination with high F-contents supports their origin as fractionation products of the associated S-type granites and leucogranites present in the thermal aureole of the Třebíč melasyenite (durbachite) pluton.

This work was supported by the research projects GAČR 19-05198S and MUNI/A/1594/2020.

REFERENCES

Buřival Z., & Novák M., 2018 − Secondary blue tourmaline after garnet from elbaite-subtype pegmatites. *Journal of Geosciences*, 63: 111-122.

Novák M. & Cempírek J., 2010 − IMA 2010 field trip guidebook CZ2.

Quartz-tourmaline intergrowths in the wall zone of the Emmons Pegmatite (Maine, USA)

Laura M. van der Does[1]*, Niels Hulsbosch[1], Philippe Claeys[2], Jan Elsen[1], Pim Kaskes[2], Philippe Muchez[1], Mona-Liza C. Sirbescu[3]

Tourmaline often occurs in the border and wall zones of internally zoned pegmatite dikes (London, 2008). Apart from coarse grain-sizes, granitic pegmatites are distinguished by anisotropic mineral textures, interpreted to result from disequilibrium crystallization and liquidus undercooling. Textures include unidirectional solidification textures and graphic intergrowths of minerals (Simmons & Webber, 2008). The crystal morphology is controlled mainly by nucleation and growth rates, which are controlled by water content and the degree of undercooling (Sirbescu *et al*., 2017). Here, tourmaline textures and chemical compositions from the outer zones of the Emmons Pegmatite (Oxford County, Maine, USA) are examined to provide insights into the early crystallization processes of an internally zoned pegmatite.

The Emmons Pegmatite is a thin dike with sharp contacts with the migmatite host-rock, indicating undercooling likely influenced the crystallization of the dike. The dike is internally zoned (Falster *et al*., 2019) (Fig. 1). Tapered, subhedral prisms and quartz-tourmaline intergrowths (QTIs) have been observed in the border and wall zone, respectively (Sirbescu & Hulsbosch, 2020). Tourmaline is black in hand sample in both assemblages. The subhedral prisms nucleate on the border growing to sizes up to, at least, 5 cm. The prisms flare inwards, creating a comb-like structure on the border. Based on transmitted light microscopy, tourmaline is zoned with pink-purple cores and brown rims. Fluid inclusions (FI) and melt inclusions (MI) both occur, but the assemblage is dominated by MI. The QTIs also form perpendicular to the host rock contact creating assemblages up to 50 cm. QTIs can be split in three different crystal morphologies: 1) large, eu- to subhedral central tourmaline, which is elongated in the growth direction, 2) second tier tourmaline, often more subhedral, extending from the tip of the central tourmaline and 3) the actual skeletal intergrowths with quartz (Fig. 2A). Type 3 tourmaline is mostly skeletal (branch-like), but, it can also include elongated, satellite portions. In transmitted light, the coarser satellite portions may possess the core-rim zonation seen in types 1 and 2 morphologies (Fig. 2A). Most importantly, all types of tourmaline within an individual QTI are optically coherent, indicating that they form a single crystal, branching out from a single initial nucleation site. The number of FI increases from the central to skeletal tourmaline. The assemblage also evolves from being MI dominated, in the central tourmaline, to being FI dominated in the skeletal tourmaline.

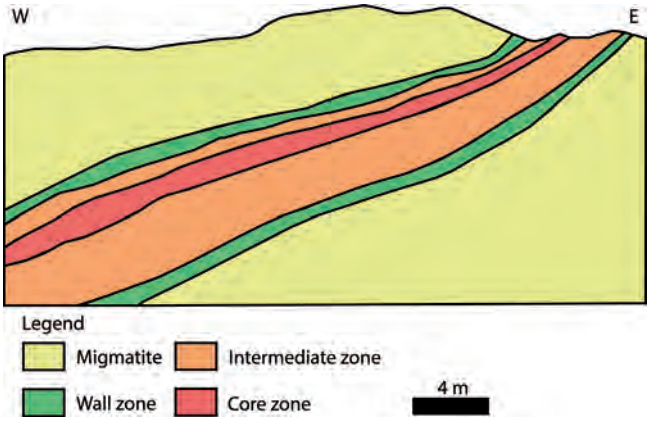

Fig. 1 - Simplified cross-section of the Emmons Pegmatite showing the internal zonation. (Modified from Hanson *et al*., 2018).

Electron microprobe analyses (EMPA; JEOL 8200 Superprobe at the University of Copenhagen) were performed to classify the tourmaline and to examine compositional variations during tourmaline growth. The tourmaline crystals belong to the alkali group (Henry *et al*., 2011), with cores trending towards the X-vacant group (Na/(Na+X-vacancy) ranging 0.52-0.68 apfu/apfu and 0.60-0.73 in cores and rims, respectively). Fur-

[1] KU Leuven, Department of Earth and Environmental Sciences, 3001 Leuven, Belgium.
[2] Vrije Universiteit Brussel, Analytical, Environmental & Geo-Chemistry Research Unit, B-1050 Brussel, Belgium.
[3] Central Michigan University, Department of Earth and Atmospheric Science, Mount Pleasant, 48859, USA.

* Corresponding author: laura.vanderdoes@kuleuven.be

thermore, the tourmaline is classified as schorl species (Henry *et al*., 2011). The prismatic tourmaline, however, has a larger dravite component, with Fe/(Fe+Mg) ranging 0.67-0.72, whereas Fe/(Fe+Mg) in the QTIs ranges 0.82-0.93.

Micro X-ray fluorescence (µXRF; Bruker M4 Tornado at Vrije Universiteit Brussel) mapping was performed to provide a high-resolution (25 µm) semi-quantitative overview of the major- and trace element variations between and within different schorl crystals (Kaskes *et al*., 2021). The µXRF maps clearly show that part of the core-rim zonation can be attributed to variations in Ti content (Fig. 2B) (Ti ranging 0.010-0.020 apfu and 0.026-0.052 apfu in cores and rims, respectively). Furthermore, these maps indicate an increase in Fe, Mn and Zn with progressive internal crystallization of the pegmatite dike from the prismatic schorl in the border zone to the QTI schorl in the wall-zone.

QTI textures are also identified elsewhere (e.g., Black Hills pegmatites, South Dakota, USA) but their formation mechanisms are currently not well understood. However, they can be of great significance for understanding the magmatic evolution of pegmatites within the light of disequilibrium crystallization (see also: Sirbescu & Hulsbosch, 2020). The different crystal morphologies, potentially indicate variations in crystallization conditions. Therefore, we plan to perform coupled tourmaline geochemistry and FI studies in order to provide valuable information on the crystallization conditions, potential boundary layer formation and localized fluid saturation in pegmatitic melts.

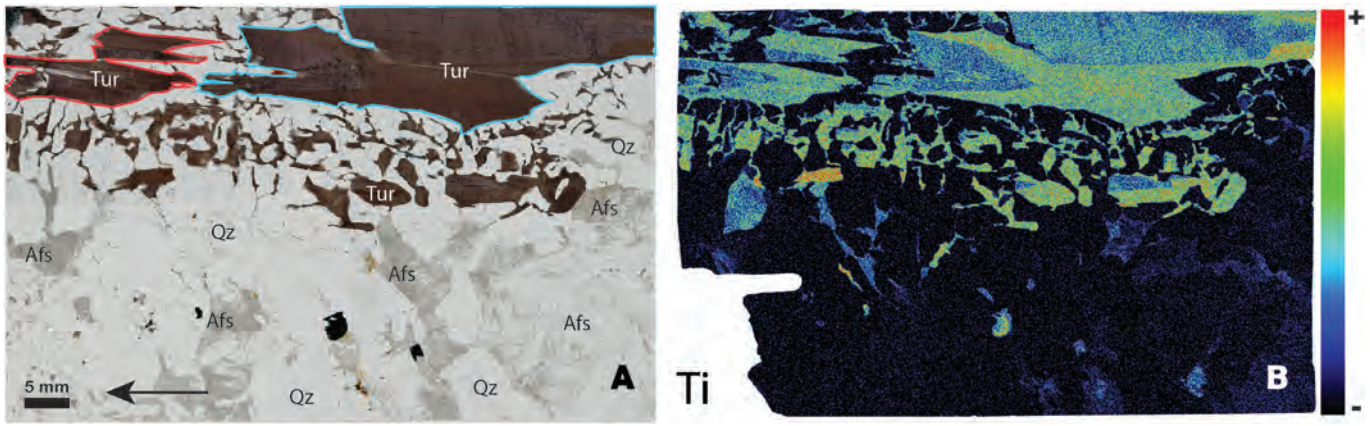

Fig. 2 - Transmitted light photo of quartz-tourmaline intergrowth (A) showing the central tourmaline (blue outline), second tier tourmaline (red outline) and skeletal tourmaline (no outline) and the corresponding µXRF heatmap of Ti (B). Tur: tourmaline, Afs: akali feldspar, Qz: quartz. Black arrow indicates growth direction.

REFERENCES

Falster A. U., Simmons W. B., Webber K. L., Dallaire D. A., Nizamoff J. W. & Sprague R. A., 2019 – The Emmons Pegmatite, Greenwood, Oxford County, Maine. *Rocks & Minerals*, 94 (6): 498-519.

Hanson S. L., Falster A. U., Simmons W. B., Sprague R., Vignola N., Andó S. & Hatert F. 2018 – Tantalowodginite, $(Mn_{0.5}\square_{0.5})TaTa_2O_8$, A New Mineral Species from the Emmons Pegmatite, Uncle Tom Mountain, Maine, U.S.A. *The Canadian Mineralogist*, 56 (4): 543-553.

Henry D. J., Novák M., Hawthorne F. C., Ertl A., Dutrow B. L., Uher P. & Pezzotta F., 2011 – Nomenclature of the tourmaline-supergroup minerals. *American Mineralogist*, 96 (5-6): 895-913.

Kaskes P., Déhais T., de Graaff S. J., Goderis S. & Claeys P., 2021 – Micro–X-ray fluorescence (µXRF) analysis of proximal impactites: High-resolution element mapping, digital image analysis, and quantifications, *Geological Society of America, Special Paper,* 550: 1-36.

London D., 2008 – Pegmatites. *The Canadian Mineralogist*, *Special Publication*, 10: 347.

Simmons W. B. & Webber K. L., 2008 – Pegmatite genesis: state of the art. *European Journal of Mineralogy*, 20 (4): 421-438.

Sirbescu M.-L. C. & Hulsbosch N., 2020 – Inclusion trapping during disequilibrium pegmatite crystallization: lessons from tourmaline-quartz intergrowths. *Goldschmidt2020 Abstract*: 2403.

Sirbescu M.-L. C., Schmidt C., Veksler I. V., Whittington A. G. & Wilke M., 2017 – Experimental Crystallization of Undercooled Felsic Liquids: Generation of Pegmatitic Textures. *Journal of Petrology*, 58 (3): 539-568.

Tourmaline elemental partitioning with melts, fluids and minerals: how to interpret tourmaline (trace element) composition

Vincent J. van Hinsberg

Tourmaline's elemental and isotopic composition has been used with great success as an indicator of provenance (e.g. Henry & Dutrow, 1996; Nascimento *et al.,* 2007), pressure-temperature conditions (e.g. van Hinsberg & Schumacher, 2007; 2009), fluid composition (e.g. Berryman *et al.*, 2015; von Goerne *et al*., 2011; van Hinsberg *et al.*, 2017) and as an ore deposit vector (e.g. Duchoslav *et al.*, 2017; Slack & Trumbull, 2011). However, the composition of a mineral in a natural rock is the net result of a range of physical and chemical parameters that both enhance and counteract each other, and in doing so may mask the variable of interest.

At equilibrium, a mineral's major and trace element composition is controlled by: **1.** The bulk composition of its growth environment, including any melt or fluid that has since departed; **2.** Physical conditions (P,T,fO_2); **3.** The element-exchanging mineral assemblage (not necessarily co-genetic); and **4.** The mineral's crystal structure as well as the crystal structure of its growth surfaces. Kinetics can modify this equilibrium composition in a number of ways, including by limiting element transport to and from the site of growth, characterized by lowered compatible over incompatible element ratios; inheritance of the elemental signature of a precursor phase; or in the meta-stable persistence of a mineral. In natural rocks, most of these parameters are not independent, but rather highly correlated. For example, P and T largely co-vary in the Earth's crust; a mineral's crystal structure reflects P-T conditions as well as major element composition; and element valence tracks fO_2.

To use a mineral's composition as an indicator of the physico-chemical conditions of its growth environment thus requires a compositional parameter that is either dominantly sensitive to only one variable, or for which the impact of other variables can be accounted for. Absolute element contents in tourmaline predominantly reflect the local bulk composition (e.g. Kalliomaki *et al*., 2017), explaining tourmaline's success as a provenance indicator.

GEOTOP Research Centre, Department of Earth and Planetary Sciences, McGill University, Montreal, Canada.
E.mail: V.J.vanHinsberg@gmx.net

The strong sensitivity to bulk composition complicates quantifying the impact of other variables. Element partitioning among phases cancels out the impact of bulk composition. Moreover, knowledge of element partitioning behaviour allows for evaluating and modelling the (re-)distribution of elements during progressive metamorphism, during melting, and in water-rock interaction. It can also identify the (ore) elements a given mineral is most sensitive to.

The element partitioning systematics of tourmaline have yet to be fully explored. Work on meta-pelites indicates that tourmaline has a strong preference for Mg over Fe compared to coexisting phases (Henry & Guidotti, 1985; van Hinsberg & Schumacher, 2009) and tourmaline-fluid experiments elucidate Ca and Na exchange (von Goerne *et al*., 2011). Only preliminary data are available for trace elements, which show minimal fractionation of the trace elements between tourmaline and a Si-poor, high-B, low X_{Mg} melt (van Hinsberg, 2011) and high D values for Cr, V and Pb with aqueous fluid (van Hinsberg *et al.,* 2017).

This contribution will review existing element partitioning data for tourmaline, and present new data for tourmaline – mineral pairs in well-equilibrated natural samples, as well as experiments with granitic melts and aqueous fluids. Results indicate that tourmaline preferentially incorporates Cr, V, the base metals and Sn, with low D values for Rb, Cs, and Ba (Fig. 1). The REE are compatible in tourmaline in melt and fluid experiments, and tourmaline prefers the LREE compared to coexisting minerals. D values range from highly incompatible to compatible, and the pattern for melt and fluid is similar, showing that tourmaline has a distinct element incorporation fingerprint. This has important implications for interpreting its composition as tourmaline will not simply sample the chemistry of its environment, but fractionate the elements as governed by the partition coefficients.

REFERENCES

Berryman E., Wunder B., Wirth R., Rhede D., Schettler G., Franz G. & Heinrich W., 2015 – An experimental study on K & Na incorporation in dravitic tourmaline and insight into the origin of diamondiferous tourmaline from the Kokchetav Massif, Kazakhstan. *Contributions to Mineralogy and Petrology*, 169: 1-16.

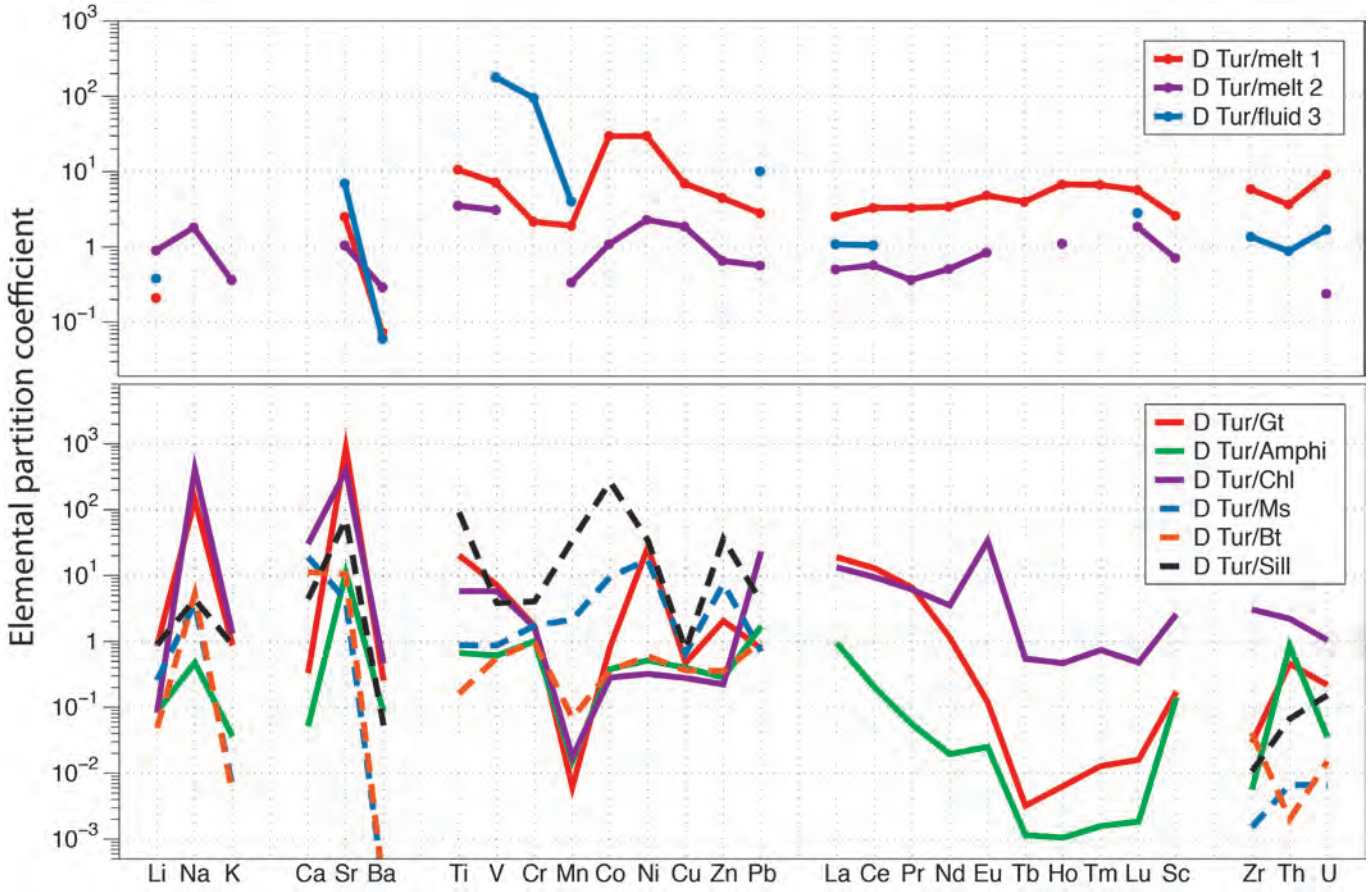

Fig. 1 - Element partition coefficients for tourmaline: 1 tourmaline-granite from Cruz & van Hinsberg (2019), 2 tourmaline – high-B, low Si melt from van Hinsberg 2011, 3 Tourmaline – aqueous fluid from van Hinsberg *et al*., 2017. The tourmaline – mineral D values are for amphibolite facies meta-pelite (Ms, Bt and Sill) and amphibolite (Gt, Amphi, Chl).

Cruz M. F. & van Hinsberg V., 2019 – Experimental investigation of orbicular tourmaline in granitic melts. *Goldschmidt conference*, Barcelona.

Duchoslav M, Marks M. A. W., Drost K., McCammon C., Marschall H. R., Wenzel T. & Markl G., 2017 – Changes in tourmaline composition during magmatic and hydrothermal processes leading to tin-ore deposition: The Cornubian Batholith, SW England. *Ore Geology Reviews*, 83: 215-234.

Henry D. J. & Dutrow B. L., 1996 – Metamorphic tourmaline and its petrologic applications. In: Boron: Mineralogy, Petrology and Geochemistry. Grew E. & Anovitz L. (eds.). *Reviews in Mineralogy*, 33 (10): 503-557.

Henry D. J. & Guidotti C., 1985 – Tourmaline as a petrogenetic indicator mineral - An example from the staurolite-grade metapelites of NW Maine. *American Mineralogist*, 70: 1-15.

Kalliomaki H., Wagner T., Fusswinkel T. & Sakellaris G., 2017 – Major and trace element geochemistry of tourmalines from Archean orogenic gold deposits: Proxies for the origin of gold mineralizing fluids? *Ore Geology Reviews*, 91: 906-927.

Nascimento M., Goes A., Macambira M. & Brod J., 2007 – Provenance of Albian sandstones in the Sao Luis-Grajau Basin (northern Brazil) from evidence of Pb-Pb zircon ages, mineral chemistry of tourmaline and palaeocurrent data. *Sedimentary Geology,* 201: 21-42.

Slack J. & Trumbull R., 2011 – Tourmaline as a recorder of ore-forming processes. *Elements*, 7: 321-326.

van Hinsberg V. J., 2011 – Preliminary experimental data on trace-element partitioning between tourmaline and silicate melt. *The Canadian Mineralogist*, 49: 153-163.

van Hinsberg V. J. & Schumacher J. C., 2007 – Intersector element partitioning in tourmaline: a potentially powerful single crystal thermometer. *Contributions to Mineralogy and Petrology*, 153: 289-301.

van Hinsberg V. & Schumacher J., 2009 – The geothermobarometric potential of tourmaline, based on experimental and natural data. *American Mineralogist*, 94: 761-770.

van Hinsberg V., Franz G. & Wood B., 2017 – Determining subduction-zone fluid composition using a tourmaline mineral probe. *Geochemical Perspectives Letters*: 160-169.

von Goerne G., Franz G. & van Hinsberg V., 2011 – Experimental determination of Na–Ca distribution between tourmaline and fluid in the system $CaO–Na_2O–MgO–Al_2O_3–SiO_2–B_2O_3–H_2O$. *The Canadian Mineralogist*, 49: 137-152.

Tourmaline reference materials for trace element analyses: a progress update

Vincent J. van Hinsberg[1]*, Haihao Guo[2]

Tourmaline's trace element composition is of growing interest as an indicator of provenance and an ore deposit vector (e.g. Marks *et al*., 2013; Duchoslav *et al.*, 2017; Kalliomaki *et al*., 2017; Sciuba *et al*., 2021), and as an archive of the trace element mobility in its host rock (*e.g.* van Hinsberg *et al*., 2017). The latter use stems from tourmaline's common growth zoning that can record a surprisingly large part of its geological history combined with tourmaline's negligible volume diffusion, which ensures preservation of this compositional record (see van Hinsberg *et al*., 2011).

Ensuring the accuracy of these trace element data and permit inter-lab comparability greatly benefits from the availability of matrix-matched standards. Here, we report on the progress towards developing a set of natural tourmalines for use as reference materials for trace elements. These reference materials will be made available to the community to promote consistency in trace element data.

Eleven natural tourmalines of sufficient size and homogeneity were selected (out of a total of more than 100 grains), spanning a wide range of tourmaline compositions from the schorl – dravite series towards uvite, elbaite, and foitite. Aliquots of these tourmalines were measured for their major element composition by EPMA in 4 labs (Barbara Dutrow and Darrell Henry – Louisiana State University; Wancai Li – University of Science and Technology of China; Jan Cempírek and Radik Škoda – Masaryk University; and our lab at McGill University), and by laser ablation ICP-MS in 5 labs (Jan Cempírek and Radik Škoda – Masaryk University, Czech Republic; Longbo Yang – Laurentian University, Canada; André Poirier – Université de Quebec à Montréal, Canada; Yanwen Tang – Institute of Geochemistry, Chinese Academy of Sciences; and our lab at McGill University). Their crystal structure was determined by Lee Groat's research group at the University of British Columbia, Canada, and Mössbauer measurements for Fe valance were conducted by Filip Jan (Palacky University, Czech Republic). Additional work is currently taking place to extend this set to Cr-rich tourmaline (samples courtesy of Ivan Baksheev).

The tourmaline reference materials cover a remarkably large range in minor and trace element concentrations (Figs. 1 and 2), with Pb, for example, varying by over 3 orders of magnitude from less than 1 to close to 700 mg/kg. REE patterns show a consistent LREE over HREE enrichment with both positive and negative Eu anomalies, and with ∑REE concentrations from 0.5 to 1620 mg/kg (Fig. 3). We expect that this compositional range will permit bracketing tourmaline analyses for most natural samples.

The tourmaline reference materials are to become available for distribution towards the end of 2021, and will be free of charge with a data-sharing requirement to allow for periodic updating of reference values.

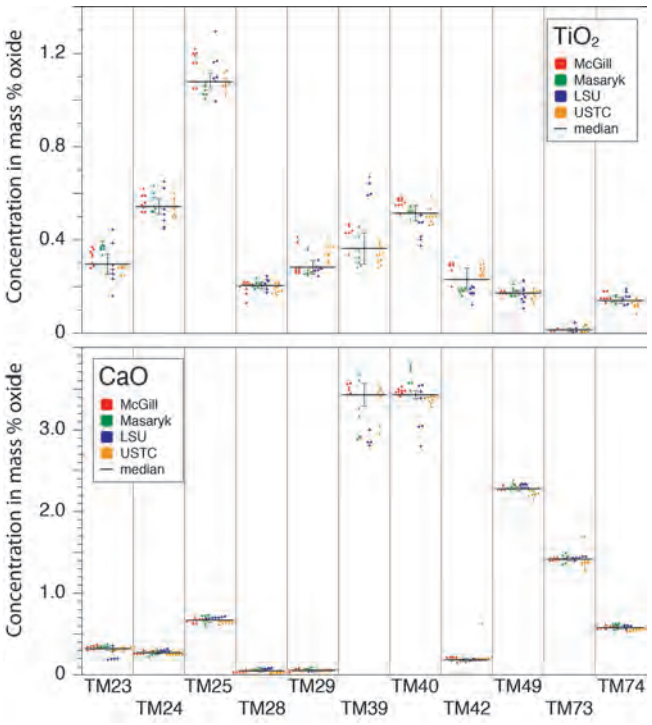

Fig. 1 - EPMA results for the tourmaline samples. Preferred reference values are given as the solid black line with 1 sd uncertainty.

[1] GEOTOP Research Centre, Department of Earth and Planetary Sciences, McGill University, Montreal, Canada.
[2] University of Orléans, CNRS, BRGM, ISTO, UMR 7327, Orléans, France.
E.mail: haihao.guo@cnrs-orleans.fr

* Corresponding author: V.J.vanHinsberg@gmx.net

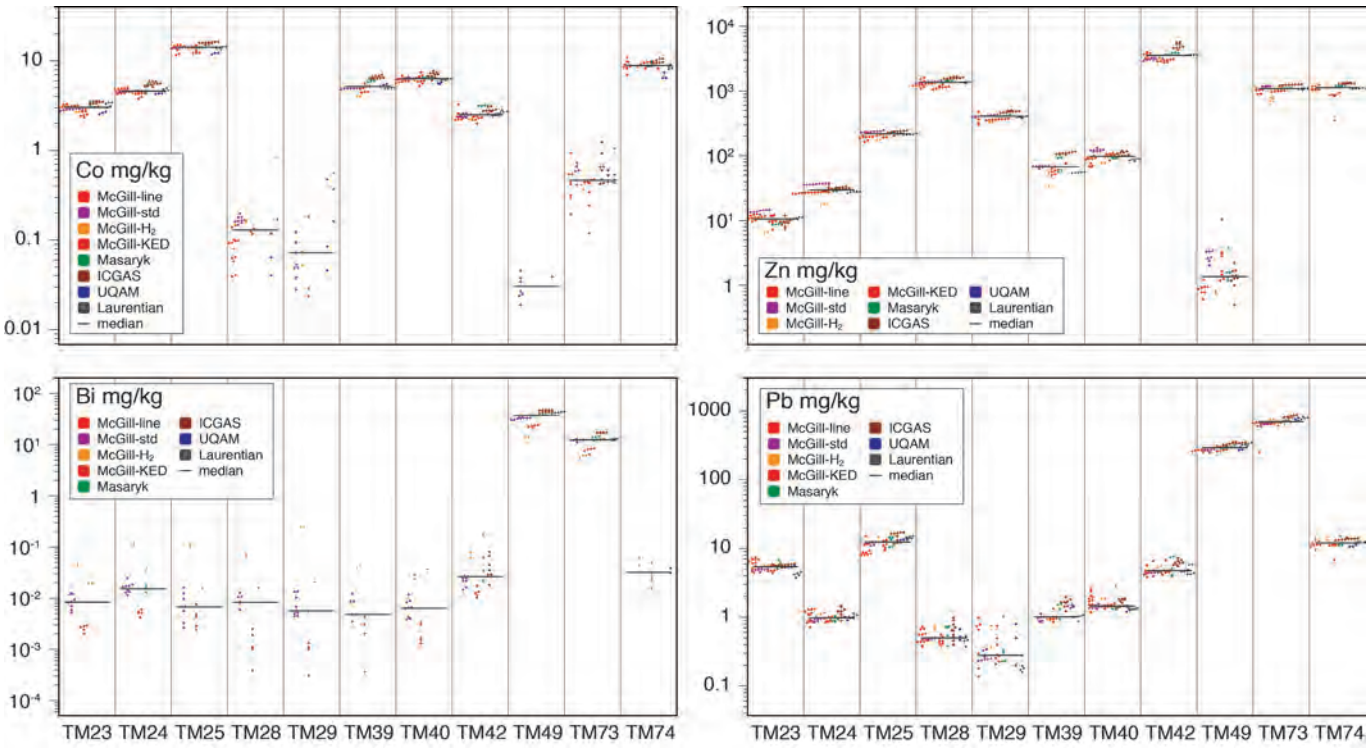

Fig. 2 - Selected trace element data for the tourmaline reference materials showing a remarkable range in concentrations.

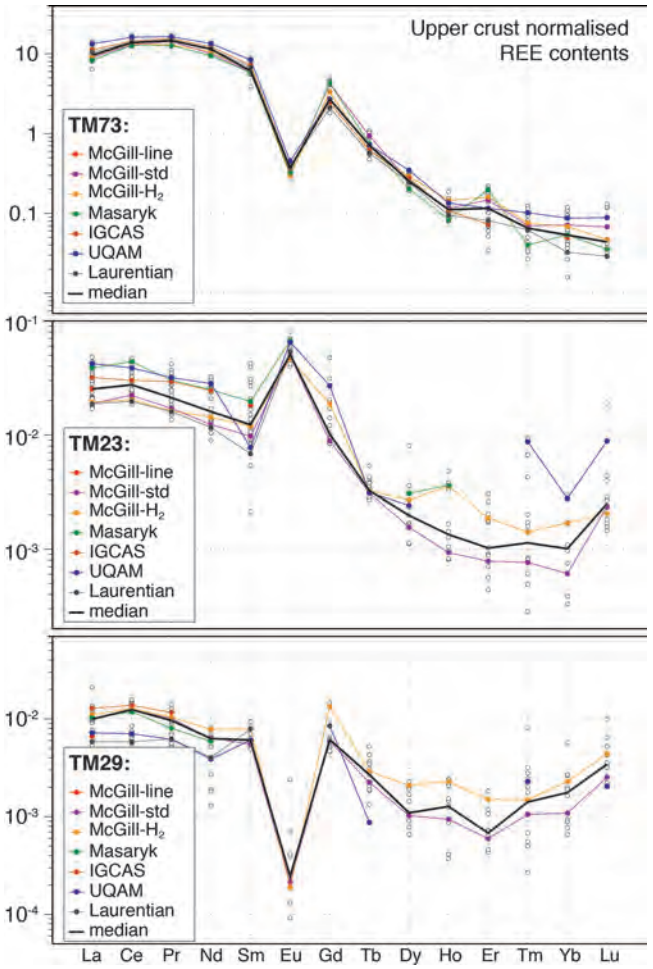

Fig. 3 - REE patterns for selected tourmaline reference materials, normalized to bulk upper crust. REE contents and patterns vary, but share a LREE/HREE enrichment.

REFERENCES

Duchoslav M, Marks M. A. W., Drost K., McCammon C., Marschall H. R., Wenzel T. & Markl G., 2017 – Changes in tourmaline composition during magmatic and hydrothermal processes leading to tin-ore deposition: The Cornubian Batholith, SW England. *Ore Geology Reviews*, 83: 215-234.

Kalliomaki H., Wagner T., Fusswinkel T. & Sakellaris G., 2017 – Major and trace element geochemistry of tourmalines from Archean orogenic gold deposits: Proxies for the origin of gold mineralizing fluids? *Ore Geology Reviews*, 91: 906-927.

Marks M. A. W., Marschall H. R., Schühle P., Guth A., Wenzel T., Jacob D. E., Barth M. & Markl G., 2013 – Trace element systematics of tourmaline in pegmatitic and hydrothermal systems from the Variscan Schwarzwald (Germany): The importance of major element composition, sector zoning, and fluid or melt composition. *Chemical Geology*, 344: 73-90.

Sciuba M., Beaudoin G. & Makvandi S., 2021 – Chemical composition of tourmaline in orogenic gold deposits. *Mineralium Deposita*, 56 (3): 537-560.

van Hinsberg V. J., Henry D. J. & Dutrow B. L., 2011 – Tourmaline as a Petrologic Forensic Mineral: A Unique Recorder of Its Geologic Past. *Elements*, 7 (5): 327-332.

van Hinsberg V., Franz G. & Wood, B., 2017 – Determining subduction-zone fluid composition using a tourmaline mineral probe. *Geochemical Perspectives Letters*: 160-169.

Towards tourmaline REE pattern explanation

Oleg Vereshchagin[1]*, Sergey N. Britvin[1], Bernd Wunder[2], Olga Frank-Kamenetskaya[1], Franziska D. H. Wilke[2]

Natural tourmalines could contain sufficient amounts of rare earth elements (up to ~1000 ppm; Bačík *et al*., 2012), exhibit both positive and negative Eu anomalies (Čopjaková *et al*., 2013) and are characterized by different light / medium / heavy rare earth elements (REE) ratios (Gadas *et al*., 2012). Even though REE patterns of natural tourmalines were studied for decades, no direct information on REE speciation in tourmaline and factors affecting REE pattern are available. Exploring the way lanthanides incorporate in tourmaline structure one could get both new functional materials and explain REE patterns of natural tourmalines.

In the course of current work we report on synthetic REE^{3+}- tourmalines (REE^{3+} = La, Nd, Eu, Yb) and discuss the role of the *X*-site cations.

REE^{3+}- tourmalines were synthesized in 11 experiments at temperatures of 700 °C and pressures of 0.2 (Fig. 1) or 4.0 GPa. Besides *REE*-tourmaline, other REE borates were obtained (<10 vol. %;): $REEAl_{2.07}(B_4O_{10})O_{0.6}$ in La-, Nd- and Eu-synthesis, $REEBSiO_5$ (stillwellite-like compounds) in La- and Nd-synthesis, $Eu_2B_2SiO_8$ and Yb-BO_3. In Yb-synthesis $Yb_2(Si_2O_7)$ (keivyte-(Yb)) was also obtained.

Elongated or needle-like prismatic tourmaline crystals from high-pressure experiments are much smaller (up to 0.5×6 μm) than those from the low-pressure experiments (up to 100×300 μm).

Based on elemental analysis data we have found that REE-content in tourmalines varies significantly (0.05 - 1.05 atoms per formula unit (apfu)) with Yb<La≤Nd<Eu independent of the pressure conditions. REE-content in tourmalines, obtained at low pressure, is 2-3 times higher than that obtained from high-pressure experiments. The Nd- and Eu-tourmalines exhibit cathode- and photoluminescence properties, which confirm their trivalent oxidation state. Single-crystal X-ray diffraction data show that Eu^{3+} and Nd^{3+} occupy the 9-coordinated *X*-site in the tourmaline structure (Table 1).

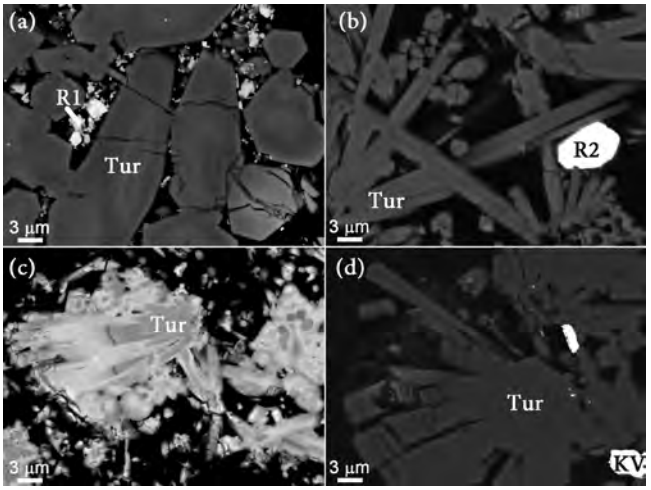

Fig. 1 - BSE images of REE-tourmalines (Tur), obtained at low pressure (2 kbar): (a) La-tourmaline and $LaBSiO_5$ (R1), (b) Nd-tourmaline and $NdBSiO_5$ (R2), (c) Eu-tourmaline, (d) Yb-tourmaline and $Yb_2(Si_2O_7)$ (KV).

Our investigations indicate pressure effect and crystal-chemical constraints on REE incorporation in tourmalines, which is of great importance for geoscientific implications.

It was suggested that the dominant factor governing the species of REE is temperature (e.g., Sverjensky, 1984). Our data on synthetic tourmalines, obtained at same temperature (700 ˚C) but at different pressures (0.2 / 4.0 GPa), clearly show that additional pressure could be a main factor, affecting tourmalines REE pattern.

It was also proposed that significant enrichment of heavy REE in tourmaline (in contrast to the REE patterns of the whole-rock samples) indicates a mobilization of heavy REE during hydrothermal processes (Yavuz *et al*., 2011). However, according to our data predominance of

[1] Institute of Earth Sciences, St Petersburg State University, Universitetskaya nab. 7/9, 199034 Saint-Petersburg, Russia.
E-mail: sergei.britvin@spbu.ru
o.frank-kamenetskaya@spbu.ru
[2] GFZ German Research Centre for Geosciences, 14473 Potsdam, Germany.
E-mail: wunder@gfz-potsdam.de
fwilke@gfz-potsdam.de

* Corresponding author o.vereshchagin@spbu.ru

light and medium REE (e.g., Eu, Nd, La) over heavy REE (Yb) in tourmalines, could be due to tourmaline crystal structure constrains, not crystallisation medium effects.

Preliminary experimental data on trace-element partitioning between tourmaline and silicate melt (van Hinsberg, 2011) predicted that Eu^{2+} is the preferential valence state in the tourmaline crystal structure and Eu^{3+} occur at octahedral sites. We have found that (1) the tourmaline crystal structure can accommodate REE as trivalent cations; and (2) REE^{3+} cations are located at the 9-coordinated *X*-site. The latter is also in a good agreement with published data, as Eu^{3+} is not even observed as six-coordinated polyhedral (Gagné *et al*., 2018). Besides that, we can conclude that tourmalines could be a phase that concentrates REE during crystallization process, as total amount of REE^{3+} can reach amounts up to 1 apfu.

It is worth to note, that the REE^{+} valence state (e.g., Eu^{3+} or Eu^{2+}) depends on the redox conditions at which tourmaline formed and that Eu^{2+}-rich tourmaline should not be completely excluded for natural occurrence. Our data do not exclude the prediction, that divalent rare-earth cation could occur at the *X*-site as REE^{2+} cations are even larger than REE^{3+} cations.

Additionally, one might conclude that natural tourmalines could contain other trivalent cations at the *X*-site (e.g., Bi^{3+}; Ertl & Bačík, 2020) and that the general classification scheme for tourmaline group may be expanded, as not only monovalent (e.g., Na, K, Li, Ag, NH_4) and divalent (e.g., Ca, Sr, Pb), but also trivalent cations could occupy this site.

Table 1 - Variations of *X*-site occupancies of natural and synthetic tourmalines.

No	*a*, Å	*c*, Å	$X_{0\text{-}1}$	<*X*-O>, Å	Y_3	<*Y*-O>, Å	Z_6	<*Z*-O>, Å	Reference
1.	15.903(5)	7.168(3)	$\square_{0.72}Eu^{3+}_{0.28}$	2.708	$Al_{1.74}Mg_{1.26}$	1.990	$Al_{5.22}Mg_{0.78}$	1.927	Eu-tourmaline
2.	15.8934(15)	7.1304(7)	$\square_{0.83}Nd^{3+}_{0.17}$	2.705	$Al_{1.95}Mg_{1.05}$	1.979	$Al_{5.28}Mg_{0.72}$	1.922	Nd-tourmaline
3.	15.910(1)	7.131(1)	$\square_{0.91}Na_{0.09}$	-	$Al_{1.62}Mg_{1.38}$	1.992	$Al_{4.92}Mg_{1.08}$	1.920	Berryman *et al*., 2016

Acknowledgment

The authors thank U. Dittmann and H.-P. Nabein for technical assistance and Resource centres of SPbSU (X-ray Diffraction Centre, Geomodel and Nanotechnology Interdisciplinary Center) for providing instrumental and computational resources.

This work was supported by grant of the President of the Russian Federation MK-1832.2021.1.5.

REFERENCES

Bačík P., Uher P., Ertl A., Jonsson E., Nysten P., Kanický V. & Vaculovič T., 2012 – Zoned *REE*-enriched dravite from a granitic pegmatite in Forshammar, Bergslagen Province, Sweden: An EMPA, XRD and LA-ICP-MS study. *The Canadian Mineralogist*, 50: 825-841.

Berryman E. J., Wunder B., Ertl A., Koch-Müller M., Rhede D., Scheid K., Giester G. & Heinrich W., 2016 – Influence of the X-site composition on tourmaline's crystal structure: investigation of synthetic K-dravite, dravite, oxy-uvite, and magnesio-foitite using SCXRD and Raman spectroscopy. *Physics and Chemistry of Minerals*, 43: 83-102.

Čopjaková R., Škoda R., Galiová M. V. & Novák M., 2013 – Distributions of Y + *REE* and Sc in tourmaline and their implications for the melt evolution; examples from NYF pegmatites of the Třebíč Pluton, Moldanubian Zone, Czech Republic. *Journal of GEOsciences*, 58 (2): 113-131.

Ertl A. & Bačík P., 2020 − Considerations About Bi and Pb in the Crystal Structure of Cu-Bearing Tourmaline. *Minerals*, 10 (8): 706.

Gadas P., Novák M., Staněk J., Filip J. & Galiová, M. V., 2012 – Compositional Evolution of Zoned Tourmaline Crystals from Pockets in Common Pegmatites of the Moldanubian Zone, Czech Republic. *The Canadian Mineralogist*, 50 (4): 895-912.

Gagné O. C., Mercier P. H. J. & Hawthorne F. C., 2018 – *A priori* bond-valence and bond-length calculations in rock-forming minerals. *Acta Crystallographica*, *Section B*, 74: 470-482.

Sverjensky D. A., 1984 – Europium redox equilibria in aqueous solution. *Earth and Planetary Science Letters,* 67: 70-78.

van Hinsberg V., 2011 – Preliminary experimental data on trace-element partitioning between tourmaline and silicate melt. *The Canadian Mineralogist*, 49 (1): 153-163.

Yavuz F., Jiang S. Y., Karakay N., Karakaya M. Ç. & Yavuz R., 2011 – Trace element, rare-earth element and boron isotopic compositions of tourmaline from a vein-type Pb-Zn-Cu ± U deposit, NE Turkey. *International Geology Review*, 53: 1-24.

Tourmaline and white mica boron isotopes in pelitic schist from the Chinese southwestern Tianshan: insight into subduction-zone fluid flow

Jie Xu[1,2]*, Guibin Zhang[1], Horst R. Marschall[2], Zeng Lü[1], Lifei Zhang[1], Nan Li[1], Xin Yang[1]

Boron geochemistry can track fluid–rock interaction during metamorphic evolution and provides important insights into mass-transfer processes in subduction zones. This study presents boron concentration and B isotope data for tourmaline and white mica (phengite and paragonite) in ultrahigh-pressure (UHP) metamorphic pelitic schists from the Chinese southwestern Tianshan (Xinjiang Province, China; Fig. 1).

Boron isotope ratios of tourmaline and white micas were measured *in-situ* using a Nu plasma II MC-ICPMS coupled with a Coherent Geolas HD excimer laser-ablation system (193 nm) at the School of Earth and Space Sciences, Peking University.

The sample investigated in detail was collected from the central part of the Kebuerte Valley, where blueschists, eclogite-facies rocks, greenschists, metabasites and serpentinites are exposed. Tourmaline and coexisting white mica record detailed information of fluid evolution from peak UHP metamorphism to late-stage exhumation.

The micaschist experienced some degree of dehydration during decompression-heating from peak conditions of 500 ºC, 3.1 GPa to 550 ºC, 2.4 GPa. This led to phengite recrystallization recorded in a correlated decrease of phengite $\delta^{11}B$ and Si content. Tourmaline grain size also increased, fed from B liberated from phengite.

During protracted exhumation at *P–T* conditions below 500 ºC and 1.5 GPa the rock was infiltrated by external fluid leading to the formation of the assemblage paragonite + tourmaline rims + chlorite.

Accessory tourmaline is hypidiomorphic to euhedral with grain diameters between 50 and 400 µm. It is observed in the rock matrix in contact with quartz and white micas (both phengite and paragonite). In thin section, tourmaline grains show (asymmetric) zonation with blue cores and brown rims. No detrital tourmaline cores were observed. The composition of all analysed tourmaline is dravitic with nearly fully occupied X-site dominated by Na (0.79–0.94) and minor Ca (≤0.08) and Mg# increase in the blue core domains from 62 to 67. The brown rims in contact to paragonite are lower again in Mg# (appr. 63) and show the highest X-site vacancy.

Boron in phengite grew isotopically lighter with a decrease in $\delta^{11}B$ from -5.71 ‰ to -16.01 ‰ (relative to NIST SRM 951) with the increase of temperature from 500 ºC to 550 ºC, which correlates positively with B abundance and Si content. Tourmaline formed at this stage also shows a decrease in $\delta^{11}B$ from core outwards concomitant with the increase in Mg# (Fig. 2).

Boron isotope fractionation during partial dehydration was modelled using known temperature-dependent B isotope fractionation factors among white mica, tourmaline and hydrous fluid (Kowalski & Wunder, 2018). The

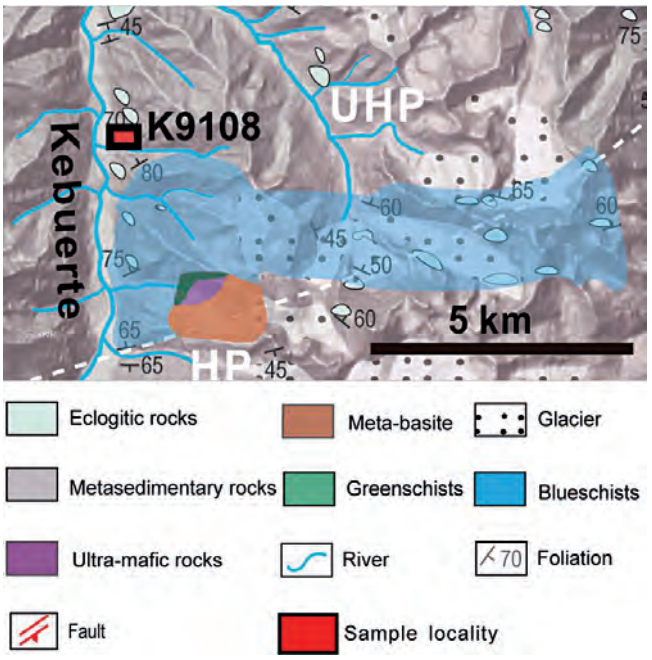

Fig. 1 - Location of study sample in the Chinese southwestern Tianshan.

[1] Key Laboratory of Orogenic Belt and Crustal Evolution, MOE; School of Earth and Space Science, Peking University, Beijing 100871, China.
[2] Institut für Geowissenschaften, Goethe-Universität, Altenhöferallee 1, 60438 Frankfurt am Main, Germany.
E-mail: marschall@em.uni-frankfurt.de

* Corresponding author: jie.xu@stud.uni-frankfurt.de

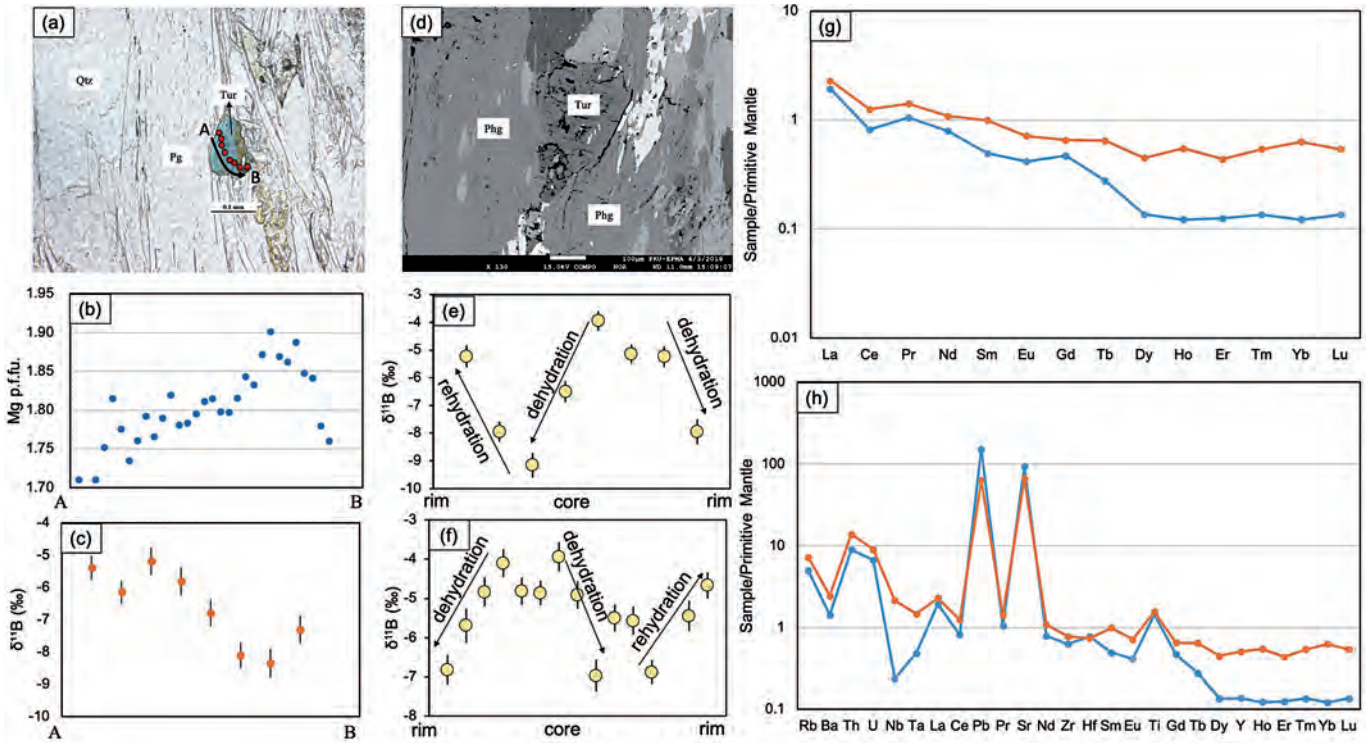

Fig. 2 - Photomicrographs and profiles of tourmaline in studied sample K9108. (a, b and c): Mg p.f.u. and boron isotope profiles for tourmaline; (d) tourmaline coexisting with phengite; (e and f): tourmaline coexisting with phengite that showed non-monotonic zonation from core to rim. Error bars correspond to internal precision (2σ). (g,h) Primitive Mantle-normalized REE patterns and multi-element diagram for tourmaline.

results suggest that fluids in equilibrium with the peak-pressure assemblage had a $\delta^{11}B$ of -1.91 ±1.35 ‰, which decreased to -6.74 ±0.93 ‰ at peak temperature.

Boron abundances in paragonite formed during exhumation and cooling shows an increase from 98 to 323 µg/g, with a concomitant increase in $\delta^{11}B$ from -15.55 to -5.63 ‰. Tourmaline rims, which grew during this stage also record the rehydration process with zonation increasing in $\delta^{11}B$ from -10.3 ‰ near the grain cores to -2.2 ‰ at the rim in contact with paragonite.

[B] and $\delta^{11}B$ of the external fluid were estimated by modeling partitioning and fractionation at 340 ±20 µg/g and +4 ±3 ‰. A likely source of this external fluid are serpentinites that are exposed nearby. Unpublished boron isotope data from serpentinite form the Chinese southwestern Tianshan revealed $\delta^{11}B$ values of +3.5 ±4.5 ‰ (Shen, unpubl.). The hypothesis of fluids derived (or interacted with) serpentinite is supported by elevated Co and Ni contents in the investigated sample compared to other micaschist samples from the area (Peng *et al*., 2018). Influx of fluids from serpentinite was also suggested for eclogites from the same locality by van der Straaten *et al.* (2008).

This study demonstrates that tourmaline is a faithful recorder of the geochemical evolution of metamorphic fluids in subduction zones that enables us to trace internally- and externally-derived fluids and relate it to the *P–T* history of the rocks.

REFERENCES

Kowalski P. M. & Wunder B., 2018 – Boron isotope fractionation among vapor–liquids–solids–melts: experiments and atomistic modeling. In: Boron Isotopes – The Fifth Element. Marschall H. R. & Foster G. L. (eds.). *Advances in Isotope Geochemistry*, *Springer*: 33-69. <doi: 10.1007/978-3-319-64666-4_3>

Peng W., Zhang L., Shen T. & Hu H., 2018 – Implications for the deep carbon cycle from the carbonation in subduction zones: A case study of carbonated micaschists from Chinese southwestern Tianshan. *Acta Petrologica Sinica*, 34 (04): 1204-1208.

van der Straaten F., Schenk V., John T. & Gao J., 2008 – Blueschist-facies rehydration of eclogites (Tian Shan, NW-China): Implications for fluid–rock interaction in the subduction channel. *Chemical Geology*, 255: 195-219. <doi: 10.1016/j.chemgeo.2008.06.037>

INDEX VOLUME 111 (1) 2021